Electrophysiological characterisation of neurons located in the Bed nucleus of the stria terminalis (BNST) in aging, sex and a model of frontotemporal dementia

Submitted by Hannah Smithers, to the University of Exeter as a thesis for the degree of Doctor of Philosophy in medical studies, September 2017.

I certify that all material in this thesis which is not my own work has been identified and that no material has previously been submitted and approved for the award of a degree by this or any other University.

Signature……

Word count: 46,713

Abstract

Chronic stress and anxiety disorders are placing an increasing economic burden on western society. The anterolateral BNST ($BNST^{ALG}$) plays a key role in mediating a number of stress related responses. There are three neuronal populations within the $BNST^{ALG}$: Type I, Type II and Type III neurons. This thesis examined the electrophysiological properties of neurons located in the $BNST^{ALG}$ in different genders, healthy aging, a mouse model of frontotemporal dementia (CHMP2B) and during the different stages of the oestrous cycle. Overall I found that the oestrous cycle had very little effect on the electrophysiological properties of these cells; the only trend observed was in the maximum rate of rise of Type II neurons: diestrus was slower than metestrus and proestrus. There were a number of intrinsic electrophysiological properties which were affected by gender; Type II cells showed a decreased excitability in the female cohort driven by changes in passive membrane properties. Specifically the observed change in input resistance may be mediated by changes in allopregnanolone, which is 8-10 fold higher in females; changes in allopregnanolone levels leads to changes in $GABA_A$ subunit expression which may mediate changes in tonic inhibition and input resistance.

In aged female mice, Type I neurons had a more hyperpolarised resting membrane potential and wider action potentials, while Type II neurons from the aged cohort displayed an increase in excitability most likely due to a more depolarised threshold. Activity in Type II neurons are thought to mediate an ‘anxiety off’ switch therefore these increases in excitability may indicate an anxiolytic role of these more excitable populations. Finally I examined the $BNST^{ALG}$ neurons in the CHMP2B model of frontotemporal dementia. Type II neurons had a more hyperpolarised threshold and faster latency. Overall these studies show that the stress regulatory brain region is susceptible to changes with gender, aging and in dementia models.

Acknowledgements

I would like to thank my supervisors Professor Andrew Randall and Dr. Jonathan Brown for all their support and encouragement over the past 4 years. I would also like to thank all the members of the Randall Brown lab who made the lab a great place to work and a special thank you to Darren, Tom and Talitha for all the coffee breaks and chats. I would also like to thank my funding body University of Exeter and AstraZeneca for providing me with the opportunity to carry out this research.

My family provided me with the support I needed to getting me this far, especially my mum who was there for me through all my years at university and gave me the strength to continue onto my PhD. A special thanks to the MagnifiCatz girls for standing by me through thick and thin; all the years of laughter and adventures made me a better person. I would like to thank Alex for all his love and support over the years he has been a shoulder to lean on when I needed it the most. Lastly I would like to thank Zach, spending my weekends being a kid was the best stress relief I could ask for.

Contents

Figures

Tables

Abbreviations

5-HT	5-hydroxytryptamine
5-HTT	5-hydroxytryptamine transporter
aCSF	artificial cerebrospinal fluid
ACTH	Adrenocorticotropic hormone
ADP	after-spike depolarisation potential
AHP	after-spike hyperpolarisation potential
ALLO	allopregnanolone
ANOVA	analysis of variance
AMPA	α-amino-3-hydroxy-5-methyl-4-isoxazolepropionic acid
AP	action potential
ATP	adenosine triphosphate
APir	amydalopiriform transitional area
BLA	basolateral amygdala
BNST	Bed nucleus of the stria terminalis
$BNST^{AL}$	Bed nucleus of the stria terminalis undefined anterolateral area
$BNST^{ALG}$	Bed nucleus of the stria terminalis anterolateral group
$BNST^{FU}$	Bed nucleus of the stria terminalis fusiform nucleus
$BNST^{JC}$	Bed nucleus of the stria terminalis juxtacapsular nucleus
$BNST^{OV}$	Bed nucleus of the stria terminalis oval nucleus
$BNST^{R}$	Bed nucleus of the stria terminalis rhomboid nucleus
$BNST^{V}$	ventral division of the Bed nucleus of the stria terminalis
BSTLD	lateral division dorsal part of BNST
BSTLJ	lateral division juxtacapsular part of BNST
BSTLP	lateral division posterior part of BNST
BSTLV	lateral division ventral part of BNST
BSTMA	medial division anterior part of BNST
BSTMPL	medial division, posteromedial part of BNST
BSTMPM	medial division posteromedial part of BNST
BSTMV	medial division ventral part
CeA	central amygdala

CHMP2B	charged multivesicular body protein 2B
CNS	central nervous system
Cyp19a1	cyctochrome P450 family 19 subfamily A member 1
CRF	Corticotropin-releasing factor
CRFR1	Corticotropin-releasing factor receptor 1
CRFR2	Corticotropin-releasing factor receptor 2
DR	Dorsal raphe
dV/dt max	maximum rate of rise
EGTA	ethylene glycol-*bis*(2-aminoethylether)-*N*,*N*,*N*',*N*'-tetraacetic acid
EPSC	excitatory post synaptic potential
ER	Estrogen receptor
fMRI	functional magnetic resonance imaging
GABA	γ-aminobutyric acid
Gabazine	SR-95531 hydrobromide (6-imino-3-(4-methoxyphenyl)-1(6*H*)-pyridazinebutanoic acid hydrobromide)
GAD	General anxiety disorder
GR	Glucocorticoid receptor
GTP	guanosine-5'-triphosphate
HCN	hyperpolarisation-activated cyclic nucleotide-gated (channels)
HEPES	4-(2-Hydroxyethyl)piperazine-1-ethanesulfonic acid
Hz	hertz
HPA	Hypothalamic-pituitary-adrenocortical
IL	infralimbic cortex
IPSP	inhibitory postsynaptic potential
K	potassium
Kiss1r	kisspeptin receptor 1
KW	Kruskal-Wallis
K^+	potassium ion
MAPT	microtubule associated protein tau
MeA	medial amygdala
mGluR	metabotropic glutamate receptor
mPFC	medial prefrontal cortex

NA	Nucleus accumbens
NBQX	2,3-dioxo-6-nitro-1,2,3,4-tetrahydrobenzo[*f*]quinoxaline-7-sulfonamide
NMDA	*N*-methyl-D-aspartate
NO	nictric oxide
Oxtr	oxytocin receptor
PAG	periaqueductal gray
PL	prelimbic cortex
PTSD	post-traumatic stress disorder
PVN	paraventricular hypothalamic nucleus
SEM	standard error of the mean
sEPSC	spontaneous excitatory post synaptic potential
TG	transgenic
Thra	thyroid hormone receptor
VS	Ventral subiculum
VTA	ventral tegmental area
WT	Wild type

1. Introduction

The bed nucleus of the stria terminalis (BNST) plays a key role in stress and anxiety. Limbic systems such as the medial prefrontal (mPFC) and the hippocampus are involved in how we respond to stressors however these regions are not directly connected to key output pathways such as the paraventricular nucleus (PVN) of the hypothalamus. The BNST acts as a relay between these regions thus regulating responses to various stressors.

1.1. Stress and Anxiety

Chronic stress, anxiety and related mood disorders have a substantial effect on the well-being of all global societies. In the developed world, conditions within this spectrum of disorders have become a major economic burden, in terms of both direct healthcare costs and lost economic productivity (Kessler Greenberg 2002).

Stress-eliciting neural drive, however, is thought typically to have its genesis in higher centres, in particular the circuits of the limbic system which are known to integrate multiple complex factors to shape emotion and mood (Herman *et al.*, 2002, 2005). However many physiological manifestations of stress-related disorders are ultimately mediated via the hypothalamus. This includes the classical neuroendocrine hypothalamo-pituitary-adrenocortical (HPA) axis and hypothalamic control of various brainstem nuclei involved in peripheral homeostatic responses such as blood pressure regulation (Klimov *et al.*, 2013; Wagner *et al.*, 2013; Schneeberger *et al.*, 2014; Kataoka *et al.*, 2014).

The HPA axis is responsible for the release of glucocorticoids into circulation (Figure 1-1). Release of corticotrophin-releasing factor (CRF) in the anterior pituitary by neurons from the PVN leads to the release of adrenocorticotropic hormone (ATCH) in the adrenal cortex which in turn affects the release of glucocorticoids into circulation (Figure 1-1).

The biological effects of glucocorticoids are mediated by the glucocorticoid receptor (GR). In the absence of a ligand the GR is located in the cytoplasm where it forms part of a complex with other proteins including Src; following the binding of a ligand the GR translocates to the nucleus where it modulates gene expression. Additionally a second component of GR activation is the release of Src which mediates non genomic effects (Cain & Cidlowski, 2015). These molecules regulate a number of

stress related responses including inflammatory and immune responses, metabolism, reproduction, growth, cell survival, cell proliferation, cognition and behaviour (Chrousos & Gold, 1992; Charmandari *et al.*, 2005; Chrousos & Kino, 2005).

Although the mammalian limbic system unquestionably has pivotal roles in eliciting and modulating stress signalling, it is not extensively connected to key hypothalamic areas involved in stress responses, such as the paraventricular hypothalamic nucleus (PVN). The PVN controls the HPA axis and also exerts substantial influences on autonomic activity via its connections to various brainstem/spinal cord networks (Kc & Dick, 2010).

Due to the above mentioned lack of direct connectivity, limbic system influences on hypothalamic and brain stem-dependent outcomes are necessarily relayed through intermediate brain areas. One area of particular interest in this regard is the anterolateral area of the BNST ($BNST^{ALG}$). The $BNST^{ALG}$ receives afferent projects from many areas of the limbic system, including the ventral subiculum and mPFC, which plays a key role in HPA axis feedback. The effect of activation of the various populations in the $BNST^{ALG}$ on the HPA axis can be either inhibitory or excitatory, however the BNST is a primarily GABAergic population, GABAergic projections from the $BNST^{ALG}$ could inhibit HPA axis activation. The excitatory drive is believed to be mediated via an internal circuit in which activation of CRF cells in the oval nucleus inhibit Type I and Type II populations within the $BNST^{ALG}$ which prevents the inhibition of the glutamatergic population within the ventral BNST (Daniel & Rainnie, 2016).

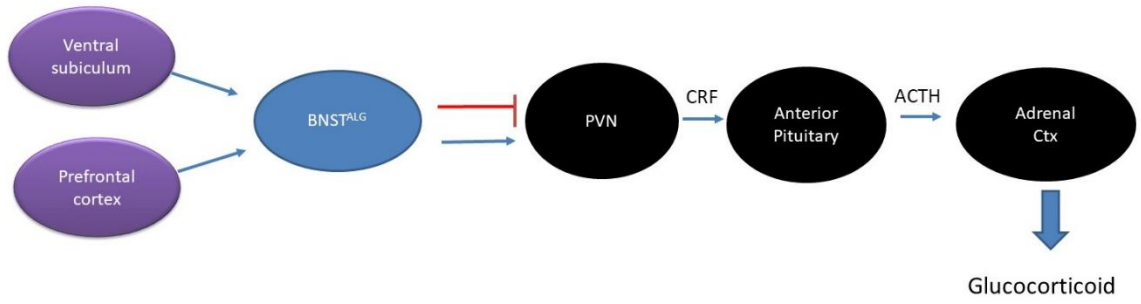

Figure 1-1 Schematic representation of the role of the anterolateral area of the BNST in the HPA function. Purple shapes represent the limbic system influences on the anterolateral BNST; the BNST is the capable of activating or inhibiting the HPA axis via its connections to the PVN. Abbreviations anterolateral BNST ($BNST^{ALG}$), paraventricular nucleus (PVN), corticotrophin releasing factor (CRF), adrenocorticotropic hormone (ACTH).

The circuit location of the BNST is suited to allow it to fulfil a gatekeeper role modulating the influences of the limbic system on the hypothalamus (Choi *et al.*, 2007; Crestani *et al.*, 2013). Notably, the BNST has been hypothesized to mediate "sustained" fear and/or anxiety after repeated stressors, as well as contextual cues that predict aversive and/or stressful stimuli (Straube *et al.*, 2007; Davis *et al.*, 2010; Janitzky *et al.*, 2015). This contrasts with the proposed roles of amygdala nuclei (such as the central amygdala amygdala (CeA) and basolateral amygdala (BLA)) which seemingly possess more pronounced roles in acute fear responses. (Gewirtz *et al.*, 1998). While the BNST and amygdala seem to display distinct roles in fear processing their functions are not completely isolated from each other; they act in conjunction with each other to provide an accurate response to fear (Walker *et al.*, 2003). Furthermore, multiple functional magnetic resonance imaging (fMRI) studies in man have demonstrated the role of BNST in the central nervous system (CNS) response to fear and anxious anticipation (Straube *et al.*, 2007; Somerville *et al.*, 2010; Yassa *et al.*, 2012).

1.1.1. The BNST

In the mammalian brain the BNST is located in the caudal pallidum, adjacent to the caudate putamen, and either side of the anterior commissure (Paxinos & Franklin, 2004*a*; Dong & Swanson, 2004*a*). It is a predominantly GABAergic region, which is sexually dimorphic. It plays a key role in stress and anxiety where its effects can be both anxiolytic and anxiogenic. This complex region is comprised of several subregions, each of which has unique cellular populations. Here I will briefly detail the subregions of the BNST with specific focus on the $BNST^{ALG}$ and its role in healthy brains and disease states.

1.1.2. Subdivisions of the BNST

The BNST is a complex region made up of several sub nuclei, the number of which vary depending upon individual classifications. These have been better characterised in the rat than in the mouse where twenty subregions have been described based mainly upon its connectivity with the amygdala (Dong *et al.*, 2001*b*). Two main classifications exist to describe the nuclei of the BNST, the first is based on detailed parcelling bundling based on intermediate, ventral, lateral and medial divisions. For the most part these are similar to the classifications used by Paxinos and Watson (Paxinos & Franklin, 2004*a*). In contrast, Swanson and Dong classifications are based more on an anterior posterior division (Dong *et al.*, 2001*b*). The differences in these classifications are detailed in Table 1-1 (Paxinos and Franklin, 2004).

The $BNST^{ALG}$ has been implicated in a number of anxiety related responses (Lee *et al.*, 2008; Hammack *et al.*, 2009; Davis *et al.*, 2010; Somerville *et al.*, 2010; Conrad *et al.*, 2011*a*; Conrad & Winder, 2011; Yassa *et al.*, 2012; Daniel & Rainnie, 2015; Daniel *et al.*, 2017), which I will be elaborating on in section 1.1.5, I will focus on this classification in my thesis. In the Dong and Swanson classification (2004) the $BNST^{ALG}$ is comprised of the rhomboid ($BNST^{R}$), oval ($BNST^{OV}$), juxtacapsular ($BNST^{JC}$) , fusiform nuclei ($BNST^{FU}$) and an undefined area ($BNST^{AL}$) surrounding them referred to as the anterolateral area; although these classifications are based in the rat, similar classifications exist within the mouse (Dong *et al.*, 2000; Paxinos &

Franklin, 2004*b*; Daniel *et al.*, 2017). Figure 1-2 shows the dorsal region of the anterolateral BNST in the mouse and rat, this is the classification used in Daniel et al., 2017 where they examined the electrophysiological properties of BNST neurons in the mouse and the rat. Below is the same slice with the subregions denoted from the Paxinos and Franklin mouse atlas (Figure 1-2).

These different subregions are populated by distinct cell types. For example corticotrophin-releasing factor (CRF) positive cells in the BNST are located within the $BNST^{OV}$ while glutamatergic neurons are primarily located in the ventral BNST ($BNST^{V}$) (Daniel & Rainnie, 2016). In this study I have focused on the dorsal component of the anterolateral group of the BNST due to its role in stress processing and well defined electrophysiological characterisation as described below. The dorsal component of the $BNST^{ALG}$ is comprised of the oval nucleus, the juxtacapsular region and the undefined anterolateral area.

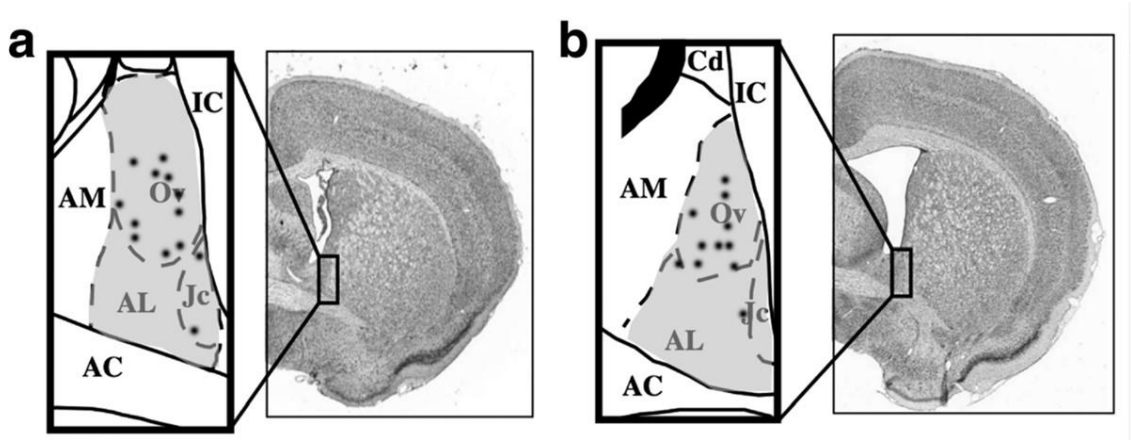

Figure 1-2 BNST subunits as depicted in Daniel et al., 2017*, this was adopted from the Dong et al 2007 classification, the dorsal anterolateral area of the BNST in the a) mouse, Bregma 0.14 mm and b) rat, Bregma -0.12 mm. Abbreviations; anterior commissure (AC), Juxtacapsular nucleus of the BNST (Jc), Oval nucleus of the BNST (Ov), undefined anterior lateral area of the BNST (AL), anterior medial division of the BNST (AM).*

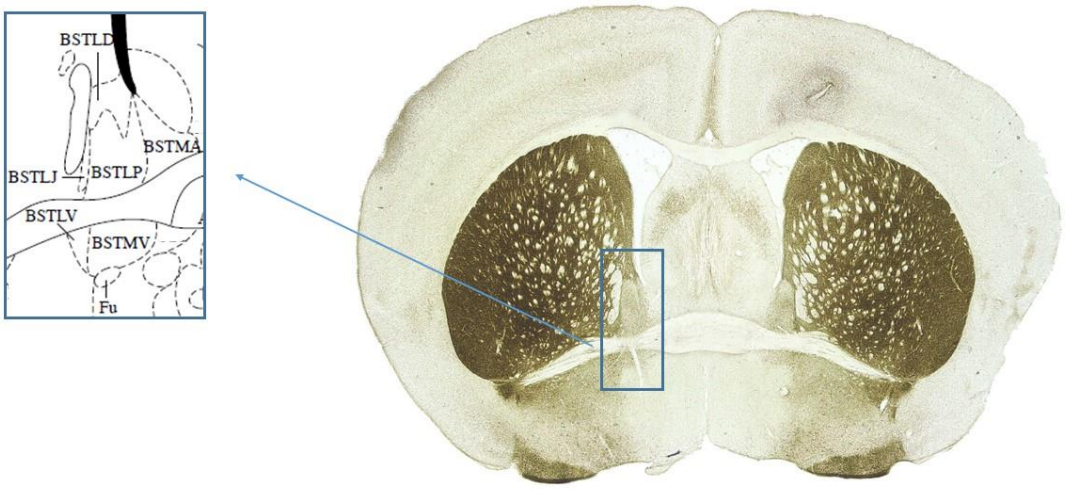

Figure 1-3 The anterolateral BNST as depicted in the Paxinos and Franklin mouse brain atlas, 2004*, Bregma 0.14 mm. abbreviations of the different subregions of the BNST: medial division ventral part (BSTMV),lateral division ventral part (BSTLV), medial division (BSTM), lateral division ventral part (BSTLV), lateral division posterior part (BSTLP), lateral division dorsal part (BSTLD), lateral division juxtacapsular part (BSTLJ).*

BNST region in paxino mouse atlas	Corresponding breakdown Ju and Swanson classification (1989)	
Lateral division (BSTL)	Anterolateral area ($BNST^{ALG}$)	Anterior division
Lateral division, dorsal part (BSTLD)		
Lateral division, juxtacapsular part (BSTLJ)		
Lateral division, posterior part (BSTLP)		
Lateral division, ventral part (BSTLV)		
Medial division, ventral part (BSTMV)	Medial group	
Medial division, posterolateral part (BSTMPL)	Posterior division	
Medial division, posteromedial part (BSTMPM)		
Supracapsular part (BSTS)		

Table 1-1 Subregions of the BNST adapted from Dong et al 2001

1.1.3. Connectivity of the anterolateral BNST with other brain regions

The $BNST^{ALG}$ has extensive connections with the amygdala, hypothalamus and midbrain regions. These brain regions are associated with pain, emotional processing, reward and autonomic function (Daniel & Rainnie, 2016). The BNST also displays a complex anatomical circuitry. Both the internal circuitry and the external efferent and afferent connections are subregion specific, briefly I will highlight the known connectivity of each of the dorsal $BNST^{ALG}$ nuclei.

The $BNST^{OV}$ has extensive connections both within the BNST and externally. Within the BNST, it densely projects to the $BNST^{FU}$, the caudal anterolateral area, $BNST^{R}$,

the subcommissural zone and the anterodorsal area. The $BNST^{OV}$ also projects to a number of areas outside of the BNST, including the dense afferents to the central amygdala (CeA), moderate input to nucleus accumbens (NA) and the periaqueductal gray (PAG) and sparse projections to the PVN (Dong *et al.*, 2001*c*) (Figure 1-6).

Similar to the $BNST^{OV}$, the $BNST^{AL}$ area projects both within the BNST and to a number of key nuclei outside of the BNST. Within the BNST it densely projects to the rhomdoid nucleus, the $BNST^{FU}$, the anteroventral nucleus and the anterodorsal area, it also has weaker connection to the $BNST^{JU}$ and the $BNST^{OV}$. Outside of the BNST it projects to several key brain areas associated with stress processing and reward including the CeA, the PVN, the NA and the VTA. The $BNST^{AL}$ also has reciprocal dorsal raphe (DR) connections (Dong & Swanson, 2004*b*) (Figure 1-4).

The $BNST^{JU}$ innervates the caudal anterolateral area of the BNST along with a number of regions outside of the BNST including the infralimbic (IL) and prelimbic (PL) cortical areas and the CA1 region of the hippocampus and the parasubthalamic and subthalamic nuclei of the hypothalamus (Dong *et al.*, 2001*c*) (Figure 1-5).

Afferent projections into the BNST also exhibit a subregion specificity. Thus, afferents from the IL cortex innervate the $BNST^{JU}$, $BNST^{OV}$ and $BNST^{AL}$. The PL cortex sends moderate connections to the $BNST^{AL}$. The ventral subiculum (VS) of the hippocampus has light connections to the $BNST^{AL}$ (McDonald *et al.*, 1999). The CeA projects to the $BNST^{OV}$ and the $BNST^{AL}$. The strongest connections to both the $BNST^{OV}$ and the $BNST^{AL}$ originate from the amydalopiriform transitional area (APir) (McDonald *et al.*, 1999). The APir is a region in the temporal lobe involved in olfactory processing (Jolkkonen *et al.*, 2001) (Figure 1-4, Figure 1-5, Figure 1-6).

Recent brain imaging-based analysis of BNST connectivity in humans indicates a very similar connectivity to that described in rodents, indicating that functional studies in rodents are likely to reflect largely human neural physiology (Lebow & Chen, 2016).

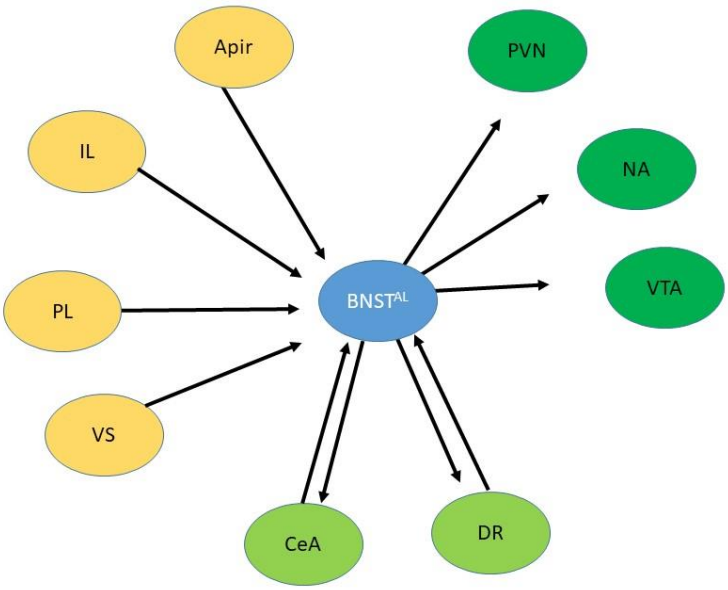

Figure 1-4 Connectivity of the BNST^{AL} to key brain regions outside of the BNST. Dark green locations represent afferent projections, yellow shapes represent efferent projections and the light green represent reciprocal connections. Abbreviations; amydalopiriform transitional area (Apir), infralimbic cortex (IL), Prelimbic cortex (PL), ventral subiculum (VS), central amygdala (CeA), dorsal raphe (DR), ventral tegmental area (VTA), nucleus accumbens (NA), paraventricular nucleus (PVN).

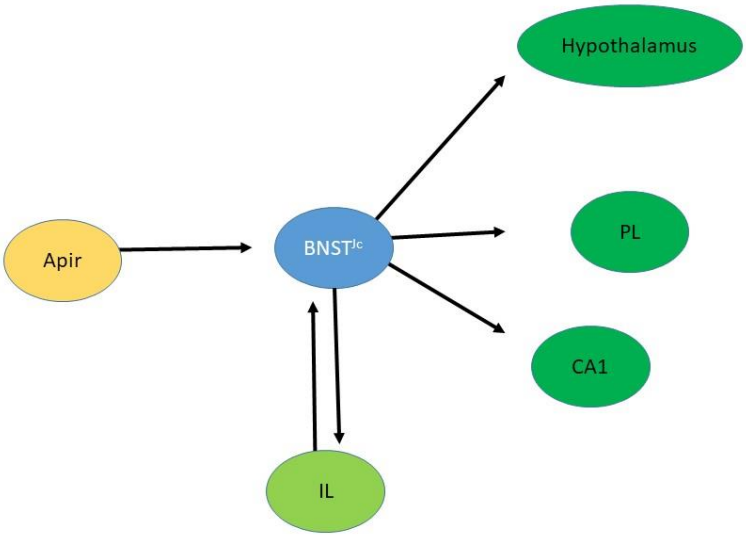

Figure 1-5 Connectivity of the BNST^{Jc} to key brain regions outside of the BNST. Dark green locations represent afferent projections, yellow shapes represent efferent projections and the light green represent reciprocal connections. Abbreviations; amydalopiriform transitional area (Apir), infralimbic cortex (IL), Prelimbic cortex (PL), the CA1 region of the hippocampus (CA1).

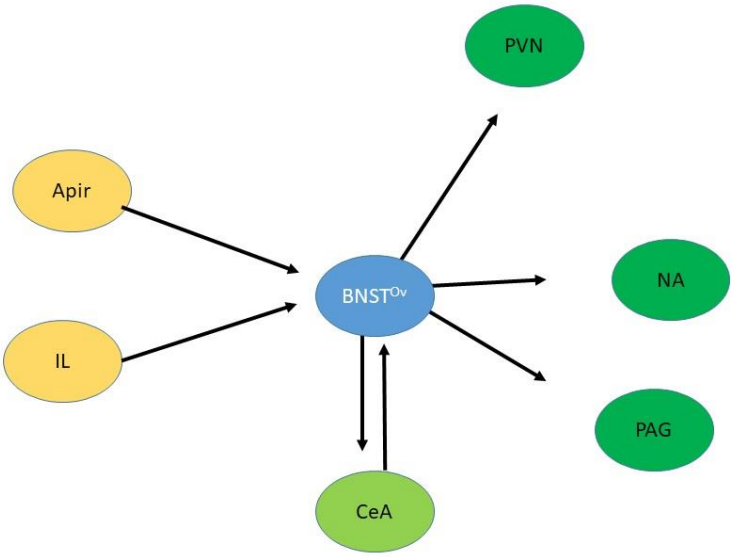

Figure 1-6 Connectivity of the BNST^{Ov} to key brain regions outside of the BNST. Dark green locations represent afferent projections, yellow shapes represent efferent projections and the light green represent reciprocal connections. Abbreviations; amydalopiriform transitional area (Apir), infralimbic cortex (IL), central amygdala (CeA), nucleus accumbens (NA), paraventricular nucleus (PVN), periaqueductal gray (PAG).

1.1.4. Electrophysiological characterisation of neurons located in the anterolateral area of the BNST

The original classification of neurons in the BNST^{ALG} of the rat identified 3 distinct population of neurons which can be characterised based on their electrophysiological properties (Hammack *et al.*, 2007*a*). Type I cells sometimes called regular spiking cells, exhibit sag in response to hyperpolarising current injections and are regular spiking in response to depolarising current injection. Type II cells also display a degree of sag in response to a hyperpolarising pulse but they also exhibit a nonlinear response to depolarising stimuli referred to as a 'hump', thought to be driven by T-type calcium channels. Type III cells display no sag in response to hyperpolarising current injection. Another key characteristic of these cells is the presence of inwardly rectifying K^+ channel (Hammack *et al.*, 2007*a*).

These neuronal classification described above were based on 24-48 day old male Sprague-Dawley rats. In 2017 Daniel et al expanded this classification to include the

C57BL/6 male mice and *Macaca mulatta* monkeys. Similar populations of cells were observed across the three species, however ~ 7% of the cells recorded in the mouse did not match the criteria for the three populations previously described. Of the cells which did not fit the Hammock classification 4/6 of these cells were regular spiking but displayed no sag in response to hyperpolarising current injections. the other 2 cells had an inward rectifying current indicating Type III but also had sag which would indicate Type I or Type II, this prevented them from fitting into any of the classifications. This would indicate that while the populations are similar there are potentially some discrepancies in their use in species other than rat (Daniel *et al.*, 2017).

A review by Daniel et al 2016 has hypothesised the role that each of these cell types play in downstream physiological effects; CRF-expressing cells are primarily located in the $BNST^{OV}$ and the $BNST^{FU}$, their physiological properties of these CRF-expressing cells correlate with type III neurons, since 95 % of type III neurons express CRF mRNA (Dabrowska *et al.*, 2013). As selective activation of CRF-expressing cells in the $BNST^{OV}$ leads to increased anxiety behaviours (Sahuque *et al.*, 2006) this population is believed to represents an ‘anxiety on’ switch. In an unpublished observation from the Rainnie lab (Daniel & Rainnie, 2015) they found that only type II neurons express mRNA for protein kinase c - δ (PKC-δ). In the CeA the PKC-δ^{+} neurons represent an ‘anxiety off’ switch through reciprocal inhibition of CRF-positive cells. A number of similarities exist between the BNST and the amygdala, the BNST is sometimes referred to as the extended amygdala (McDonald *et al.*, 1999; Dong *et al.*, 2001*b*; Janitzky *et al.*, 2014; Pleil *et al.*, 2015). Given the similarities between the amygdala and the BNST this would translate to a situation in which type III neurons represent “anxiety on” and type II neurons represent “anxiety off” switch. The role of Type I neurons is less clear; while the Daniel et al 2016 review have proposed that type I neurons exhibit an ‘anxiety off’ switch the reasoning behind this is unclear (Daniel & Rainnie, 2016).

1.1.5. The role of the BNST in stress processing

As indicated earlier, the BNST can elicit both anxiolytic and anxiogenic responses, mediated by a number of key modulators including CRF and serotonin. Injection of CRF into the ventricle enhances the startle response in rodents (Swerdlow *et al.*, 1986), but this effect can be blocked via lesions to the lateral BNST or microinjection of a CRF antagonist into the $BNST^{ALG}$ (Lee & Davis, 1997). A number of other anxiety related behaviours can be enhanced via micro infusion of CRF directly into the BNST, such as decreased time in the open arm on the elevated plus maze. The elevated plus maze is commonly used test for anxiety; a decrease in the proportion of time spent in the open component of the maze vs the walled area is an indicator of heightened anxiety. The micro infusion of CRF into the BNST also causes a reinstatement of drug seeking behaviour (Erb & Stewart, 1999; Liang *et al.*, 2001). Chemogenetic inhibition of CRF neurons in the BNST leads to decreases in anxiety like behaviour (Pleil *et al.*, 2015). The $BNST^{OV}$ contains a population of CRF neurons, within this population, CRF mRNA increases in response to stress (Makino *et al.*, 1994; Funk *et al.*, 2006) indicating a key role of this region in stress processing.

There are 2 CRF receptors, type 1 (CRFR1) and the type 2 (CRFR2) CRF receptors, they are plasma membrane G-protein coupled receptors (Liapakis *et al.*, 2011). CRFR1 predominantly acts through the Gsα pathway; this pathway leads to a cascade of events beginning with the activation of adenylyl cyclase causing the formation of cyclic AMP which phosphorylates protein kinase A (PKA) (Jedema & Grace, 2004). PKA mediated signalling has been implicated in in upregulation of BDNF in cerebral cultures (Bayatti *et al.*, 2005), inactivation of potassium channels in locus ceruleus neurons (Jedema & Grace, 2004) and activation of serine threonine kinase (SGK-1) in primary hippocampal cultures (Sheng *et al.*, 2008); SGK-1 is involved in the mediation of synaptic plasticity and cell survival. Another CRFR1 pathway activated via cyclic AMP involves extra-cellular signal-regulated kinase-mitogen-activated protein kinase (ERK-MAPK) which can regulate BDNF signalling in cultured neurons from the LC (Jedema & Grace, 2004). To my knowledge no one has examined the signalling cascades of CRFR1 in the BNST.

While CRFR1 is expressed solely in the CNS, CRFR2 is expressed both in the CNS and peripheral tissue. The CRFR2 differs from the CRFR1 in its endogenous ligands. It has a lower affinity for CFR in comparison to CRFR1 but unlike CRFR1 it has a high affinity for urocortin (Ucn), specifically Ucn2 and Ucn3. Urocortins play a key role in stress responses, cardiovascular responses and metabolism (Pal *et al.*, 2010). CRFR2 also mediates its downstream effects via adenyl cyclase and the formation of cAMP (Lewis *et al.*, 2001).

Within the $BNST^{ALG}$, CRF acts presynaptically to enhance glutamatergic transmission and increases the frequency of spontaneous excitatory post synaptic potential (sEPSCs) in a CRF receptor (CRFR1) dependent manner (Kash *et al.*, 2008). This would indicate that glutamatergic input into the BNST is modulated in a stress dependent manner by a CRF population; however it is currently unknown which glutamatergic inputs are being modulated. This could be addressed using optogenetic targeting of the different afferent projections; however to my knowledge this has not been carried out. The BNST also receives CRF afferents from the amygdala (Sakanaka *et al.*, 1986; Day *et al.*, 1999) so it is difficult to attribute these actions solely to the CRF population within the BNST.

Within the BNST, CRF neurons send inhibitory afferents to the $BNST^{AL}$. The $BNST^{ALG}$ is predominantly GABAergic therefore inhibition of it may lead to decreased inhibition in other key circuits in the stress pathway (Turesson *et al.*, 2013). BNST CRF-expressing neurons also innervate a number of nuclei outside of the BNST including the DR, PVN, VTA, PAG and LC (Dabrowska *et al.*, 2016). These circuits play a key role in stress modulation therefore it is highly probable that the anxiogenic effects of CRF are being mediated within a combination of these regions (Daniel & Rainnie, 2016). More specific targeting would be required to address the downstream effects of the CRF population within the BNST.

Another key neurotransmitter system involved in the modulation of stress in the BNST is that of serotonin. Serotonin (or 5-hydroxytryptamine (5-HT)) is a monoamine neurotransmitter; there are seven families of 5-HT receptors in the CNS (Liapakis *et al.*, 2011). One of the most commonly used classes of drugs for the treatment of both anxiety related disorders and depression are selective serotonin reuptake inhibitors (SSRIs) (Stokes & Holtz, n.d.; Kent *et al.*, 1998). SSRIs do not act

directly on 5-HT receptors, rather they increase the amount of serotonin in the synaptic cleft by limiting its reabsorption into the presynaptic cell. This is mediated via inhibition of the serotonin transporter. There are a number of clinically available SSRIs, these include Fluoxetine, Fluvoxamine, Paroxetine, Ciitalopram and Sertraline (Rang *et al.*, 2007).

In the BNST availability of serotonin transporter (5-HTT) positively correlates with anxiety-like behaviour in monkeys (Oler *et al.*, 2009). The $BNST^{ALG}$ receives dense inputs from serotonergic dorsal raphe cells, which can act in an anxiolytic or anxiogenic manner depending upon the receptor which it innervates. Presynaptically, activation of $5\text{-}HT_{1B}$ receptors causes increases in glutamatergic transmission in the $BNST^{ALG}$ (Guo & Rainnie, 2010). While the effects of specific activation of the $5\text{-}HT_{1B}$ receptor within the BNST are unknown, activation of this receptor in the wider CNS leads to increased aggression and impulsivity (Saudou *et al.*, 1994; Nautiyal *et al.*, 2015). Postsynaptically, $5\text{-}HT_{1A}$ hyperpolarises cells, producing an anxiolytic effect (Levita *et al.*, 2004). When activated $5\text{-}HT_{2c}$ depolarises cells in the BNST, contributing to an anxiogenic state, albeit this study found these changes in the ventral part of the BNST (Marcinkiewcz *et al.*, 2015). From this we can see that the serotonergic circuitry has opposing action on BNST populations.

Serotoninergic cells within the DR are subject to modulation by CRF in a dose dependent manner; at low doses CRF is inhibitory acting primarily via CRFR1 due to its higher affinity for this receptor, at higher doses CRF becomes excitatory most likely through its actions on CRFR2 (Kirby *et al.*, 2000; Amat *et al.*, 2004; Hale *et al.*, 2010). As CRF neurons innervate the BNST, stress related changes in CRF expression may lead to increased activation of DR serotonergic neurons. The primary action of serotonergic inputs into the BNST is inhibitory (Daniel & Rainnie, 2016). A negative feedback loop has been hypothesised by Hammack et al 2009, in which stress induced CRF release from $BNST^{ALG}$ neurons leads to activation of DR serotonergic neurons. These DR neurons innervates the CRF-expressing neurons within the $BNST^{ALG}$ where they block stress induced CRF release. (Hammack *et al.*, 2009).

Due to the central role of the BNST in stress and anxiety it has been implicated in a number of different anxiety-related disorders including general anxiety disorder

(GAD)(Pigott, 2003; Conrad *et al.*, 2011*b*, 2011*c*; Yassa *et al.*, 2012), drug addiction (specifically stress-induced relapse)(Shaham *et al.*, 2003; Dumont *et al.*, 2005; Li *et al.*, 2012; Jennings *et al.*, 2013) and post-traumatic stress disorder (PTSD) (Hammack *et al.*, 2012; Lebow *et al.*, 2012; Janitzky *et al.*, 2015; Rodriguez-Sierra *et al.*, 2016).

1.1.5.1. The role of the BNST in PTSD

PTSD is a debilitating psychiatric disorder characterised by flashbacks, increased activity of HPA axis, increases in arousal and difficulty sleeping. PTSD sufferers often live in a hypervigilant sustained fear state (Bremner *et al.*, 1997*a*; Admon *et al.*, 2009; Somerville *et al.*, 2010; Brinkmann *et al.*, 2017).

While this sustained fear state alone would indicate the involvement of the BNST, a number of other aspects of PTSD involve processes mediated by the BNST (McElligott & Winder, 2008; Lebow *et al.*, 2012). A commonly used, albeit debated, marker of PTSD is increased cortisol levels; HPA regulation is mediated by the BNST as discussed in the previous section (Klaassens *et al.*, 2012; Zaba *et al.*, 2015). One of the most commonly used treatments for PTSD include SSRIs which mediate a number of their actions via the serotonergic system in the BNST which was discussed earlier (Schneier *et al.*, 2015; MacNamara *et al.*, 2016).

The CRF circuit within the BNST has been implicated in aspects of PTSD-like behaviours in rodents; activation of the CRF circuit in the posterior area of the BNST either by optogenetic stimulation (Henckens *et al.*, 2016) or overexpression of CRFR2 decreased anxiety. Furthermore optogenetic activation of CRFR2 neurons in the posterior BNST following trauma reduces susceptibility to PTSD-like behaviour.

Human studies have also produced similar findings, linking the CRF system within the BNST with PTSD. In human patients, heightened levels of CRF have been found in the cerebrospinal fluids of veteran's suffering from PTSD (Bremner *et al.*, 1997*b*; Baker *et al.*, 1999). Human imaging studies have also found an increase in activation of the BNST in female PTSD patients in anticipation of aversive stimuli (Brinkmann *et al.*, 2017), with these patients also displaying increased anxiety in anticipation of the aversive stimuli of a human scream.

While the BNST plays a role in PTSD it is worth noting that this is not isolated from other key regions such as the amygdala; Admon et al., (2009) found that increased activity in the amygdala increased ones susceptibility to PTSD. When an individual is faced with a real threat, both the BNST and the amygdala are involved in the fear response: exposure to an actual tarantula elicited responses in both brain regions (Mobbs et al., 2010). Also Münsterkötter et al., 2015 found enhanced functional connectivity between the amygdala and the BNST in individuals with spider phobias when looking at pictures of spiders.

1.1.5.2. Integration of social cues and stressful stimuli

The BNST displays connectivity to key regions associated with social interaction, such as the vomersonsal cavity, VTA, medial amygdala (MeA) and the hypothalamus including the ventromedial hypothalamus, preoptic area and anterior hypothalamus (Dong *et al.*, 2001*c*). These circuits play a key role in behaviour and mood; the central role of the BNST allows it to dictate a positive or negative response to various inputs thereby contributing to social regulation. It is involved in parental attachment, mating behaviours and aggression (Lebow & Chen, 2016). While these behaviours are driven more by the medial and posterior parts of the BNST there is a complex internal network which links these systems to the anterolateral area (McDonald *et al.*, 1999; Dong *et al.*, 2001*b*).

This social regulation can play a key role in fear processing; negative social interaction can induce anxiety in both rodents and humans, evidenced by the fact that a commonly used PTSD model is that of a larger intruder (Hammack *et al.*, 2012; Hammels *et al.*, 2015; Huang *et al.*, 2016). The opposing circuits discussed above in relation to responses to stress observed of the BNST (Daniel & Rainnie, 2016) may play a key role in recognising social interactions from threats allowing for appropriate responses. While this theory is a compelling one, the breakdown of these key social interactions via manipulation of various BNST circuitry has yet to be explored.

1.2. Intrinsic properties of neurons

The central nervous system (CNS) encompasses the brain and spinal cord, it is composed primarily of two distinct population of cells, neurons and glial cells. Glial cells are comprised of three major populations; oligodendrocytes, astrocytes and microglia.

The main role of oligodendrocytes is to create a myelin sheath for axons in the CNS; this is similar to the function to the role of Schwann cells in the peripheral nervous system, these sheath play a key role in electrical propagation along the axis (Simons & Nave, 2016). Astrocytes are the most abundant cell type in the central nervous system (CNS) and constitute almost 20-40% of the total brain cell population(Khakh & Sofroniew, 2015).These star-like glial cells participate in many fundamental biological processes such as maintenance of ion homeostasis, neurovascular coupling, gliotransmitter release, modulating synaptic activity, metabolic support of neurons and immune responses(Suzuki *et al.*, 2011; Panatier *et al.*, 2011; Ransom & Ransom, 2012). During normal healthy conditions astrocytes are in a resting state(Sofroniew, 2009; Gallo & Deneen, 2014; Lee & MacLean, 2015). However, once activated, they undergo morphological changes, becoming more proliferative and begin releasing pro-inflammatory cytokines and growth factors, as well as nitric oxide (Zhao *et al.*, 2011; Batarseh *et al.*, 2016).

While astrocytes are involved in immune responses the primary glial cell involved in immunity and inflammation in the brain are microglia. Microglia have a well characterised phagocytic function as well as playing a key role in both adaptive immune responses and non-specific inflammation. Microglia are capable of detecting dysfunction both within and outside of cells, CNS stimulus of microglia leads to an “activation” or maturation of the microglia. Following maturation these cells they increase expression of a number of pro-inflammatory cytokines and activation of immune genes such as mannose receptors and CD14 (Aloisi, 2001). Microglial function is not limited to immunity it also plays a role in synaptic pruning; this process is necessary for both development (Paolicelli *et al.*, 2011) and synaptic plasticity (Clark *et al.*, 2015).

Dysfunction within glial populations have also been implicated in a number of disease states including depression, schizophrenia and Alzheimer’s disease. While

glial cells play a vital role in a healthy functioning brain this thesis will focus on neurons; however more information on glial populations and their role in neuronal function can be found in these reviews (Smiałowska *et al.*, 2013; Takahashi & Sakurai, 2013; Öngür *et al.*, 2014; Goldman *et al.*, 2015).

Neurons are electrically active cells which transmit information through electrical and chemical means. They are comprised of four key compartments; the cell body, the axon, the dendrites and the presynaptic terminal (Kandel *et al.*, 2000). Neurons can conduct electrical currents across large distances, this is mediated via the movement of ions across the cell membrane. Here I will go into detail on mechanisms involved in electrical conductances of neurons including both active and passive membrane properties.

1.2.1. Resting membrane potential

The resting membrane potential of neurons arises from differences in the electrical charges on either side of the cell membrane. The concentration of certain ionic species in the inside and the outside of the cell differs. This difference in the concentration provides the foundation for the resting membrane potential. The electrical charge outside of the cell is arbitrarily defined at zero and so any charges within the membrane are subtracted leading to a determination of the membrane potential,

$V_m = V_{in} - V_{out}$

In a neuron there are 4 main ions which drive this electrical gradient these are Na^+, Cl^-, K^+ and organic anions (A^-). Na^+ and Cl^- have higher concentrations outside the cell while K^+ and A^- are in higher concentrations inside the cell (Table 1-2).

Leak ion channels play a key role in maintaining the resting membrane potentials of cells. In nerve cells nongated channels can be selective for a number of different ions. In these channels the passage of ions is driven by passive diffusion; two key parameters play a role in this 1) the concentration gradient of the ion and 2) the electrical gradient which is affected by the charge of the ion. For example K^+ ions will flow through leak channels when a cell is at its resting membrane potential. The concentration gradient of K^+ will drive the ions out of the cell through these pores,

however this ion has a positive charge and as the charge outside the cell begins to become more positive it will drive the ion back into the cell. This balance between the two parameters is referred to as the equilibrium potential for any given ion. The Nernst equation, stated below, can be used to calculate the equilibrium potential of an ion (Kandel *et al.*, 2000).

The Nernst equation:

$$E_x = \frac{RT}{zF} \ln \frac{[X]_o}{[X]_i}$$

Where R is the gas constant, T is temperature measured in Kelvin, Z is the valence of the ion, F is the Faraday constant, $[X]_o$ is the concentration of the ion outside the cell and $[X]_I$ is the concentration inside the cell.

In a stereotypical neuron the equilibrium potential of each of these ions are listed below along with their intracellular and extracellular concentrations (Wright, 2004).

Ion	Intracellular concentration (mM)	Extracellular concentration (mM)	Equilibrium potential (mV)
Cl^-	4	116	-88
Na^+	12	140	+64
K^+	135	4	-92

Table 1-2 Concentration of ions in a typical neuron

Leak channels allow the passive diffusion of Na^+, K^+ and Cl^- across the membrane. In the case of Na^+ and K^+ their electrical charge means that their actions cancel out the electrical gradient change, however, should this process continue uninterrupted the concentration gradients of the ions would run down and reduce the resting membrane potential of the cell. In order to correct this change in concertation gradient the Na^+-K^+ pump moves these ion against their net electrochemical gradients; this requires energy which is provided in the form of ATP. The Na^+-K^+ pump is a transmembrane protein which has binding site for Na^+ and ATP intracellularly and a K^+ binding site extracellularly. The pump hydrolyses a single molecule of ATP providing it with sufficient energy to expel 3 Na^+ ion and transport 2

K^+. This discrepancy in electrical gradient is offset by the electrogenic nature of the pump itself (Kandel *et al.*, 2000).

In the case of the Cl^- ion there are two possibilities, in some cells the passive diffusion is corrected via a Cl^- pump. As the equilibrium potential of Cl^- in neurons generally leads to an inward flow of the ion the Cl^- pump is responsible for expelling excess Cl^- from the cell. Some populations of neurons do not have these Cl^- pumps and so in these cells passive diffusion across the membrane determines the resting membrane potential ie. the resting membrane potential will be equal to E_{Cl}.

Cl^-, Na^+, and K^+ are the main ions which flow across the membrane when the cell is at rest. A modified version of the Nernst equation referred to as the Goldman-Hodgkin-Katz equation has been derived to calculate the resting membrane potential based on the movement of these ions.

The Goldman-Hodgkin-Katz equation:

$$V_m = \frac{RT}{F} \ln \frac{P_K[K^+]_o + P_{Na}[Na^+]_o + P_{Cl}[Cl^-]_i}{P_K[K^+]_i + P_{Na}[Na^+]_i + P_{Cl}[Cl^-]_o}$$

V_m is the membrane potential of the cell and P is the relative permeability of the different ions

Current flow is defined as the direction of net movement of positive charge; this rule defines the way in which we describe net changes in electrical charge across the membrane. An influx of positive ions into the cell or an efflux of negative ions out of the cell, causes a net positive charge inside the cell, this is referred to as a depolarisation of the membrane potential. The opposite is true of hyperpolarisation of the membrane, where a net negative change inside the cell leads to hyperpolarisation of the cell.

1.2.2. Ion channels

The membrane of cells is comprised of a lipid bilayer; due to the hydrophobic environment of the lipid bilayer charged ions are more likely to favour the hydrophilic environment that exists both within and outside of cells. Electrical signalling requires the rapid movement of ions across the membrane, as ions are unlikely to pass through this lipid membrane a number of pores exist within it to allow the transport of ions. These pores are comprised of proteins which can allow selective transport of different ions. Ion channels allow the passive transport of ions across the membrane meaning that large quantities of ions can move across the membrane without expending any metabolic energy (Kandel *et al.*, 2000).

Two forms of ion channels exist gated and non-gated. Gated channels can be further subdivided into voltage-gated, ligand-gated, light-gated, mechanically-gated and temperature-gated. Ligand gated channels open in response to activation by an agonist. Light gated ion channels change their conformation in repose to specific wavelengths of light, Channelrhodopsins are a naturally occurring example of this. These receptors now widely used as a tool in neuroscience to allow the activation and inactivation of specific populations in response to specific wavelengths of light and have been invaluable in enhancing our understanding of neuronal circuits (Boyden *et al.*, 2005; Zhang *et al.*, 2006; Han & Boyden, 2007; Boyden, 2015).

Voltage gated channels open in response to changes in the membrane potential; the opening and closing of ion channels involves conformational changes in the protein. When Hodgkin and Huxley examined the electrophysiological properties of the giant squid axon they found voltage gated Na^+ and K^+ channels (Hodgkin &Huxley, 1952). These ion channels have since been found in neuronal populations throughout the brain, since these experiments voltage gated Ca^{2+} channels and voltage gated Cl^- have also been identified.

Voltage gated Na^{2+} channels can be classified into two families. In the first family there are nine subtypes have been identified, each type has specific expression patterns. In the CNS $Na_v1.1$, $Na_v1.2$, $Na_v1.3$, $Na_v1.6$ are expressed, $Na_v1.6$, $Na_v1.7$, $Na_v1.8$ and $Na_v1.9$ are expressed in the peripheral nervous system (PNS), $Na_v1.6$ is expressed in skeletal muscles and $Na_v1.6$ is expressed in cardiac muscles. In mammals, voltage gated sodium channels consist of the pore-forming α subunit and

one or two β subunits (de Lera Ruiz & Kraus, 2015). The second family, Na_V2, is expressed in the heart, lung and Schwann cells. Its expression is restricted in the CNS and has been hypothesised to play a role in regulation of salt and water intake (Watanabe *et al.*, 2000).

There are twelve families of voltage gated K channels (Kv): Kv1 to Kv12. Kv are key regulators of excitability and the largest family of K^+ channels. Their role in neuronal excitability is distinct to each family; Kv1, Kv4 and Kv7 are low-voltage activated channels and regulate threshold potential. Kv2 is a high-voltage activated slowly inactivating channel, which is involved in modulating firing during high frequency firing periods. Kv channels are also involved in regulating a number of neurological processes, including apoptosis, which has made it a potential target in a number of neurological disease (Shah & Aizenman, 2014).

Another key example of voltage gated ion channels is the hyperpolarisation-activated cyclic nucleotide-gated (HCN) channels. In response to hyperpolarising stimuli, membranes often do not charge in a linear manner, one aspect of this is the presence of a ‘sag’ in response to hyperpolarising current injections. This is response is driven by voltage gated HCN channels which lead to an excitatory current in neurons referred to as I_h in response to hyperpolarising stimuli. These channels are involved in regulating the presynaptic release of neurotransmitters, dendritic excitability and initiation of rhythmic firing (He *et al.*, 2014).

The role of HCN channels in neuronal excitability is cell type for specific, for example in hippocampal pyramidal cells HCN channels are located on distal dyndrites where they play more of a role in functional connectivity (Lörincz *et al.*, 2002). I_h currents also impact input resistance, HCN channels which are open at rest depolarise the membrane pushing cells closer to their threshold potential thus increasing their excitability (He *et al.*, 2014). This diverse functions allows these channels to act as regulators of neuronal function at both the dendritic and soma level.

1.1.1. Passive membrane properties

The passive electrical properties of neurons play a key role in regulating excitability and determining responses to synaptic inputs, these will be discussed in detail below. Here I will discuss how input resistance, capacitance and the membrane time constant can influence the behaviour of a cell.

The input resistance of a cell is mediated by the resistance of the membrane, this is a reflection of the leak channels discussed above. As the membrane itself functions as a resistor, we can use Ohm's law to determine the level of resistance. It is measured as the amount that the membrane deflects in response to a steady state current injection.

Ohm's law:

$$V = IR$$

Where I is current, V is voltage change and R is resistance (Ω).

As we are interested in the resistance of the cell we can rearrange the equation to

Ohm's law

$$R = \frac{V}{I}$$

The resistance of the membrane can have a large impact on spike generation in cells; larger input resistances will cause a larger deflection from baseline voltage in response to changes in current. In this manner synaptic events will generate a larger response in a cell with a higher input resistance increasing the likelihood of that cell reaching action potential threshold and generating an action potential.

If a membrane functioned as a true resistor, then a step change in current would lead to an immediate step change in voltage, however there is a delay in the voltage deflection observed. This delay in the voltage deflection is due to the fact that neuronal membranes function not only as a resistor, but also as a capacitor. The charging of the membrane is exponential in nature, in order to quantify this curve the membrane time constant is examined.

The time constant is

$$1 - \frac{1}{e}$$

This equates to ~63.2% of the final peak value reached. The membrane time constant can play a significant role in action potential generation, due to the fast nature of synaptic events slower time constants can prevent the cell from reaching threshold in this short period.

A capacitor stores electrical charge in a manner proportional to the size of the membrane. Due to this a higher capacitance of a cell would indicate a larger membrane area and therefore a larger cell. A second variable can affect capacitance which is the size of the insulator; in the case of neurons the lipid bilayer is assumed to be constant at 4 nm this means the capacitance of the membrane can be calculated, in neuronal cells this is ~ 1µF/cm^2 of membrane. The capacitance of the membrane is directly related to the input resistance and the membrane time constant of a cell. This allows the capacitance to be calculated based on these other parameters as described below:

$$C = \frac{Tau}{R}$$

Where C is the capacitance, R is the resistance and Tau is the membrane time constant.

1.2.3. Action potentials

Large depolarising changes in the membrane potential such as those caused by excitatory synaptic events can lead to an action potential. Before a neuron can generate an action potential it must reach threshold potential; threshold is a membrane potential which the cell must reach to initiate the all or nothing action potential. Should one of these inputs reach threshold a number of voltage activated Na^+ channels will open. Once this happens, the influx of Na^+ into of the cell becomes larger than the K^+ efflux and leads to depolarisation of the cell. This causes more voltage gated Na^+ channels to open leading to an even greater influx of Na^+ ions.

This process causes the rising phase of an action potential. The Na^+ equilibrium potential in neurons is approximately +64 mV, however even on the rising phase of an action potential K^+ is flowing preventing the cell from reaching this membrane potential. The downward phase of an action potential is driven by two forces, the inactivation of the Na^+ channels and the delayed opening of voltage gated K^+ channels. A final aspect of the action potential is the after-spike potential; there are two main after-spike potentials which can be either hyperpolarising ie. an afterhyperpolarization potential (AHP) or depolarising ie. an afterdepolarization potential (ADP) (Kandel *et al.*, 2000).

The action potential is propagated along the axon in the same manner in which it was generated. Voltage gated Na^+ channels open along the axon followed by the delayed opening of the K^+ channels allowing the current to flow along the axon. In some neuronal populations, such as those in the spinal cord the axons are surrounded by insulating glial cells which increase the efficiency of this propagation (Kandel *et al.*, 2000).

While the basic properties of action potential generation are generally the same for all CNS neurons the variety and differences in expression levels of the ion channels can vary greatly from cell to cell. This can have a large impact on the action potential of a given cell affecting a number of properties such as changes in threshold or action potential height and width. Changes in threshold will alter the required current needed to initiate an action potential. Changes the action potential width or peak height can have an impact on the release of neurotransmitters from the cell.

1.2.4. Synapses and synaptic transmission

Synaptic transmission is the mechanism by which nerve cells communicate. A synapse is comprised of a presynaptic terminal on the axon of a neuron which communicates with a postsynaptic terminal in the dendrite of another neuron.

The release of neurotransmitters is mediated by an influx of Ca^{2+} into the cell as the extracellular concentration of Ca^{2+} is higher than the intracellular concentration this influx is mediated by passive diffusion through voltage-gated Ca^{2+} channels. Voltage gated Ca^{2+} channels are conjugated at the neuromuscular junction, the high local

concentration of these voltage gated Ca^{2+} channels in the 'active zone' allows for a rapid localised increase in Ca^{2+}. The calcium sensors which are responsible for the release of the vesicle have a low binding affinity between 50-100 µM whereas most enzymatic reactions require only ~1 µM. The rapid influx allows high enough concentrations to be reached however due to passive diffusion these high concentrations are only maintained for ~1 ms; this mediated the speed of synaptic transmission. Neurotransmitters are stored in vesicles at the synaptic terminal, once neurotransmitter release is instigated, exocytosis of the contents of the vesicle takes place. This process is mediated by a protein complex involving soluble NSF-attachment protein receptor (SNARE) and Sec1/Munc 18-like (SM) protein which mediate the formation of a fusion pore. The formation of a fusion pore which expels the neurotransmitter into the synaptic cleft (Kandel *et al.*, 2000).

Most neurotransmitter release is mediated via depolarisation of the cell; tetrodotoxin, a compound which blocks Na^{+} channels inhibits action potential generation preventing calcium induced binding of the SNARE protein thereby preventing neurotransmitter release. Miniature IPSCs can be observed in the presence of TTX; these reflect spontaneous neurotransmitter release (Ropert *et al.*, 1990).

These neurotransmitters then act on receptors on the post synaptic terminal. There are two broad classes of receptors at synapses, ionotropic and metabolic receptors. Ionotropic receptors contain an ion channel which opens in response to agonist binding allowing movement of ions across the cell membrane thereby eliciting an electrical response. Actions at metabotropic receptors are mediated via a second messenger system inside the postsynaptic cell (Kandel *et al.*, 2000).

Neurotransmitters can be both excitatory and inhibitory; the two most abundant neurotransmitters in the mammalian brain are L-Glutamate and GABA. While glutamate is primarily considered to be excitatory and GABA is generally inhibitory, the effect of any given neurotransmitter is dependent on the type of receptor on the postsynaptic cell and the effect that receptor has on the properties of the cell.

Glutamate acts at 2 broad classes of receptors; these are ionotropic and metabotropic. The three main ionotropic receptors these are AMPA receptors, NMDA receptors and kainate receptors. These channels are ion permeable channels which allow the flow of Na^{+} and K^{+} and, in some cases, Ca^{2+}. Opening of these

channels leads to a depolarisation of the cell; for this reason glutamate is seen as the primary excitatory neurotransmitter in the brain. The second major class of Glutamate receptors are metabotropic glutamate receptors (mGluR) which are G-protein coupled receptors. mGluRs are involved in the modulation of cell excitability and synaptic transmission via second messengers (Niswender & Conn, 2010).

1.1.1.1. GABA

There are three main receptor classes at which GABA is functionally active; these are known as $GABA_A$, $GABA_B$ and $GABA_C$ receptors. Briefly the $GABA_B$ receptor is a metabotropic receptor, activation of which causes a second messenger cascade mediated by G protein. The downstream effect of $GABA_B$ receptor activation is dependent upon the associated G protein, the effects include the opening of a K^+ channel (Kandel *et al.*, 2000), stimulation of adenyl cyclase (A.R Knight, 1996; Olianas & Onali, 1999) or inhibition of Ca^{2+} channels (Bowery *et al.*, 2002; Bettler *et al.*, 2004).

$GABA_A$ and $GABA_C$ (Bormann & Feigenspan, 1995) receptors are anionic selective channels that are permeable to Cl^-. Increased permeability of Cl^- in most mature neurons leads to a reduction in neuronal excitability. In most mature neurons the external concentration of Cl^- is higher than the internal concentration of Cl^-, the opening of this channel leads to an influx of Cl^- and hyperpolarisation of the cell (Olsen & Sieghart, 2008).

There are 16 subunits which can combine in a variety of manners to form $GABA_A$ receptors, consisting of 6 α subunits, 4 β subunits and 4 γ subunits, a δ subunit, a ε subunit, a π subunit, a Θ subunit. There are also 3 ρ receptors, however these contribute to $GABA_C$ receptors. Each of these subunits have various splice variants, leading to a wide array of possible subunits (Olsen & Sieghart, 2008). $GABA_A$ receptors are made up of 5 subunits usually comprising 2 α subunits, 2 β subunits and 1 other subunit (Chang *et al.*, 1996); the expression of these subunits differs greatly throughout the brain (Lovick, 2006).This has a major impact on function of the receptors as subunit composition of these receptors affects the pharmacology of the receptor. The γ subunit is necessary for the synaptic location of the $GABA_A$ receptor, while those lacking this subunit will often contain the δ subunit and are extrasynaptic (Wei *et al.*, 2003).

Neurons will invariably receive a combination of synaptic inputs both from the neurotransmitters discussed here and the various other neurotransmitters in the brain which can be both excitatory and inhibitory in nature. A single excitatory synaptic input is usually not large enough to drive a cell to threshold, this often requires multiple synaptic events at multiple synapses. The effect of these excitatory inputs can be counterbalanced by the action of inhibitory synapses in the region. Therefore it is the balance between excitatory and inhibitory synaptic input which determine the impact of synaptic events on action potential generation.

1.3. The oestrus cycle

The oestrus cycle is regulated via the hypothalamus-pituitary-gonad axis; gonadotrophin-releasing hormone (GnRH) is released in the anterior pituitary by GnRH cells which project from the hypothalamus and septal area. This leads to the peripheral release of follicle-stimulating hormone (FSH) and luteinizing hormone (LH) from the gonadotrophs, these hormones stimulate the ovary leading to ovulation (Caligioni, 2009).

Estradiol, one of the estrogens often referred to as E2, is released by the ovaries prior to ovulation which provides a positive feedback loop stimulating GnRH neurons. This peak in E2 levels has been shown to have effects on other key processes in the body including cardiac (Scharfman *et al.*, 2003) and neuronal (Walf & Frye, 2007) function.

The diestrus phase of the mouse and rat oestrus cycle and the premenstrual phase of the human oestrus cycle are characterised by a decline in plasma levels of progesterone (Figure 1-7). Progesterone plays a key role in many aspects of pregnancy and is required to produce mammalian offspring. As this thesis has focused on virgin females I will not go into much detail on this; more details can be found in a review by Spencer et al 2002 (Spencer & Bazer, 2002). In cycling females, progesterone is involved in the negative feedback of the GnRH cells (Skinner *et al.*, 1998). Progesterone also plays a key role in stress modulation, the effect of which may be partially mediated by the BNST and will be discussed in the following section.

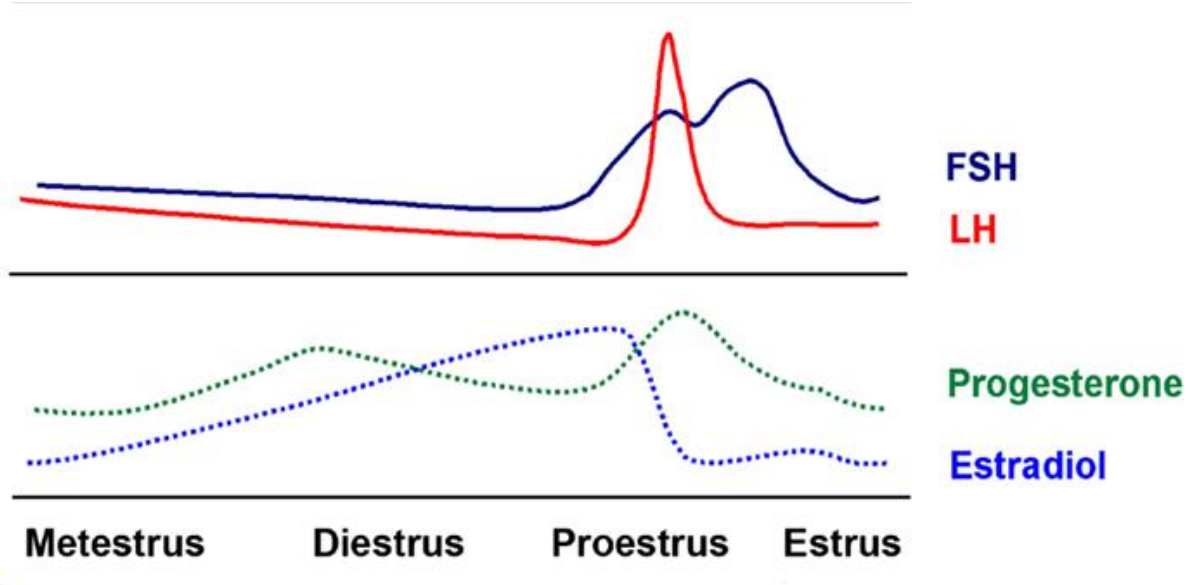

Figure 1-7 Changes in hormone levels during the mouse estrus cycle as depicted in Miller and Takahashi, 2014

1.4. The sexually dimorphic nature of the BNST

The BNST is a sexually dimorphic region in both the rodent and the human. In the rat, the encapsulated region of the BNST is twice the size in males in comparison to females (Hines *et al.*, 1992), this is driven by heightened cell death in females during development (Hines *et al.*, 1992). The sexually dimorphic nature of the BNST plays a role not only in gender specific behaviours but also in sexual identity. In human the central subdivision has been found to be larger in males than females. Interestingly male to female transsexuals have the BNST of females, this has led to the hypothesis that the BNST plays a key role in sexual identity (Hines *et al.*, 1992; Kruijver *et al.*, 2000). The BNST also mediates a number of sexually distinct behaviours such as maternal behaviour, aggression in males and sexual behaviour.

The BNST plays a key role in anxiety and anxiety-related disorders; the incidence of anxiety related disorders in the population is estimated to be ~60% higher in females, some estimates put levels of PTSD in females at twice that observed in male population (Kessler *et al.*, 1995; Breslau & Kessler, 2001). There is debate within the field whether the main reason for this is down to neurological differences in the processing of stress within the brain or if societal effects are playing a role (Tolin & Foa, 2006). While societal effects are undoubtedly influencing these altered

susceptibilities, a number of regions associated with stress processing including the hippocampus, PAG and BNST are sexually dimorphic.

A key difference between males and females is the levels of circulating hormones which play a role in reproduction. Females will undergo constantly changing levels of hormones which due to their lipophilic nature can easily cross the blood brain barrier and elicit significant effects at nuclear receptors and lipid bound receptors. Both estrogen and progesterone receptors are located throughout the brain; this would indicate that their function is not limited to reproduction.

Estradiol is a key hormone involved in reproduction as discussed above, it also has a number of vital functions outside of the reproductive system including in bone health (Albright et al., 1941), and in the CNS where estrogen receptors are abundantly expressed. Estradiol is upregulated during stress (Shors *et al.*, 1999) but its effects are anxiolytic (Walf & Frye, 2007).

Progesterone receptors function in three major ways, through regulation of gene expression, activation of cell signalling cascades and modulation of neurotransmitter systems (Brinton *et al.*, 2008). Progesterone has been implicated in a number of stress related responses; in fact progesterone levels have been found to increase during acute stress (Barbaccia *et al.*, 2008). The main effect of progesterone on stress is thought to be mediated not by the hormone itself but by one of its key metabolites, Allopregnalone (ALLO) (Gulinello *et al.*, 2003; Lovick, 2006, 2012; Shen *et al.*, 2007; Nagaya *et al.*, 2015*a*). Levels of ALLO and progesterone are tightly linked; at the end of the proestrus phase of the mouse cycle where a drop in progesterone is observed there is equal drop in ALLO (Lovick, 2012).

ALLO affects excitability of neurons, both withdrawal from progesterone (Smith *et al.*, 1998*a*, 1998*b*; Devall *et al.*, 2009) and increases in progesterone (Shen *et al.*, 2005) induce upregulation of extra synaptic $GABA_A$ by activating the genes encoding α4, β1 and δ subunit. As discussed earlier, the presence of the δ subunit into the $GABA_A$ complex leads to the extrasynaptic placement of the receptor. The extrasynaptic placement of these receptors leads to an increase in tonic inhibition which causes a decrease in excitability.

A large body of evidence has linked the anxiogenic effects of progesterone withdrawal to effects mediated by the periaqueductal gray matter (PAG). The PAG is

a key pathway in pain modulation and processing of stress, two characteristics which show gender specific behaviours. Cycle-specific changes in excitability have been observed in this region which highlights its susceptibility to fluctuations in hormones. Similar to a number of other brain regions characterisation of the PAG was based primarily in males, however recently more females are being studied due to the evident role of hormones in this area (Lovick, 2006, 2012; Brack & Lovick, 2007*a*; Johnson *et al.*, 2012; Jiang *et al.*, 2014).

The PAG has reciprocal connections with the BNST which also has a high concentration of both estrogen receptors and progesterone receptors specifically within the anterolateral area. Similar to the PAG most of the characterisation of this region has focused on males especially within the rodent. However recent evident is starting to emerge of the central role of the BNST in gender specific responses to stress.

Systemic administration of ALLO blocks CRH-enhanced startle response in female rats (Toufexis *et al.*, 2004), thought to be a BNST-mediated process. Nagaya et al (2015) examined the gender-specific effects of ALLO on the BNST by altering levels of ALLO in the BNST in a gender specific manner. This was carried out firstly via local infusion of ALLO into the BNST of male rats and secondly either an inhibitor of ALLO synthesis or an ALLO antagonist into the BNST of female rats. In males, the attenuation of ALLO in the BNST leads to a decrease in contextual freezing while in females reduction of ALLO activity in the BNST elicited enhanced contextual freezing (Nagaya *et al.*, 2015*a*). This sexually dimorphic response to changes in ALLO highlights the importance of gaining greater understanding of the role of this compound, and the pathways it triggers, in the BNST.

At nanomolar concentrations, ALLO acts as an allosteric modulator of the $GABA_A$ receptor (Shen *et al.*, 2007). Systemic administration of ALLO has also been shown to change the expression levels of the delta subunit of the $GABA_A$ receptor in hippocampus leading to greater extra synaptic placement of the receptor (Shen *et al.*, 2005). This extrasynaptic placement means its effects are not limited to GABAergic synapses, indeed it has been shown that ALLO can modulate glutamate release presynaptically via extrasynaptic $GABA_A$ (Iwata *et al.*, 2013).

1.5. Health ageing

Healthy aging is associated with a number of cognitive and behavioural changes. Over the lifespan of both humans and rodents there is a decrease in cognitive function (Disterhoft *et al.*, 2004) along with changes in susceptibility to anxiety-like disorders (Garrido, 2011). The changes in cognitive function are mediated at least in part by changes in hippocampal function where changes in excitability of neurons have been observed (Wilson *et al.*, 2005; Randall *et al.*, 2012). Aging has been shown to impact intrinsic properties in a number limbic brain regions such as the hippocampus and prefrontal cortex (Disterhoft *et al.*, 2004; Chang *et al.*, 2005*a*; Wilson *et al.*, 2005; Randall *et al.*, 2012; Hermann *et al.*, 2014; Prenderville *et al.*, 2015; Tamagnini *et al.*, 2015; Rodríguez-Arellano *et al.*, 2016). A number of underlying factors have been attributed to these changes including changes in Na^+ channel function which leads to changes in excitability in the hippocampus (Randall *et al.*, 2012), changes in GAD-67 expression in hippocampal interneurons (Stanley & Shetty, 2004) and AHP magnitude (Landfield & Pitler, 1984; Kumar & Foster, 2002). While to my knowledge no similar differences have been reported in the BNST, changes in other brain regions provide some basis to examine alterations in intrinsic electrophysiological properties within the BNST.

Changes in stress processing across the lifespan occur in a sex specific manner, I have already discussed the impact of sex hormones on stress processing so it is unsurprising that changes in hormone levels can have an impact on various neurological functions. In humans females undergo menopause in approximately the fifth to sixth decade of life, in mice this is referred to as senescence and occurs at ~18 months (Ehrchen *et al.*, 2004).

In senescence rats anxiety levels have been shown to be higher in males than in females when measured in the open field. The administration of 21 days of restraint stress, 6 h/day, reduced anxiety shown by female rats and increased the anxiety shown in the males (Bowman *et al.*, 2006); producing a highly gender specific response. Testosterone has been shown to regulate the HPA axis function via vasopressin and CRF synthesis (Viau, 2002). This effect is not mediated via testosterone itself but rather mediated via a metabolite of testosterone, 3β-diol (Lee *et al.*, 2001). Males also undergo senescence, sometimes referred to as hypogonadism, which can be observed in both humans (Wu *et al.*, 2008, 2010;

Ahern & Wu, 2015) and rodents (Lovick, 2012; Donner & Lowry, 2013) and is characterised by a decrease in testosterone. The drop in testosterone could account for the changes in anxiety observed.

Female menopause, or senescence, is characterised by a decline in a number of sex hormones including estradiol and progesterone both of which have been shown to have anxiolytic properties (Chen *et al.*, 2004; Walf & Frye, 2007; Lovick, 2012). Progesterone has been shown to be protective against a number of age-associated disease such as Alzheimer's disease and stroke (Lee *et al.*, 2001). The key role of progesterone in stress processing along with the gender specific nature of its effects was addressed earlier. Decreases in these key hormones may lead to increased anxiety and increases in a number of age-associated diseases such as Alzheimer's disease and osteoporosis.

Little research has been carried out on the BNST in healthy aging and to my knowledge no studies have looked at the electrophysiological properties of the BNST in aging; however some research has been carried out in gene expression levels of various key mediators within the BNST. Nutsch et al 2017 examined the expression levels of a number of key genes associated with behaviour in the both the BNST and several other regions associated with hypothalamic modulation. They found a decrease in expression of six genes; *Cyp19a1*, *Esr2*, *Kiss1r*, *Nos1*, *Oxtr* and *Thra* (Nutsch *et al.*, 2017) in male Spague-Dawley male rats at 18 months in the BNST compared with 5 months. While the role of these genes has often not been studied in great detail in the BNST some studies have touched upon the effect they may be playing within this circuit. Cyp19a1 is the gene associated with aromatase, a key enzyme in the production of estradiol. While this paper did not examine protein levels one could hypothesise that a decrease in expression could lead to a decrease in local estradiol production. The Kiss1r gene encodes the kisspeptin receptor which is involved in sexual behaviour (Gresham *et al.*, 2016) and oestrogen signalling in the amygdala of male rats (Stephens *et al.*, 2016).

The decrease in expression of Nos1 and Esr2 would indicate a decrease in NO production in the BNST with age, this is based on observation in the PVN where estrogen increases NO production through interaction with ERβ (Gingerich & Krukoff,

2005, 2006). In the BNST, NO is anxiolytic, as such a reduction should lead to decrease in anxiety responses (Faria *et al.*, 2016).

Decreases in oxytocin binding within the BNST have previously been associated with increases in parental care (Perea-Rodriguez *et al.*, 2015) and increases in aggression (Calcagnoli *et al.*, 2014). Perea-Rodriguez et al (2015) found that a decrease in Oxtr mRNA observed in first time fathers was associated with an increase in parental care in comparison to virgin males. However it is worth noting in this study they also observed decreases in expression of the progesterone and vasopressin receptors as such the behavioural observations may not be entirely attributable to the decrease in OXR expression. The role of the Oxytocin system in aggression was addressed by Calcagnoli et al (2014) where they observed increases in OXTR binding in the BNST and CeA were associated with highly aggressive rats.

The final gene identified was the *Thra* gene; while the role of this gene has not been studied in the BNST, the knockout model displays heightened anxiety and facilitated sexual behaviour (Vasudevan *et al.*, 2013). These shifts in behaviour specifically with regards to the increases in anxiety would implicate the involvement of the BNST to some extent possibly through interaction with the oxytocin system (Vasudevan *et al.*, 2001).

To my knowledge, the only other study to assess the role of the BNST in healthy aging found a decrease in vasopressin in mRNA in aged male Fischer 344 rats (Dobie *et al.*, 1991). This effect was rescued via administration of testosterone (Dobie *et al.*, 1992). Vasopressin plays a key role in a number of social behaviours including social approach and communication, with pharmacological inhibition leading to anxiogenic effects (Faria *et al.*, 2016).

It is worth noting that both of these studies were carried out in male rats however in this study I plan to address the role of electrophysiological properties in female mice. However from the above studies I can infer that a number of key modulators of social behaviour change in the BNST during heathy aging, we would expect these changes to impact the functionality of neurons within this circuit.

1.6. Frontotemporal dementia

Frontotemporal dementia is an umbrella term used to describe a group of neurodegenerative diseases characterised by deficits in executive function, behaviour or language (Bang *et al.*, 2015). It is the leading type of early onset dementia, the third most common dementia following Alzheimer's disease and dementia with Lewy bodies (Vieira *et al.*, 2013) and the second most common early onset dementia following Alzheimer's disease (Ratnavalli *et al.*, 2002; Harvey *et al.*, 2003). There are three main forms of the disease, behavioural-variant frontotemporal dementia and primary progressive aphasia which is further subcategorised as non-fluent variant primary progressive aphasia and semantic-variant primary progressive aphasia. Further details on their clinical diagnosis can be found in Bang et al., 2015.

Frontotemporal dementia is characterised by neuronal loss, microvascular changes and gliosis with different subtypes displaying distinct protein depositions (Mackenzie *et al.*, 2010). There are three common proteins which account for nearly all cases of frontotemporal dementia; the microtubule-associated protein tau (MAPT), the fused – in-sarcoma (FUS) protein and the TAR DNA-binding protein with molecular weight 43 KDa (TDP-43). There are some rarer cases which contain no inclusions or ubiquitin-only positive inclusions (Mackenzie *et al.*, 2010; Bang *et al.*, 2015).

An understanding of the genetic causes of disease gives researchers the ability to generate models, specifically mouse models. There are a number of commonly used mouse models for FTD, these include models with mutations in TDP-43, progranulin and tau. Another model to more recently emerge in the field of FTD is those containing mutations in CHMP2B. Briefly I will describe some of these models and asses how closely related to FTD they are.

TDP-43 positive inclusions are found in most familial and sporadic cases of FTD indicating a key role in disease pathogenesis (Cairns *et al.*, 2007). Mouse models containing the entire human TDP-43 gene or mutant TDP-43 display several features of FTD including neuronal inclusions and motor dysfunction (Swarup *et al.*, 2011). While this captures aspects of the disease the protein levels observed in tissue was three times that of the endogenous protein, such an increase in protein may lead to other pathological functions not observed in the human brain.

70 mutations in the progranulin gene (GRN) have been identified in FTD, these mutations lead to a loss of function (Chen-Plotkin *et al.*, 2011). Therefore a number of knockout models have been developed. From these mouse models progranulin has been implicated in neuro-inflammation (Yin *et al.*, 2010; Ahmed *et al.*, 2010) and protein mishandling (Kayasuga *et al.*, 2007). These mice are homozygous for the missing gene, however, humans homozygous for GRN mutations develop another disease known as neuronal ceroid lipofuscinosis (Smith *et al.*, 2012). Future research into the role of progranulin in FTD should focus on heterozygous mice (Roberson, 2012).

Unlike a number of genes involved in other mouse models of dementia a large proportion of the genes involved in FTD have a high rate of conservation with those observed in human. In the case of the CHMP2B gene used in this study is 100% conserved. Inclusion of human CHMP2B into mice has no effect equally knockout mice display no phenotype, this has indicated a gain of function role of the mutated proteins. The CHMP2B gene forms part of the endosomal sorting complex required for transport III (ESCRT-III). Mutations within intron 5 of CHMP2B leads to a failure to disconnect from the ESCRT-III impairing its function (Cox *et al.*, 2010). Insertion of this mutated gene into mice leads to the presence of ubiquitin positive inclusions and axonal swelling implicating a role in neuronal degeneration (Ghazi-Noori *et al.*, 2012*a*).

Approximately half of patients with frontotemporal dementia will experience symptoms of anxiety (Cummings, 1997; Liu *et al.*, 2004). While this heightened anxiety may implicate the involvement of the BNST, to my knowledge no known changes in HPA axis function have been reported. This is in contrast to Alzheimer's disease, where the involvement of this pathway has been implicated (Hebda-Bauer *et al.*, 2013). The lack of literature on the effect of frontotemporal dementia on the HPA axis could be caused by one of two factors, one factor being that no studies have been carried out to examine the effect either in mouse models or in patients, despite the observed changes in anxiety levels.A second possibility is that there are no changes in HPA axis function however I have found no literature to support this, potentially due to publication bias towards positive results.

1.7. Hypothesis

Intrinsic properties of neurons located within the $BNST^{ALG}$ differ in sex, aging and in a model of frontotemporal dementia.

Differences in intrinsic properties of cells will be cell type dependent and this unstressed model may represent susceptibility to changes in anxiety and anxiety disorders which may arise following stress.

1.8. Aims

The overall aim of this project was to characterise the electrophysiological properties of BNST neurons and determine the effect of gender, age and frontotemporal dementia pathology on these properties. A robust and information rich way to study the function and plasticity of CNS circuits is through direct real-time neurophysiological measurements of neural activity using various approaches. Such neurophysiological approaches have been applied to aspects of BNST function since the mid to late 1970s, starting with in vivo unit recording in anaesthetized animals (Bueno & Pfaff, 1976) and subsequently including brain slice studies performed in vitro (Sawada *et al.*, 1980; Rainnie, 1999).

Differences in gender, healthy aging and dementia including frontotemporal dementia display a wide variety of changes in neurological function including changes in anxiety and susceptibility to anxiety-related disease. In the case of aging and gender there are also known changes to the HPA axis, a process regulated by the BNST. In the case of frontotemporal dementia there is evidence of heightened anxiety in patients (Cummings, 1997; Liu *et al.*, 2004). Due to the central role of the BNST in processing of stress it is possible that changes in anxiety levels of patients may be driven by functional changes in the BNST. Here we plan to address how changes in electrophysiological properties of neurons located in the $BNST^{ALG}$ differ in these unstressed models to isolate possible mechanism for changes in anxiety and susceptibility to anxiety-related disorders.

A key reason for the use of males over females is the unknown effect of the estrus cycle on neuronal properties which may lead to increased variability. Here I addressed this by examining the electrophysiological properties of BNST neurons in the different stages of estrus to determine if the circulating hormones had impacted intrinsic electrophysiological properties

2. Methods

2.1. Animals

One transgenic line was used in this project; the CHMP2B line. This line was developed and breed at UCL in the lab of Dr. Adrian Isaacs (Ghazi-Noori *et al.*, 2012*b*). The cohort was transported to the University of Exeter in the weeks preceding the experiments. The remainder of the project focused on C57BL/6 mice; the aged female study the mice were bred at Charles River and transported to the University of Exeter a week prior to the commencement of the project. For the remaining studies the C57BL/6 mice were breed in house using stock from Charles River. All animals were housed in a 12:12 hour light-dark cycle with *ad libitum* access to food and water. All procedures were carried out in accordance with the Animals (Scientific procedures) act 1986.

2.2. Behavioural tasks

Anxiety levels were examined using the elevated zero maze (Faria *et al.*, 2016). This maze comprises an elevated circular track which is covered on two sides Figure 2-1. Anxiety is thought to be related to the proportion of time spent in the open area. A light source was placed in the centre of the maze which allowed the two ‘closed’ components of the maze to remain dark while the ‘open’ components of the maze were illuminated by white light. Animals were placed in the maze for 5 minutes and the proportion of time spent in the open vs closed component was calculated. In the CHMP2B chapter 5 animals of each genotype were run over two days and the results were averaged. In the sex chapter the animals were run once on the morning of experiments prior to culling.

The proportion of time in each component was carried out using a stop watch; the experimenter was blinded by to animal’s genotype or sex during visual analysis.

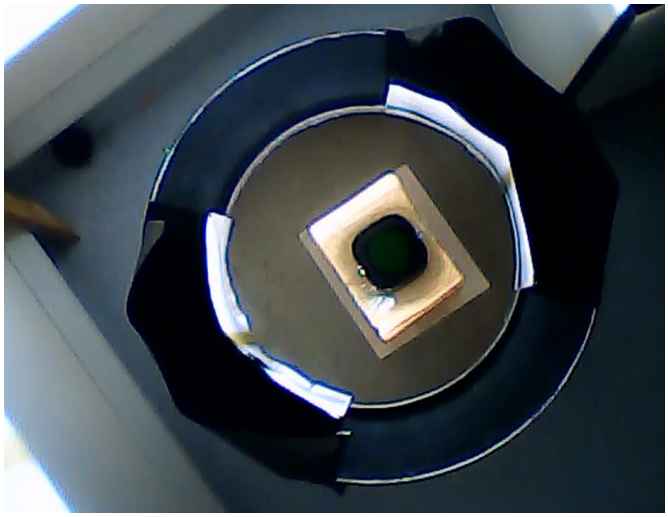

Figure 2-1 Image of the elevated zero maze taken from experimental videos.

2.3. Slice preparation and electrophysiological recordings

2.3.1. Solutions

A number of internal and external solutions were used to prepare slices and carry out patch clamp recordings. Two external solutions were used (Table *2-1*); a sucrose based solution used in slice preparation and artificial cerebrospinal fluid (aCSF) was used to maintain slices in both the holding chamber and the recording chamber. All external solutions were constantly bubbled with carbogen (95 % O_2, 5 % CO_2), these solutions had a pH of 7.3 and osmolality of 290-300 mOsm.

	Sucrose (mM)	aCSF (mM)
Sucrose	189	
D-glucose	10	10
$NaHCO_3$	26	24
KCl	3	3
$MgSO_4$	5	1
$CaCl_2$	0.1	2
NaH_2PO_4	1.25	1.25
NaCl		124

Table 2-1 Composition of external solutions

K-gluconate based internal solutions were used throughout the project. Two different varieties were used as detailed in Table 2-2 below. The 15 mV junction potential error produced by pairing this pipette solution with our aCSF was corrected for

during analysis. Internal solutions had an osmolality of 280 – 290 mOsm and a pH of 7.3.

	K-Gluconate (mM)	K-Gluconate with biocytin (mM)
K-Gluconate	130	120
KCl	20	20
HEPES free acid	10	10
EGTA	0.2	0.2
GTP-Na salt	0.3	0.3
ATP-Mg salt	4	4
KOH	pH to 7.3	pH to 7.3
Biocytin		13.4

Table 2-2 Composition of internal solutions

2.3.2. Slice preparation

Animals were killed by cervical dislocation, the brains were quickly removed and placed into ice-cold sucrose solution (Table *2-1*). A Leica VT1200 vibratome was used to cut serial 300 μm thick coronal sections. Slices containing the $BNST^{ALG}$ came from approximately Bregma -.1 to +0.3, and were identified with the aid of the Paxinos and Franklin mouse brain atlas (Paxinos & Franklin, 2004*a*) using the anterior commissure as a key landmark. Cells came from the dorsal portion of the $BNST^{ALG}$ Figure 2-2. Typically one or two BNST-containing coronal sections per animal could be used and by bisecting these along the dorsal-ventral midline I was able to obtain up to four usable tissue sections per mouse.

Following their preparation slices were allowed to recover at room temperature for at least 60 mins in our standard aCSF (Table *2-1*). A Flaming Browning P-97 micropipette puller was used to produce the microelectrodes used in this study. These electrodes had a resistance of 3-5 MΩ when filled with the K-Gluconate-based internal solution used for all recordings..

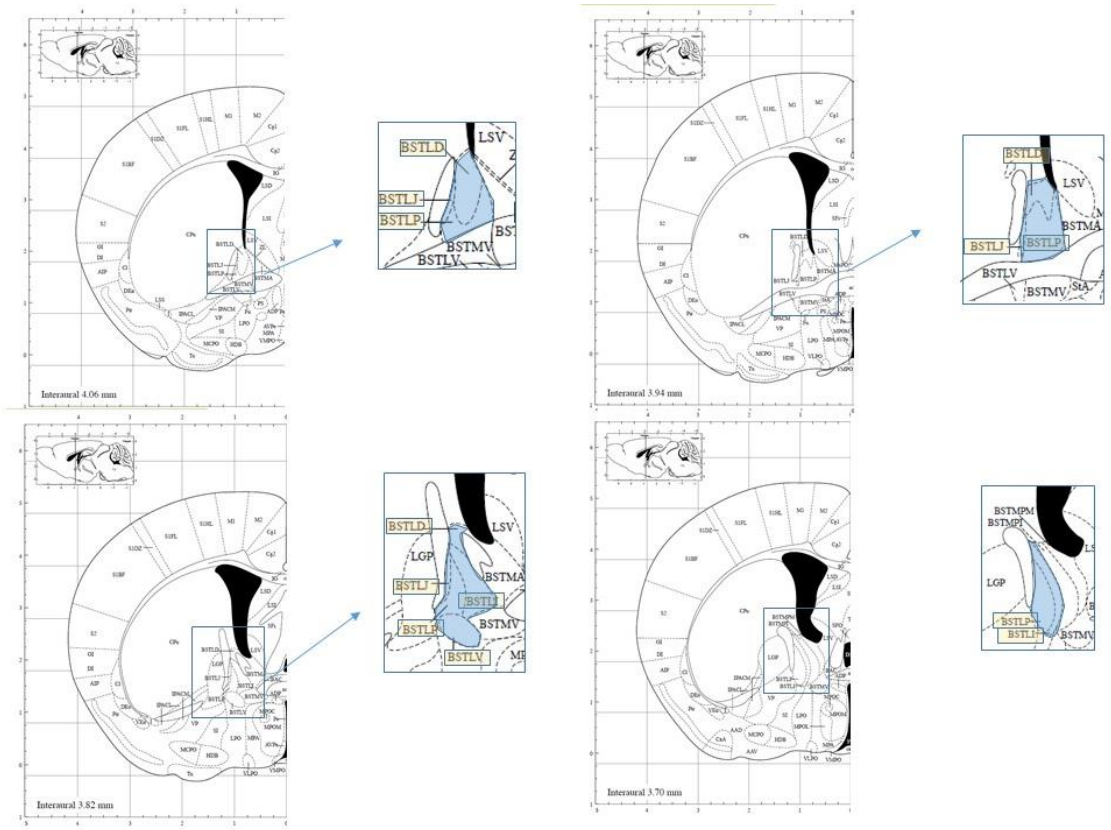

Figure 2-2 BNST^{ALG} location enlarged boxes show the anterolateral area of the BNST as taken from the Paxino and Franklin mouse brain atlas (Paxinos & Franklin, 2004a)abbreviations of the different subregions of the BNST: medial division ventral part (BSTMV),lateral division ventral part (BSTLV), medial division anterior part (BSTMA), medial division posteromedial part (BSTMPM), medial division, posteromedial part (BSTMPL), lateral division ventral part (BSTLV), lateral division posterior part (BSTLP), lateral division dorsal part (BSTLD), lateral division juxtacapsular part (BSTLJ). Blue shaded area with in the enlarged images depict the anterolateral area of the BNST. Bregma -0.1 to +0.3.

2.3.3. Whole cell patch clamp recordings

The recording chamber was mounted on the stage of an upright microscope (Olympus BX51). Slices were placed in the recording chamber and continuously diffused with aCSF heated to between 32-35 ^{o}C. Cells within the BNST were visually identified using the microscope's infrared differential interference contrast optics and a coupled IR-sensitive CMOS camera (Thor Labs) as seen in Figure 2-3. All recordings were made with a Multiclamp 700B amplifier (Molecular Devices) interfaced to a Digidata 1440A computer interface (Molecular Devices). Data was collected using the Clampex programme within the pClamp 10.4 software suite. All

data were stored directly onto a personal computer (Hewlett-Packard) and backed-up to a network drive.

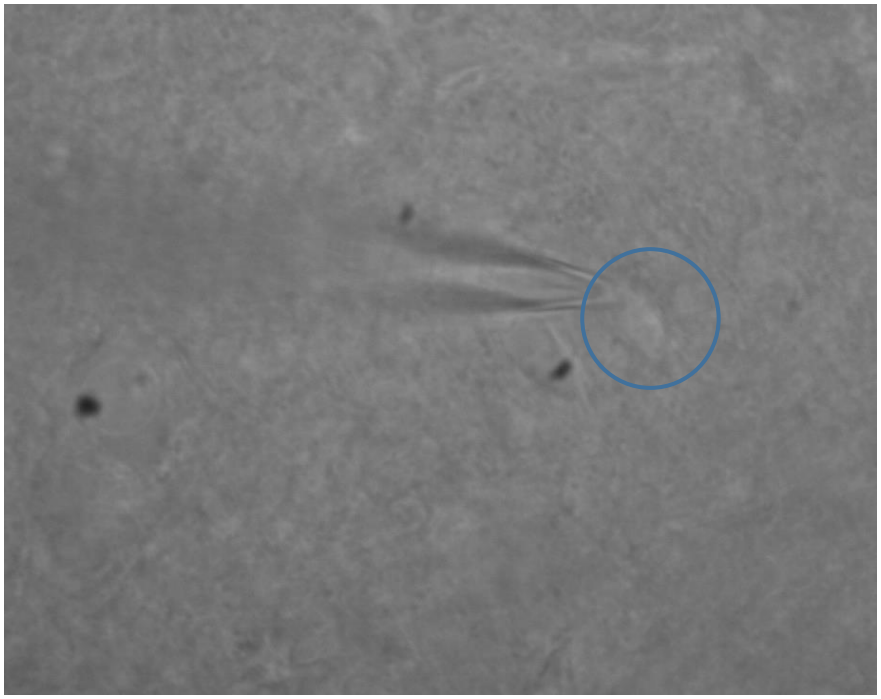

Figure 2-3 Visualisation of cell

2.3.3.1. Voltage clamp recordings

After forming a gigaseal and subsequently gaining whole cell access, in all recordings I first recorded a 60 s period in voltage clamp at a holding potential of -70 mV at a sampling rate of 10 kHz. From this recording the amount of holding current, the mean frequency and amplitude of the spontaneous inward-going synaptic events were measured. The holding current was taken as the mean current in the 1 minute trace.

To assess the frequency and amplitude of inward-going synaptic events traces were bandpassed filtered using a 5 Hz highpass filter and 1000 Hz for a Gaussian lowpass filter. A threshold detection was used to isolate all events over 8pA. Cells which displayed a large quantity of noise were excluded. The event frequency measured in hertz was calculated by dividing the number of events by 60. The amplitude of all events was averaged for each cell.

2.3.3.2. Current clamp recordings

Following the initial 60 s period in voltage clamp, the amplifier was switched to current clamp mode for the remainder of the recording allowing cellular voltage responses to be studied. Firstly, a period of activity in the absence of any injected current was recorded (i.e. at the resting potential).at a sampling rate of 10 kHz. The proportion of cells exhibiting any spontaneous action potential firing was also examined. Cells were subsequently held at a prestimulus membrane potential at defined levels of -70 mV or -80 mV; the amount of current required to hold cells at these potentials was defined as I_{hold} (pA) and recorded for each cohort. A number of protocols were used to examine passive properties and firing properties of each cell. We began with the step protocol; this was comprised of a series of nine, 500 ms duration, current injections ranging from -40 to +80 pA in 15 pA increments recorded at a sampling rate of 100 kHz. The time between the stimuli was 10 s. This was followed by a rheobase protocol which examined the amount of current required to generate an action potential in a cell also recorded at a sampling rate of 100 kHz.

2.3.3.2.1. Passive membrane properties

The -40 pA hyperpolarizing current injections from the 9 step series were used to determine passive, subthreshold membrane properties as shown in Figure 2-4. Input resistance was calculated using ohms law (R = I/V, R = input resistance, I = current injection, V = voltage change); the voltage deflection was the difference between the pre-stimulus voltage and average voltage during the final 100 ms of the hyperpolarizing current stimulus.

The rebound is the voltage change between the depolarising peak following the switching off of the current and the baseline. % Sag is the (((peak negative deflection – average voltage of last 100 ms of hyperpolarising current stimulus)/ peak negative deflection) *100).

The membrane time constant is the amount of time required to charge the membrane to 63.2% of the peak negative deflection; this is calculated following the injection of -40 pA of current. Finally capacitance was calculated from the membrane time constant and the input resistance (capacitance = (membrane time constant/

input resistance) * 1000 pF). Figure *2-4* depicts a cell at a holding potential of -80 mV; the same measurements were made on cells held at -70 mV.

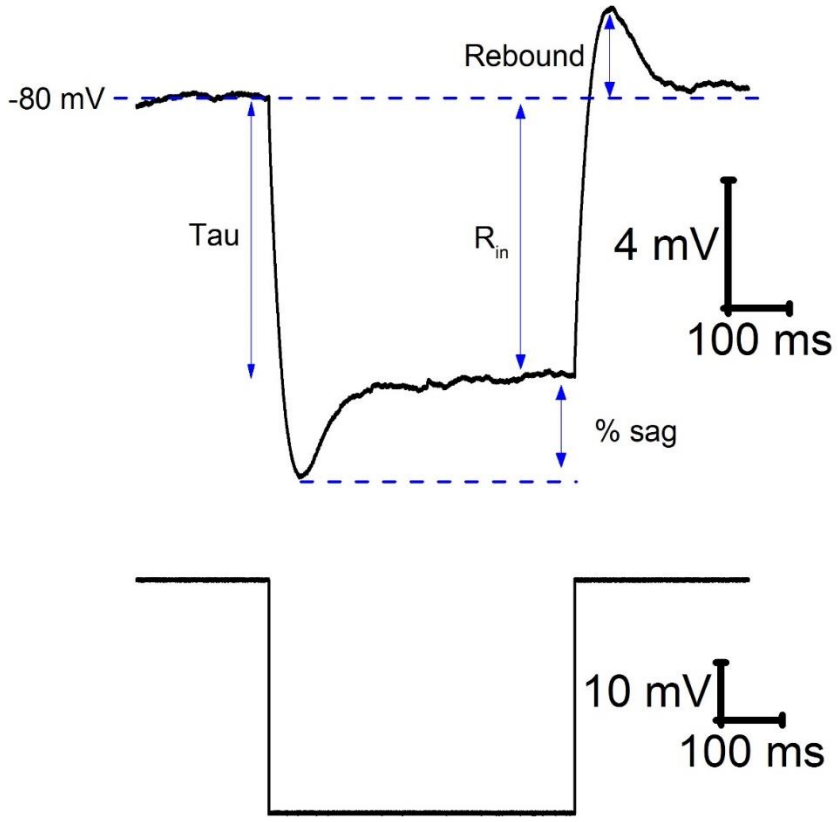

Figure 2-4 Passive membrane properties isolated from a 40 pA current injection, this sample trace displays a prominent sag along with a rebound following the switching off of the current. The areas where key calculations from the voltage deflection to a -40 pA current injection are highlighted using blue arrows.

2.3.3.2.2. Active properties

The action potential properties of each cell were characterised from the first action potential generated in response to a series of depolarising current injections. For each recording we measured action potential threshold, maximum rate of rise, zenith and action potential width as depicted in Figure *2-5*.

Threshold was measured at the first point at which the rate of rise exceeded 20 mV/ms. AP zenith was the peak depolarisation reached; AP width was measured at 2 points, from a set point of -20 mV and at threshold. The maximum rate of rise was

calculated based on the first derivative of the action potential as depicted in Figure 2-6.

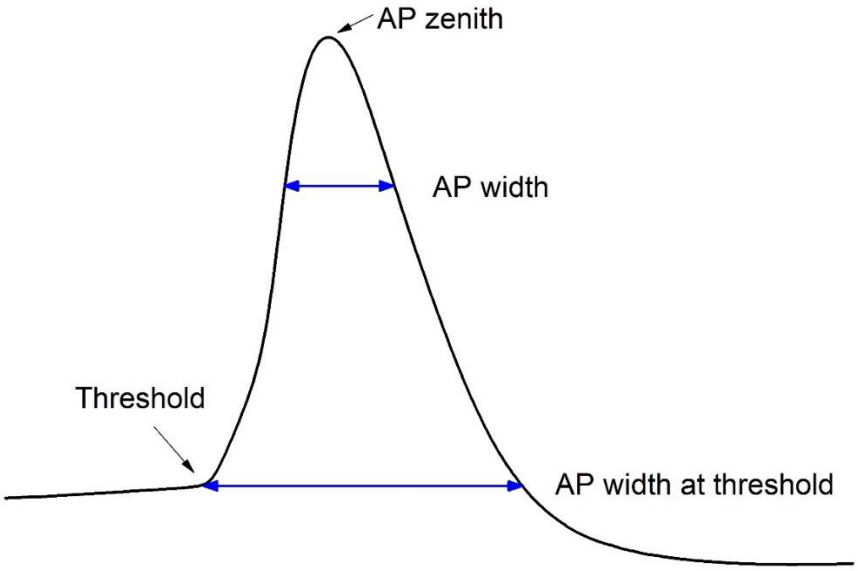

Figure 2-5 Action potential properties. AP zenith is the maximum point which the action potential reaches (mV), AP width is the width of the action potential at a specific membrane potential of 20 mV (ms), threshold is the point at which the rate of rise goes above 20 mV/ms (mV). AP width at threshold is the width of the action potential at this point (ms).

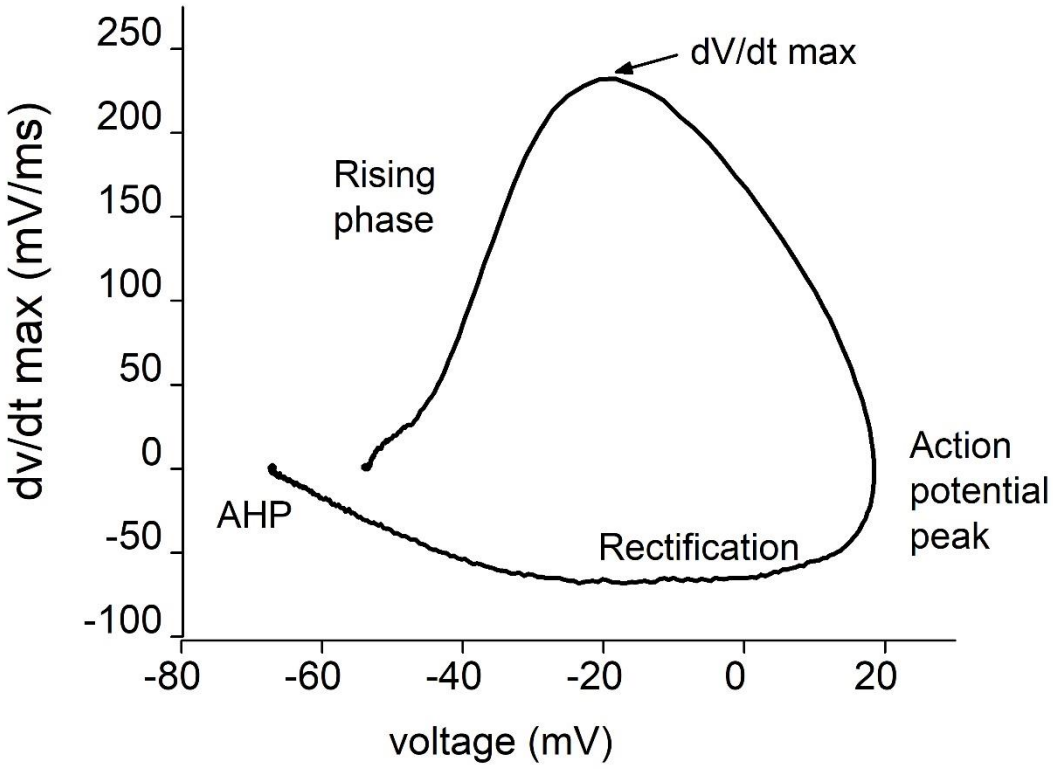

Figure 2-6 dV/dt max plotted against the voltage change of a single cell. dV/dt max is taken at the maximum rate of rise reached by the cell (mV/ms).

2.3.3.2.3. Firing properties

The series of depolarising pulses in the step protocol were used to characterise the firing properties of the cells (Figure 2-7). This included the proportion of cells firing in response to each amplitude of depolarising injection, the frequency of action potentials and latency to generate an action potential. Latency to the first action potential was measured on 2 sweeps; the first sweep when an action potential was generated and the final sweep in the step protocol ie. the injection of +80 pA of current. Another way to examine excitability is to look at rheobase (i.e. the amount of depolarizing current required to elicit any spiking). This was achieved by applying current injections lasting 300 ms that were increased in amplitude by 2 pA per sweep until a spike was observed, the time between stimuli was 1 s (Figure 2-8).

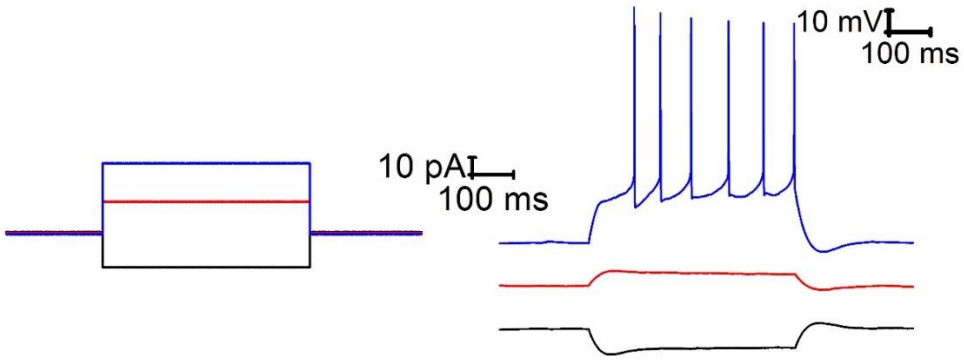

Figure 2-7 sample trace of step protocol. Depicts 3 out of the 9 current injections offset for visualisation purposes.

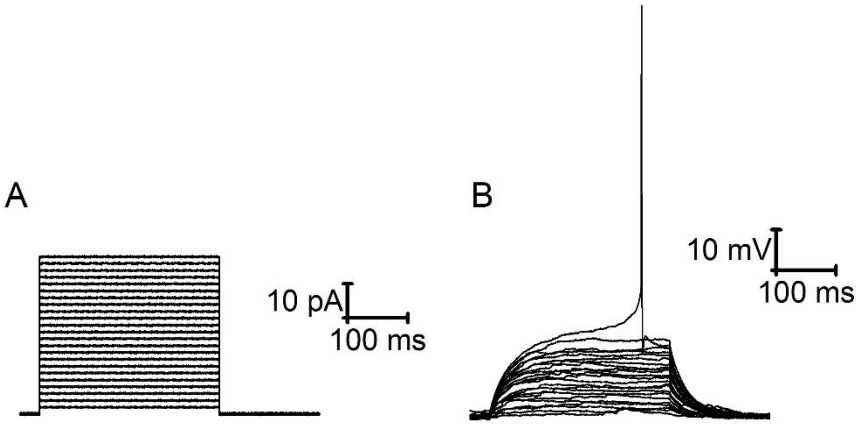

Figure 2-8 Sample rheobase current injection (A) and trace (B)

2.3.3.2.4. Pharmacological recordings

Pharmacological examination of gaboxadol was carried out via injection of alternating hyperpolarising (-40 pA), depolarising (80 pA) pulses to examine firing frequencies as well as passive membrane properties in current clamp mode while holding the cells at -80 mV.

The nature of inward synaptic events was determined by using agents which block glutamatergic synaptic transmission specifically NBQX and L689-560 in voltage clamp mode holding cells at -70 pA.

2.4. Statistics and graphs

Several statistical test were carried out throughout this project dependent upon the dataset being examined. Comparisons between proportions of cells firing action potentials was examined using a chi squared test carried out in Excel. All other statistical tests were carried out in SPSS. Comparisons of firing frequencies on each step was carried out via a two-way ANOVA. For all other parameters the Shapiro-Wilk normality test was used to address the distribution of the populations. Populations which were normally distributed were compared using an unpaired t-test. Non-normally distributed populations were examined via Mann-U-Whitney test. Identification of statistical tests used are listed in figure legends.

Graphs were all made in Origin 2016; for all box plots the scatter plots to the left are individual recordings. The small symbol within the box is the mean, the box reflects the Standard error of the mean (SEM) and line traversing the box is the median.

2.5. Characterisation of cells based on their electrophysiological properties

Cells were sorted into 3 different populations based on the characterisation from Hammack *et al* 2007 paper. A key component of Type I and Type II calls is a depolarising sag mediated by I_h current in response to a hyperpolarising current injection. Type I cells have a regular spiking pattern in response to depolarising current injection (Figure 2-9). A key characteristic of Type II cells is a depolarising 'hump' peaking within 150 ms of the depolarising current being switched on. This 'hump' contributes to the burst firing observed within these cells. Finally type III cells have no 'sag' in response to a hyperpolarising current injection. A sample of each of these cells is depicted in Figure *2-9*.

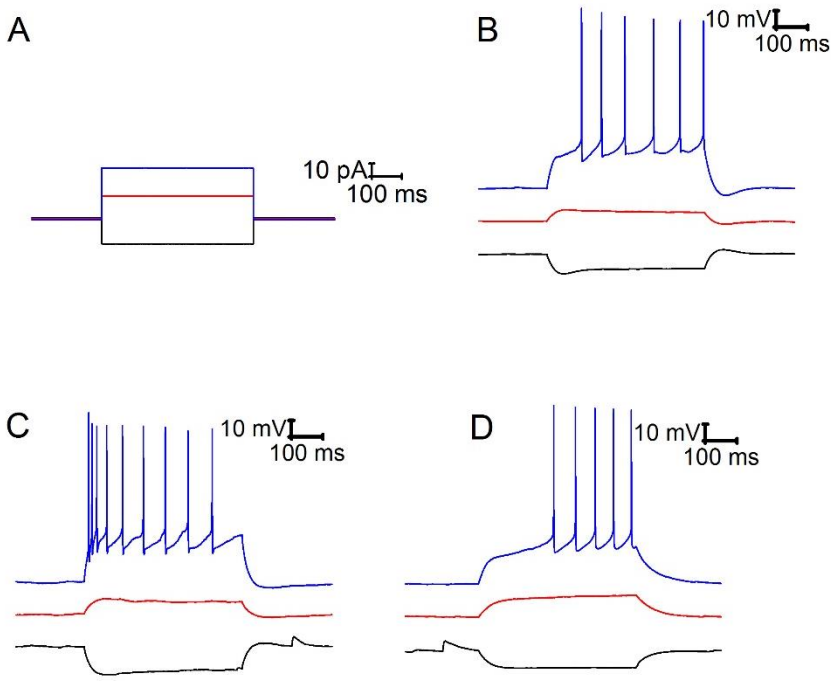

Figure 2-9 Sample of each cell type A) sample of current injection showing 3 out of the 9 injections, B) sample type I cell, C) sample Type II cell and D) sample Type III cell.

2.6. Oestrous cycle testing

Following the cervical dislocation of female mice and the removal of the brain into ice cold sucrose solution as described below the stage of oestrous was examined via a wet smear for chapters three and four. 10 µL of PBS was inserted ~ 5mm into the mouse's vagina and gently flushed two to three times. The final flush was collected and placed on to a slide for visual examination. The unstained sample was examined under a x10 objective using a Nikon eclipse E800 microscope. Oestrous cycle stage was determined by the proportion of each cell type present as described in Caligioni, 2009. During proestrus the sample is predominantly populated with nucleated epithelial cells, during estrus it is predominantly anucleated cornified cells, in metestrus it is a combination of leukocytes, cornified and nucleated epithelial cells and during diestrus it is predominantly leucocytes (Figure 2-10).

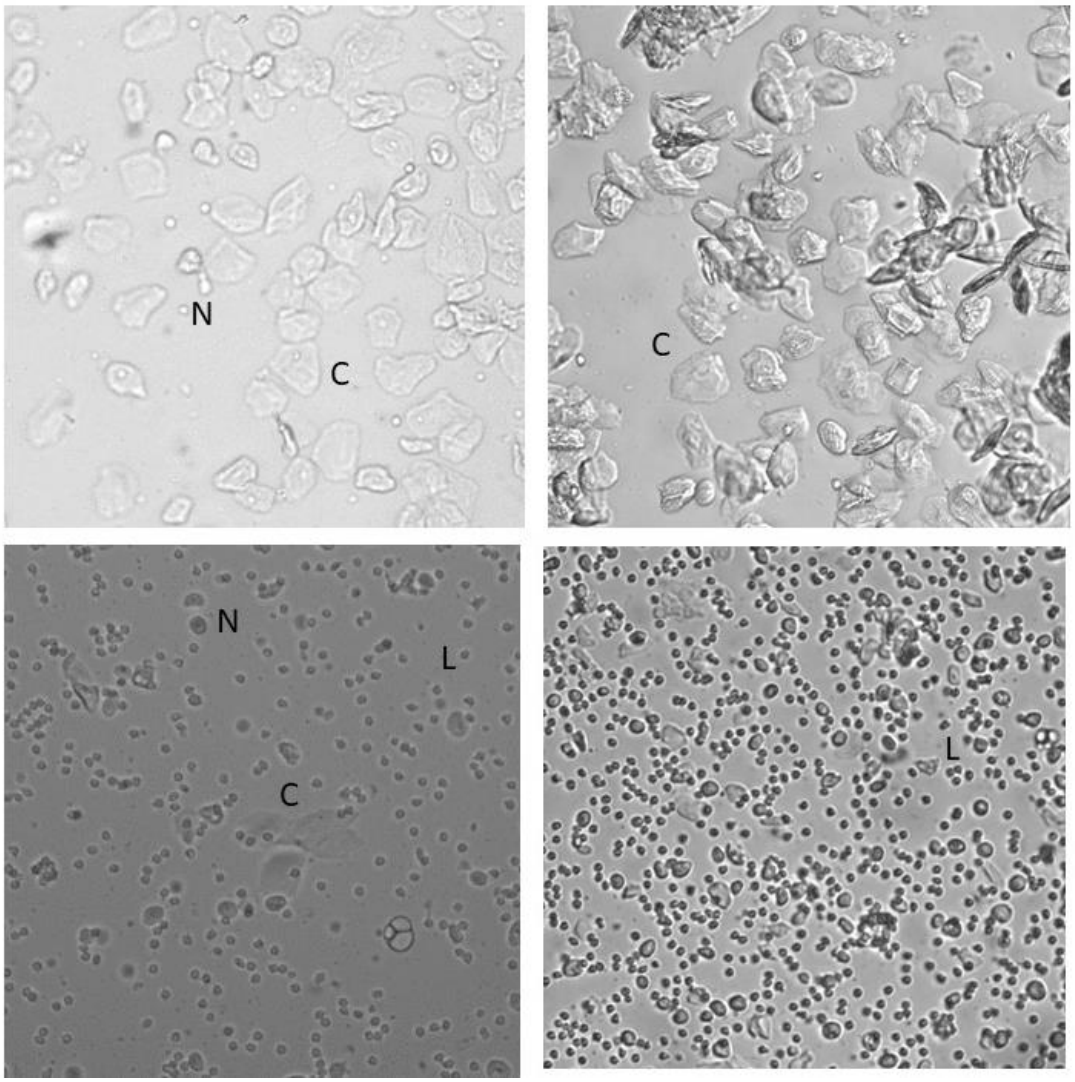

Figure 2-10 Different stages of the oestrus cycle, a) proestrus, b) estrus, c) metestrus, d) diestrus. N is adjacent to a nucleated epithelial cells, C di adjacent to a cornified cells, L is adjacent to leucocytes.

2.7. Pharmacology

To assess spontaneous synaptic transmission cells were voltage clamped at -70 mV. Events were then detected and measured as described in the methods chapter. The receptor basis of synaptic events in Type I neurons was examined by applying the glutamate receptor blockers of NBQX and L689560 (both 5 μM)

Pharmacological activation of $GABA_A$ receptors containing the δ subunit was carried out in current clamp mode from a prestimulus potential of -80 mV in the constant presence of NBQX and L689-560, alternating 500 ms pulses of -40 pA and +80 pA were applied at 10 second intervals. Following a 5 minute baseline, 30 μM Gaboxadol was added, 8 minutes later the $GABA_A$ receptor antagonist GABAzine (5 μM) was co-applied with the Gaboxadol. After another 8 minutes Gaboxadol and GABAzine were washed out.

3. Effect of the estrus cycle on neurons located in the BNST

3.1. Introduction

The reproductive cycle in females is a key component of fertility, in humans this cycle is referred to as the menstrual cycle and last ~ 28 days. The premenstrual phase of the menstrual cycle is often associated with increase in anxiety as well as mood swings. Due to the central role of the BNST in anxiety-related behaviour, these mood changes could be at least in part mediated by the BNST. In the mouse, this cycle is referred to as the oestrus cycle and lasts approximately 4-5 days. This process leads to changes in circulating levels of a number of hormones that have been shown to have an effect on neurological function (Brack & Lovick, 2007*a*; Johannessen *et al.*, 2011; Singh & Su, 2013; Bailey & Silver, 2014).

One such hormone is progesterone, this hormone has been shown to have a number of CNS activities outside of hypothalamic function, evident by the widespread expression of its receptor in various brain regions. For example, progesterone has been shown to be involved in cognitive function as well as key neuronal processes, including neuronal differentiation, outgrowth, survival, plasticity and regeneration (Singh & Su, 2013).

3.1.1. Effect of the oestrus cycle on neurophysiological properties

A number of studies have identified changes in neuronal excitability in different CNS cellular populations. In the periaqueductal grey (PAG) increases in bicuculline-induced firing in estrus and diestrus were observed in comparison to proestrus and metestrus (Brack & Lovick, 2007*b*). In the hippocampus larger maximal population spikes were evoked in proestrus and estrus were observed in comparison with metestrus in CA1 cells following Schaffer collateral stimulation (Scharfman *et al.*, 2003).

Outside the CNS oestrus-dependent changes in intrinsic excitability of neurons have also been observed in the trigeminal ganglion where an increase in excitability in proestrus and estrus was seen in comparison to diestrus (Saleeon

et al., 2016). Here we plan to examine whether these hormonal fluctuations affect intrinsic properties of neurons located in the $BNST^{ALG}$.

1.1.1 Effect of oestrus cycle in the BNST and stress

The role of the oestrus cycle in stress processing is a complex one with the role of fluctuating hormones sometimes having opposing effects. Estrus, the stage with the lowest levels of circulating E2 and progesterone, has been found to be protective against social isolation-induced anxiety (Ramos-Ortolaza *et al.*, 2017) while also increasing susceptibility to the development of PTSD-like states in female rats (Mironova *et al.*, 2015).

The BNST plays a key role in anxiety-related disorders; these disorders also have higher incidence in females over males in the human population. Despite this there is very little research which examines the BNST in female rodents. One contributing factor for this bias is a lack of understanding of the effects of hormonal fluctuation on the intrinsic properties of BNST neurons. To address this, I compared the properties of BNST neurons from mice in each stage of oestrus to identify oestrus cycle dependent changes on intrinsic electrophysiological properties.

3.2. Hypothesis

Hormone fluctuations during oestrous cycle may lead to changes in the intrinsic properties of neuron located in the $BNST^{ALG}$. These hypothesised changes may account for expected changes in anxiety observed at different stage of the oestrous cycle.

3.3 Aims

To determine if the intrinsic properties of neurons located within the $BNST^{ALG}$ are affected by the different stages of oestrous.

1.2 Methods

This study focused on female mice aged 3-5 months; all mice used in this study were breed in house using stock from Charles River with *ab libitum* access to food and water. A proportion of animals underwent behavioural testing on the elevated zero maze; these tests were carried on the morning of experimental days. Animals were then killed by cervical dislocation, the brain was removed and placed into an ice cold sucrose solution. Once the brain was removed the stage of oestrus cycle was determined via a wet vaginal smear. 300 μm coronal slices containing the $BNST^{ALG}$ were prepared and placed into aCSF.

Whole cell patch clamp recordings were made using a K-Gluconate solution containing biocytin. A series of electrophysiological protocols were used as described in methods chapter to characterise the intrinsic properties of neurons located within the anterolateral area of the BNST. The compositions of all solutions listed here are described in detail in the methods chapter.

Determination of statistical test used was based on normal distribution of the data based on a Shapiro-Wilk normality test. A number of properties were examined from only one membrane potential, ie. firing frequency at rest; for these parameters if data was normally distributed an unpaired t-test was carried out, if data was not normally distributed a Mann-Whitney U was carried out. Part of the data were examined from two prestimulus potentials; if the data was normally distributed at both prestimulus membrane potentials a repeated measure two-way ANOVA was carried out with oestrus cycle stage as the between subject effect and prestimulus membrane potential as the within subject effect. If the data was not normally distributed a Kruskal-Wallis test was performed at each prestimulus membrane potential. If the data was normally distributed at only one prestimulus membrane potential a one-way ANOVA was carried out on this set and a Kruskal-Wallis on the non-normally distributed set. Firing frequencies in response to each depolarising current injection were analysed via repeated measure two-way ANOVA. All statistics were carried out in SPSS. Proportion of cells firing was determined by chi squared; tests were carried out in Excel.

1.3 Results

1.3.1 Behaviour

Anxiety levels were assessed using the elevated zero maze, mice were run on the maze in the early stages of their lights-on stage. Average time spent in the open arm vs dark arm was calculated over a 5 minute time period. No differences in % time spend in the open vs the closed arm were detected between the groups (Figure 3.1.1 -1, Table 3-1).

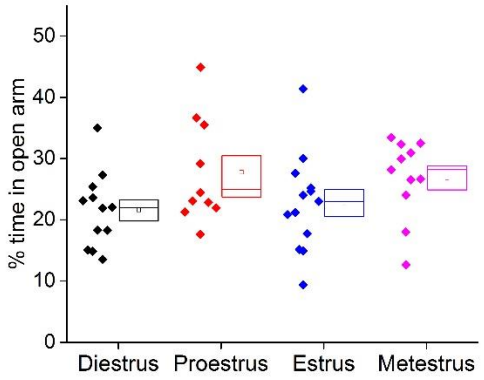

Figure 3.1.1 -1 % time spent in the open arm of the elevated zero maze.

	Diestrus	Proestrus	Estrus	Metestrus	P value	Statistical test
% time in the open arm	21 ± 2 (n = 12)	28 ± 3 (n = 10)	23 ± 2 (n = 13)	27 ± 2 (n = 11)	0.1	One-way ANOVA

Table 3-1 % time spend in the open of each cohort on the elevated zero maze

1.3.2 Electrophysiological characterisation of neurons located in the anterolateral area of the BNST

1.3.2.1 Type I neurons

A total of 66 Type I cells were recorded in this study, of these 21 were from mice in diestrus, 16 from mice in proestrus, 13 from mice in estrus and 16 from mice in metestrus. The cells in diestrus were recorded from 11 animals with a maximum of 3 cells per animals, the cells in proestrus were recorded from 8 animals with a maximum of 5 cells from each animal, the cells in estrus were recorded from 8 animals with a maximum of 4 cells being recorded from each animal and the recordings in metestrus were recorded from 11 animals with a maximum of 3 cells being recorded from each animal.

Initially I began by using voltage clamp to examine the synaptic properties of Type I neurons in the BNST. The stage of the oestrus cycle had no effect on either the amount of current required to hold cells at -70 mV, the frequency of events observed or the averaged amplitude of such events (Figure 3-2, Table 3 -2).

	Diestrus	Proestrus	Estrus	Metestrus	P value	Statistical test
I_{hold} (pA)	-10 ± 6 (n = 17)	-7 ± 6 (n = 16)	-4 ± 7 (n = 7)	-3 ± 9 (n = 13)	0.9	One-way ANOVA
Frequency (Hz)	7 ± 2 (n = 17)	9 ± 3 (n = 16)	5 ± 3 (n = 7)	6 ± 1 (n = 13)	0.6	KW
Amplitude (pA)	-14 ± 1 (n = 18)	-16 ± 1 (n = 16)	-14 ± 1 (n = 7)	-14 ± 1 (n = 13)	0.6	KW

Table 3 -2 Properties measured from VC recordings held at -70 mV. Statistical tests performed Kruskal-Wallis (KW) test or one-way ANOVA.

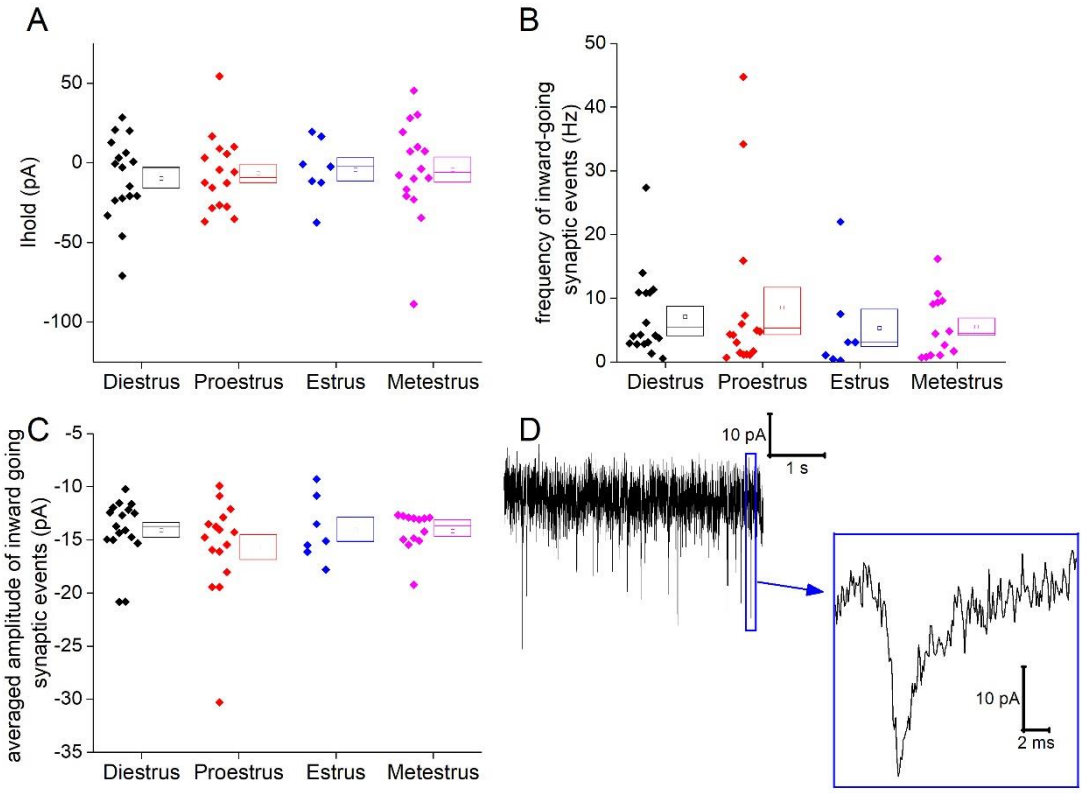

Figure 3-2. Spontaneous synaptic events in Type I neurons. A) Holding current required to hold cells at -70 mV, B) frequency of inward-going synaptic events, C) average amplitude of spontaneous inward going-synaptic events, D) Sample trace of unfiltered cell in voltage clamp mode with a zoomed in image of a synaptic event in the blue box.

Following this the cells were switched into current clamp mode where their properties at their resting membrane potential were examined. The resting membrane potential was not dependent on the stage of the oestrus cycle in Type I neurons. The proportion of cells firing action potentials in the initial 1 minute recording was also not dependent upon the oestrus cycle (estrus 8/13 cells firing, metestrus 7/16 cells firing, diestrus 9/21 cells firing, proestrus 6/10 cells firing, chi squared test , $p = 0.4$). The firing frequency of cells which were firing at rest was not affected by the oestrus cycle. Of the cells which were not firing at rest the rheobase was examined, this was not depended on the oestrus cycle (Figure 3-3, Table 3-3).

In order to assess the intrinsic properties of these cells current was injected to hold cells at a prestimulus membrane potential of either -70 mV or -80 mV; the amount of current required to hold these cells at these potentials was not dependent upon the oestrus cycle (Table 3-3).

Parameter and prestimulus membrane potential		Diestrus	Proestrus	Estrus	Metestrus	P value	Statistical test
RMP (mV)		-68 ± 2 (n = 21)	-70 ± 2 (n = 16)	-64 ± 4 (n = 13)	-70 ± 3 (n = 16)	0.4	One-way ANOVA
Frequency (Hz)		9 ± 3 (n = 9)	5 ± 2 (n = 6)	2 ± 1 (n = 8)	5 ± 2 (n = 7)	0.2	One-way ANOVA
I_{hold} (mV)	-70 mV	-11 ± 7 (n = 21)	-1 ± 7 (n = 16)	-25 ± 14 (n = 13)	-2 ± 7 (n = 14)	0.6	KW
	-80 mV	-32 ± 7 (n = 21)	-17 ± 6 (n = 16)	-44 ± 16 (n = 13)	-22 ± 8 (n = 14)	0.5	KW
Rheobase (pA)		28 ± 10 (n = 7)	28 ± 7 (n = 5)	26 ± 9 (n = 5)	26 ± 6 (n = 5)	1	One-way ANOVA

Table 3-3. Properties of cells at their resting membrane potential and holding currents, statistical tests Kruskal-Wallis (KW) test and one-way ANOVA.

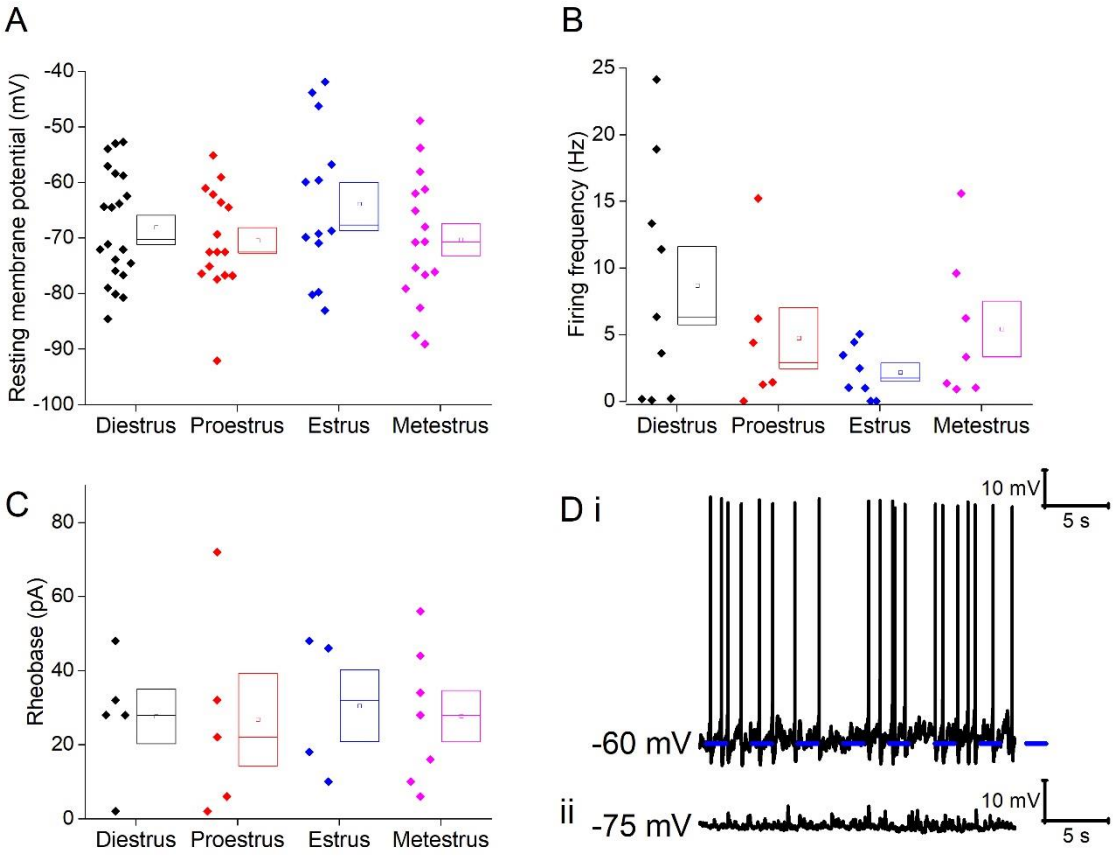

Figure 3-3 Properties of type I neurons at their resting membrane potential, A) Resting membrane potential of cells in the different stages of oestrus, B) firing frequency of cells which fired at rest, C) Rheobase of cells which did not fire at rest, D) Sample trace showing cell which was firing at rest (i) and a cell which was not firing at rest (ii).

The passive membrane properties were examined following the injection of -40 pA of current; the averages for each cohort can be seen in Figure 3-*4*. Oestrus cycle had no effect on input resistance, membrane time constant, sag or capacitance (Figure 3-*4*, Table 3-*4*).

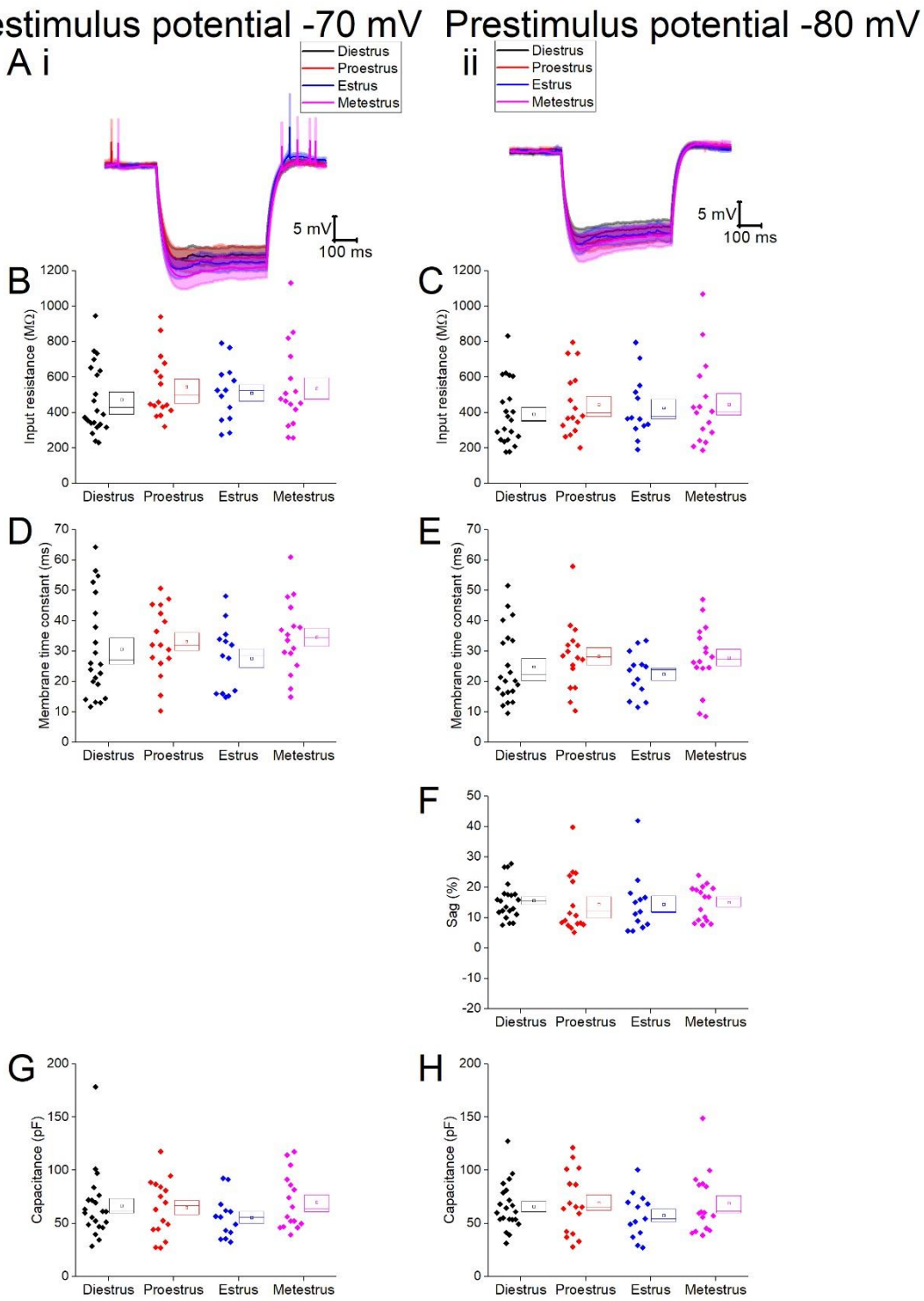

Figure 3-4 Passive membrane properties of Type I neurons, A) average trace following the injection of -40 pA of current from a prestimulus membrane potential of -70 mV (i) and -80 mV (ii), B, C) Input resistance measured frrm a prestimulus membrane potential of – 70 mV and – 80 mV respectively, D, E) Membrane time constant of cells from a prestimulus membrane potential of -70 mV and -80 mV respectively, F) % sag from a prestimulus membrane potential of -80 mV respectively, G, H) Capacitance from a prestimulus membrane potential of -70 mV and -80 mV respectively.

Parameter and holding current		Diestrus	Proestrus	Estrus	Metestrus	P	Statistical test
R_{in} (MΩ)	-70 mV	473 ± 43 (n = 21)	544 ± 45 (n = 16)	510 ± 46 (n = 13)	536 ± 59 (n = 16)	0.6	KW
	-80 mV	391 ± 39 (n = 21)	446 ± 46 (n = 16)	427 ± 49 (n = 13)	446 ± 61 (n = 16)	0.8	KW
Tau (ms)	-70 mV	31 ± 4 (n = 21)	33 ± 3 (n = 16)	28 ± 3 (n = 13)	35 ± 3 (n = 16)	0.5	KW
	-80 mV	25 ± 3 (n = 21)	28 ± 3 (n = 16)	22 ± 2 (n = 13)	28 ± 3 (n = 16)	0.4	KW
Sag (%)	-80 mV	16 ± 1 (n = 21)	15 ± 2 (n = 16)	14 ± 3 (n = 13)	15 ± 1 (n = 16)	0.5	KW
Capacitance (pF)	-70 mV	67 ± 7 (n = 21)	65 ± 7 (n = 16)	56 ± 5 (n = 13)	70 ± 7 (n = 16)	0.4	KW
	-80 mV	66 ± 5 (n = 21)	70 ± 7 (n = 16)	57 ± 6 (n = 13)	69 ± 7 (n = 16)	0.8	One-way ANOVA

Table 3-4 Passive membrane properties of Type I neurons, statistical test used were Kruskal-Wallis (KW) and one-way ANOVA.

		Diestrus	Proestrus	Estrus	Metestrus	P	Statistical test
Zenith (mV)	-70 mV	15 ± 2 (n = 21)	14 ± 2 (n = 16)	18 ± 2 (n = 13)	17 ± 2 (n = 16)	0.4	KW
	-80 mV	17 ± 2 (n = 21)	14 ± 2 (n = 16)	20 ± 2 (n = 13)	17 ± 2 (n = 16)	0.3	KW
Width (ms)	-70 mV	0.7 ± 0.03 (n = 21)	0.8 ± 0.03 (n = 16)	0.7 ± 0.03 (n = 13)	0.8 ± 0.04 (n = 16)	0.6	KW
	-80 mV	0.7 ± 0.04 (n = 21)	0.7 ± 0.04 (n = 16)	0.7 ± 0.03 (n = 13)	0.7 ± 0.05 (n = 16)	0.8	KW
Threshold (mV)	-70 mV	-52 ± 1 (n = 21)	-54 ± 2 (n = 16)	-52 ± 1 (n = 13)	-50 ± 2 (n = 16)	0.6	Repeated measure two-way ANOVA
	-80 mV	-52 ± 1 (n = 21)	-50 ± 1 (n = 16)	-50 ± 2 (n = 13)	-51 ± 1 (n = 16)		
dV/dt max (mV/ms)	-70 mV	265 ± 16 (n = 21)	234 ± 12 (n = 16)	272 ± 23 (n = 13)	282 ± 16 (n = 16)	0.2	KW
	-80 mV	294 ± 17 (n = 21)	256 ± 12 (n = 16)	308 ± 24 (n = 13)	302 ± 19 (n = 16)	0.2	KW

Table 3-5 Action potential properties of Type I neurons, statistical tests used were Kruskal-Wallis (KW) and one –way ANOVA

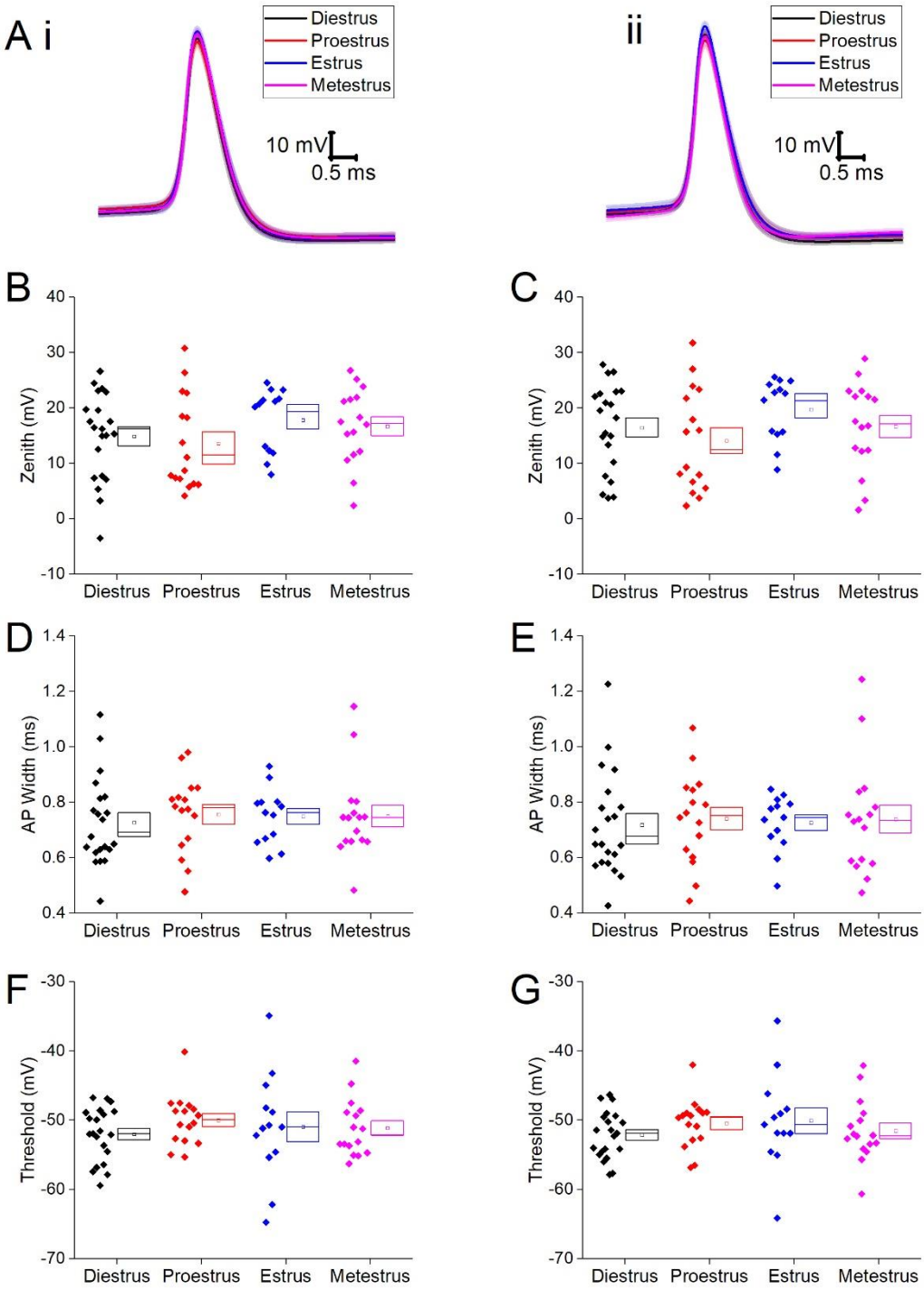

Figure 3-5. Action potential properties of Type I neurons, A) averaged action potential of the first action potential generated from a prestimulus membrane potential of -70 mV (i) and -80 mV (ii), B, C) Action potential zenith from a prestimulus membrane potential of -70 mV and -80 mV respectively, D, E) Action potential width measured at – 20 mV from a prestimulus membrane potential of -70 mV and -80 mV respectively, F, G) Threshold from prestimulus membrane potential of -70 mV and -80 mV respectively.

The action potential properties were measured from the first action potential generated in response to depolarising current injections, the averages of these are shown in Figure 3-5. The action potential zenith, width and threshold were examined; none of these were affected by the oestrus cycle (Figure 3-5, Table 3-5). We also examined the first derivative of the action potential to establish the maximum rate of rise, this was not dependent on oestrus in type I neurons (Figure 3-6, Table 3-5).

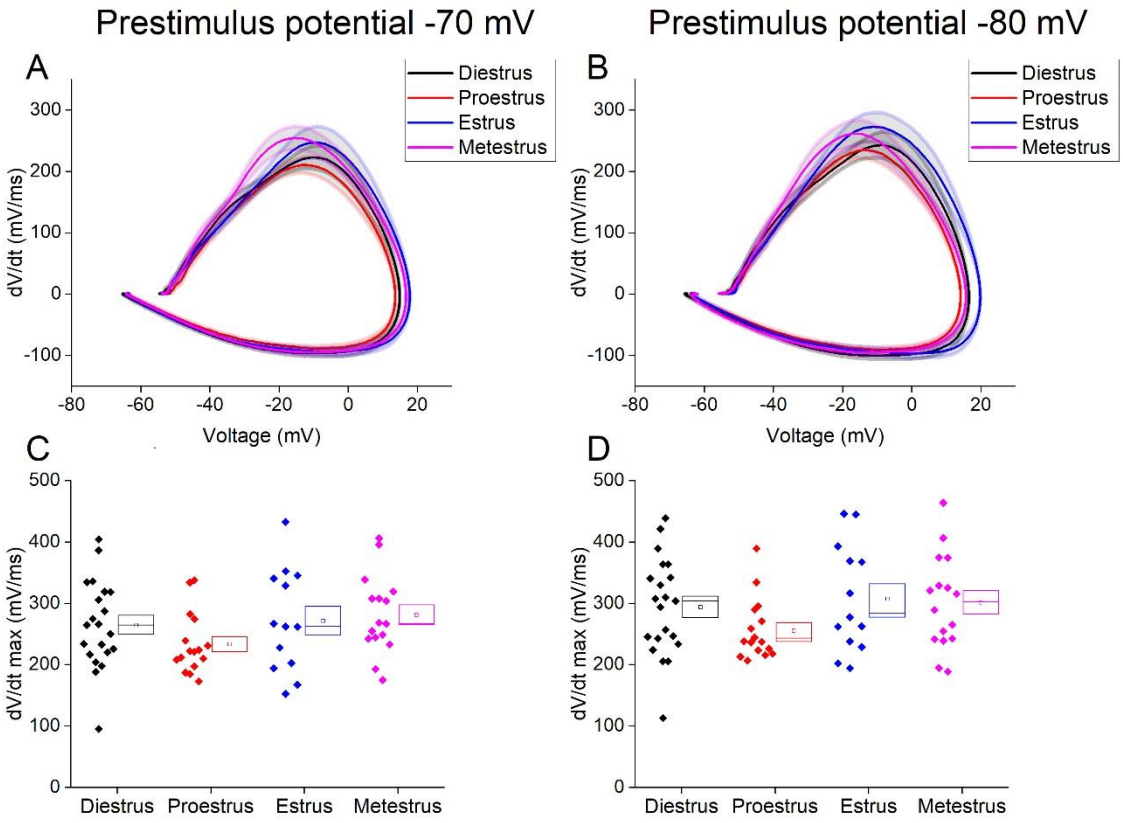

Figure 3-6. dV/dt of first action potential generated by Type I neurons, A, B) averaged dV/dt (line is the mean and shaded area is the standard error of the mean) plotted against the average action potential of cells from a prestimulus membrane potential of -70 mV and -80 mV, respectively, C, D) dV/dt maximum from a prestimulus membrane potential of -70 mV and -80 mV, respectively.

Using the series of depolarising pulses the excitability of cells was examined; neither the frequency of firing (repeated measure two-way ANOVA, $p = 0.6$) nor the proportion of cells firing were affected by the oestrus cycle (Figure 3-7,Table 3-6, Table 3-7, Table 3-8, Table 3-9). Equally rheobase was not affected by oestrus cycle (Figure 3-7, Table 3-10), this is unsurprising given the fact that

neither the resting membrane potential nor excitability on the step protocol was affected by oestrus.

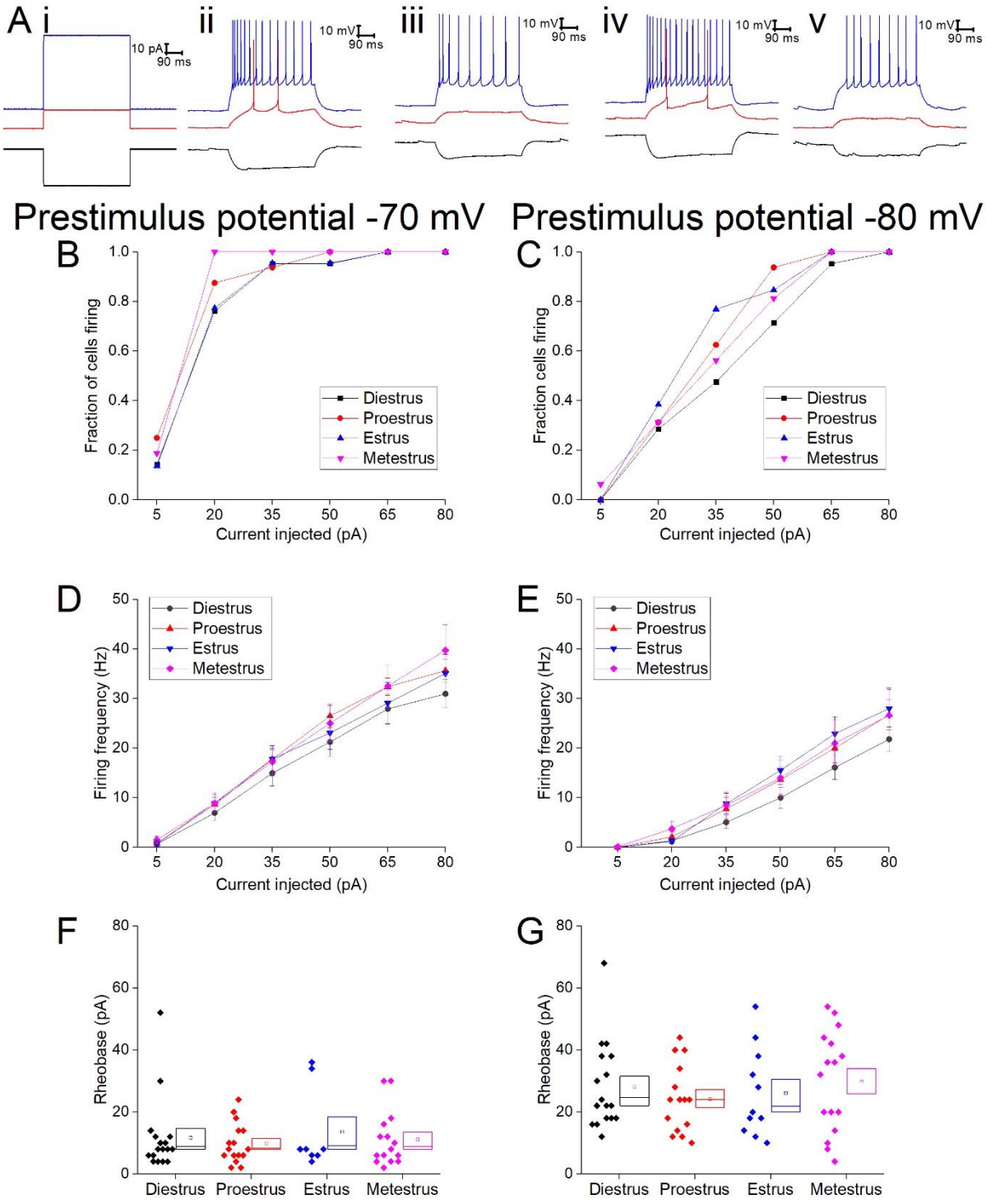

Figure 3-7 Firing properties of Type I neurons A) sample traces of cells in each stage of oestrus i) sample current injection, ii) diestrus, iii) proestrus, iv) estrus, v) metestrus, B, C) fraction of cells firing action potentials in response to various current injections from a prestimulus membrane potential of -70 mV and -80 mV respectively, D, E) frequency of firing in response to various current injections from a prestimulus membrane potential of -70 mV and -80 mV respectively, F, G) Rheobase from a prestimulus membrane potential of -70 mV and -80 mV respectively.

	Diestrus (Hz)	Proestrus (Hz)	Estrus (Hz)	Metestrus (Hz)
5 pA	1 ± 0.4	1 ± 0.4	1 ± 1	1 ± 1
20 pA	7 ± 1	9 ± 1	9 ± 2	9 ± 2
35 pA	15 ± 2	18 ± 2	18 ± 3	17 ± 3
50 pA	21 ± 3	27 ± 3	23 ± 3	25 ± 4
65 pA	28 ± 3	32 ± 2	29 ± 4	32 ± 4
80 pA	30 ± 3	36 ± 2	35 ± 4	40 ± 5

Table 3-6 Firing frequency on each current injection from a prestimulus membrane potential of -70 mV

	Diestrus	Proestrus	Estrus	Metestrus
5 pA	0 ± 0	0 ± 0	0 ± 0	0.1 ± 0.1
20 pA	1 ± 0.5	2 ± 1	1 ± 0.5	4 ± 2
35 pA	5 ± 1	8 ± 2	9 ± 2	9 ± 3
50 pA	10 ± 2	14 ± 3	16 ± 3	14 ± 4
65 pA	16 ± 2	20 ± 3	23 ± 3	21 ± 5
80 pA	22 ± 3	27 ± 3	28 ± 4	27 ± 5

Table 3-7 Firing frequency on each current injection from a prestimulus membrane potential of -80 mV

	P value	Diestrus	Proestrus	Estrus	Metestrus
5 pA	0.9	3/21	3/16	2/13	4/16
20 pA	0.2	16/21	16/16	10/13	14/16
35 pA	0.6	20/21	16/16	13/13	15/16
50 pA	0.5	20/21	16/16	13/13	16/16
65 pA	NS	21/21	16/16	13/13	16/16
80 pA	NS	21/21	16/16	13/13	16/16

Table 3-8 Proportion of cells firing in response to current injection from a prestimulus membrane potential of -70 mV

	P value	Diestrus	Proestrus	Estrus	Metestrus
5 pA	0.4	0/21	0/16	0/13	1/16
20 pA	0.9	6/21	5/16	5/13	5/16
35 pA	0.4	10/21	10/16	10/13	9/16
50 pA	0.3	15/21	15/16	11/13	13/16
65 pA	0.5	20/21	16/16	13/13	16/16
80 pA	NS	21/21	16/16	13/13	16/16

Table 3-9 Proportion of cells firing action potentials from a prestimulus membrane potential of -80 mV

Due to the speed of synaptic events the delay between onset of current injection and action potential generation is a key measure. This is referred to as the latency, it was measured in two manners, the delay between current onset and the first action potential generated in response to the complete set of incremental depolarising current injections and the delay between injection of 80 pA of current and the generation of an action potential, neither of these measurements were oestrus cycle-dependent (Figure 3-8, Table 3-10).

		Diestrus	Proestrus	Estrus	Metestrus	P	Statistical test
Rheobase (pA)	-70 mV	12 ± 3 (n = 17)	10 ± 2 (n = 15)	12 ± 4 (n = 9)	11 ± 2 (n = 15)	0.99	KW
	-80 mV	28 ± 3 (n = 17)	24 ± 3 (n = 15)	29 ± 5 (n = 9)	32 ± 4 (n = 15)	0.6	KW
Latency 1st AP (ms)	-70 mV	129 ± 32 (n = 21)	153 ± 30 (n = 16)	98 ± 32 (n = 13)	98 ± 15 (n = 16)	0.2	KW
	-80 mV	109 ± 20 (n = 21)	115 ± 20 (n = 16)	122 ± 27 (n = 13)	131 ± 24 (n = 16)	0.9	KW
AP Latency last sweep (ms)	-70 mV	14 ± 3 (n = 21)	13 ± 2 (n = 16)	10 ± 1 (n = 13)	14 ± 2 (n = 16)	0.4	KW
	-80 mV	46 ± 14 (n = 15)	32 ± 8 (n = 13)	17 ± 2 (n = 16)	35 ± 10 (n = 9)	0.3	KW

Table 3-10 firing properties of Type I neurons, statistical test performed Kruskal-Wallis (KW)

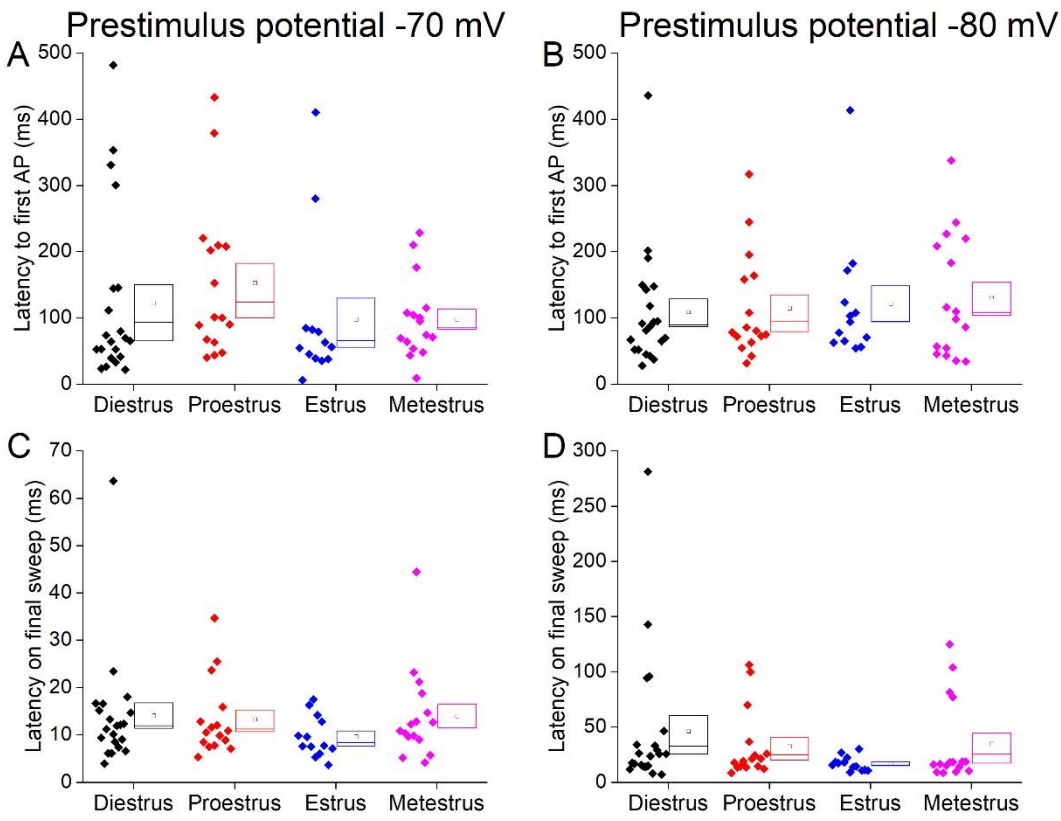

Figure 3-8 Latency to action potential generation in Type I cells A, B) latency to the first action potential generated in response to depolarising current injection from a prestimulus membrane potentials of -70 mV and -80 mV, respectively, C, D) latency to action potential generation in response to injection of 80 pA from a prestimulus membrane potential of -70 mV and -80 mV respectively.

1.3.2.2 Type II neurons

A total of 53 Type II cells were recorded from, of these cells 15 were recorded from mice in diestrus, 13 were recorded from mice in proestrus, 16 were recorded from mice in estrus and 9 were recorded from mice in metestrus. The recordings made in diestrus were recoded from 10 animals with a maximum of 3 cells recorded from each animal, the recordings made in proestrus were recorded from 8 animals with a maximum of 4 cells being recorded per animal, the recordings made in estrus were recorded from 10 animals with a maximum of 3 cells being recorded from each animal and the recordings carried out in metestrus were recorded from 7 animals with a maximum of 2 cells being recorded from each animal.

When examining the cells in voltage clamp mode no differences were found in the frequency or average amplitude of inward-going synaptic events of Type II neurons, equally the amount of current required to clamp cells at -70 mv did not depend on oestrus (Figure 3-9, Table 3-11).

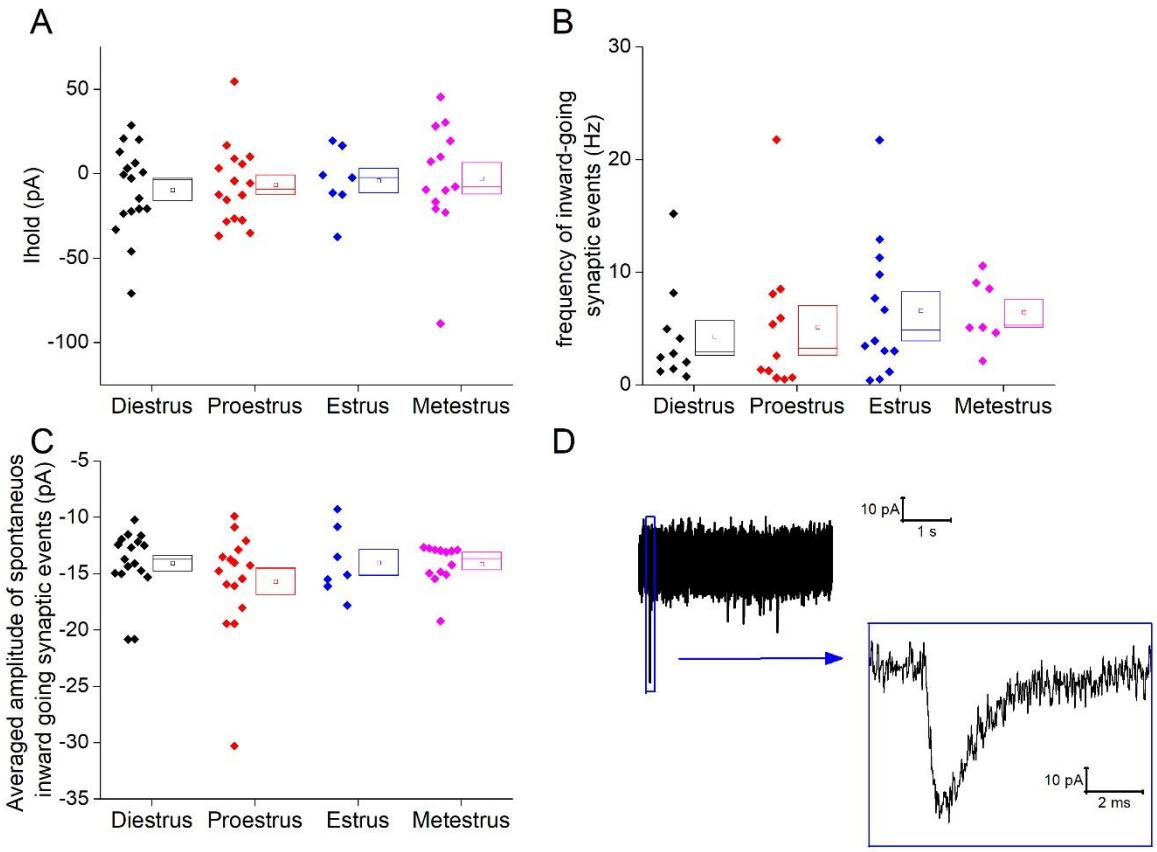

Figure 3-9. Spontaneous synaptic events in Type II neurons. A) Holding current required to hold cells at -70 mV, B) frequency of inward-going synaptic events, C) average amplitude of spontaneous inward going-synaptic events, D) Sample trace of unfiltered trace in voltage clamp mode with a zoomed in image of a synaptic event in the blue box.

	Diestrus	Proestrus	Estrus	Metestrus	P value	Statistical test
I_{hold} (pA)	-2 ± 4 (n = 10)	0 ± 7 (n = 11)	-8 ± 8 (n = 13)	-6 ± 6 (n = 7)	0.8	One-way ANOVA
Frequency (Hz)	4 ± 1 (n = 10)	5 ± 2 (n = 11)	7 ± 2 (n = 13)	6 ± 1 (n = 7)	0.4	KW
Amplitude (pA)	-12 ± 1 (n = 10)	-14 ± 1 (n = 11)	-14 ± 1 (n = 13)	-14 ± 1 (n = 7)	0.056	KW

Table 3-11. Synaptic properties of Type II neurons

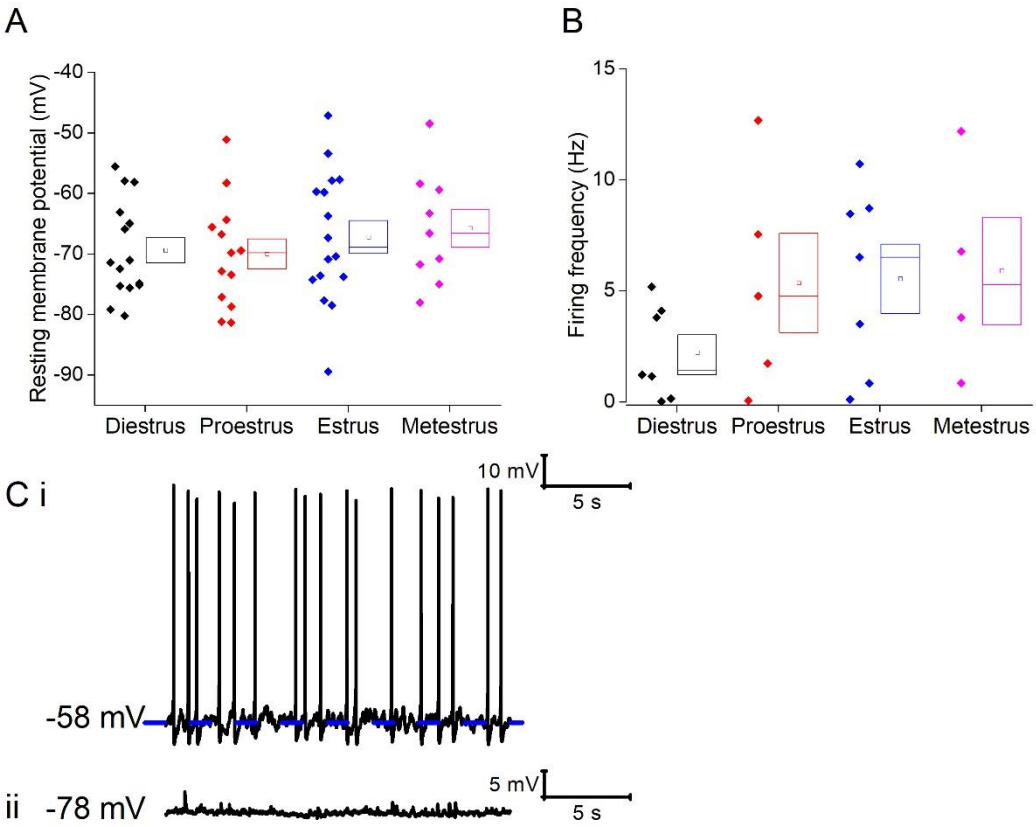

Figure 3-10. Properties of type II neurons at their resting membrane potential, A) Resting membrane potential of cells in the different stages of estrus, B) firing frequency of cells which fired at rest, C) Sample trace showing cell which was firing at rest (i) and a cell which was not firing at rest (ii).

		Diestrus	Proestrus	Estrus	Metestrus	P value	Statistical test
RMP (mV)		-69 ± 2 (n = 15)	-70 ± 2 (n = 13)	-67 ± 3 (n = 16)	-66 ± 3 (n = 9)	0.7	One-way ANOVA
Frequency (Hz)		2 ± 1 (n = 7)	5 ± 2 (n = 5)	5.5 ± 2 (n = 7)	6 ± 2 (n = 4)	0.3	One-way ANOVA
I_{hold} (mV)	-70 mV	-9 ± 5 (n = 15)	-6 ± 5 (n = 13)	-9 ± 6 (n = 14)	-7 ± 9 (n = 9)	0.9	KW
	-80 mV	-30 ± 6 (n = 15)	-31 ± 3 (n = 13)	-23 ± 7 (n = 14)	-38 ± 8 (n = 9)	0.4	KW

Table 3-12. Properties of Type II cells at their resting membrane potential

Cells were then transferred into current clamp mode where the properties of cells at their resting membrane potential were examined. The resting membrane potentials and firing frequency of firing cells which fired at rest did not differ between the cohorts (Figure 3-10, Table 3-12). Not enough observations were gathered to examine the rheobase from the resting membrane potential.

The passive membrane properties were measured from the injection of -40 pA of current: averages are shown in Figure 3-11A. Input resistance, membrane time constant, capacitance and sag were not dependent on estrus in Type II neurons (Figure 3-11, Table 3-13).

Parameter and prestimulus potential		Diestrus	Proestrus	Estrus	Metestrus	P value	Statistical test
R_{in} (MΩ)	-70 mV	453 ± 41 (n = 15)	445 ± 55 (n = 13)	571 ± 69 (n = 16)	422 ± 95 (n = 9)	0.2	KW
	-80 mV	342 ± 42 (n = 15)	339 ± 42 (n = 13)	456 ± 66 (n = 16)	315 ± 79 (n = 9)	0.2	KW
Tau (ms)	-70 mV	27 ± 2 (n = 15)	33 ± 3 (n = 13)	36 ± 3 (n = 16)	29 ± 2 (n = 9)	0.2	KW
	-80 mV	23 ± 2 (n = 15)	25 ± 2 (n = 13)	28 ± 3 (n = 16)	21 ± 3 (n = 9)	0.3	One-way ANOVA
Sag (%)	-80 mV	21 ± 2 (n = 15)	17 ± 1 (n = 13)	18 ± 2 (n = 16)	20 ± 3 (n = 9)	0.4	KW
Capacitance (pF)	-70 mV	65 ± 4 (n = 15)	78 ± 6 (n = 13)	69 ± 7 (n = 16)	85 ± 12 (n = 9)	0.4	KW
	-80 mV	77 ± 7 (n = 15)	78 ± 6 (n = 13)	70 ± 7 (n = 16)	81 ± 12 (n = 9)	0.8	One-way ANOVA

Table 3-13 Passive membrane properties of Type II neurons. Statistical test based on Kruskal-Wallis (KW) and one-way ANOVA.

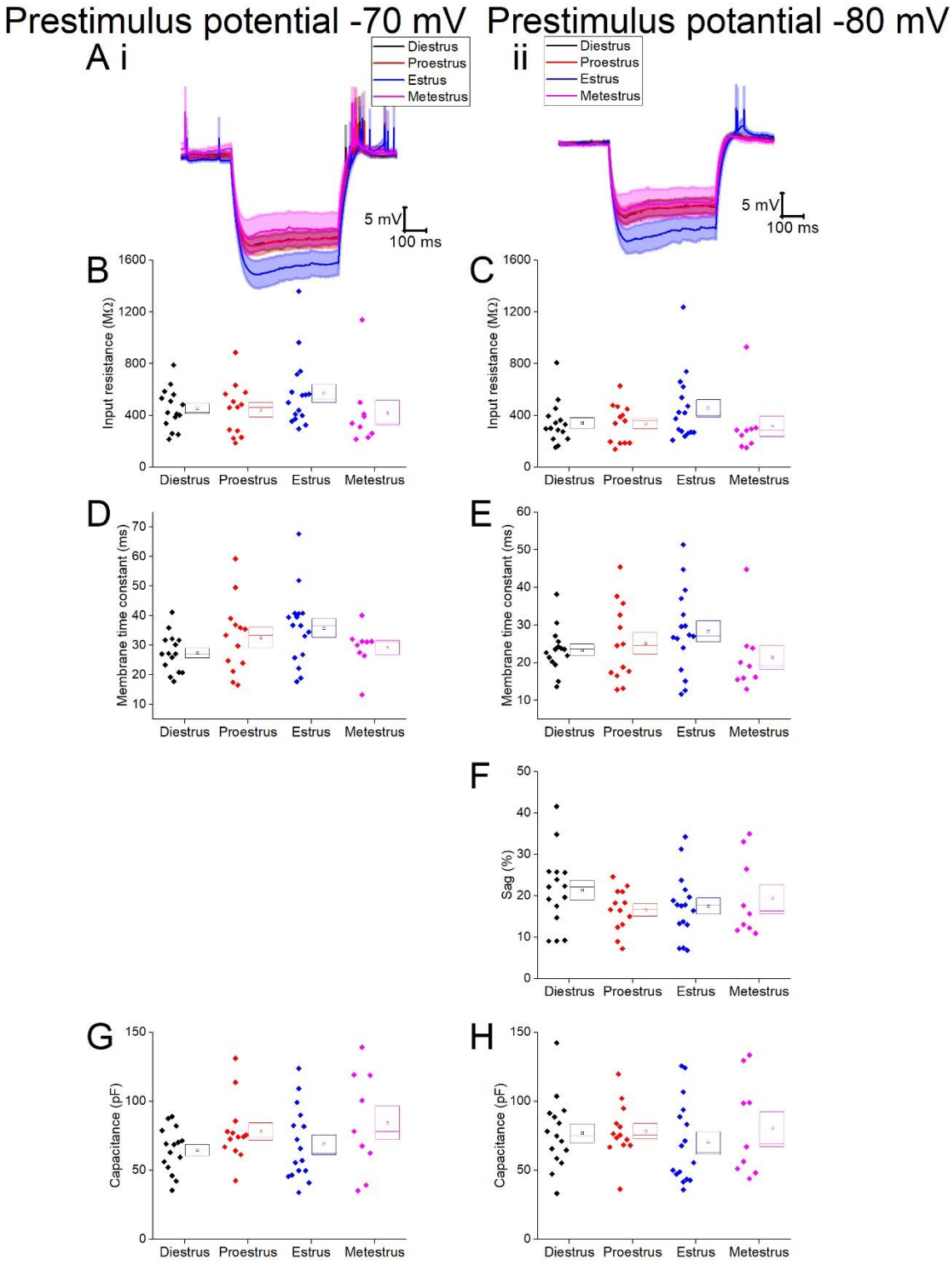

Figure 3-11 Passive membrane properties of Type II neurons, A) average trace following the injection of -40 pA of current from a prestimulus membrane potential of -70 mV (i) and -80 mV (ii), B, C) Input resistance from a prestimulus membrane potential of – 70 mV and – 80 mV respectively, D, E) Membrane time constant of cells from a prestimulus membrane potential of -70 mV and -80 mV, respectively, F) % sag from a prestimulus membrane potential of -70 mV G, H) Capacitance from a prestimulus membrane potential of -70 mV and -80 mV respectively.

Following this I examined the action potential properties; the averages are shown in Figure 3-12A. There were no differences observed in action potential zenith, width or threshold from either holding potential (Figure 3-12, Table 3-14). Following this the first derivative of the action potential was examined and the maximum rate of rise determined, averages of the rate of rise plotted against the average action potential are shown in Figure 3-13 A, B. No statistically significant differences were observed in the maximum rate of rise, however there was a trend towards a lower maximum rate of rise in diestrus when compared to metestrus (LSD post hoc analysis, p = 0.02) and proestrus (LSD post hoc analysis p = 0.03).

Following this I examined the firing properties of Type II neurons, a sample trace from each cohort is displayed in Figure 3-14A; no changes were found in the proportion of cells firing (Table 3-17, Table 3-18) or the frequency of firing of cells (Table 3-15, Table 3-16, repeated measure two-way ANOVA, p = 0.9) in response to depolarising current injection, there were also no differences in rheobase or latency of action potentials (Figure 3-14, Figure 3-15, Table 3-19).

		Diestrus	Proestrus	Estrus	Metestrus	P value	Statistical test
Zenith (mV)	-70 mV	10 ± 2 (n = 15)	16 ± 1 (n = 13)	14 ± 3 (n = 16)	16 ± 2 (n = 9)	0.8	KW
	-80 mV	11 ± 2 (n = 15)	16 ± 2 (n = 13)	16 ± 3 (n = 16)	17 ± 2 (n = 9)	0.6	KW
Width (ms)	-70 mV	0.75 ± 0.03 (n = 15)	0.7 ± 0.03 (n = 13)	0.8 ± 0.03 (n = 16)	0.7 ± 0.03 (n = 9)	0.3	Repeated measure two-way ANOVA
	-80 mV	0.7 ± 0.03 (n = 15)	0.7 ± 0.03 (n = 13)	0.8 ± 0.04 (n = 16)	0.7 ± 0.03 (n = 9)		
Threshold (mV)	-70 mV	-52 ± 1 (n = 15)	-54 ± 2 (n = 13)	-52 ± 1 (n = 16)	-50 ± 2 (n = 9)	0.7	KW
	-80 mV	-54 ± 1 (n = 15)	-53 ± 1 (n = 13)	-54 ± 1 (n = 16)	-51 ± 2 (n = 9)	0.8	KW
dV/dt max (mV/ms)	-70 mV	222 ± 13 (n = 15)	271 ± 15 (n = 13)	236 ± 14 (n = 16)	279 ± 18 (n = 9)	0.055	Repeated measure two-way ANOVA
	-80 mV	256 ± 15 (n = 15)	298 ± 15 (n = 13)	273 ± 16 (n = 16)	308 ± 19 (n = 9)		

Table 3-14 Action potential properties of Type II neurons, statistical tests used Kruskal-Wallis (KW) and repeated measure two-way ANOVA.

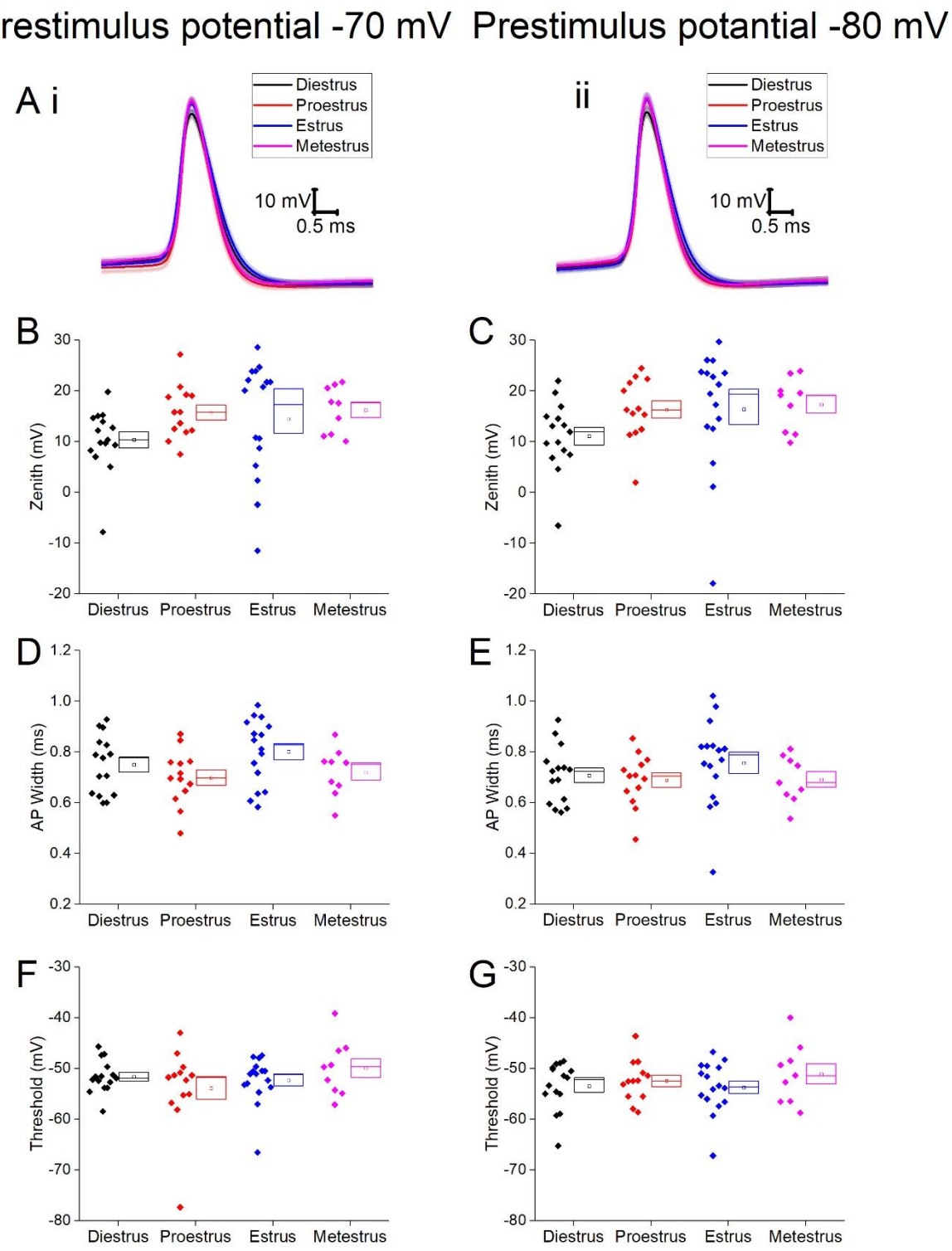

Figure 3-12. Action potential properties of Type II neurons, A) averaged action potential of the first action potential generated, B, C) Action potential zenith from a prestimulus membrane potential of -70 mV and -80 mV, respectively, D, E) Action potential width measured from – 20 mV from a prestimulus membrane potential of -70 mV and -80 mV, respectively, F, G) Threshold from a prestimulus membrane potential of -70 mV and -80 mV, respectively.

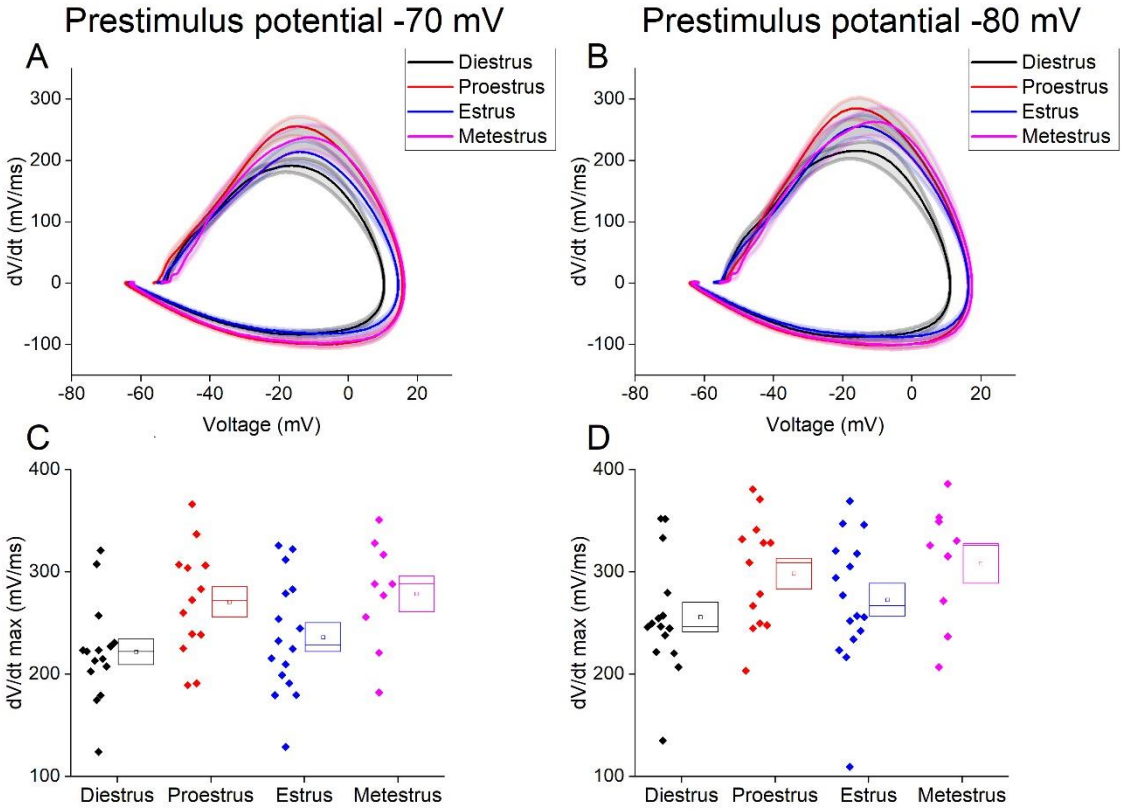

Figure 3-13. dV/dt of first action potential generated by Type II neurons, A, B) averaged dV/dt (shaded area Standard error of the mean) plotted against the average action potential on cells from a prestimulus membrane potential of -70 mV and -80 mV, respectively, C, D) dV/dt maximum from a prestimulus membrane potential of -70 mV and -80 mV, respectively.

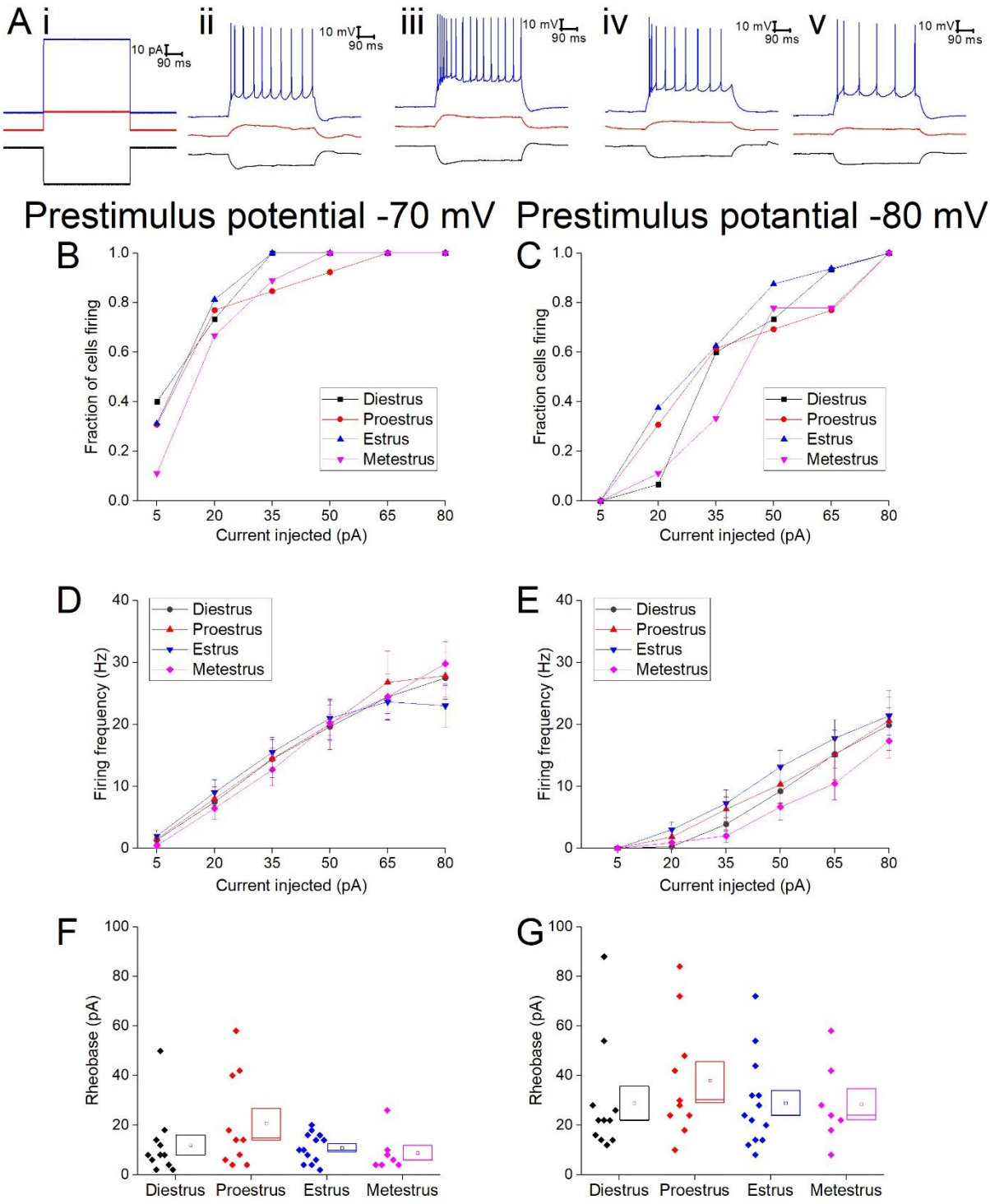

Figure 3-14. Firing properties of Type II neurons A) sample traces of cells in each stage of the oestrus cycle i) Diestrus, ii) Proestrus, iii) Estrus, iv) Metestrus, B, C) fraction of cells firing action potentials in response to various current injections from prestimulus membrane potentials of -70 mV and -80 mV, respectively, D, E) frequency of firing in response to various current injections from a prestimulus membrane potential of -70 mV and -80 mV, respectively, F, G) Rheobase from a prestimulus membrane potential of -70 mV and -80 mV, respectively.

	Diestrus (n = 15)	Proestrus (n = 13)	Estrus (n = 16)	Metestrus (n = 9)
5 pA	1 ± 0.5	2 ± 1	2 ± 1	0.4 ± 0.4
20 pA	7 ± 1	8 ± 2	9 ± 2	6 ± 2
35 pA	14 ± 2	14 ± 3	15 ± 2	13 ± 2
50 pA	20 ± 2	20 ± 4	21 ± 3	20 ± 3
65 pA	24 ± 3	27 ± 5	24 ± 3	24 ± 4
80 pA	27 ± 3	28 ± 4	23 ± 3	30 ± 4

Table 3-15 Firing frequency on each current injection from a prestimulus membrane potential of -70 mV

	Diestrus (n = 15)	Proestrus (n = 13)	Estrus (n = 16)	Metestrus (n = 9)
5 pA	0 ± 0	0 ± 0	0 ± 0	0 ± 0
20 pA	0.3 ± 0.2	2 ± 1	3 ± 1	1 ± 1
35 pA	4 ± 1	6 ± 2	7 ± 2	2 ± 1
50 pA	9 ± 2	10 ± 3	13 ± 3	7 ± 2
65 pA	15 ± 2	15 ± 4	18 ± 3	10 ± 3
80 pA	20 ± 3	21 ± 5	21 ± 3	17 ± 3

Table 3-16 Firing frequency on each current injection from a prestimulus membrane potential of -80 mV

	P value	Diestrus	Proestrus	Estrus	Metestrus
5 pA	0.5	6/15	4/13	5/16	1/9
20 pA	0.9	11/15	10/13	13/16	6/9
35 pA	0.2	15/15	11/13	16/16	8/9
50 pA	0.4	15/15	12/13	16/16	9/9
65 pA	NS	15/15	13/13	16/16	9/9
80 pA	NS	15/15	13/13	16/16	9/9

Table 3-17 Proportion of cells firing action potentials from a prestimulus membrane potential of -70 mV

	P value	Diestrus	Proestrus	Estrus	Metestrus
5 pA	NS	0/15	0/13	0/16	0/9
20 pA	0.1	1/15	4/13	6/16	1/9
35 pA	0.5	9/15	8/13	10/16	3/9
50 pA	0.7	11/15	9/13	14/16	7/9
65 pA	0.4	14/15	10/13	15/16	7/9
80 pA	NS	15/15	13/13	16/16	9/9

Table 3-18 Proportion of cells firing action potentials from a prestimulus membrane potential of -80 mV

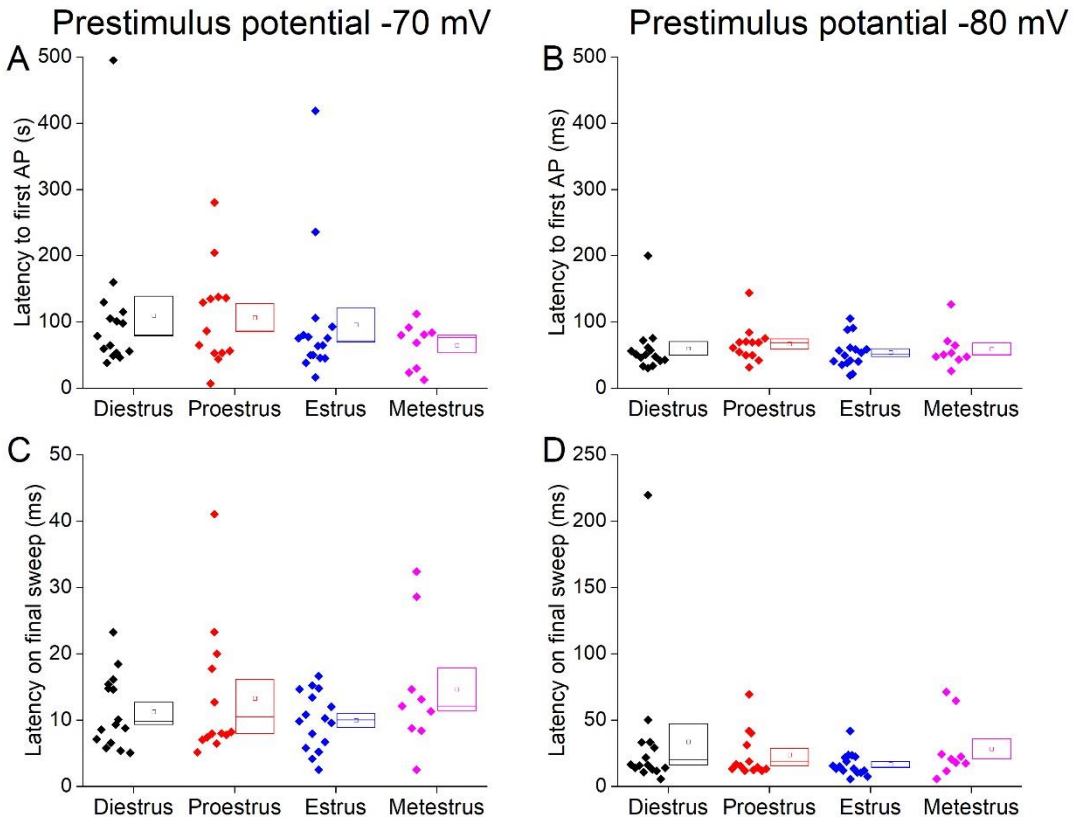

Figure 3-15 Latency to action potential generation in Type II cells A, B) Latency to the first action potential generated in response to depolarising current injection from a prestimulus membrane potential of -70 mV and -80 mV, respectively, C, D) latency to action potential generation in response to injection of 80 pA from a prestimulus membrane potential of -70 mV and -80 mV, respectively.

		Diestrus	Proestrus	Estrus	Metestrus	P value	Statistical test
Rheobase (pA)	-70 mV	12 ± 4 (n = 11)	21 ± 6 (n = 10)	11 ± 2 (n = 13)	9 ± 3 (n = 7)	0.4	KW
	-80 mV	29 ± 7 (n = 11)	38 ± 8 (n = 10)	29 ± 5 (n = 13)	29 ± 5 (n = 7)	0.6	KW
Latency 1st AP (ms)	-70 mV	110 ± 29 (n = 15)	106 ± 21 (n = 13)	96 ± 25 (n = 16)	65 ± 11 (n = 9)	0.6	KW
	-80 mV	60 ± 11 (n = 15)	67 ± 8 (n = 13)	54 ± 6 (n = 16)	59 ± 9 (n = 9)	0.4	KW
Latency last sweep (ms)	-70 mV	11 ± 1 (n = 15)	13 ± 3 (n = 13)	10 ± 1 (n = 16)	15 ± 3 (n = 9)	0.7	KW
	-80 mV	34 ± 14 (n = 15)	24 ± 5 (n = 13)	17 ± 2 (n = 16)	28 ± 8 (n = 9)	0.5	KW

Table 3-19 firing properties of Type II neurons

Type III neurons

Four Type III cells were recorded from Estrus and proestrus, five Type III cells were recorded from Metestrus, Diestrus. No more than two Type III cells were recorded from each animals.

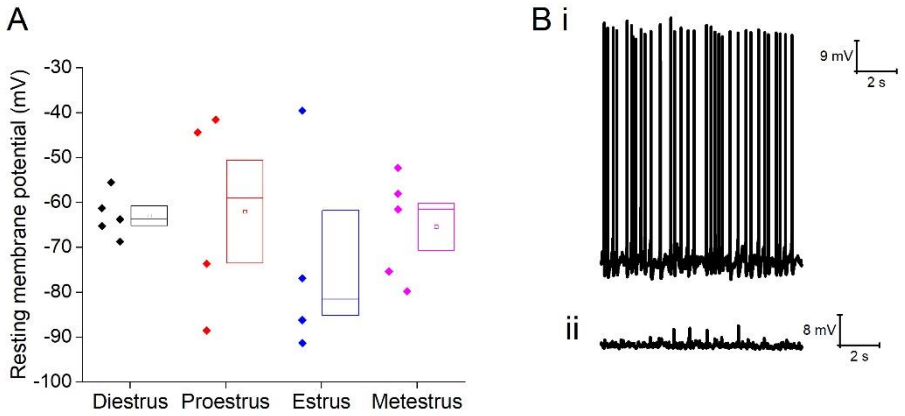

Figure 3-16 Resting membrane potential of Type III cells in the different stages of estrus (A). Sample cell firing at rest (ii) and not firing at rest (ii).

		Diestrus	Proestrus	Estrus	Metestrus	P value	Statistical test
RMP (mV)		-63 ± 2 (n = 5)	-62 ± 9 (n = 4)	-74 ± 12 (n = 4)	-65 ± 5 (n = 5)	0.7	One-way ANOVA
I_{hold} (mV)	-70 mV	-37 ± 21 (n = 4)	-32 ± 31 (n = 4)	24 ± 28 (n = 4)	-23 ± 23 (n = 5)	0.4	Repeated measure two-way ANOVA
	-80 mV	-29 ± 12 (n = 4)	-58 ± 40 (n = 4)	-11 ± 19 (n = 4)	-28 ± 19 (n = 5)		

Table 3-20 Properties of Type III cells at their resting membrane potential

Cells were then transferred into current clamp mode where the properties of cells at their resting membrane potential were examined. The resting membrane potentials did not differ between the cohorts or the amount of current required to hold cells at either holding potentials (Figure 3-10, Table 3-12). Not enough observations were gathered to examine the rheobase or firing frequency from the resting membrane potential.

The passive membrane properties were measured from the injection of -40 pA of current, averages are shown in Figure 3-11A; input resistance, membrane time constant, capacitance were not dependent on estrus in Type II neurons

(Figure 3-11, Table 3-13). Sag was not examined as a lack of sag was the key factor in identifying these cells as Type III.

Parameter and prestimulus potential		Diestrus	Proestrus	Estrus	Metestrus	P value	Statistical test
R_{in} (MΩ)	-70 mV	351 ± 137 (n = 5)	371 ± 47 (n = 4)	388 ± 98 (n = 4)	515 ± 83 (n = 5)	0.2	Repeated measure two=way ANOVA
	-80 mV	536 ± 130 (n = 5)	288 ± 39 (n = 4)	311 ± 56 (n = 4)	460 ± 53 (n = 5)		
Tau (ms)	-70 mV	20 ± 7 (n = 5)	28 ± 4 (n = 4)	34 ± 12 (n = 4)	31 ± 8 (n = 5)	0.8	Repeated measure two-way ANOVA
	-80 mV	28 ± 6 (n = 5)	24 ± 4 (n = 4)	33 ± 15 (n = 4)	25 ± 5 (n = 5)		
Capacitance (pF)	-70 mV	59 ± 9 (n = 5)	76 ± 1 (n = 4)	79 ± 12 (n = 4)	59 ± 10 (n = 5)	0.3	Repeated measure two-way ANOVA
	-80 mV	60 ± 12 (n =)	84 ± 4 (n =)	100 ± 41 (n =)	57 ± 11 (n =)		

Table 3-21 Passive membrane properties of Type III neurons, statistical test based on Kruskal-Wallis (KW) and one-way ANOVA.

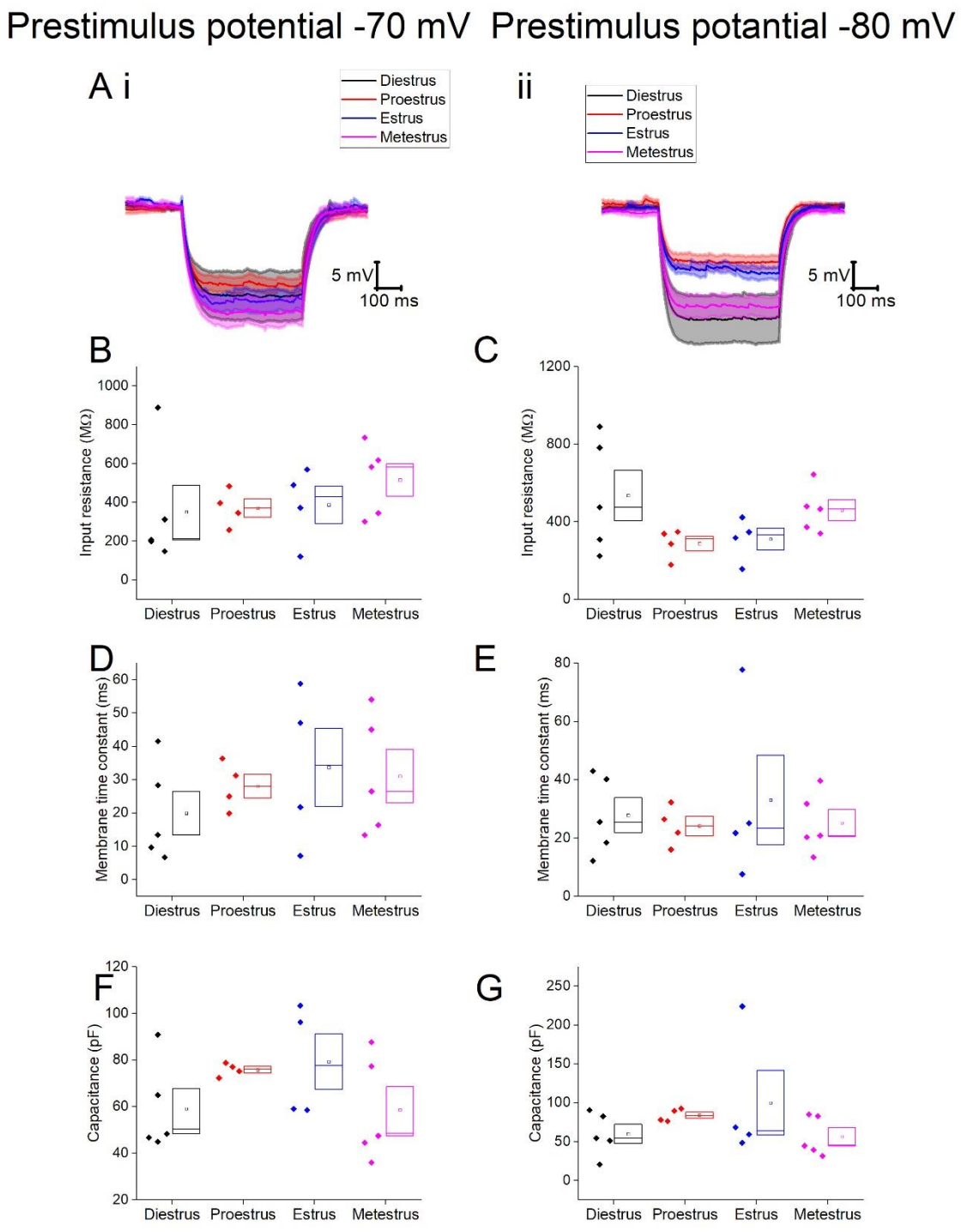

Figure 3-17 Passive membrane properties of Type III neurons, A) average trace following the injection of -40 pA of current from a prestimulus membrane potential of -70 mV (i) and -80 mV (ii), B, C) Input resistance from a prestimulus membrane potential of – 70 mV and – 80 mV respectively, D, E) Membrane time constant of cells from a prestimulus membrane potential of -70 mV and -80 mV, respectively, F, G) Capacitance from a prestimulus membrane potential of -70 mV and -80 mV respectively.

Following this I examined the action potential properties; there were no differences observed in action potential zenith or threshold from either holding

potential. Following this the first derivative of the action potential was examined and the maximum rate of rise was determined. No statistically significant differences were observed in the maximum rate of rise (Figure 3-12, Table 3-14). There was a significant effect of oestrous cycle on AP width however using Bonferroni post hoc analysis no statistically significant effects were observed.

Following this I examined the firing properties of Type III neurons, a sample trace from each cohort is displayed in Figure 3-14A; no changes were found in the frequency of firing of cells (Table 3-15, Table 3-16, repeated measure two-way ANOVA, p = 0.2) in response to depolarising current injections. The proportion of cells firing was not examined in this cohort as this requires n numbers above five which were not present in this group.

		Diestrus	Proestrus	Estrus	Metestrus	P value	Statistical test
Zenith (mV)	-70 mV	9 ± 7 (n = 5)	8 ± 7 (n = 4)	16 ± 4 (n = 4)	21 ± 4 (n = 5)	0.4	Repeated measure two-way ANOVA
	-80 mV	14 ± 7 (n = 5)	10 ± 7 (n = 4)	16 ± 4 (n = 4)	21 ± 3 (n = 5)		
Width (ms)	-70 mV	0.6 ± 0.07 (n = 5)	0.9 ± 0.1 (n = 4)	1 ± 0.1 (n = 4)	0.7 ± 0.01 (n = 5)	0.02	Repeated measure two-way ANOVA
	-80 mV	0.7 ± 0.1 (n =)	0.9 ± 0.1 (n = 4)	1 ± 0.1 (n = 4)	0.6 ± 0.04 (n = 5)		
Threshold (mV)	-70 mV	-51-± 5 (n = 5)	-55 ± 4 (n = 4)	-50 ± 2 (n = 4)	-50 ± 3 (n = 5)	0.6	Repeated measure two-way ANOVA
	-80 mV	-46 ± 3 (n = 5)	-52 ± 3 (n = 4)	-53 ± 4 (n = 4)	-50 ± 2 (n = 5)		
dV/dt max (mV/ms)	-70 mV	244 ± 54 (n = 5)	206 ± 59 (n = 4)	239 ± 39 (n = 4)	310 ± 17 (n = 5)	0.2	Repeated measure two-way ANOVA
	-80 mV	261 ± 63 (n = 5)	213 ± 59 (n = 4)	244 ± 28 (n = 4)	335 ± 11 (n = 5)		

Table 3-22 Action potential properties of Type II neurons, statistical tests used Kruskal-Wallis (KW) and repeated measure two-way ANOVA.

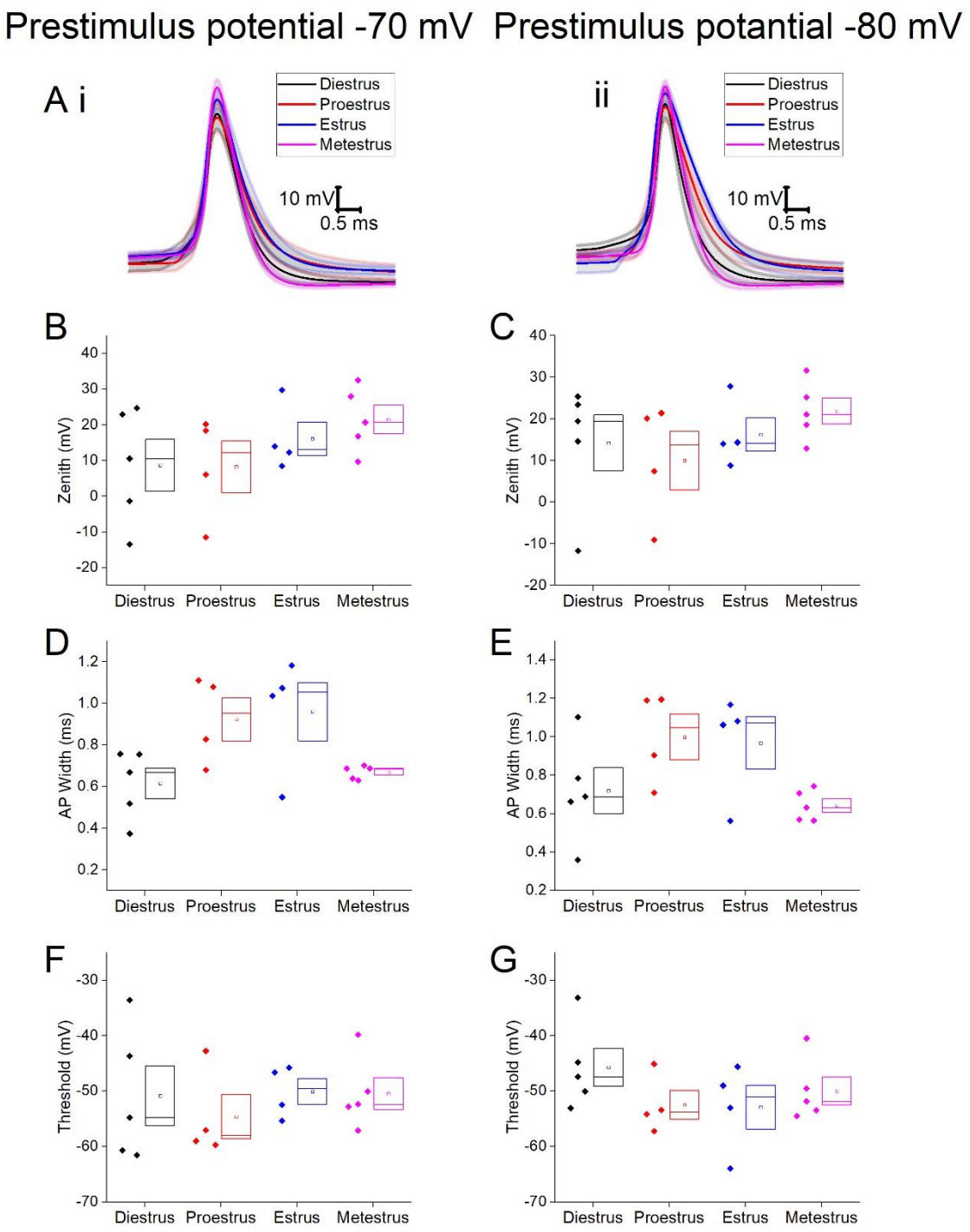

Figure 3-18 Action potential properties of Type III neurons, A) averaged action potential of the first action potential generated, B, C) Action potential zenith from a prestimulus membrane potential of -70 mV and -80 mV, respectively, D, E) Action potential width measured from – 20 mV from a prestimulus membrane potential of -70 mV and -80 mV, respectively, F, G) Threshold from a prestimulus membrane potential of -70 mV and -80 mV, respectively.

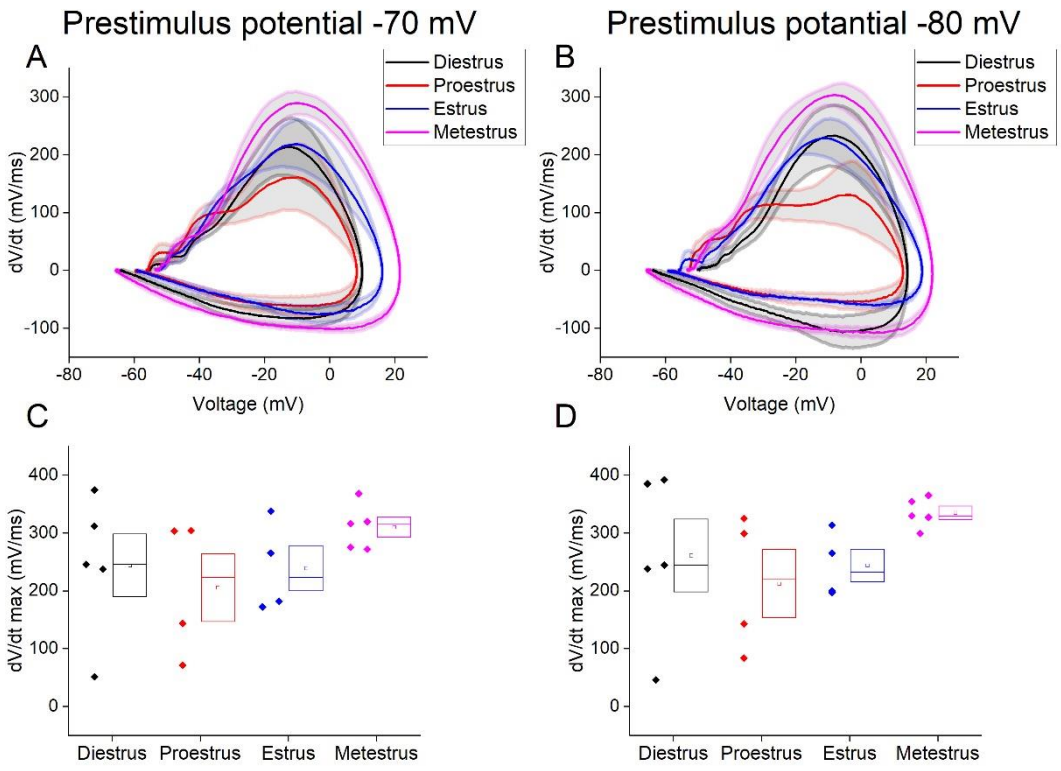

Figure 3-19 dV/dt of first action potential generated by Type III neurons, A, B) averaged dV/dt (shaded area Standard error of the mean) plotted against the average action potential on cells from a prestimulus membrane potential of -70 mV and -80 mV, respectively, C, D) dV/dt maximum from a prestimulus membrane potential of -70 mV and -80 mV, respectively.

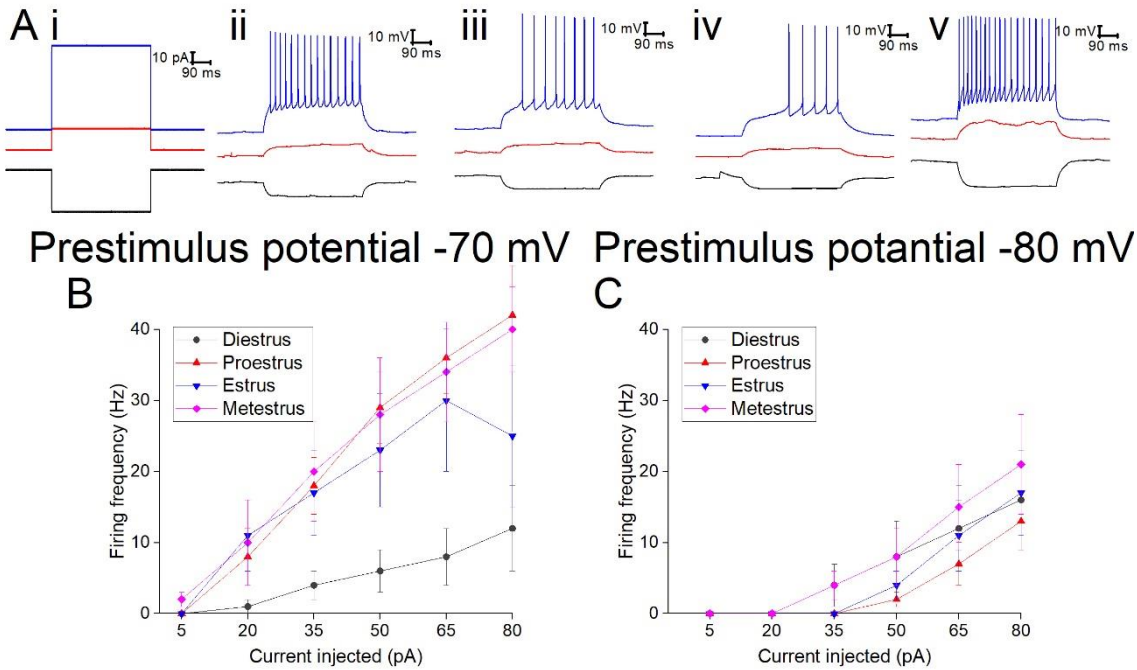

Figure 3-20 Firing properties of Type III neurons A) sample traces of cells in each stage of the oestrus cycle i) Diestrus, ii) Proestrus, iii) Estrus, iv) Metestrus, B, C) fraction of cells firing action potentials in response to various current injections from prestimulus membrane potentials of -70 mV and -80 mV, respectively, D, E) frequency of firing in response to various current injections from a prestimulus membrane potential of -70 mV and -80 mV respectively, F, G) Rheobase from a prestimulus membrane potential of -70 mV and -80 mV, respectively.

	Diestrus (n = 5)	Proestrus (n = 4)	Estrus (n = 4)	Metestrus (n = 5)
5 pA	0 ± 0	0 ± 0	0 ± 0	2 ± 1
20 pA	1 ± 1	8 ± 4	11 ± 5	10 ± 6
35 pA	4 ± 2	18 ± 4	17 ± 6	20 ± 7
50 pA	6 ± 3	29 ± 5	23 ± 8	28 ± 8
65 pA	8 ± 4	36 ± 5	30 ± 10	34 ± 7
80 pA	12 ± 6	42 ± 7	25 ± 10	40 ± 6

Table 3-23 Firing frequency on each current injection from a prestimulus membrane potential of -70 mV

	Diestrus (n = 5)	Proestrus (n = 4)	Estrus (n = 4)	Metestrus (n = 5)
5 pA	0 ± 0	0 ± 0	0 ± 0	0 ± 0
20 pA	0 ± 0	0 ± 0	0 ± 0	0 ± 0
35 pA	4 ± 3	0 ± 0	0 ± 0	4 ± 2
50 pA	8 ± 5	2 ± 1	4 ± 2	8 ± 4
65 pA	12 ± 6	7 ± 3	11 ± 5	15 ± 6
80 pA	16 ± 7	13 ± 4	17 ± 6	21 ± 7

Table 3-24 Firing frequency on each current injection from a prestimulus membrane potential of -80 mV

1.4 Discussion

This study examined neurons located within the $BNST^{ALG}$ across the four stages of oestrus to determine the effect of circulating hormones on intrinsic neurophysiological properties. These data would suggest that oestrus cycle has minimal effect on the intrinsic properties of neurons in the $BNST^{ALG}$. No statistically significant effect was seen on any parameter examined with only one trend being seen in maximum rate of rise of action potentials of Type II neurons.

The electrophysiological characterisation of BNST neurons was originally based on male rats; these have since been expanded to mice and even primates (Daniel *et al.*, 2017). Here we have shown that a similar classification can also be applied to female mice and that the amount of variability across the stages of oestrus is minimal. The BNST plays a key role in a number of anxiety-related disorders including GAD and PTSD, as discussed in the introduction, however the electrophysiological characterisation of this key brain region is currently biased towards males, despite far higher incidences of these pertinent disorders being diagnosed in females. To my knowledge, only one study examining electrophysiological properties has contained female mice (Silberman *et al.*, 2013). In this study male and female mice were examined in the same cohort, neither the sexually dimorphic nature of this brain region nor the influences of oestrus cycle were addressed in the Silberman et al study perhaps due to limited numbers of transgenic mice.

Drops in progesterone levels have been shown to lead to changes in plasticity of $GABA_A$ receptors in various brain regions. In the PAG changes in endogenous hormone levels lead to changes in subunit expression of the $GABA_A$ receptor; in diestrus mice there is an increase in expression of the δ subunit (Brack & Lovick, 2007*a*). The delta subunit causes extrasynaptic placement of the $GABA_A$ receptor leading to tonic inhibition. Through a decrease in input resistance (shunting inhibition) as well as a possible hyperpolarization of the resting potential increases in tonic inhibition would typically lead to decreased excitability (Kullmann *et al.*, 2005; Marowsky & Vogt, 2014), although this would, to some extent, depend on the nature of Cl^- equilibrium potential. In the PAG the plastic changes in $GABA_A$ receptors appear to be limited to GABAergic neurons. The BNST is a primarily GABAergic

population making it a possible target to observe similar effects however no changes in excitability or input resistance were observed in either population in this study.

The one observed trend was seen in the maximum rate of rise of the action potential which was lower in diestrus in comparison to metestrus and proestrus. The central role of voltage gated sodium channels in the rising phase of the action potential would indicate some alteration in function of these channels. Progesterone has been shown to act as σ-receptors where it inhibits endogenous ligands.; These endogenous ligands are capable of modulating voltage gated sodium channels in HEK293 cells (Johannessen *et al.*, 2011). The σ-receptors is also found in the BNST (Lein *et al.*, 2007) therefore similar actions may be taking place within the BNST. During diestrus circulating progesterone levels are at their lowest, the largest peak in progesterone levels is observed in proestrus while a smaller peak is observed in metestrus. These peeks in progesterone could be altering the rate of rise of these action potentials via indirect interactions with voltage gated sodium channels.

Chen et al 2009 found increased neuronal activity within the BNST during estrus in comparison to proestrus when exposed to predator scent (Chen *et al.*, 2009). The Chen et al study was carried out *in vivo* while this study took place in vitro; due to the nature of *in vitro* slice preparation the afferent connections into this region are lost however the axonal projections would remain and no differences were observed in synaptic events or in excitability. It is possible that exposure to a stressor causes differences; no stressors were introduced to these animals.

In the neurophysiological literature as a whole there is a distinct biased towards the use of male animals, a contributing reason for this is the uncertainty regarding the neuronal effects of the oestrus cycle. This can have detrimental effects especially when examining anxiety-related disorders such as general anxiety disorder and PTSD which have far higher incidences in the female population. This bias carries through to the clinic where changes in procedure to include more females in clinical trials has still not lead to necessary changes in drug development (Mazure & Jones, 2015). Here, we have shown that the intrinsic properties of Type I and Type II neurons in the BNST appear largely

unaffected by the oestrus cycle. In future studies related to the BNST I propose the use of both genders to ensure an accurate understanding of this key brain region and the circuits in which it participates.

4. In the BNST type II neurons show higher excitability in males than in females

4.1. Introduction

Despite our understanding of the sexually dimorphic properties of the brain the electrophysiological characterisations of various brain regions including the BNST are often biased toward males. A common reason for this is the uncertainty of the effect of the oestrus cycle on neuronal properties and the variability of female data due to hormone fluctuations. In the previous chapter, I have addressed the effect of the oestrus cycle on the intrinsic properties of cells in the BNST and found no statistically significant effects; as no statistically significant effects were observed the cohort was grouped together for comparison with age matched males from the same colony.

In humans, incidences of anxiety-related disorders are ~60% higher in females than males (Kessler *et al.*, 2005), and in the case of PTSD they are twice as high. Some controversy still surrounds the basis for this and while a component of this may be down to societal effects of gender roles, eg. females are far more likely to experience sexual trauma, a key instigator for PTSD, the stress system in mammals is sexually dimorphic. In particular, as discussed in the introduction, the sexually dimorphic properties of the BNST are quite well characterised. This key circuit is also responsible for carrying out sex-specific behaviours such as maternal behaviours (Numan & Numan, 1995, 1996), heightened aggression in males (Masugi-Tokita *et al.*, 2016) and reproductive behaviours in both males and females (Emery & Sachs, 1976; Claro *et al.*, 1995; Liu *et al.*, 1997; Klampfl *et al.*, 2016).

Circulating levels of a number of hormones greatly differ between males and females, for example levels of ALLO are 8 -10 fold higher in females than in males (Purdy *et al.*, 1990; Corpéchot *et al.*, 1993; Cheney *et al.*, 1995) . ALLO is a neuroactive metabolite of progesterone thought to be involved in anxiety (Shen *et al.*, 2007). Components of these actions are mediated via the BNST, for example systemic administration of ALLO blocks CRH-enhanced startle in female rats (Toufexis *et al.*, 2004), a BNST-mediated response.

Gaboxadol (4,5,6,7-Tetrahydroisoxazolo[5,4-*c*]pyridin-3-ol hydrochloride), also known as THIP, is a $GABA_A$ agonist with a high affinity for the $GABA_A$ receptors containing the delta subunit. Here we plan to address the functional properties of these receptors in the BNST via administration of Gaboxadol and determine if the effects are sex-specific. I will also examine the intrinsic neuronal properties of cells in the anterolateral area of the BNST in both male and female C57BL/6 mice to determine any sex-related functional differences in Type I and/or Type II cells within this region.

Hypothesis

The sexually dimorphic nature of the BNST includes changes in the intrinsic properties of neurons located in this brain region; these changes may be related to changes in susceptibility to anxiety related disorders such as PTSD.

Aim

The aim of the current study is to address the role of sex on the intrinsic properties of neurons located within the $BNST^{ALG}$

4.2. Methods

All animals used in this study were breed in house using stock from Charles River; Male and female C57BL/6 mice aged 3-5 months were interleaved throughout the study, the females used in this study were the same cohort described in the previous chapter. A proportion of the animals underwent behavioural tests which were carried out on the morning of experimental days in the early hours of the animals' light cycle. Following this animals were killed by cervical dislocation and the brain was removed and placed into ice-cold sucrose solution. 300 μm thick coronal slices were prepared, slices which contained the $BNST^{ALG}$ were placed into a holding chamber where they were left to recover for one hour prior to commencement of experiments.

Slices were transferred into the recording chamber where whole cell patch clamp recordings were carried out using a K-gluconate solution containing biocytin as described in the methods chapter.

To assess spontaneous synaptic transmission cells were voltage clamped at -70 mV. Events were then detected and measured as described in the methods chapter. The receptor basis of synaptic events in Type I neurons was examined by applying the glutamate receptor blockers of NBQX and L689560 (both 5 μM)

Pharmacological activation of $GABA_A$ receptors containing the δ subunit was carried out in current clamp mode from a prestimulus potential of -80 mV in the constant presence of NBQX and L689-560, alternating 500 ms pulses of -40 pA and +80 pA were applied at 10 second intervals. Following a 5 minute baseline, 30 μM Gaboxadol was added, 8 minutes later the $GABA_A$ receptor antagonist GABAzine (5 μM) was co-applied with the Gaboxadol (30 μM). After another 8 minutes Gaboxadol and GABAzine were washed out.

4.3. Results

4.3.1. Behaviour

Anxiety levels were assessed using the elevated zero maze, mice were run on the maze in the early hours of their lights on stage. Anxiety is measured as the % of time the animals spend in the light component of the maze; while the females spent approximately 4% less time in the open in comparison to the males (Male, 28 ± 2 %, n = 20, Female 24 ± 1%, n = 46) this was not statistically significant (unpaired t-test, p = 0.07, Figure 4-1).

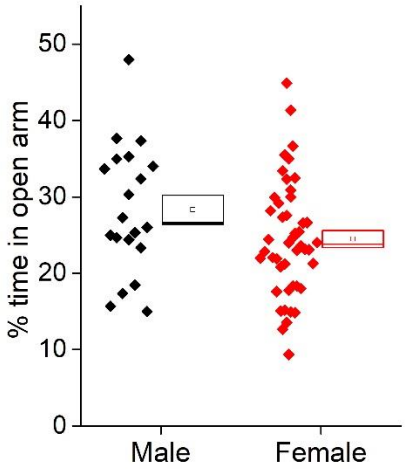

Figure 4-1. % time spent in the open of the elevated zero maze

4.3.2. Electrophysiological properties of neurons located in the anterolateral area of the BNST

4.3.2.1. Type I neurons

A total of 21 Type I neurons were recorded from males, these were recorded from 15 animals with a maximum of 3 cells being recorded from each animal. 66 Type I neurons were recorded from females, these were recorded from 36 animals with a maxiumum of 5 cells being recorded from each animal. I began by looking at the synaptic events in voltage clamp mode while holding the cells at -70 mV; no differences were observed in the amount of current required to clamp cells at -70 mV (Male -6 ± 5 pA, n = 16, female -6 ± 4 pA, n = 53,

unpaired t-test, p = 1, Figure 4-2), the frequency of inward-going post synaptic events (Male 8 ± 3 Hz, n = 16, Female 7 ± 1 Hz, n = 53 Mann-Whitney U, p = 0.9, Figure 4-2) or the average amplitude of inward-going post synaptic events (Male -14 ± 0.8 pA, n = 16, female -15 ± 0.5 pA, n = 53, Mann-Whitney U, p = 0.5, Figure 4-2).

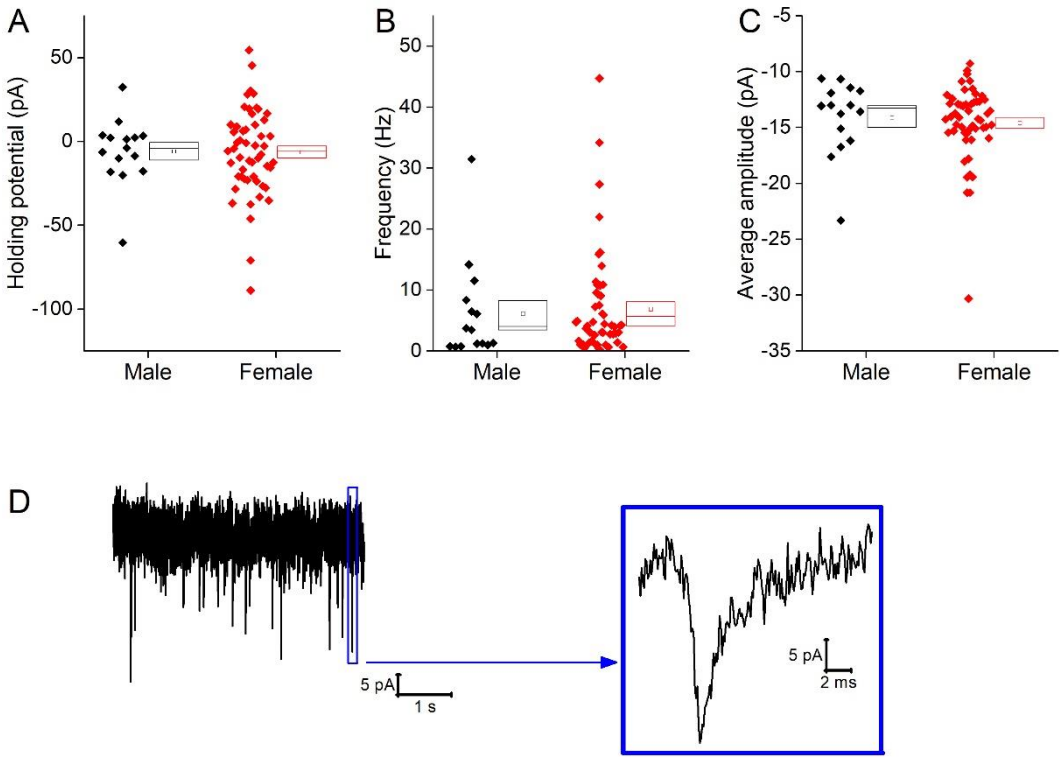

Figure 4-2 Synaptic properties of Type I neurons A) Amount of current required to hold cells at -70 mV, B) the frequency on inward-going postsynaptic events, C) Averaged amplitude of inward-going post-synaptic events, D) sample trace with an enlarged synaptic event in the blue box.

In order to assess the nature of these synaptic events antagonists of key glutamate receptors were applied; NBQX, an antagonist of AMPA receptors, and L689560, an antagonist of NMDA receptors. The synaptic inputs to these cells are almost entirely blocked by the addition of these compounds (paired t-test, p = 0.01, n = 3) indicating that they are comprised mostly of excitatory glutamatergic inputs (Figure 4-3).

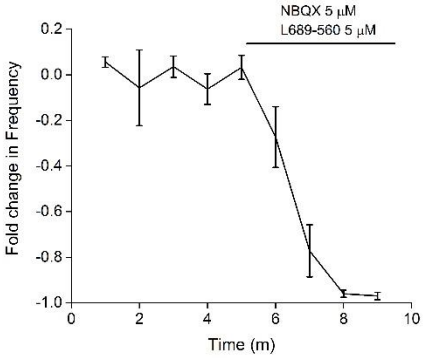

Figure 4-3. % change in the frequency of inward going-synaptic events following the addition of NBQX (5μM) and L689560 (5μM).

Following this the cells were switched into current clamp mode where properties of the cells at their resting membrane potential were assessed. As suggested by the holding current measurements in voltage clamp, sex does not play a significant role in resting membrane potential with both cohorts resting at approximately -68 mV (Male -69 ± 2 mV, n = 21, Female -68 ± 1 mV, n = 66, unpaired t-test, p = 0.9, Figure 4-4). There was also no sex-specific differences in the proportion of cells firing with 9/21 (43%) of male cells firing action potentials at rest and 30/66 (45%) of the female cells firing at rest (chi squared, p = 0.8). The cells which were firing at rest fired at a mean of 2 ± 0.6 Hz in the males and 5 ± 1 Hz in the females, however, this was not significantly different (Mann-Whitney U, p = 0.3, Figure 4-4). Notably in the females there appeared to be a population of cells firing faster than 5 Hz that was absent in the males. Of the cells which were not firing at rest there was no difference in rheobase (Male 39 ± 20 pA, n = 5, Female 28 ± 5 pA, n = 16 unpaired t-test, p = 0.5).

The intrinsic properties of the neurons were examined from two prestimulus potentials, -70 mV and -80 mV. The amount of current required to hold cells at these potentials was not dependent upon sex (-70 mV, Male -12 ± 6 pA, n =21, Female -9 ± 4 pA, n = 66, Mann-Whitney U, p = 0.5; -80 mV, Male -28 ± 6 pA, n = 21, Female -29 ± 5 pA, n = 66, Mann-Whitney U, p = 0.8).

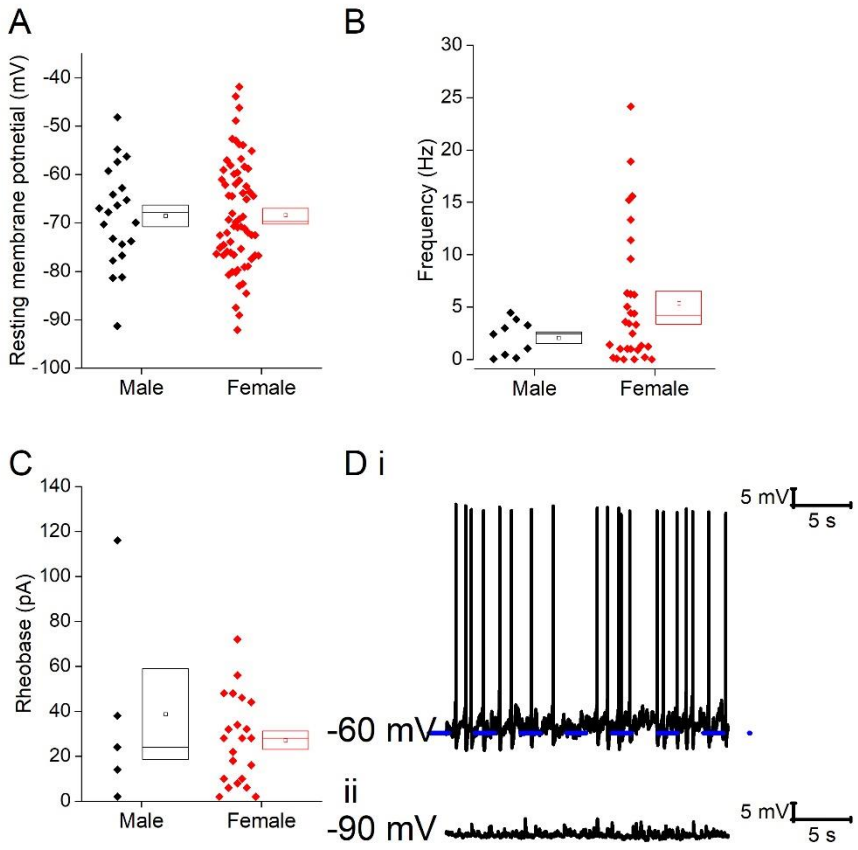

Figure 4-4. Properties of Type I neurons at their resting membrane potentials. A) resting membrane potential of cells, B) the frequency of firing of cells which generated at least one action potential during a one minute epoch, C) rheobase of cells which were not firing at rest, D) sample cell firing at rest (i) and not firing at rest (ii).

The passive membrane properties were examined following the injection of -40 pA of current. the averages of these traces can be seen in Figure 4-5; no differences were observed in input resistance (-70 mV, Male 489 ± 43 MΩ, n = 21, Female 513 ± 24 MΩ, n = 66, Mann-Whitney U, p = 0.5; -80 mV, Male 374 ± 34 MΩ, n = 21, Female 425 ± 24 MΩ, n = 66, Mann-Whitney U, p = 0.4, Figure 4-5), membrane time constant (-70 mV, Male 34 ± 3 ms, n = 21, Female 32 ± 2 ms, n = 66, unpaired t-test, p = 0.4; -80 mV, Male 26 ± 2 ms, n = 21, Female 26 ± 1 ms, n = 66, Mann-Whitney U, p = 0.7, Figure 4-5), sag (-80 mV, Male 16 ± 1 %, n = 21, Female 15 ± 1 %, n = 66, Mann-Whitney U, p = 0.3, Figure 4-5) and capacitance (-70 mV, Male 74 ± 5 pF, n = 21, Female 65 ± 3 pF, n = 66, Mann-Whitney U, p = 0.07; -80 mV, Male 75 ± 6 pF, n = 21, Female 66 ± 3 pF, n = 66, Mann-Whitney U, p = 0.2, Figure 4-5).

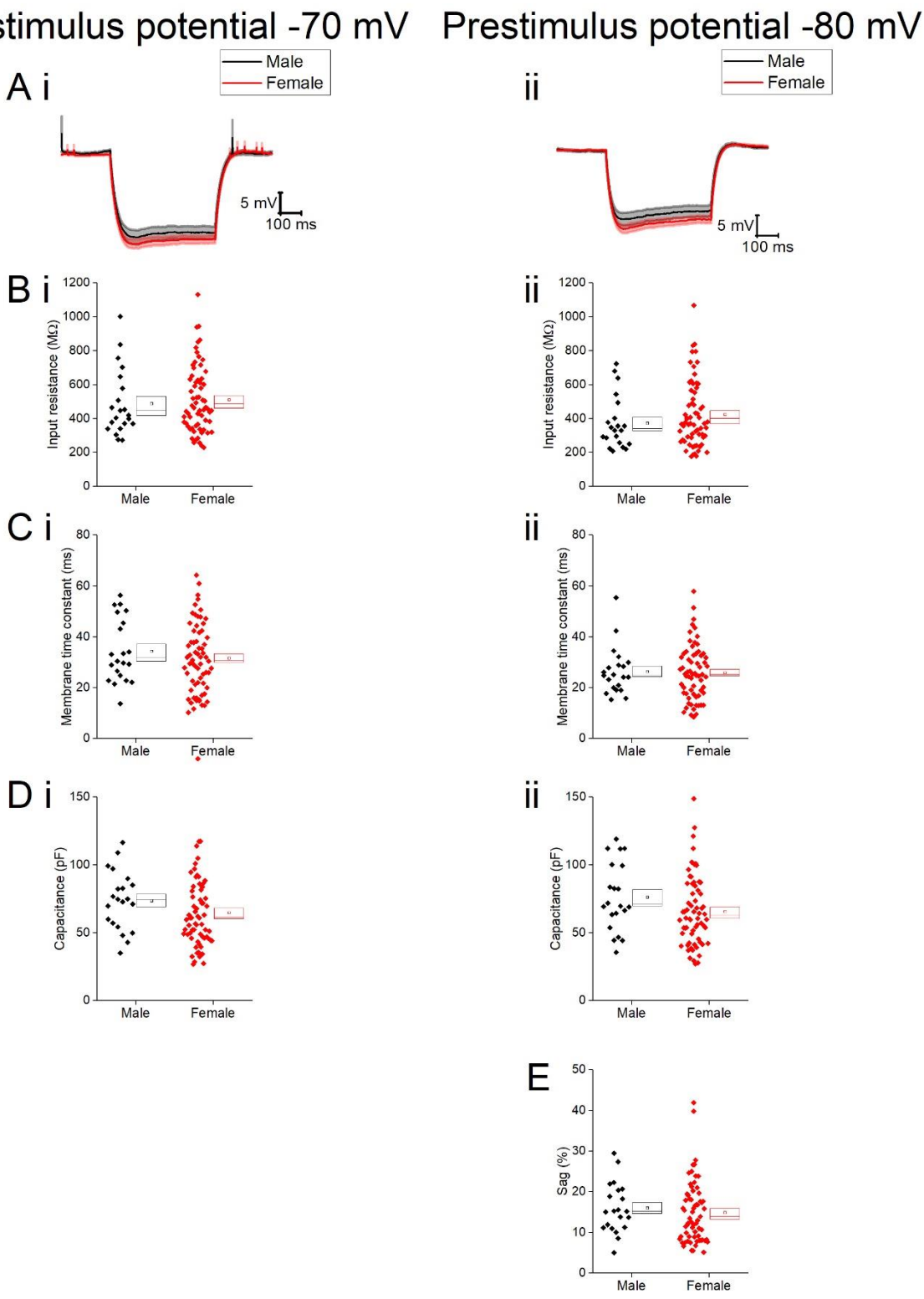

Figure 4-5. Passive membrane properties of Type I neurons, A) average responses to the injection of -40 pA of current, i) averaged responses from a prestimulus potential of -70 mV and ii) average responses from a prestimulus potential of -80 mV, B) Input resistance from a prestimulus potential of -70 mV (i) and -80 mV (ii), C) membrane time constant from a prestimulus potential of -70 mV (i) and -80 mV (ii), D) capacitance from a prestimulus potential of -70 mV (i) and -80 mV (ii), E) sag from a prestimulus potential of -80 mV.

The action potential properties were examined from the first action potential generated in response to a series of depolarising stimuli. The averages of these action potentials can be seen in Figure 4-6. No sex-related differences were seen in the action potential width (-70 mV, Male 0.7 ± 0.04 ms, n = 21, Female 0.7 ± 0.02 ms, n = 66, unpaired t-test, p = 0.4; -80 mV, Male 0.7 ± 0.03 ms, n = 21, Female 0.7 ± 0.02 ms, n = 66, Mann-Whitney U, p = 0.7, Figure 4-6), zenith (-70 mV, Male 16 ± 2 mV, n = 21, Female 16 ± 1 mV, n = 66, unpaired t-test, p = 0.99; -80 mV, Male 17 ± 2 mV, n = 21, Female 17 ± 1 mV, n = 66, Mann-Whitney U, p = 0.9, Figure 4-6), threshold (-70 mV, Male -51 ± 1 mV, n = 21, Female -51 ± 1 mV, n = 66, Mann-Whitney U, p = 0.4; -80 mV, Male -51 ± 1 mV, n = 21, Female -51 ± 1 mV, n = 66, unpaired t-test, p = 0.9, Figure 4-6) or maximum rate of rise (-70 mV, Male 262 ± 13 mV/ms, n = 21, Female 263 ± 8 mV/ms, n = 66, unpaired t-test, p = 0.96; -80 mV, Male 289 ± 17 mV/ms, n = 21, Female 289 ± 9 mV/ms, n = 66, Mann-Whitney U, p = 1, Figure 4-7).

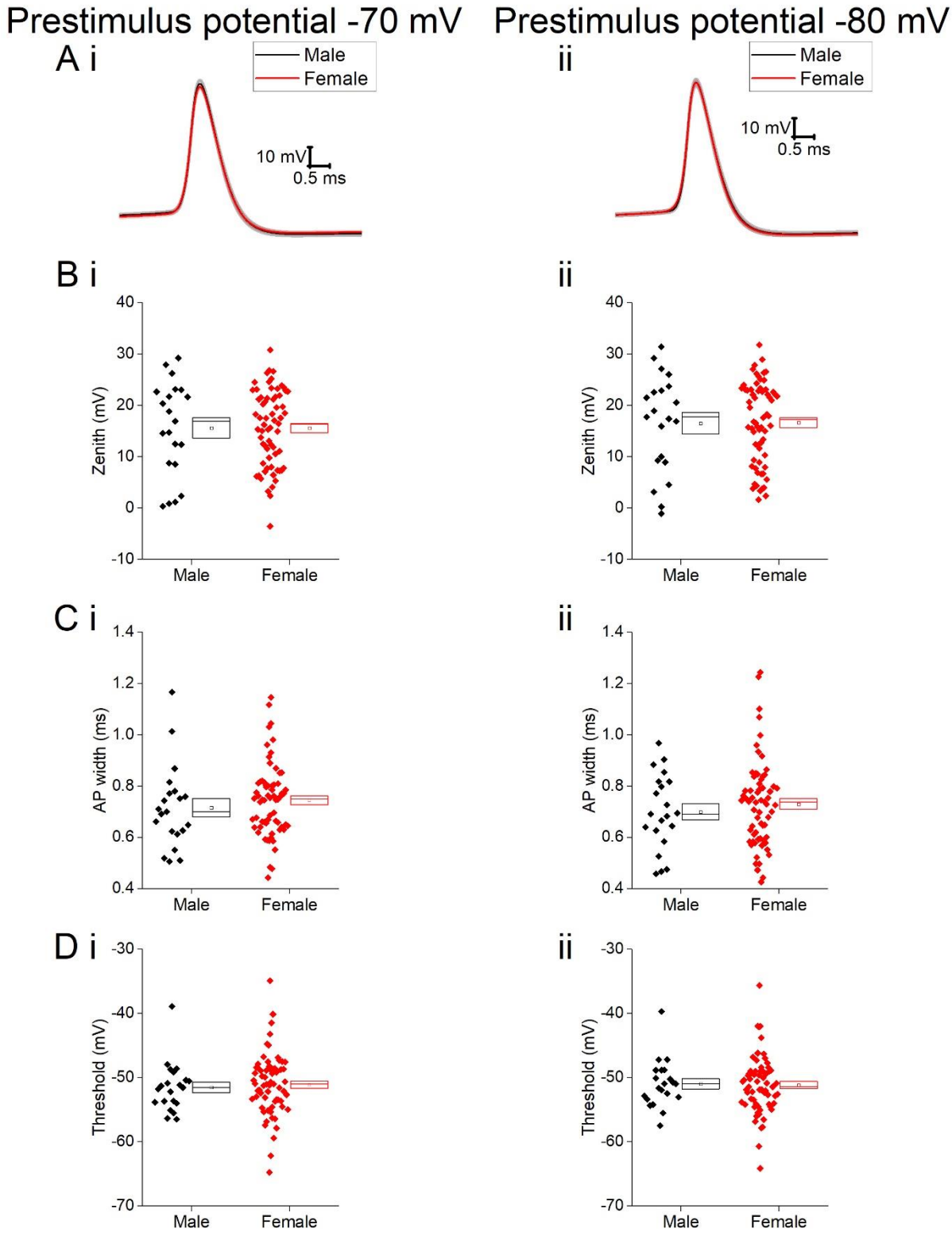

Figure 4-6. Action potential properties of Type I neurons, A) Averages of first action potential generated in response to a series of depolarising current injections from a prestimulus potential of -70 mV (i) and -80 mV (ii), B) Action potential zenith from a prestimulus potential of -70 mV (i) and -80 mV (ii), C) action potential width measured at -20 mV from a prestimulus potential of -70 mV (i) and -80 mV (ii), Threshold of action potential from a prestimulus potential of -70 mV (i) and -80 mV (ii).

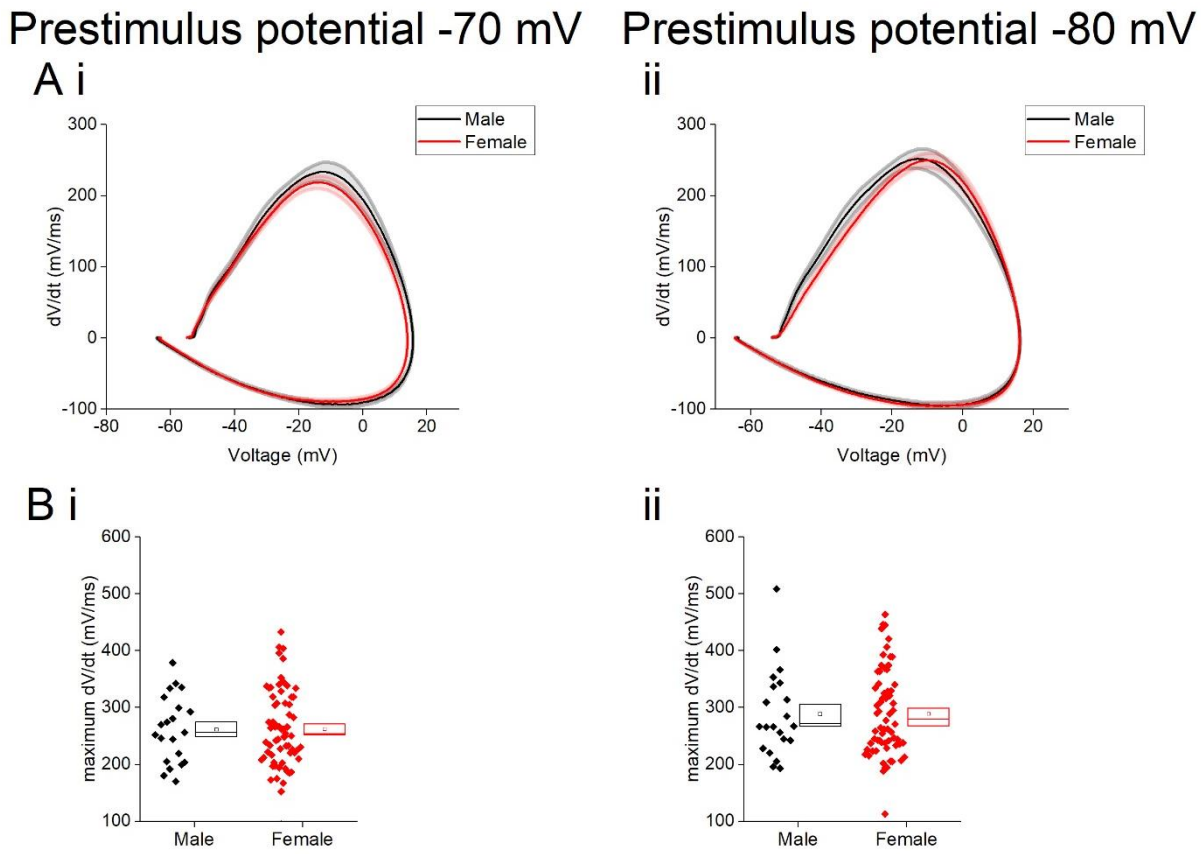

Figure 4-7. Maximum rate of rise of Type I neurons A) First derivative of action potentials plotted against the average action potential for each cohort, line is the mean and shaded area is the standard error of the mean, from a prestimulus potential of -70 mV (i) and -80 mV (ii), B) the maximum rate of rise of each cell from a prestimulus potential of -70 mV (i) and -80 mV (ii).

To measure excitability a series of depolarising pulses were injected into the cell, the proportion of cells which fired in response to each stimulus and the firing frequency (repeated measure two-way ANOVA, sex p = 0.9, Figure 4-8) were not sex-specific in Type I neurons. Rheobase was also not sex-dependent (-70 mV, Male 11 ± 3 pA, n = 21, Female 11 ± 1 pA, n = 66, Mann-Whitney U, p = 0.8; -80 mV, Male 28 ± 6 pA, n = 21, Female 28 ± 2 pA, n = 66, Mann-Whitney U, p = 0.4, Figure 4-8).

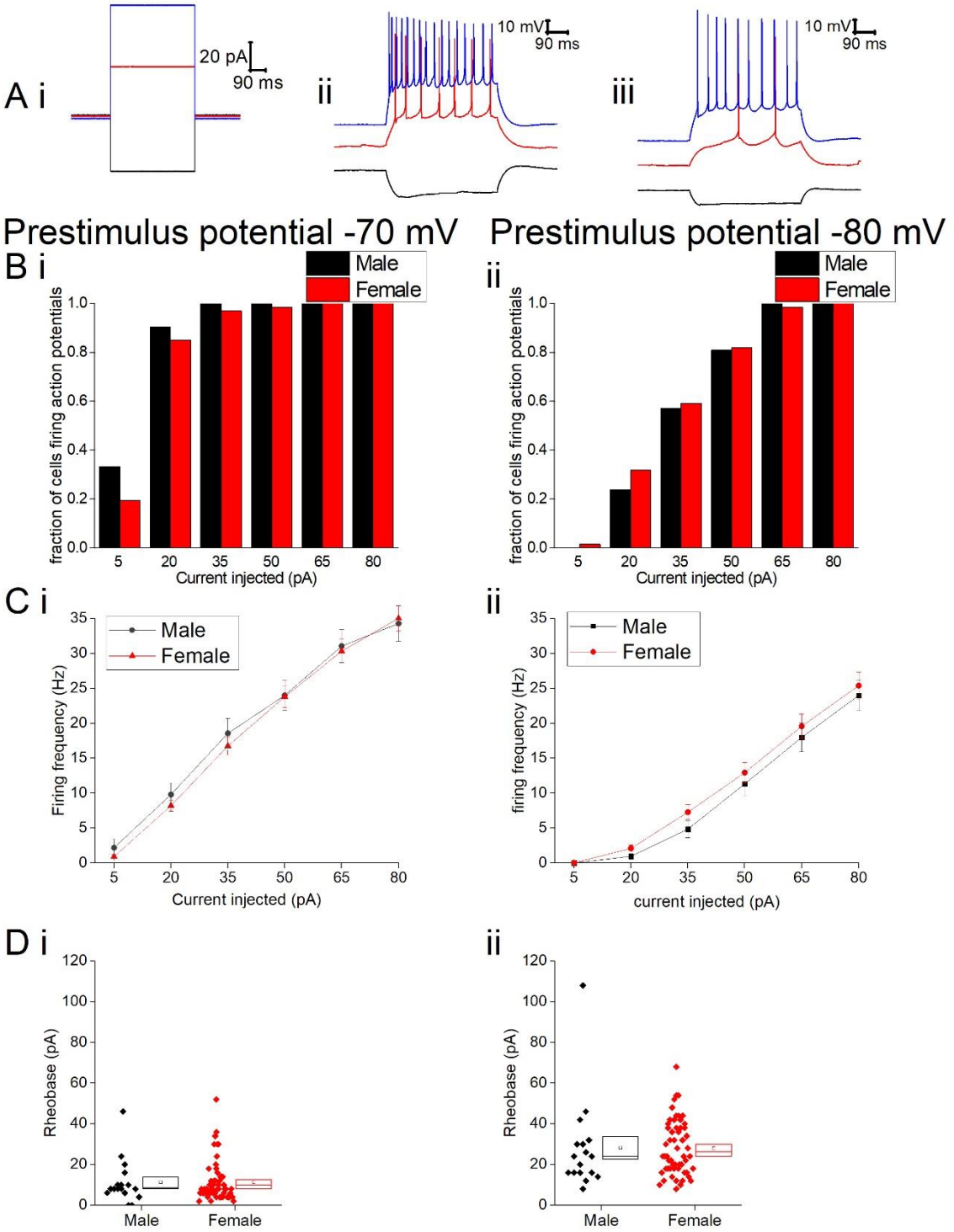

Figure 4-8. Firing properties of Type I neurons. A) Sample cell from prestimulus potential of -80 mV, i) sample current injection, ii) sample cell from the male cohort, iii) sample cell from the female cohort, B) proportion of cells firing action potentials in response to a series of depolarising current injections from a prestimulus potential of -70 mV (i) and -80 mV (ii), C) frequency of action potentials in response to depolarising current injections from a prestimulus potential of -70 mV (i) and -80 mV (ii), D) Rheobase from a prestimulus potential of -70 mV (i) and -80 mV (ii).

The delay between the injection of current and the generation of the first action potential, latency, was not dependent on sex either for the first action potential generated in response to depolarising stimuli (-70 mV, Male 137 ± 25 ms, n = 21, Female 121 ± 14 ms, n = 66, Mann-Whitney U, p = 0.4; -80 mV, Male 147 ± 28 ms, n = 21, Female 118 ± 11 ms, n = 66, Mann-Whitney U, p = 0.6, Figure 4-9) or following the injection of +80 pA of current (-70 mV, Male 11 ± 1 ms, n = 21, Female 13 ± 1 ms, n = 66, Mann-Whitney U, p = 0.6; -80 mV, Male 25 ± 3 ms, n = 21, Female 34 ± 5 ms, n = 66, Mann-Whitney U, p = 0.2, Figure 4-9).

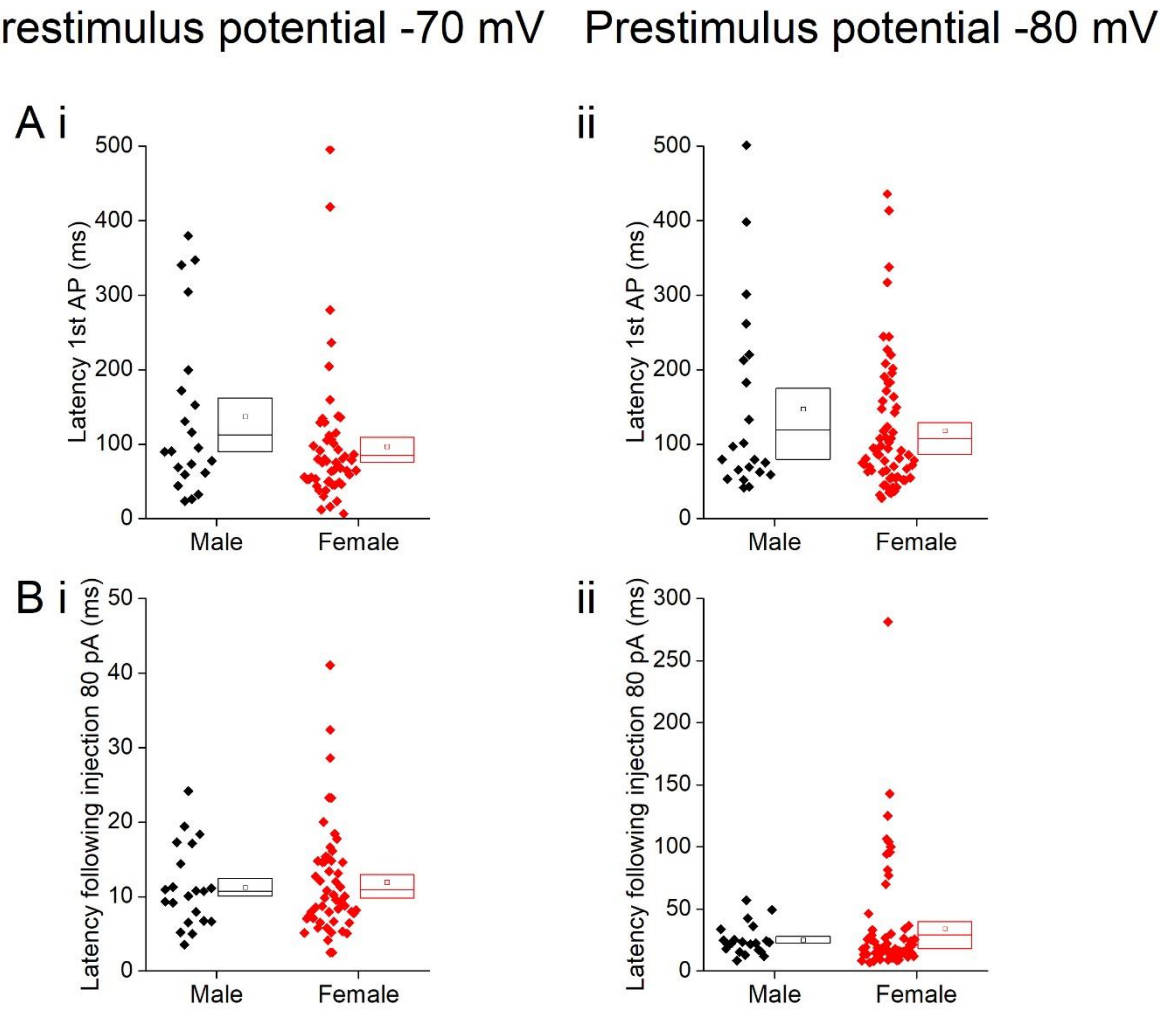

Figure 4-9 Latency of Type I neurons in generation of action potentials, A) Latency of first action potential generated in response to depolarising stimuli from a prestimulus potential of -70 mV (i) and -80 mV (ii).

In order to address the role of the different cell populations described here with the anxiety-like behaviours of animals, a series of correlations were examined between the % time spent in the open part of the maze and the intrinsic properties of neuronal populations in the BNST. A strong correlation was observed with increased frequency of synaptic events correlating with decreased anxiety like behaviour in the elevated zero maze in the male cohort (Figure 4-10, Table 4-1). A more depolarised resting membrane potential was also highly correlated with decreases in anxiety like-behaviour in Type I neurons, once again this was only in the male cohort (Figure 4-11, Table 4-2).Given this correlation between resting membrane potential and behaviour it is unsurprising that a correlation was observed between holding current and behaviour in both voltage clamp mode (Figure 4-10, Table 4-1) and current clamp mode (Figure 4-11, Table 4-2). Finally higher membrane time constants correlated with decreased anxiety-like behaviour on the elevated zero maze (Figure 4-11, Table 4-3). No other correlations were observed between intrinsic properties and anxiety like behaviours.

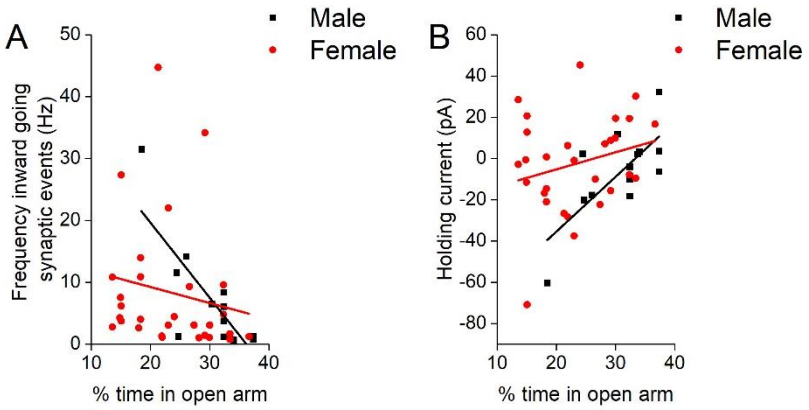

Figure 4-10. Correlation between % time spent in the open on the elevated zero maze and frequency of inward going synaptic events (A) and the amount of current required to hold cells at -70 mV (B).

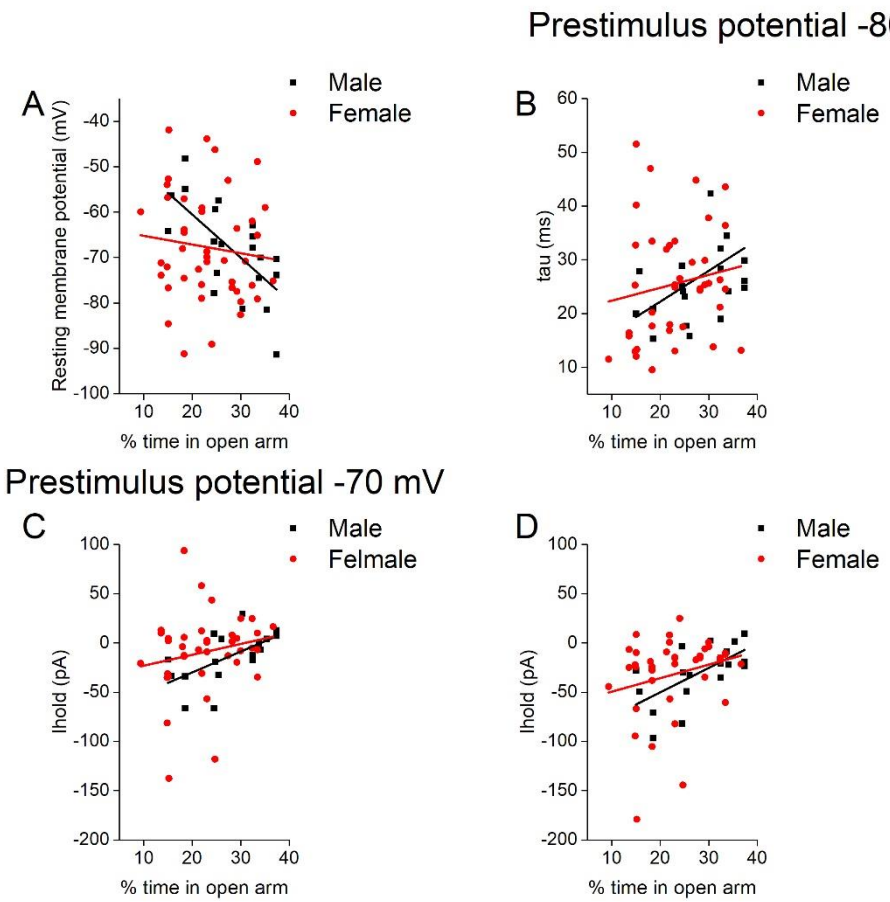

Figure 4-11. Correlation between the amount of time spent in the open on the elevated zero maze and A) resting membrane potential, B) membrane time constant from a prestimulus potential of -80mV and holding current from a prestimulus potential of -70 mV (C) and -80 mV (D).

Parameter	**Male**		**Female**	
	R-squared	P value	R-squared	P value
Holding current	0.48	0.004	0.03	0.2
Frequency of events	0.62	0.0005	-0.007	0.4
Average amplitude	-0.07	0.7	-0.02	0.5

Table 4-1. Correlation statistics between % time spent in the open component of the elevated zero maze and properties of cells examined in voltage clamp mode.

Parameter		Male		Female	
		R-squared	P value	R-squared	P value
Resting membrane potential		0.4	0.001	-0.01	0.5
Frequency at rest		0.3	0.08	-0.05	0.7
I_{hold}	**-70 mV**	0.3	0.004	0.009	0.25
	-80 mV	0.4	0.003	0.03	0.15

Table 4-2. Correlation statistics between % time spent in the open component of the elevated zero maze and properties of cells at their resting membrane potentials and holding current required to obtain a prestimulus potential of -70 mV and -80 mV.

Parameter		Male		Female	
		R-squared	P value	R-squared	P value
Input resistance	**-70 mV**	0.02	0.24	-0.004	0.4
	-80 mV	0.007	0.3	-0.01	0.4
Membrane time constant	**-70mV**	-0.04	0.65	0.002	0.3
	-80 mV	0.2	0.049	$-6.8\ E^{-4}$	0.3
Capacitance	**-70 mV**	0.02	0.3	0.004	0.29
	-80 mV	-0.03	0.6	-0.02	0.6
Sag	**-80 mV**	-0.009	0.4	0.7	-0.02

Table 4-3. Correlation statistics between % time spent in the open component of the elevated zero maze and passive membrane properties.

Parameter		Male		Female	
		R-squared	P value	R-squared	P value
AP zenith	**-70 mV**				
	-80 mV	-0.05	0.97	-0.005	0.4
AP width	**-70mV**	-0.05	0.9	-0.02	0.6
	-80 mV	-0.05	0.75	-0.01	0.5
Threshold	**-70 mV**	0.02	0.3	-0.01	0.4
	-80 mV	-0.05	0.8	-0.02	0.6
dV/dt max	**-70 mV**	-0.05	0.9	-0.02	0.9
	-80 mV	-0.03	0.5	-0.01	0.5

Table 4-4. Correlation statistics between % time spent in the open component of the elevated zero maze and action potential properties.

Parameter		Male		Female	
		R-squared	P value	R-squared	P value
Frequency-injection 80 pA	**-70 mV**	-0.05	0.9	-0.008	0.4
	-80 mV	0.04	0.2	-0.03	0.9
Latency 1st AP	**-70mV**	0.08	0.11	-0.03	0.98
	-80 mV	-0.04	0.7	-0.03	0.9
Latency injection 80 pA	**-70 mV**	0.01	0.3	-0.02	0.8
	-80 mV	-0.05	0.8	-0.009	0.4

Table 4-5. Correlation statistics between % time spent in the open component of the elevated zero maze and properties of neuronal excitability.

4.3.2.2. Type II neurons

A total of 29 Type II cells were recorded from males, these were recorded from 16 animals with a maximum of 4 cells being recorded from each animals. 53 Type II cells were recorded from females, these recordings were made from 34 animals with a maximum of 4 cells being recorded from each animal. Upon examining synaptic properties in voltage clamp mode no differences were observed in the amount of current required to hold cells at -70 mV (male -14 ± 7 pA, n = 18, Female -4 ± 3 pA, n = 41, unpaired t-test, p = 0.2, Figure 4-12), the frequency of inward-going post synaptic events (Male 4 ± 0.8 Hz, n = 18, Female 6 ± 1 Hz, n = 41 Mann-Whitney U, p = 0.5, Figure 4-12) or the average amplitude of inward-going post synaptic events (Male -13 ± 0.5, n = 18, Female -13 ± 0.4, n = 41, Mann-Whitney U, p = 1, Figure 4-12).

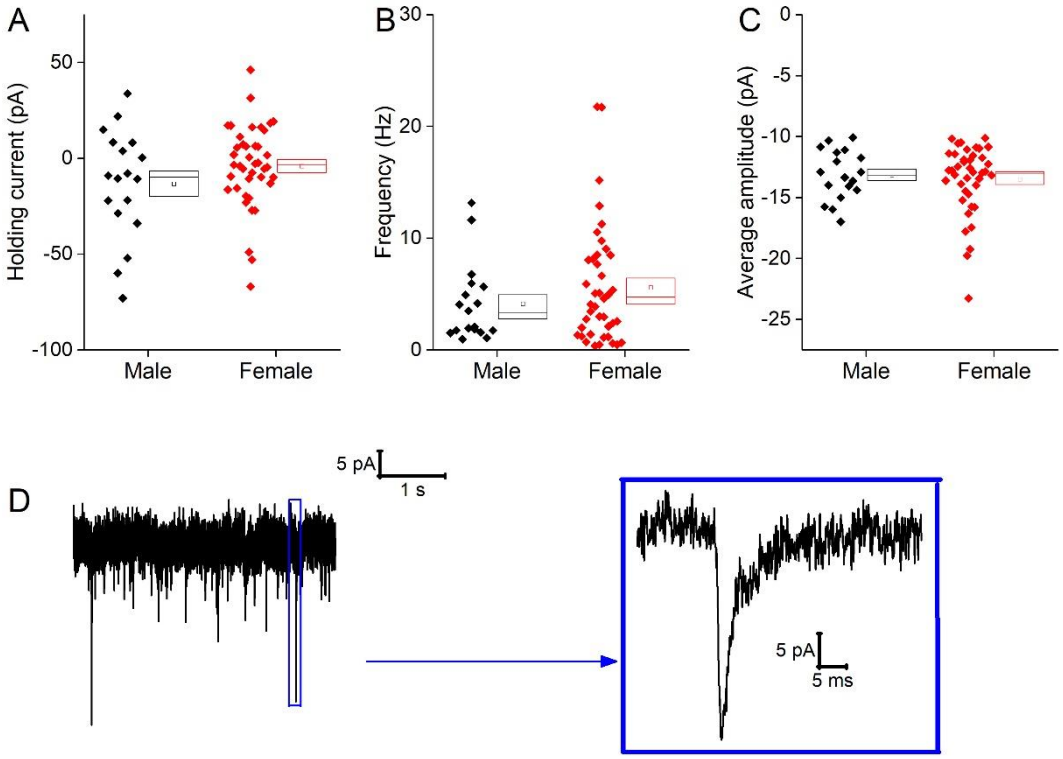

Figure 4-12 Synaptic properties of Type II neurons A) Amount of current required to hold cells at -70 mV, B) the frequency on inward-going post synaptic events, C) Averaged amplitude of inward-going post-synaptic events, D) sample trace with an enlarged synaptic event in the blue box.

Following this the recording was switched into current clamp mode to examine the properties of the cells at their resting membrane potential. The resting membrane potentials of Type II neurons was not sex-dependent (Male -66 ± 2

mV, n = 29, Female -68 ± 1 mV, n =53, unpaired t-test, p = 0.3, Figure 4-13). Approximately half of the cells from each cohort were firing action potentials in the initial 1 minute recording of the cells at their resting membrane potential with 14/29 male cells firing and 23/53 female cells firing. The firing frequency of the cells which were generating action potentials did not differ with sex (Male 6 ± 2 Hz, n = 14, Female 5 ± 1 Hz, n = 23, Mann-Whitney U, p = 0.99, Figure 4-13). Of the cells which did not fire at rest rheobase was examined, this was not sex-specific averaging 23.6 ± 7 pA (n = 5) in the males and 28.5 ± 5 pA (n = 16) in the females (unpaired t-test, p = 0.6, Figure 4-13).

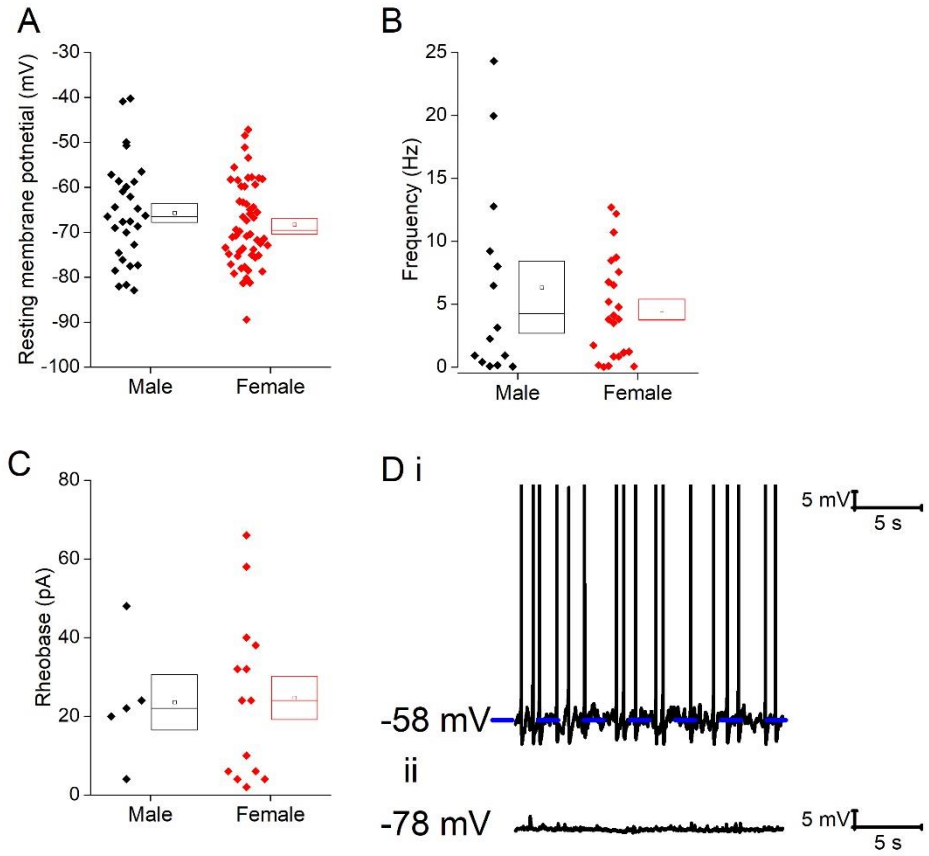

Figure 4-13. Properties of Type II neurons at their resting membrane potentials, A) resting membrane potential of cells, B) the frequency of firing of cells which generated at least one action potential during a one minute epoch, C) rheobase of cells which were not firing at rest, D) sample cell firing at rest (i) and not firing at rest (ii)

The intrinsic properties were examined from set prestimulus membrane potentials of -70 mV and -80 mV. The amount of current required to hold the cells at the prestimulus potential of -70 mV averaged -7 pA in both male and female groups (Male -6 ± 4 pA, n = 24, Female -8 ± 3 pA, n =51, unpaired t-

test, p = 0.7); whereas the depolarising current required to hold the cells at -80 mV averaging -22 ± 4 pA (n = 24) in males and -30 ± 4 pA (n = 51) in females, (Mann-Whitney U, p = 0.2).

The passive membrane properties were examined from the responses to the injection of -40 pA of current (averages are shown in Figure 4-14). The input resistance was a mean of ~100 MΩ (~21%) higher in the male cohort from a prestimulus potential of -70 mV this however was not statistically significant (Male 581 ± 58 MΩ, n = 29, Female 482 ± 32 MΩ, n =53, Mann-Whitney U, p = 0.14, Figure 4-14); from -80 mV the mean was also 100 MΩ (26%) higher in the male cohort which was statistically significant (Male 470 ± 45 MΩ, n = 29, Female 372 ± 29 MΩ, n =53, Mann-Whitney U, p = 0.02, Figure 4-14). Capacitance was ~15 pF higher in the female cohort in comparison to the male cohort (-70 mV, Male 56 ± 4 pF, n =29, Female 73 ± 4 pF, n = 53, Mann-Whitney U, p = 0.006; -80 mV, Male 60 ± 4 pF, n = 29, Female 76 ± 4 pF, n = 53, unpaired t-test, p = 0.006, Figure 4-14). No differences were observed in the membrane time constant (-70 mV, Male 30 ± 2 ms, n = 29, Female 32 ± 1 ms, n = 53, Mann-Whitney U, p = 0.6; -80 mV, Male 25 ± 1 ms, n = 29, Female 25 ± 1 ms, n = 53, Mann-Whitney U, p = 0.4, Figure 4-14), as the influence of the higher capacitance of cells in females is balanced out by their lower input resistance. Sag was only examined from a prestimulus potential of -80 mv due to the voltage dependent kinetics of I_h; this was found to be significantly larger in the female cohort (Male 15 ± 1 %, n = 29, Female 19 ± 1 %, n = 53, Mann-Whitney U, p = 0.02, Figure 4-14).

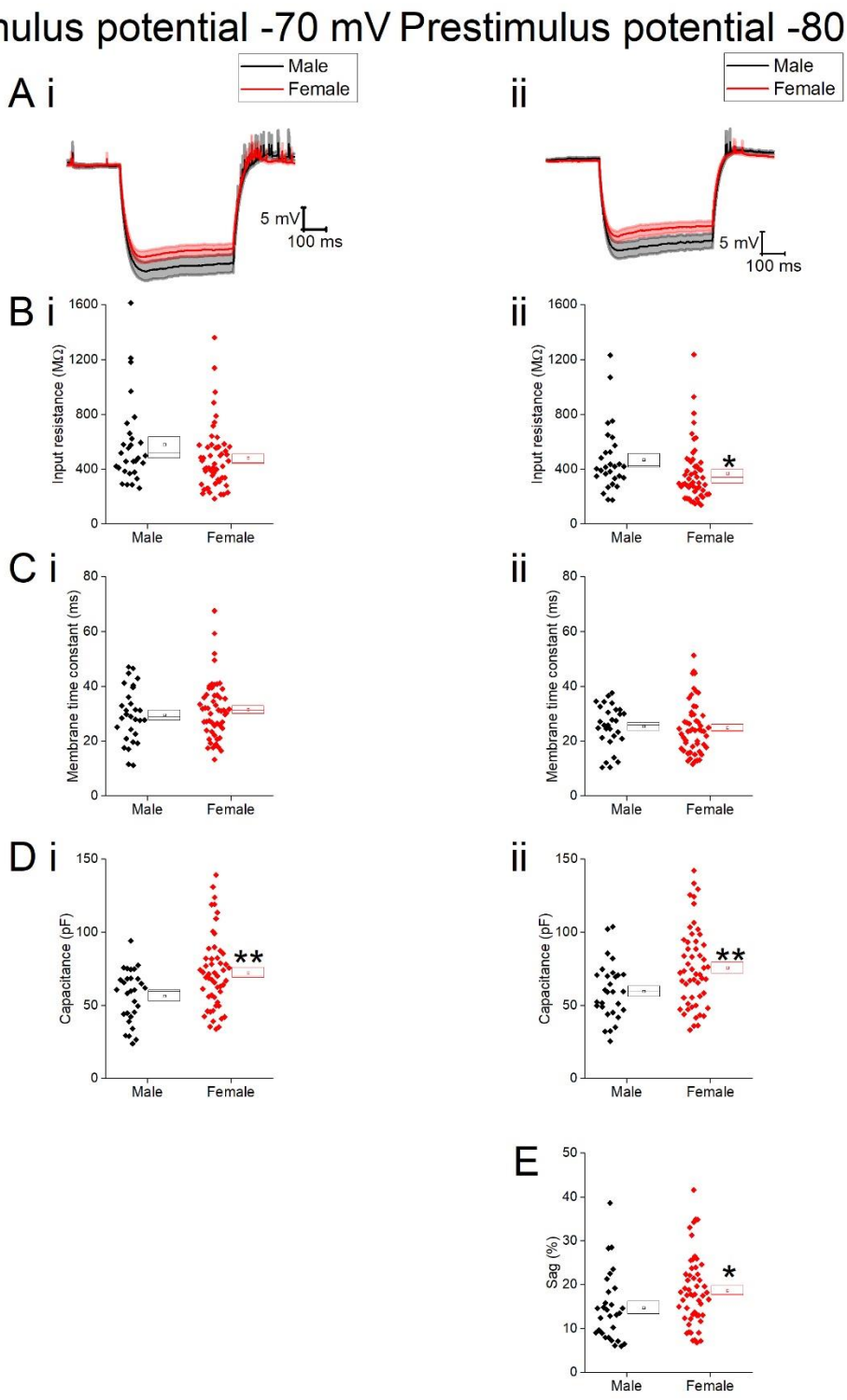

Figure 4-14 Passive membrane properties of Type II neurons, A) average responses to the injection of -40 pA of current, i) sample current injection, ii) averaged responses from a prestimulus potential of -70 mV and iii) average responses from a prestimulus potential of -80 mV, B) Input resistance from a prestimulus potential of -70 mV (i) and -80 mV (ii), C) membrane time constant from a prestimulus potential of -70 mV (i) and -80 mV (ii), D) capacitance from a prestimulus potential of -70 mV (i) and -80 mV (ii), E) sag from a prestimulus potential of -80 mV. Significance indicated via *, * $p<0.05$, ** $p<0.01$.

Averages of action potentials, examined from the first action potential generated in response to depolarising stimuli, are shown in Figure 4-15. No differences were observed in action potential zenith (-70 mV, Male 12 ± 2 mV, n = 29, Female 14 ± 1 mV, n = 53, Mann-Whitney U, p = 0.3; -80 mV, Male 13 ± 2 mV, n = 29, Female 15 ± 1 mV, n = 53, Mann-Whitney U, p = 0.14, Figure 4-15), width (-70 mV, Male 0.7 ± 0.03 ms, n = 29, Female 0.7 ± 0.02 ms, n = 53, unpaired t-test, p = 0.4; -80 mV, Male 0.7 ± 0.02 ms, n = 29, Female 0.7 ± 0.02 ms, n = 53, Mann-Whitney U, p = 0.14, Figure 4-15) or the threshold (-70 mV, Male -52 ± 1 mV, n = 29, Female -52 ± 1 mV, n = 53, Mann-Whitney U, p = 0.8; -80 mV, Male -54 ± 1 mV, n = 29, Female -53 ± 1 mV, n = 53, Mann-Whitney U, p = 0.7, Figure 4-15). The maximum rate of rise, was also not affected by sex (-70 mV, Male 240 ± 15 mV/ms, n = 29, Female 248 ± 8 mV/ms, n = 53, unpaired t-test, p = 0.6; -80 mV, Male 272 ± 16 mV/ms, n = 29, Female 280 ± 8 mV/ms, n = 53, Mann-Whitney U, p = 0.4, Figure 4-16).

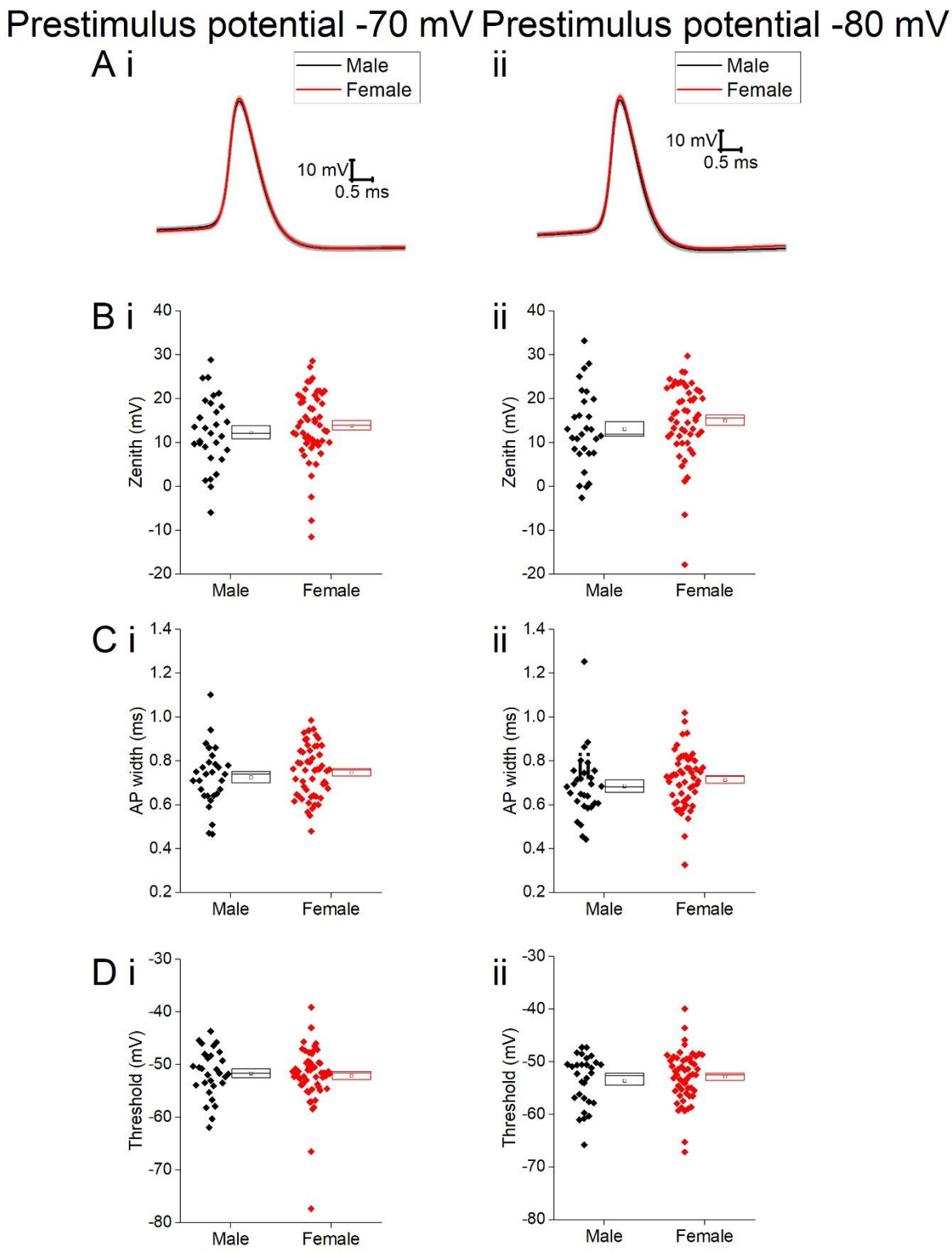

Figure 4-15 Action potential properties of Type II neurons, A) Averages of first action potential generated in response to a series of depolarising current injections from a prestimulus potential of -70 mV (i) and -80 mV (ii), B) Action potential zenith of action potentials from a prestimulus potential of -70 mV (i) and -80 mV (ii), C) action potential width measured at -20 mV from a prestimulus potential of -70 mV (i) and -80 mV (ii), Threshold of action potential from a prestimulus potential of -70 mV (i) and -80 mV (ii).

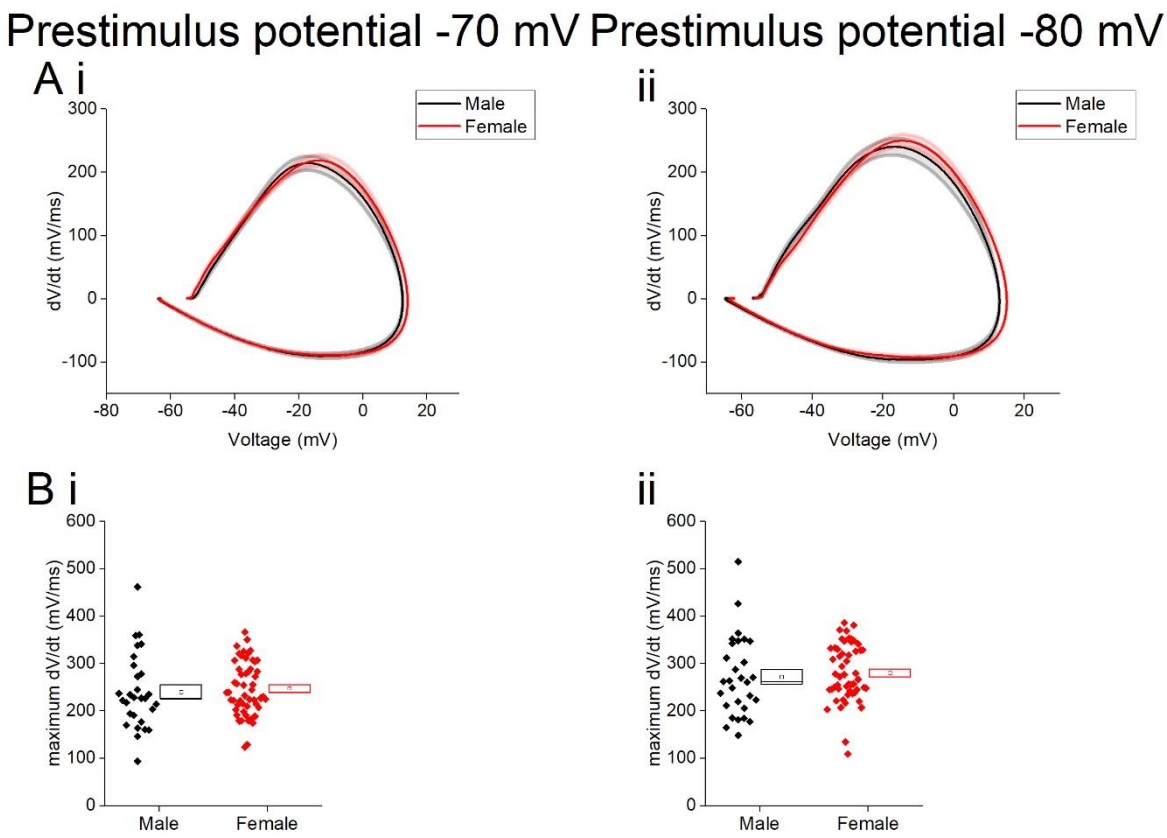

Figure 4-16. Maximum rate of rise of Type II neurons A) First derivative of action potentials plotted against the average action potential for each cohort, line is the mean and shaded area is the standard error of the mean, from a prestimulus potential of -70 mV (i) and -80 mV (ii), B) the maximum rate of rise of each cell from a prestimulus potential of -70 mV (i) and -80 mV (ii).

Finally I measured the excitability of Type II neurons. From a prestimulus potential of -70 mV there were no differences in proportions of cells firing in response to depolarising currents (Figure 4-17B), most likely down to the high proportion of cells firing even in response to smaller stimuli. From a prestimulus potential of -80 mV the male neurons had an increased likelihood of firing in response to the injection of 5 pA (3/29 male cells fired while 0/59 female cells fired, $p = 0.01$) and 20 pA (15/29 male cells fired and 14/59 female cells fired, $p = 0.009$), by 35 pA a large proportion of both cohorts were firing (22/ 29 male cells were firing and 33/59 female cells were firing, $p = 0.07$, Figure 4-17B) which continued to increase to the point that all cells in both cohorts were firing by the injection of 80 pA. Male Type II neurons fired at a higher frequency than females in response to a series of depolarising current injections (repeated

measure two-way ANOVA on both prestimulus potentials, sex, p = 0.02, Figure 4-17C). This indicated greater excitability in males compared to females.

Rheobase of Type II neurons was not dependent on sex (-70 mV, Male 12 ± 2 pA, n = 17, Female 13 ± 2 pA, n = 41, Mann-Whitney U, p = 0.8; -80 mV, Male 27 ± 2 pA, n = 17, Female 31 ± 3 pA, n = 41, Mann-Whitney U, p = 0.8, Figure *4-17*). Latency between current injection and the generation of the first action potential was not effected by sex (-70 mV, Male 112 ± 16 ms, n = 29, Female 97 ± 12 ms, n = 53, Mann-Whitney U, p = 0.4; -80 mV, Male 99 ± 17 ms, n = 29, Female 59 ± 4 ms, n = 53, Mann-Whitney U, p = 0.09, Figure *4-18*), however following the injection of 80 pA of current the male cohort generated an action potential faster than the females (-70 mV, Male 8 ± 0.1 ms, n = 29, Female 12 ± 1 ms, n = 53, Mann-Whitney U, p =0.02; -80 mV, Male 15 ± 1 ms, n = 29, Female 25 ± 4 ms, n = 53, Mann-Whitney U, p = 0.02, Figure *4-18*).

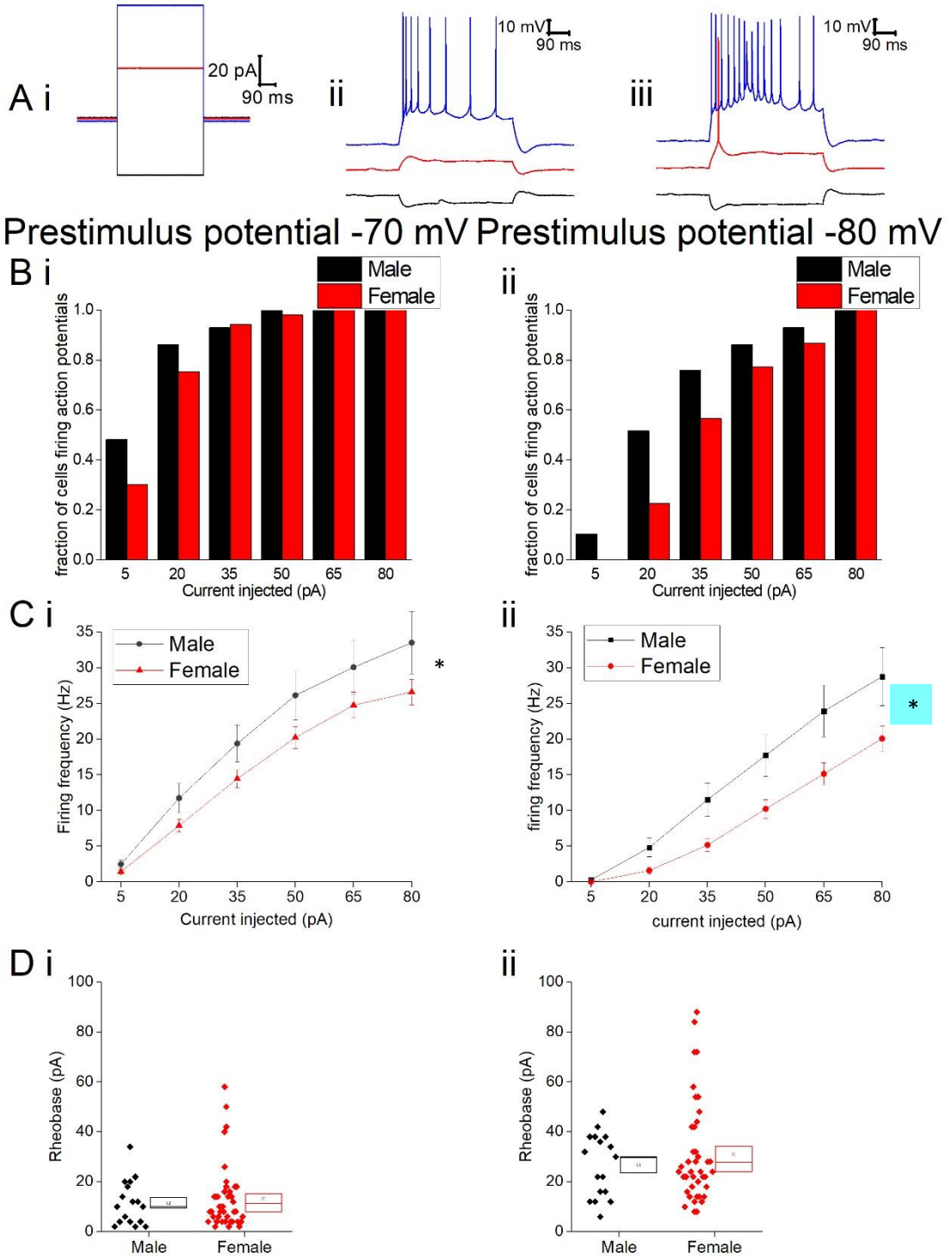

Figure 4-17. Firing properties of Type II neurons A) Sample cell from prestimulus potential of -80 mV, i) sample current injection, ii) sample cell from the male cohort, iii) sample cell from the female cohort, B) proportion of cells firing action potentials in response to a series of depolarising current injections from a prestimulus potential of -70 mV (i) and -80 mV (ii), C) frequency of action potentials in response to depolarising current injections from a prestimulus potential of -70 mV (i) and -80 mV (ii), D) Rheobase from a prestimulus potential of -70 mV (i) and -80 mV (ii). * indicates significance * $p < 0.05$.

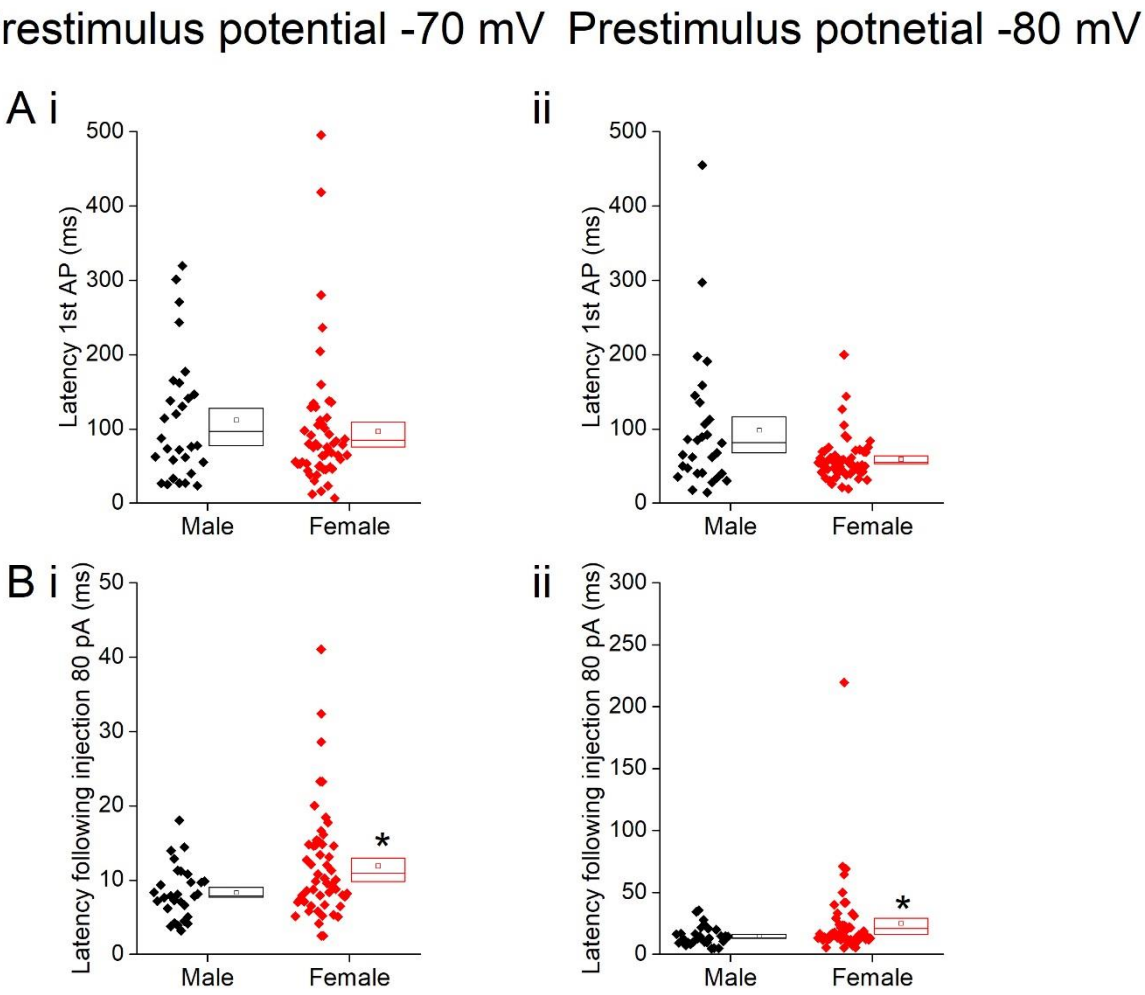

Figure 4-18. Latency of Type II neurons in generation of action potentials, A) Latency of first action potential generated in response to depolarising stimuli from a prestimulus potential of -70 mV (i) and -80 mV (ii).

The >20% average higher input resistance observed in the males is most likely playing a role in the increased excitability observed within the cohort. ALLO has been shown to impact the extrasynaptic placement of $GABA_AR$ through increased expression of the δ subunit; this can lead to increases in input resistance due to increased tonic inhibition. To determine the impact of these receptors on input resistance Gaboxadol (30 μM), a $GABA_AR$ agonist with a high affinity for the $GABA_AR$ containing the δ subunit, was added. To confirm that the effect was mediated by $GABA_A$ GABAzine (a $GABA_AR$ agonist) was also added; this was examined via alternating injections of -40 pA and +80 pA. Frequency of cells firing following the depolarising pulse was measured and input resistance was assessed on the hyperpolarising current injection. Addition of Gaboxadol to both male (n = 5) and female (n = 6) Type II neurons caused a

decrease in input resistance and a decrease in firing of action potentials. Despite a mean larger decrease of over 100 MΩ in the Female cohort the difference was not statistically significant (unpaired t-test, sex, p = 0.07, Figure *4-19*), following this the decreases in action potentials were examined between the cohorts and no statistically significant differences were observed (Mann-Whitney U, sex, p = 0.4, Figure *4-19*). While these findings were not statistically significant there is a trend towards a larger effect in the female cohort.

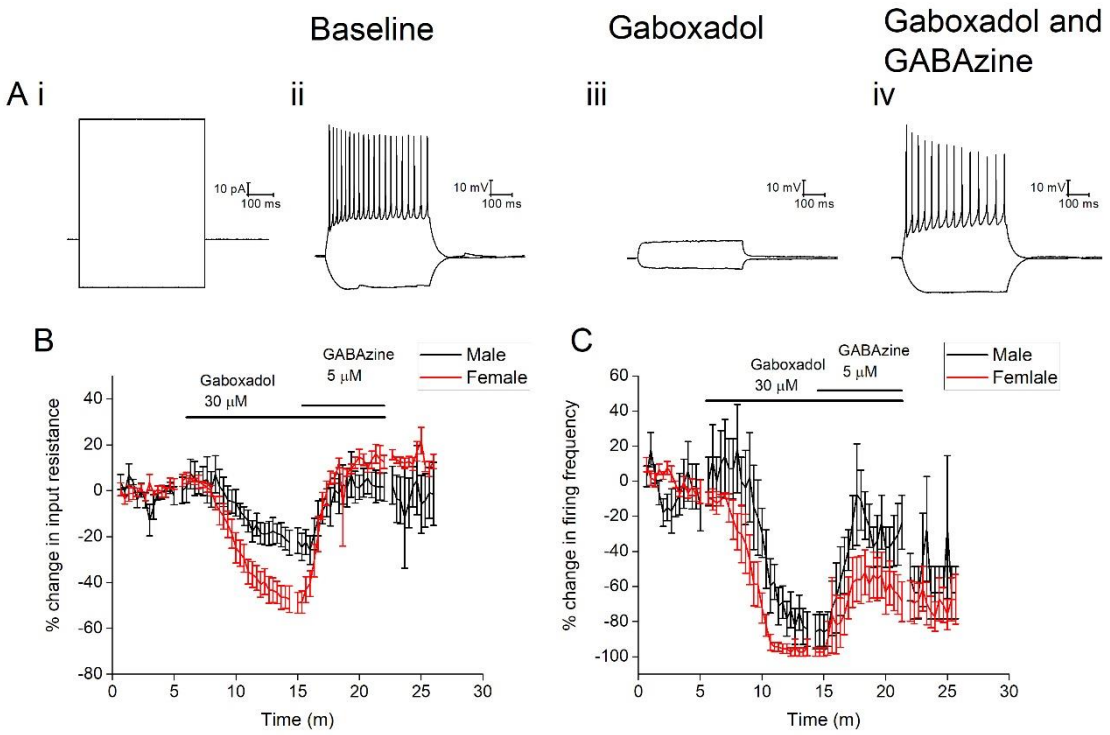

Figure 4-19 Effect of Gaboxadol on B) input resistance and C) firing frequency of Type II neurons. A) Sample traces of the different stages of the drug recording, i) sample current injection, ii) Baseline, ii) in the presence of Gaboxadol, iii) in the presence of Gaboxadol and GABAzine

In order to address the roles of the intrinsic properties of these cells in behaviour correlations between % time spent in the open of the elevated zero maze and the intrinsic properties of cells were examined. A correlation was found between the firing frequency of Type II neurons following the injection of +80 pA and % time spent in the open, this correlation was only observed in the males (-70 mV, Pearson's r = 0.43, ANOVA, p = 0.03; -80 mV, Pearson's r = 0.41, ANOVA, p = 0.04, Figure *4-20*, Table *4-6*) but not in the females (-70 mV, Pearson's r = 0.29, ANOVA, p = 0.1; -80 mV, Pearson's r = 0.03, ANOVA, p =

0.88, Figure *4-20*, Table *4-6*). No other correlations were observed between intrinsic properties of Type II neurons and % time spent in the open on the zero maze (Table *4-6*, Table *4-7*, Table *4-8*, Table *4-9*, Table *4-10*).

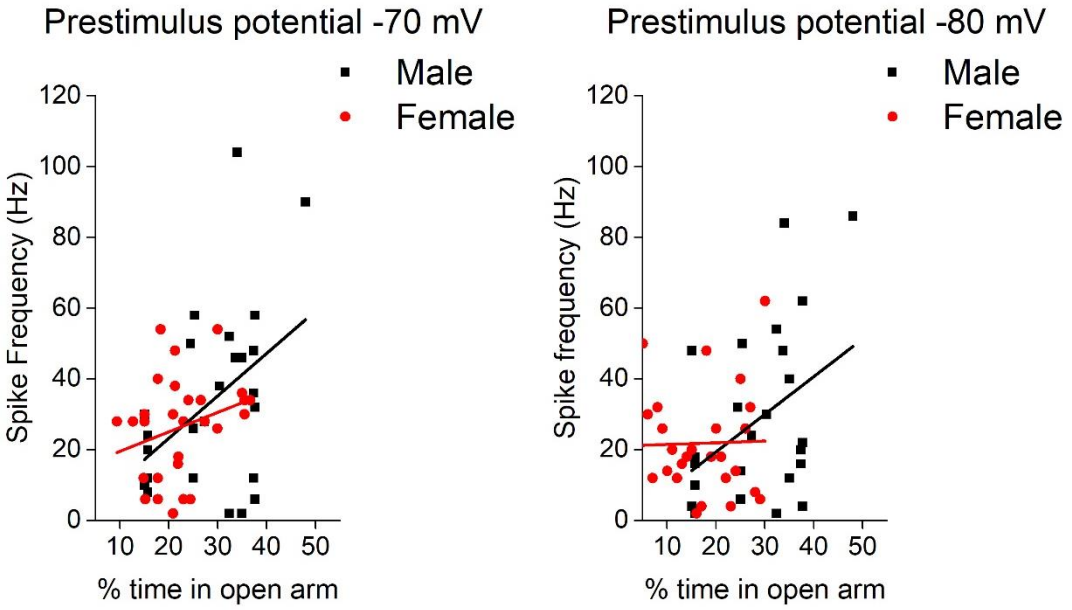

Figure 4-20. Correlation between firing frequency of Type II neurons and the % time spent in the open on the elevated zero maze.

Parameter	**Male**		**Female**	
	R-squared	P value	R-squared	P value
Holding current	0.02	0.3	-0.04	0.6
Frequency of events	0.19	0.057	-0.03	0.5
Average amplitude	-0.05	0.6	-0.05	0.9

Table 4-6. Correlation statistics between % time spent in the open component of the elevated zero maze and properties of cells examined in voltage clamp mode.

Parameter		Male		Female	
		R-squared	P value	R-squared	P value
Resting membrane potential		0.01	0.3	-0.02	0.5
Frequency at rest		-0.02	0.4	0.03	0.3
Rheobase		0.16	0.4	-0.3	0.8
I_{hold}	**-70 mV**	-0.02	0.4	-0.04	0.8
	-80 mV	-0.05	0.8	-0.04	0.96

Table 4-7. Correlation statistics between % time spent in the open component of the elevated zero maze and properties of cells at their resting membrane potentials and holding current required to obtain a prestimulus potential of -70 mV and -80 mV.

Parameter		Male		Female	
		R-squared	P value	R-squared	P value
Input resistance	**-70 mV**	0.08	0.09	0.04	0.14
	-80 mV	0.06	0.13	-0.01	0.4
Membrane time constant	**-70mV**	0.04	0.17	0.07	0.09
	-80 mV	-0.03	0.6	-0.003	0.4
Capacitance	**-70 mV**	-0.02	0.5	-0.01	0.4
	-80 mV	0.01	0.3	-0.035	0.9
Sag	**-80 mV**	-0.04	0.7	0.026	0.2

Table 4-8. Correlation statistics between % time spent in the open component of the elevated zero maze and passive membrane properties.

Parameter		Male		Female	
		R-squared	P value	R-squared	P value
AP zenith	**-70 mV**	-0.02	0.5	-0.02	0.5
	-80 mV	-0.02	0.4	-0.01	0.4
AP width	**-70mV**	0.02	0.2	0.01	0.3
	-80 mV	0.02	0.2	-0.02	0.6
Threshold	**-70 mV**	-0.04	0.9	0.07	0.09
	-80 mV	-0.04	0.4	-0.01	0.8
dV/dt max	**-70 mV**	-0.04	0.9	-0.002	0.3
	-80 mV	-0.04	0.9	-0.001	0.3

Table 4-9. Correlation statistics between % time spent in the open component of the elevated zero maze and action potential properties.

Parameter		Male		Female	
		R-squared	P value	R-squared	P value
Frequency-injection 80 pA	**-70 mV**	0.15	0.03	0.05	0.12
	-80 mV	0.01	0.04	-0.03	0.9
Latency 1st AP	**-70mV**	-0.04	0.9	0.003	0.3
	-80 mV	-0.03	0.6	-0.003	0.3
Latency injection 80 pA	**-70 mV**	0.09	0.08	0.06	0.1
	-80 mV	-0.04	0.76	0.06	0.1

Table 4-10. Correlation statistics between % time spent in the open component of the elevated zero maze and neuronal excitability.

Type III neurons

A total of 14 type III cells were recoded from males, these recordings were made from 11 animals with a maximum number of 2 being recorded from each animal. A total of 19 type III cells were recorded from females, these were recorded from 16 animals with a maximum of 2 cells being recorded from each animal.

I began by examining cells at their resting membrane potential of cells, there was no significant effect of sex on either resting membrane potential (Male, -72 ± 4 mV, n = 14, Female, -66 ± 4 mV, unpaired t-test p = 0.2) or the proportion of cells firing (6/14 Male cells fired while 10/19 Female cells fired, chi squared, p = 0.6), Of the cells which were firing at rest there was no significant effect of sex in Type III neurons (Male 4 ± 2 Hz, n = 6, Female 4 ± 1 Hz, n = 9, unpaired t-test p = 0.9) (Figure *4-21*).

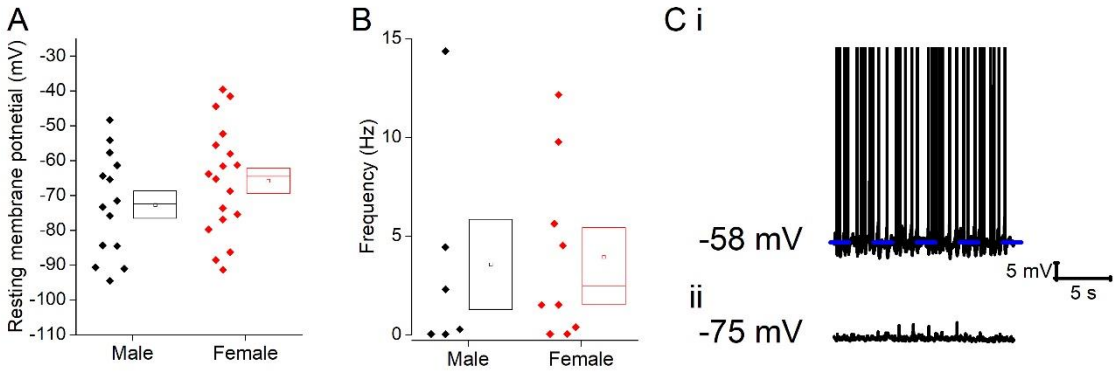

Figure 4-21 Properties of cells at their resting membrane potential of Type III neurons, A) resting membrane potential, B) Firing frequency at rest and C) sample cell firing at rest (i) and not firing at rest (ii).

Cells were then held at a prestimulus potential of -70 mV or -80 mV to examine the intrinsic properties of the neurons. I began by looking at the passive membrane properties. There was no significant effect of sex on the input resistance (-70 mV: Male, 588 ± 94 MΩ, n = 14, Female, 409 ± 49 MΩ, -80 mV: Male, 498 ± 72 MΩ, n = 14, Female, 410 ± 46 MΩ ,repeated measure two-way ANOVA p = 0.08), membrane time constant (-70 mV: Male, 38 ± 6 ms, n = 14, Female, 28 ± 4 ms, -80 mV: Male, 27 ± 3 ms, n = 14, Female, 27 ± 4 ms ,repeated measure two-way ANOVA p = 0.3) or capacitance (-70 mV: Male, 70 ± 7 pF, n = 14, Female, 67 ± 5 pF, unpaired t-test, p = 0.7, -80 mV: Male, 60 ± 6 pF, n = 14, Female, 73 ± 10 pF, Mann-Whitney U, p = 0.4) (Figure *4-22*). Sag

was not examined as the main criteria for Type III neurons is an absence of sag.

Following this the action potential properties were examined, as previously described this was recorded from the first action potential generated in response to a series of depolarising current injections. There was no effect of sex on the action potential width (-70 mV: Male, 0.9 ± 0.1 ms, n = 14, Female, 0.8 ± 0.1 ms, -80 mV: Male, 0.7 ± 0.1 ms, n = 14, Female, 0.8 ± 0.1 ms, repeated measure two-way ANOVA p = 0.3), threshold (-70 mV: Male, -51 ± 2 mV, n = 14, Female, -51 ± 2 mV, -80 mV: Male, -51 ± 2 mV, n = 14, Female, -50 ± 2 mV, repeated measure two-way ANOVA p = 0.9) or zenith (-70 mV: Male, 10 ± 3 mV, n = 14, Female, 14 ± 3 mV, -80 mV: Male, 12 ± 3 mV, n = 14, Female, 16 ± 3 mV, repeated measure two-way ANOVA p = 0.3) (Figure *4-23*). There was also no effect on the maximum rate of the rise of the action potential (-70 mV: Male, 198 ± 21 mV/ms, n = 14, Female, 253 ± 22 mV/ms, -80 mV: Male, 220 ± 20 mV/ms, n = 14, Female, 267 ± 24 mV/ms, repeated measure two-way ANOVA p = 0.1) (Figure *4-24*).

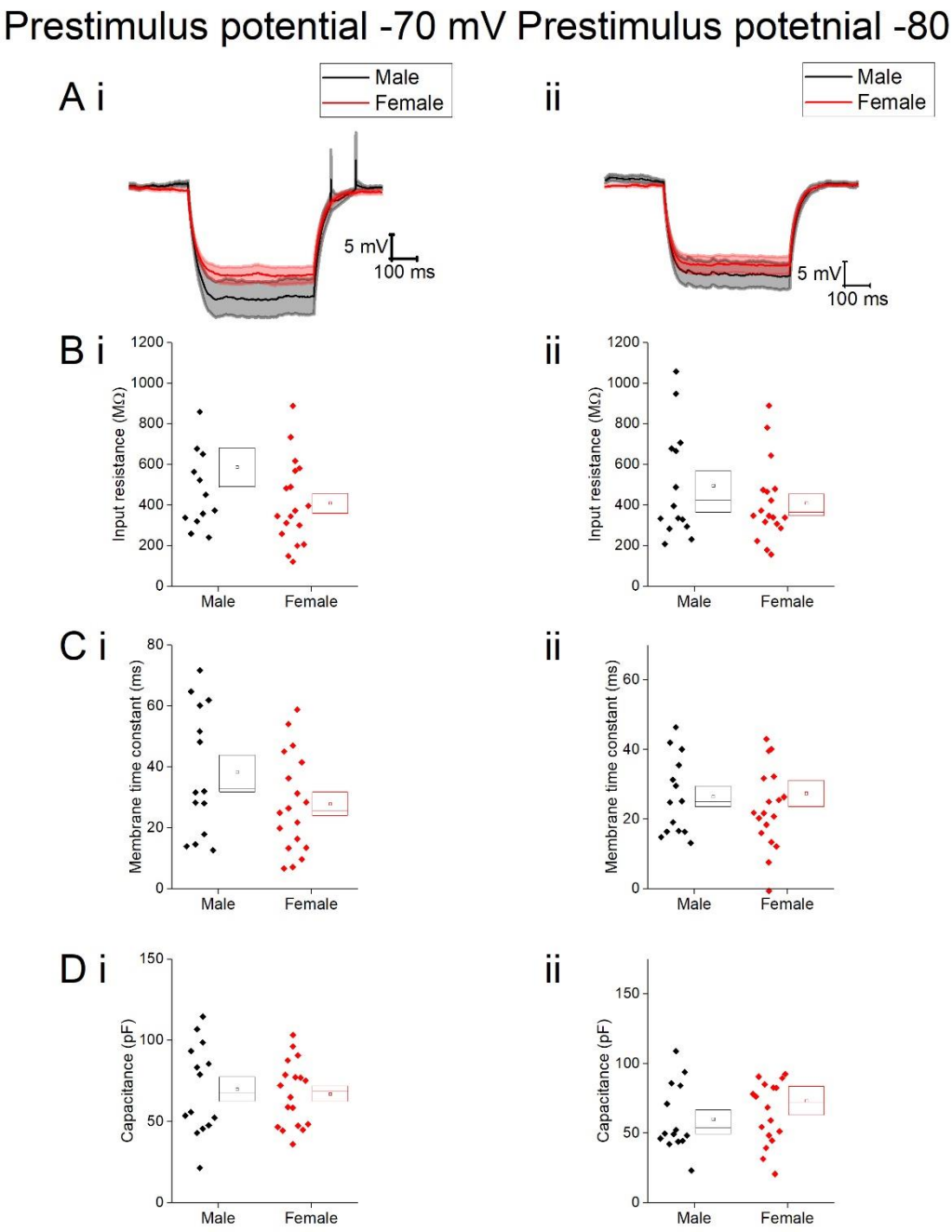

Figure 4-22 Passive membrane properties of Type III neurons A) average response to the injection of -40 pA of current from a prestimulus potential of -70 mV and -80 mV, B) input resistance from a prestimulus potential of -70 mV and -80 mV, C) membrane time constant from a prestimulus potential of -70 mV and -80 mV and D) capacitance from a prestimulus potential of -70 mV and -80 mV.

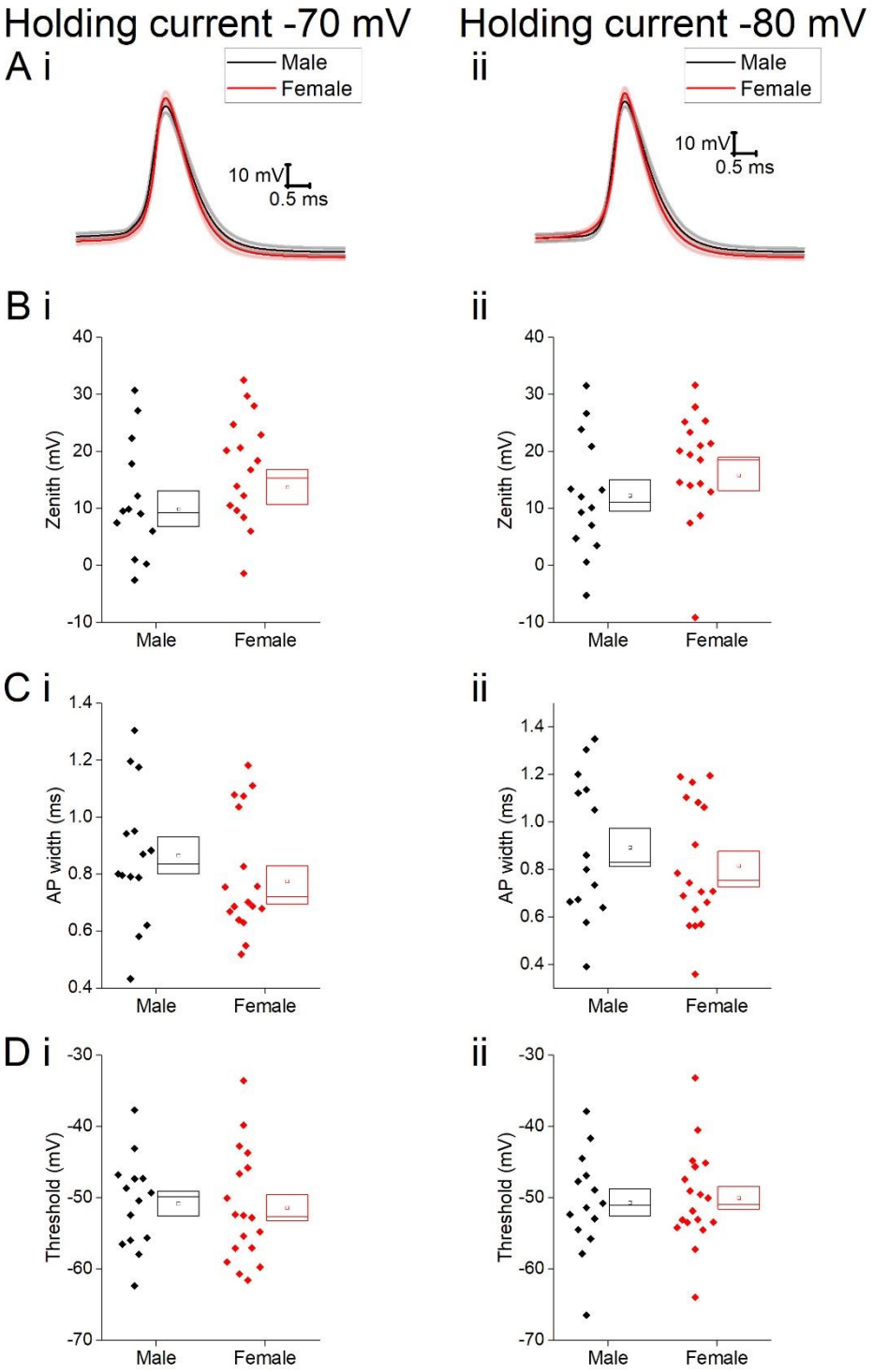

Figure 4-23 Action potential properties of Type III neurons, A) average action potential from a prestimulus potential of -70 mV and -80 mV, B) action potential zenith from a prestimulus potential of -70 mV and -80 mV, C) Action potential width from a prestimulus potential of -70 mV and -80 mV and D) action potential threshold from a prestimulus potential of -70 mV and -80 mV.

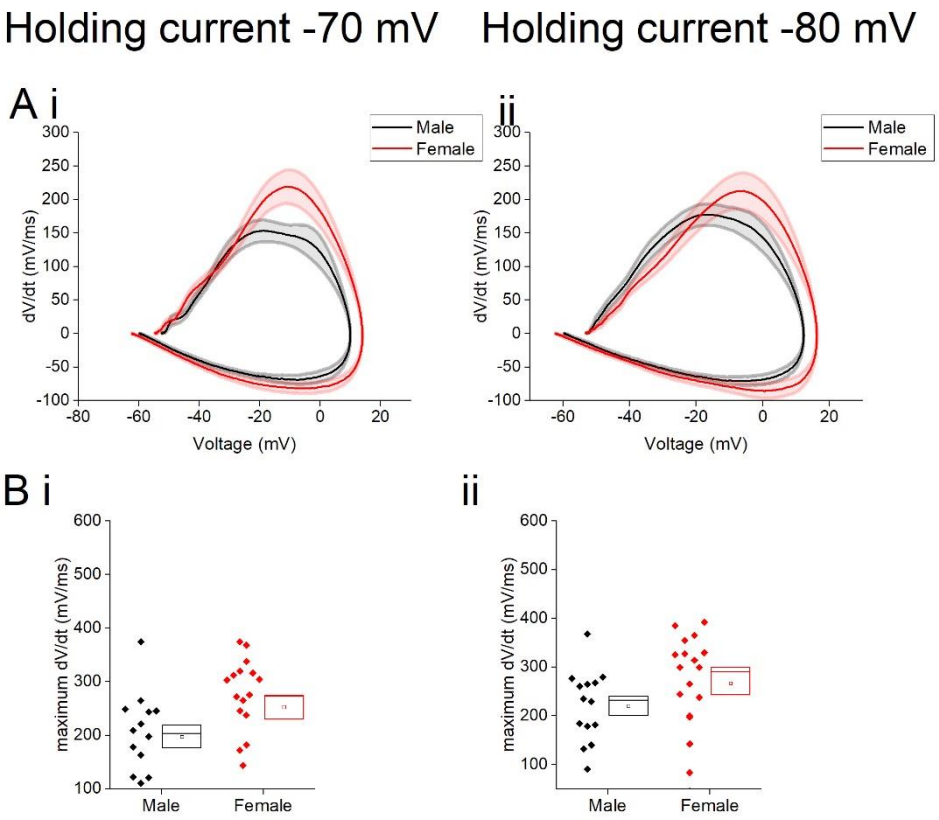

Figure 4-24 maximum rate of rise of the action potential, A) average rate of rise of the action potential plotted against the voltage change during the action potential. B) maximum rate of rise of the action potential from a prestimulus potential of -70 mV (i) and -80 mV (ii).

Finally I examined the firing properties of Type III, there was no significant effect of sex on either the proportion of cells firing in response to a series of depolarising pulses or the firing frequencies in response to a series of depolarising current injections (Figure *4-25*).

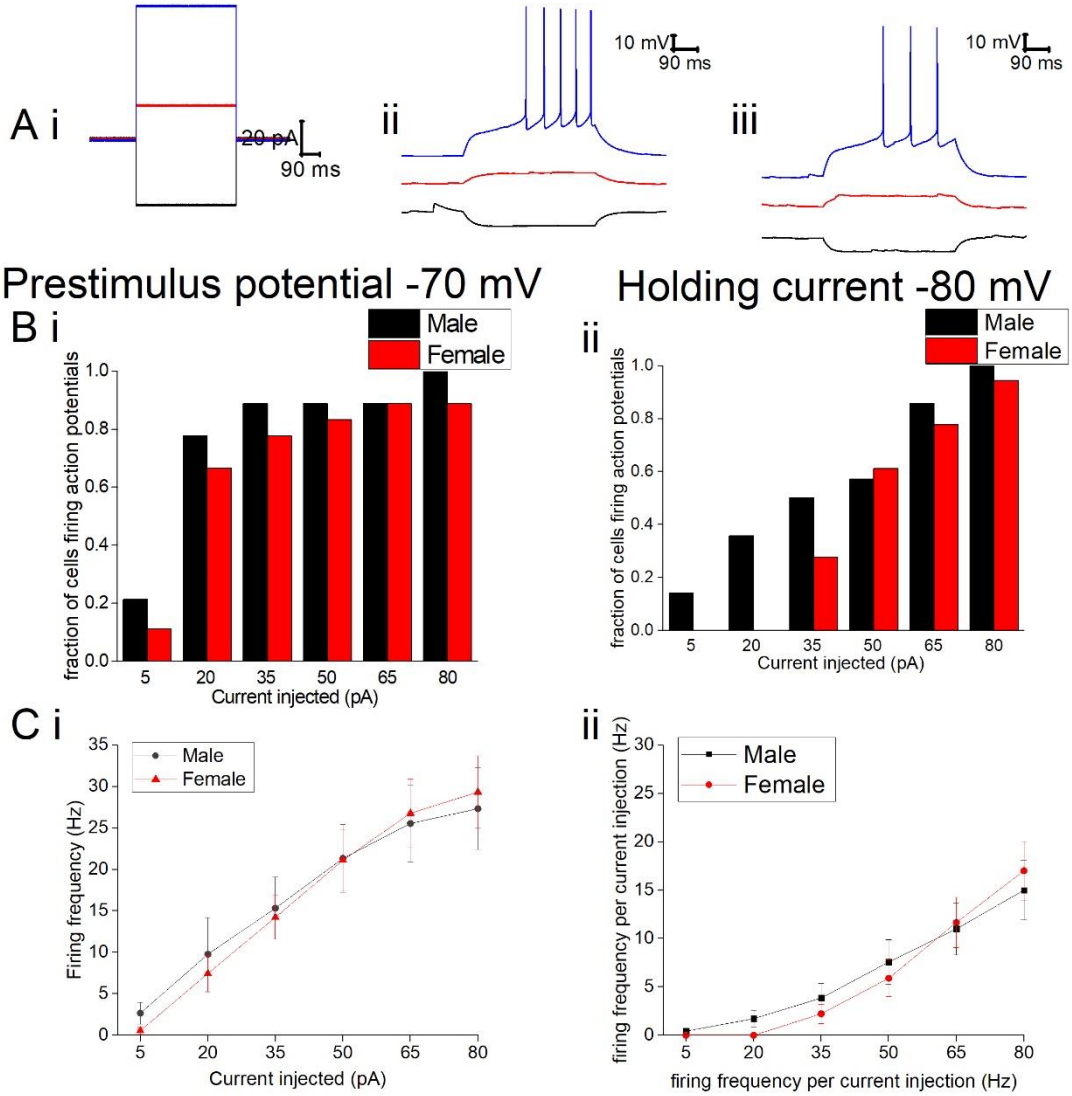

Figure 4-25 firing properties of Type III neurons A) sample trace in response to a current injection (i) from a male (ii) and female (iii) cell, B) fraction of cells firing in response to a series of depolarising stimuli (i) and C) firing frequency of cells n response to the injection a series of depolarising stimuli.

4.4. Discussion

This study examined the intrinsic electrophysiological properties of Type I and Type II neurons in the $BNST^{ALG}$ in young adult male and female mice. The main finding in this study was a greater excitability in Type II neurons in males. Theoretically such a sex-associated change in excitability could result from a number of underlying sources, such as a negative shift in AP threshold, altered AHPs, or changes in input resistance. In the case of Type II neurons in the $BNST^{ALG}$ the >20% higher input resistance observed in the male cohort is a likely contributing factor. This difference in input resistance was only statistically significant from a prestimulus potential of -80 mV. However from the more depolarised prestimulus potential of -70 mV there was a trend towards a higher input resistance in the males.

I addressed these changes in input resistance by examining the effects of Gaboxadol and found that Type II neurons in the females showed a trend towards larger changes in response to administration. While the higher levels of ALLO in female rats (Shen *et al.*, 2005) have been shown to increase expression of the delta subunit in the hippocampus. to my knowledge no one has examined this in the BNST however the trend observed here would indicate that similar processes may be taking place in the BNST.

The widespread expression of progesterone and estrogen receptors throughout the brain implies that their functions are not limited to reproduction. Indeed they have been shown to be involved in neuronal growth, survival, differentiation and plasticity (Singh & Su, 2013). Progesterones neuroprotective properties have also been characterised in Alzheimer's disease, stroke and traumatic brain injury (Singh & Su, 2013). A key metabolite of progesterone is allopregnalone which may impact BNST properties. The role of ALLO in anxiety is both age and sex specific (Shen *et al.*, 2007; Nagaya *et al.*, 2015*b*).

Here we have shown that Gaboxadol trends towards a higher impact on female Type II neurons indicating more $GABA_A$ receptor containing the δ subunit may be present in the $BNST_{ALG}$ of females. ALLO is an allosteric modulator which enhances actions of GABA at $GABA_A$ receptors containing the δ subunit, it also alters subunit expression of the $GABA_A$ receptor. The activation of these

receptors in this neuronal population reduces the input resistance of cells thereby reducing firing. As Type II neurons are responsible for reducing anxiety, a reduction in their firing could lead to an increase in activity in downstream targets such as the PVN thereby causing an increase in anxiety.

The anxiolytic actions of ALLO may be mediated via other components of the limbic system such as the hippocampus where short term treatment with ALLO treatment enhances δ subunit expression of $GABA_A$ receptors. However, the attenuation of CFR-enhanced startle by progesterone (Toufexis *et al.*, 2004) would implicate the involvement of the BNST. There is a population of CRF neurons within the BNST but this population was not addressed in this study due to low n numbers. However, if the effects seen in the Type II neurons were also observed in these anxiety-inducing CRF cells they may be medicating the effect.

The electrophysiological characterisation of cells in the BNST was originally based on male rats (Hammack *et al.*, 2007*b*). This characterisation was recently expanded to other mammals including mice and rhesus macaque; where a similar classification of cells appears to exist. These newer studies were also based solely on males (Daniel *et al.*, 2017). While these studies have hypothesised a role for these different populations based mainly on similar populations within the amygdala, their functional role has not been fully addressed. The BNST is a primarily GABAergic population but other cell types are present in this region including CRF cells. The CRF cells are thought to be Type III and act as anxiety-inducing neurons. The Type I and Type II cells are thought to be GABAergic and function as 'anxiety off' cells (Daniel & Rainnie, 2016). The correlation in behaviour of Type II cells supports this hypothesis. With an increase in excitability of neurons correlating with the higher percentage of time that was spent in the open component of the maze. The GABAergic nature of this population would allow it to inhibit neurons in the PVN leading to a reduction in anxiety-like responses.

The correlations observed in Type I neurons in this study would indicate an anxiety inducing function in this unstressed model. The more hyperpolarising resting membrane potentials in the male cohort correlated with a decrease in anxiety. In theory a more hyperpolarised resting membrane potential would indicate a decreased likelihood of firing as larger amounts of depolarising

current would be required to bring the cell to threshold. A trend was also seen in the frequency of cells which were firing; lower firing frequencies correlated with lower levels of anxiety. Finally a lower frequency of inward going synaptic events correlated with decreases in anxiety. The synaptic input into Type I cells was mostly blocked by administration of NBQX and L689560 indicating that these events are primarily glutamatergic in nature. There are substantial GABAergic projections into this region (Dong *et al.*, 2001*b*), however, given the chloride equilibrium of the solutions used (-50 mV) their detection could have been impaired. A higher frequency of glutamatergic input could increase the likelihood of spike generation. These correlations would indicate that the decreases in activity of Type I cells are related to decreases in the anxious behaviour of animals. To my knowledge this is the first study to directly compare anxiety like behaviour in relation to Type I and Type II cells in the BNST and have provided insight into the possible functionality of these different populations in the BNST.

The correlation between anxiety and behaviour discussed here would provide support for the physiologically distinct cell types in the region. However, these correlations were only significant in the male cohorts. This would lead one to question if such classifications are physiologically relevant in females. There are a number of possibilities why these classifications may alter between sexes, for example changes in I_h, which would alter the sag of the cells, sag is one of the key parameters on which Type I and Type II cells are characterised. Equally changes in I_T which is believed to be responsible for the nonlinear responses of cells to depolarising current injections leading to a ‘hump’, the presence of this ‘hump’ was a key component of identifying Type II neurons. Reclassification of the cells may be required for an accurate representation of the roles of BNST cell populations in females. These discrepancies in classification highlights the problem of sex bias in our electrophysiological characterisation of populations, especially those in a sexually dimorphic brain regions such as the BNST.

Here we have provided insight into the differences in intrinsic of neurons in the BNST between sexes in an unstressed model. These differences may provide a component of the physiological basis for changes in susceptibility to anxiety-related disorders. An interesting advancement of this work would be to address the effect of stress on the electrophysiological properties of BNST neurons in

both males and females. One proposed model of PTSD in rodents is predator scent exposure which shows lasting changes in anxiety (Adamec *et al.*, 2006), this model showed some sex-specific behaviours making it an ideal starting point to better understand responses to stressors. The electrophysiological characterisation of the BNST in this model would provide a key insight into possible changes in susceptibility of the different sexes to PTSD.

5. Heightened intrinsic excitability in Type II neurons of the bed nucleus of the stria terminalis in aged mice

Having determined the sexually dimorphic nature of the intrinsic properties of neurons located in the $BNST^{ALG}$ I was next interested to determine the impact of age on these properties. Due to availability of tissue this study was carried out in female mice.

5.1. Introduction

Although seen at most ages from childhood onwards, the development and nature of chronic stress exhibits a complex age-related nature (Garrido, 2011; Prenderville *et al.*, 2015).The glucocorticoid theory of brain aging hypothesises the role of these key molecules in healthy aging; chronic exposure to glucocorticoids leads to damage of brain structures. Indeed, in aging there is an impairment of the negative feedback of the HPA axis leading to chronically elevated glucocorticoid levels (Gupta & Morley, 2014). One key component of this is the downregulation of the glucocorticoid receptor within the hippocampus (Sapolsky *et al.*, 1986). The role of the BNST in this feedback loop has not been previously addressed however, given the key position of the BNST as a relay between the hippocampus and the PVN, it is highly probable that the BNST may contribute to these observed alterations

Little research has been carried out on the BNST in healthy aging and to my knowledge no one has looked at the electrophysiological properties of the BNST in aging, however some research has been carried out in gene expression levels of various key mediators within the BNST. Nutsch *et al* 2017 examined the expression levels of a number of key genes associated with behaviour in the both the BNST and several other regions associated with hypothalamic modulation. They found a decrease in expression of six genes; *Cyp19a1*, *Esr2*, *Kiss1r*, *Nos1*, *Oxtr* and *Thra* in male Spague-Dawley male rats at 18 months in comparison to 3 month olds (Nutsch *et al.*, 2017).

To my knowledge the only other study to assess the role of the BNST in healthy aging found a decrease in vasopressin mRNA in aged male Fischer 344 rats (Dobie *et al.*, 1991). This effect was rescued via administration of testosterone (Dobie *et al.*, 1992). Vasopressin plays a key role in a number of social behaviours including social approach and communication, with pharmacological inhibition leading to anxiogenic effects (Faria *et al.*, 2016).

The above studies implicate the BNST as a key region in mediating changes in anxiety associated with aging, functional characterisations were not carried out in any of these studies but we would expect the above mentioned changes to impact the functionality of neurons within this circuit.

In male C57BL/6 mice, levels of glucocorticoid were found to decrease at 16 months however this was a circadian-dependent effect seen only in the morning with no changed observed in the evening (Dalm *et al.*, 2005). I hypothesized that the changes to HPA activity associated with healthy aging may, at least in part, be driven by changes in the electrophysiological properties of neurons located within the BNST. To address this I performed a study in which I compared the neurophysiological properties of Young (3-4 month old) and Aged (29-30 month old) neurons in the $BNST^{ALG}$ in female C57BL/6 mice. This initial study focused on the role of aging in female mice, this was due to the availability of tissue, and in future it would be interesting to expand this characterisation to male mice. I believe this to be the first cell-level study to examine the effects of healthy aging on the neurophysiological function of the BNST.

Hypothesis

Sex specific changes in stress and anxiety observed in aging may be mediated by changes to the intrinsic properties of neuron located within the $BNST^{ALG}$.

Aims

To identify changes in intrinsic properties of the different population within the $BNST^{ALG}$.

5.2. Methods

5.2.1. Animals

All tissues for this study were harvested from female C57BL/6 mice purchased from Charles River. In this investigation animals aged 3-4 months (Young) were compared to animals aged 29-30 months (Aged). Experimental days employing brain slices obtained from the two different ages of mouse were interleaved throughout the duration of the study.

Graphs were generated using Origin; for all box plots the symbols to the left are individual recordings. The small symbol within the box is the mean, the box reflects the Standard error of the mean (SEM) and line traversing the box is the median.

5.3. Results

A total of 28 cells from the Aged cohort and 44 cells from the Young cohort were recorded in the $BNST^{ALG}$. The aged neurons consisted of 8 Type I cells from 4 animals with a maximum of 4 cells from any one animal, 16 Type II cells from 9 animals with a maximum of 4 cells from any one animal and 3 Type III cells, the young neurons consisted of 19 Type I cells from eight animals with a maximum of four cells from any one animal, 18 Type II cells from seven animals with a maximum of four cells from any one animal and 7 Type III neurons. Due to the low n numbers of Type III cells they were not included in this report.

5.3.1. Type I neurons

Initially, I began by examining spontaneous synaptic events while clamping the voltage at -70 mV. The mean holding current required to maintain cells at -70 mV in voltage clamp mode was more positive in the aged cohort (14 ± 4 pA, n = 14) than the Young group (-5 ± 5 pA, n = 6) (Unpaired t-test p=0.02, t = -2.5, Figure 5-1). Imposed upon the baseline current of both groups was a considerable barrage of spontaneous inward-going synaptic events (Figure 5-1). The frequency of these events (Figure 5-1) varied considerably from cell to cell but did not differ with age (Young: 9 ± 2 Hz, n = 14, aged: 10 ± 3 Hz, n = 6, Mann-Whitney U, p = 0.7, Z = -0.5). The average amplitude of these events was -16 pA (Young -16 ± 1 mV, n = 14, Aged -16 ± 2 pA, n = 6, Mann-Whitney U, p = 0.97, Z = 0.1, Figure 5-1) and was not age-dependent.

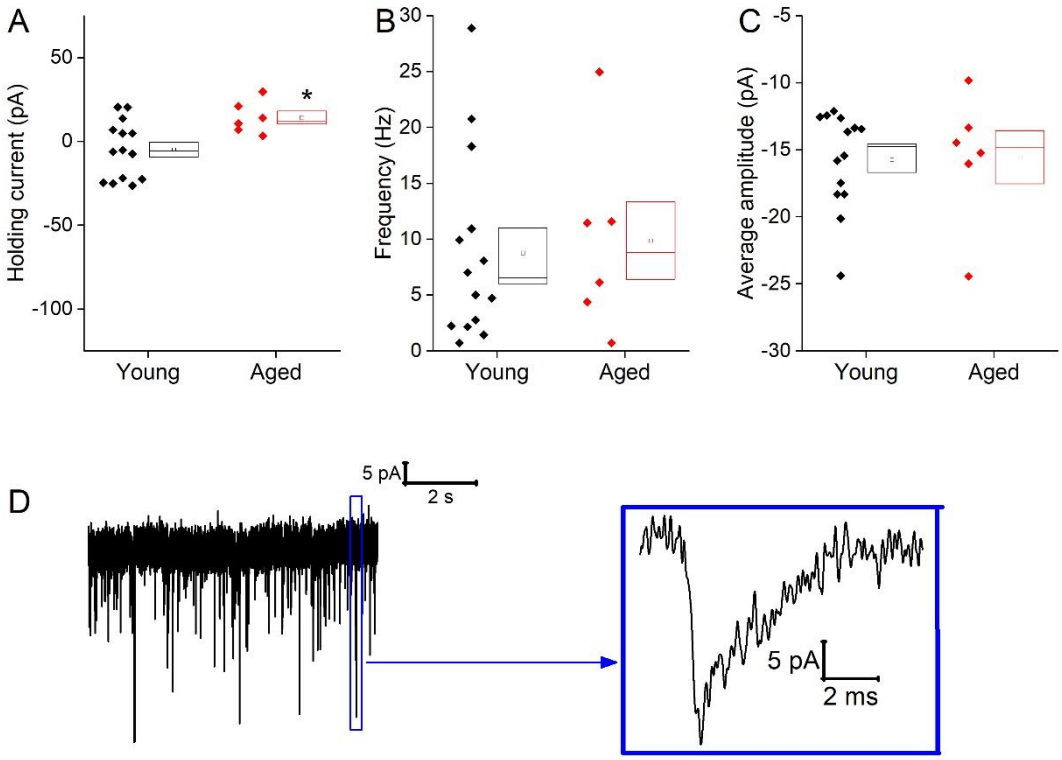

Figure 5-1. Spontaneous inward post-synaptic current properties of Type I neurons **A)** the holding current required to hold cells at -70 mV, **B)** Mean inward postsynaptic current frequency from 60 s voltage clamp recordings at -70 mV, **C)** Corresponding mean inward postsynaptic current averaged amplitudes, **D)** Sample trace from a typical BNST neuron showing numerous spontaneous inward-going postsynaptic currents and a zoomed in image of a single spontaneous synaptic events. For all graphs in figure - Young n= 14, Aged n = 6.

Given the significant difference in the amount of current required to hold cells at -70 mV in the voltage clamp recordings it is unsurprising that the mean resting membrane potential of the young cohort (-68 ± 3 mV, n = 18) was over 10 mV more depolarised than that of the Aged population (-80 ± 2 mV, n = 8), (unpaired t-test, p= 0.01, t = 2.6, Figure 5-2). This difference in resting membrane potential did not lead to a significant difference in the proportion of cells exhibiting any spontaneous action potential firing; 12 % fired spontaneously in the Aged slices (1 of 8 cells) while 50% were firing in the Young group (9 of 18 cells; Chi-squared test p = 0.07). Of the cells which did not fire spontaneously there was no difference in rheobase (Young 46 ± 11 pA, n = 5, Aged 34 ± 11 pA, n = 7, Mann-Whitney U, p = 0.3, Z = -1, Figure 5-2).

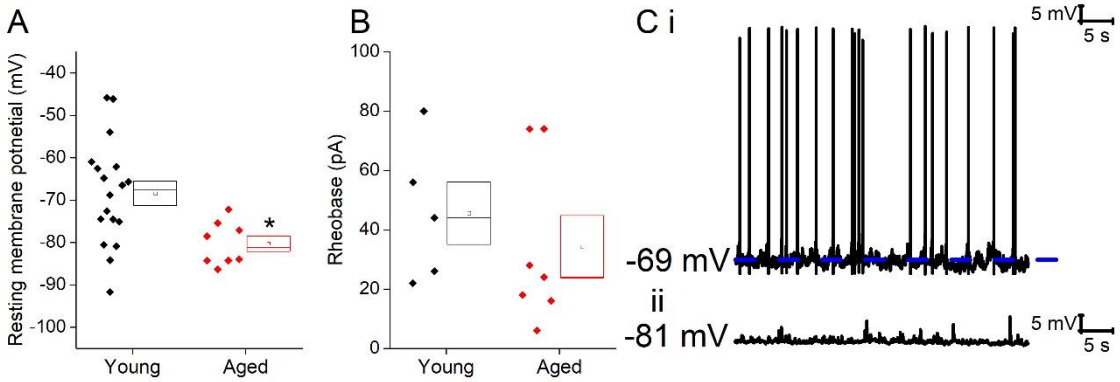

Figure 5-2. Aged Type I neurons have a more depolarised resting membrane potential. **A)** Resting membrane potential (RMP), **B)** Rheobase of cells which did not fire action potentials in initial minute of recording (pA), **C)** Sample cell firing spontaneously (i), sample cell not firing at rest (ii) and a sample current injection (iii).

Holding cells at a set membrane potential was achieved by application of suitable level of “steady state” bias current. The amount of current required to hold cells at -70 mV (Young 5.5 ± 6 pA, n = 18, Aged 23.6 ± 5 pA, n = 7) and -80 mV (Young -27 ± 7 pA, n = 19, Aged 4 ± 3 pA, n = 7) was dependent on age (repeated measure two way ANOVA, age p = 0.03, F = 5).

Once cells were held at a set membrane potential a series of depolarising and hyperpolarising steps were injected. Injection of -40 pA of current was used to assess passive membrane properties of the cells; the averages of these traces are shown in Figure 5-3. From a holding potential of -70 mV the cells from the Young population charged with a mean membrane time constant of 31 ± 4 ms (n = 18) which is significantly faster than those from the Aged population (48 ± 4 ms, n = 8, Mann-Whitney U p = 0.005, Z = -2.5, Figure *5-3*). This was also faster from a prestimulus potential of -80 mV averaging 29 ± 3 ms in the young cohort (n = 19) and 35 ± 4 ms in the aged cohort (n = 8) which was not significantly different (Mann-Whitney U, p = 0.14, Z = -1.6, Figure *5-3*).

There was no statistically significant effect of age on input resistance (-70 mV Young: 413 ± 37 MΩ, n = 18, Aged 539 ± 61 MΩ, n = 8; -80 mV Young 352 ± 32 MΩ, n = 18, Aged: 420 ± 69 MΩ, n = 8, repeated measure two-way ANOVA, age p = 0.14, F = 2.4 Figure 5-3) or capacitance (-70 mV Young: 79 ± 9 pF, n = 18, Aged: 97 ± 15 pF, n = 8, Mann-Whitney U, p = 0.16, Z = -1.4; -80 mV

Young: 90 ± 9 pF, Aged : 90 ± 8 pF, Mann-Whitney U, p = 0.6, Z = 0.56, Figure 5-3). All Type 1 neurons exhibit some degree of hyperpolarization activated “sag” at -80 mV. Sag was not age dependent averaging 16 ± 2 % in the Young neurons (n = 18) and 15 ± 3 % in the Aged (n = 8) neurons (Mann-Whitney U, p = 0.7, Z = -0.4, Figure 5-3).

The relationship between current injected and proportion of cells firing one of more spikes is shown in figures 5-4B and C for prestimulus potentials of -70 mV and -80 mV, respectively. Examples of current injections from both age cohorts are shown in Figure 5-4. As expected less current was required to generate spiking from the more depolarized holding potential. From both prestimulus potentials, age had no effect on the likelihood of spike generation (Figure 5-4). Figure 5-4 C describes the total spike outputs generated during the 500 ms depolarizing stimuli (including traces with zero spikes) related to stimulus amplitude, this also did not differ with age at either -70 mV (Two way ANOVA p = 0.2, F = 1.4) or -80 mV (Two way ANOVA p = 0.6, F = 0.4).

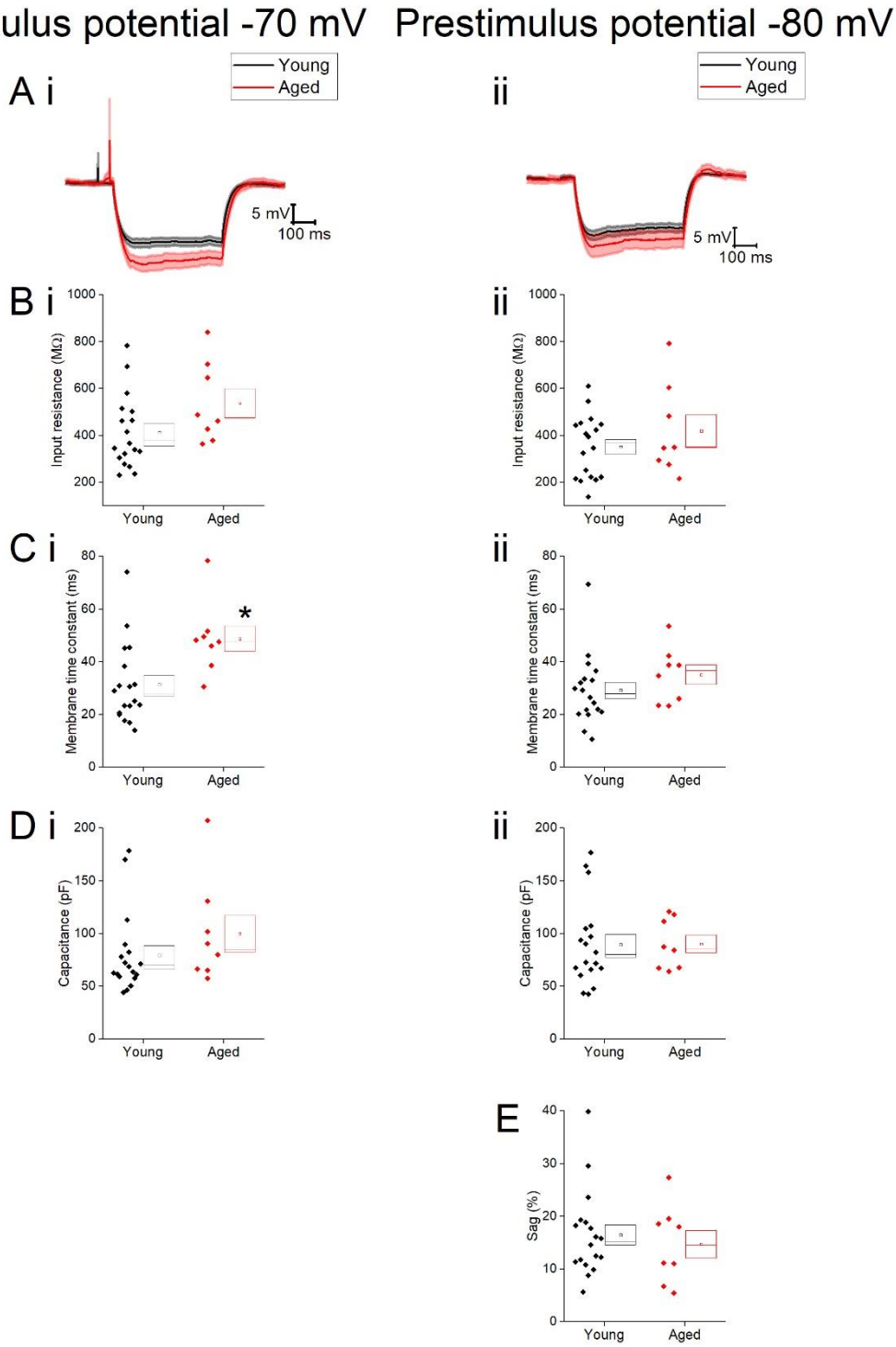

Figure 5-3. Passive membrane properties of type I cells. **A)** Averaged traces of voltage response to a -40 pA current step in the Young and Aged cohort from a holding potential of -70 mV (i) or -80 mV (ii) (the shaded areas are the standard error of the mean**), B)** Input resistance (R_{in}) from -70 mV (i) and -80 mV (i) **C)** membrane time constant (tau) from -70 mV (i) and -80 mV (i), **D)** Capacitance from -70 mV (i) and -80 mV (ii) **E)** % sag from -80 mV.

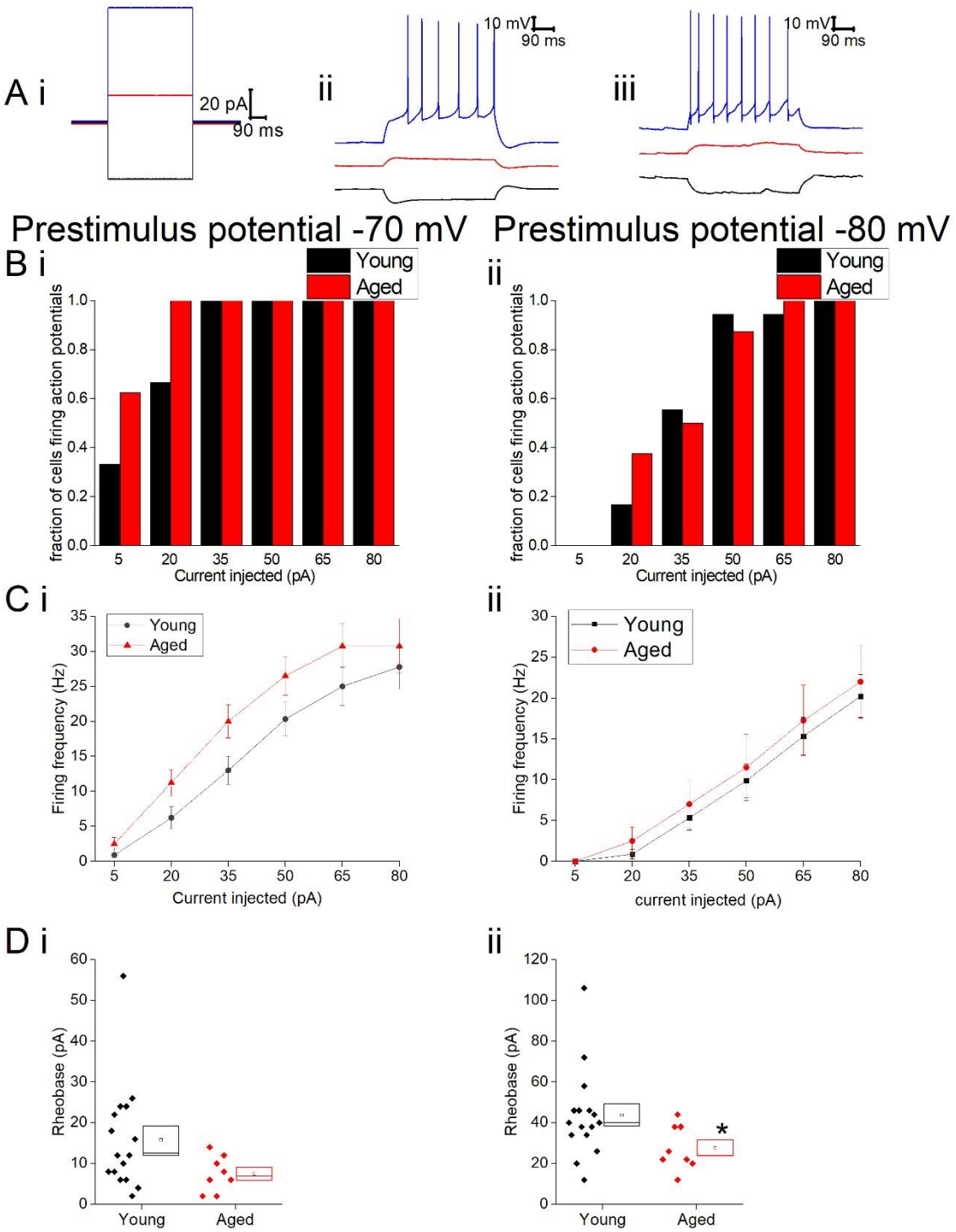

Figure 5-4. Type I neurons exhibit no age dependent changes in excitability in response to depolarising stimuli. **A)** For -40 pA, +20 pA and +80 pA stimuli applied at a prestimulus voltage of -80 mV the applied current injection (i) and observed voltage response from an example Young cell (ii) and Aged cell (iii) are presented. **B)** Fraction of cells which fired at least 1 action potential in response to each amplitude of depolarising current injection applied from holding potentials of -70 mV (i) and -80 mV (i). **C)** Mean number of action potentials for each level of current injection from holding potentials of -70 mV (i) and -80 mV (ii),(error bars SEM) **D)** Rheobase from a holding potential of -70 mV (i) and -80 mV (ii).

Although no differences were observed in firing properties from set membrane potentials the rheobase was significantly higher from the prestimulus potential of -80 mV in the Young neurons (44 ± 5 pA, n= 16) than in the Aged cohort (28 ± 4 pA, n = 8) (Mann-Whitney U p = 0.04, Z = -2.047, Figure 5-4). From a prestimulus membrane potential of -70 mV the mean rheobase was ~8 pA higher in Young cohort (16 ± 3 pA, n = 16) in comparison to the Aged neurons (7.5 ± 2 pA, n = 8) but was not statistically different (Mann-Whitney U, p = 0.08, Z = -1.8, Figure 5-4).

The action potential properties were measured from the 1st action potential generated in response to depolarising current injections. Average APs from the Young and Aged groups are presented in Figure 4. The threshold (-70 mV, Young -53 ± 1 mV, n = 18, Aged -54 ± 2 mV, n = 8; -80 mV, Young -54 ± 1 mV, n = 18, Aged -56 ± 1 mV, n = 8, repeated measure two-way ANOVA, age p = 0.9, F = 0.3, Figure 5-6), maximum rate of rise (dV/dt max; -70 mV, Young 269 ± 18 mV/ms, n = 18, Aged 259 ± 27 mV/ms, n = 8; -80 mV Young 297 ± 16 mV/ms, n = 18, Aged 271 ± 26 mV/ms, n = 8, repeated measure one-way ANOVA, age p = 0.6, F = 0.4, Figure 5-5) and action potential zenith (70 mV, Young 17 ± 2 mV, n = 18, Aged 22 ± 4 mV, n = 8 Unpaired t-test, p = 0.1, t = -1.7; -80 mV, Young 19 ± 2 mV, n = 18, Aged 23 ± 4 mV, n = 8, Mann-U-Whitney, p = 0.1, Z = -1.6, Figure 5-6) did not differ with age.

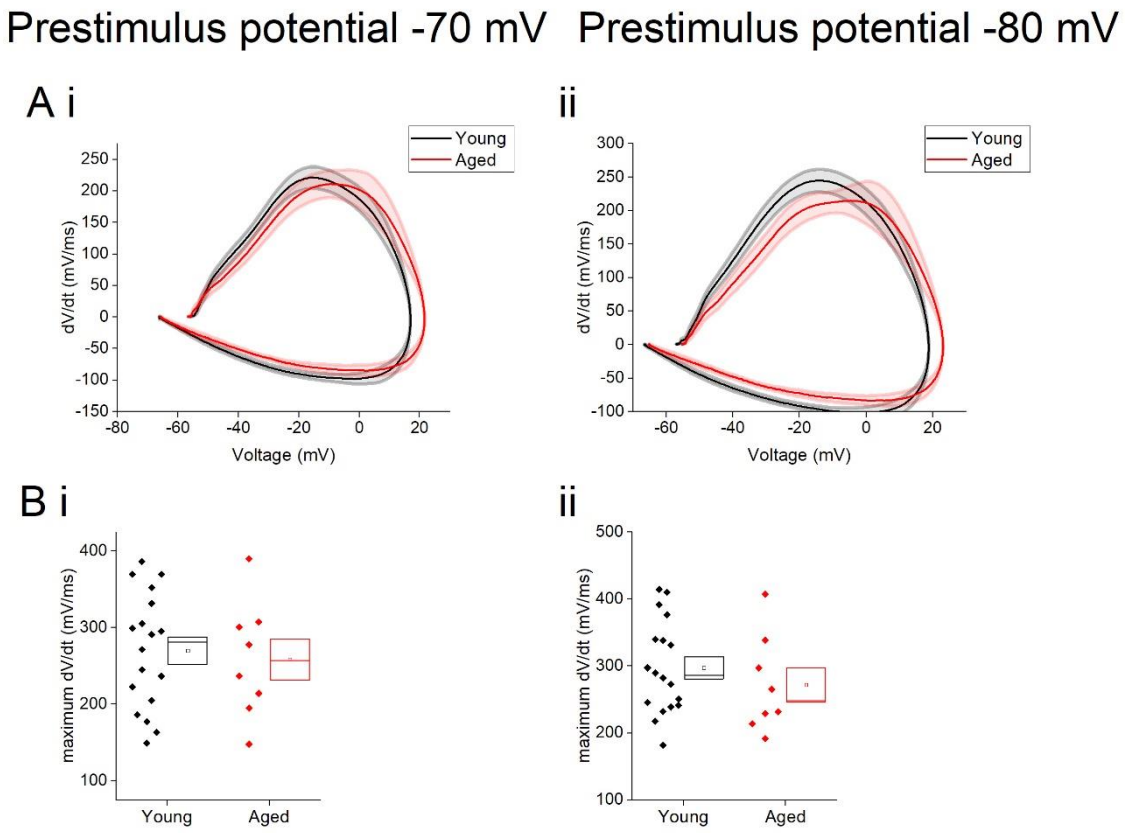

Figure 5-5. dV/dt of first action potential generated, **A)** averaged dV/dt of action potentials plotted against the average voltage of aforementioned action potentials from a holding current of -70 mV (i) and -80 mV (ii). **B)** dV/dt max from a holding potential of -70 mV (i) and -80 mV (ii).

The action potential width measured at the threshold was a mean of >0.4 ms wider in the Aged cohort in comparison to the Young cohort (-70 mV, Young 1.5 ± 0.1 ms, n = 18, Aged: 2 ± 0.2 ms, n = 8; -80 mV, Young 1.6 ± 0.1 ms, n = 18, Aged, 2 ± 0.2 ms, n = 8, repeated measure one-way ANOVA, age p = 0.04, Figure 5-6). From a set measurement of -20 mV there was no differences in action potential width (-70 mV, Young: 0.8 ± 0.05 ms, n = 18, Aged: 0.9 ± 0.08 ms, n = 8; -80 mV, Young: 0.8 ± 0.05 ms, Aged: 1 ± 0.1 ms, repeated measure one-way ANOVA, age p = 0.07, Figure 5-6).

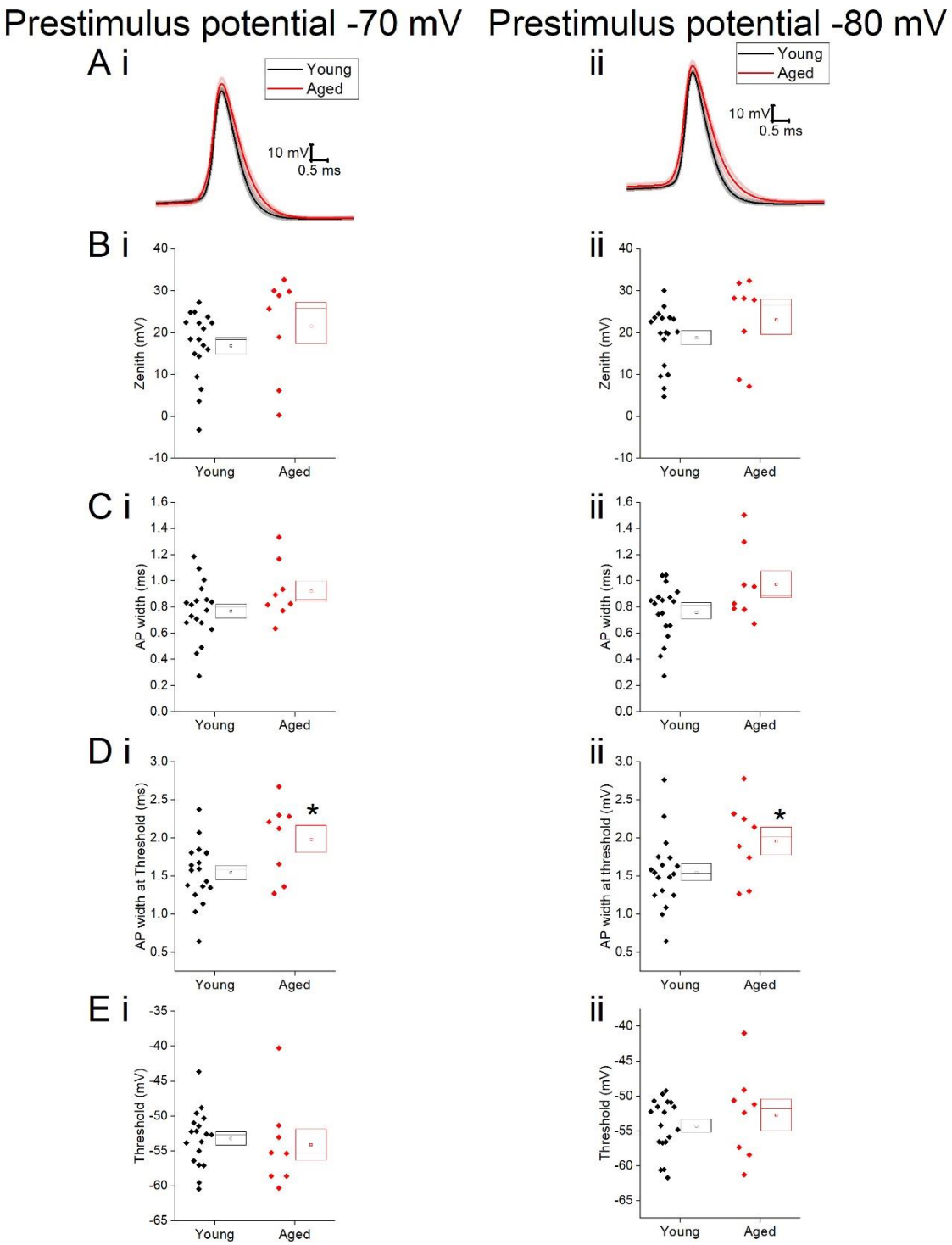

Figure 5-6. Aged Type I neurons have wider action potentials**.** The properties of the first action potential produced by a 500 ms duration depolarizing pulse **A)** averaged action potential for 1st Action potential from -70 mV (i) and -80 mV (ii). **B)** action potential Zenith from holding potential of -70 mV (i) and -80 mV (ii), **C)** action potential width from holding potential of -70 mV (i) and -80 mV (ii), **D)** action potential width at threshold from holding potential of -70 mV (i) and -80 mV (ii), **E)** threshold from holding potential of -70 mV (i) and -80 mV (ii).

Finally I examined the delay between the injection of the current and the generation of an action potential. This was examined on 2 steps the first was a measurement of the first action potential generated during this protocol. There was no difference in the latency to the first action potential generated at either holding potential (-70 mV, Young: 137 ± 30 ms, n = 18, Aged 168 ± 58 ms, n = 8, Mann-Whitney U, p = 0.5, Z = -0.7; -80 mV, Young: 166 ± 33 ms, n = 18, Aged: 245 ± 55 ms, n = 8, Mann-Whitney U, p = 0.2, Z = -1.2, Figure 5-7). Secondly I looked at the latency to the first action potential generated following the injection of 80 pA, no age-dependent differences were observed (-70 mV, Young 11 ± 1 ms, n = 18, Aged: 11 ± 2 ms, n = 8, Mann-Whitney U p = 1, Z = 0; -80 mV, Young: 57 ± 22 ms, n = 18, Aged: 85 ± 28 ms, n = 8, Mann-Whitney U, p = 0.5, Z = -0.7 Figure 5-7).

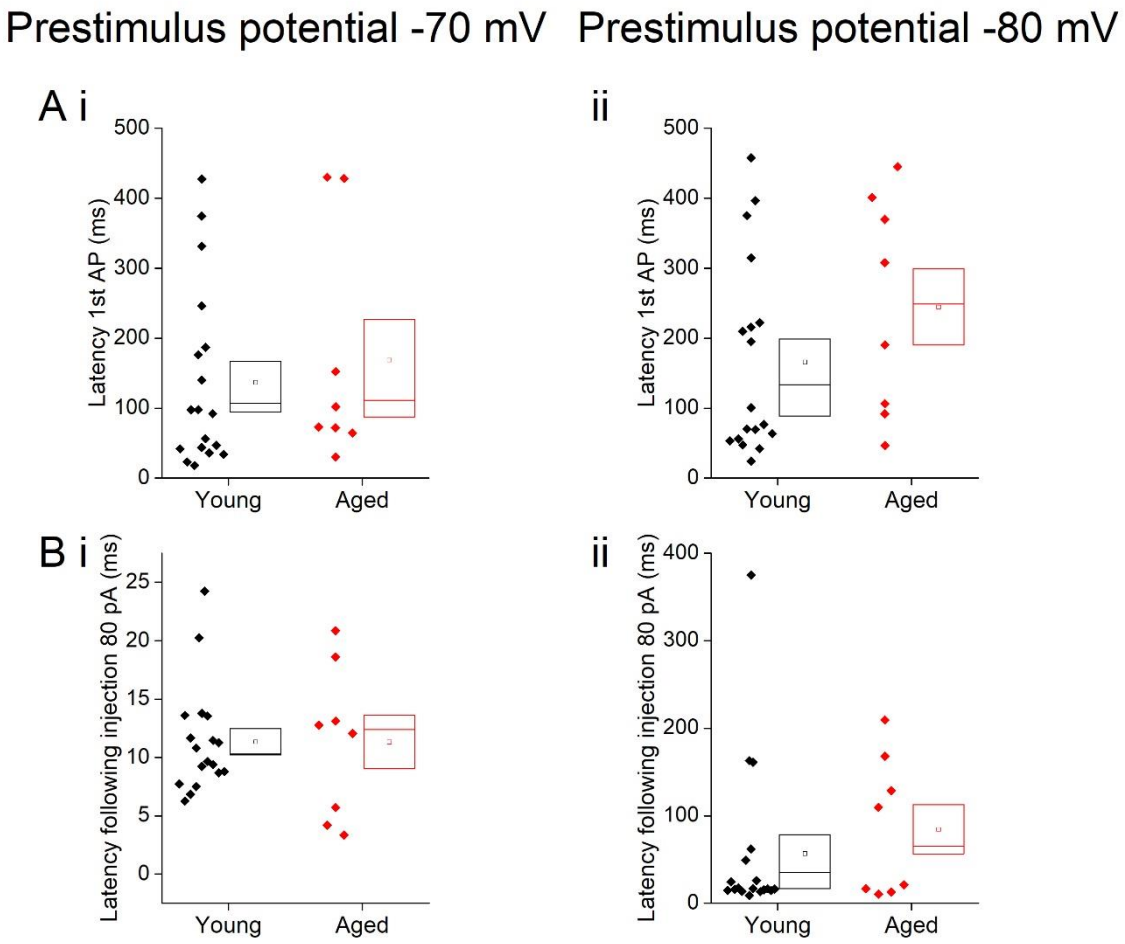

Figure 5-7. Latency to generation of first Action potential of Type I neurons **A, B)** Latency to the 1st Action potential generated in response to depolarising current injections from a holding current of -70 mV and -80 mV, respectively. **C, D)** Latency to the first action potential generated in response to the injection of 80 pA of current from a holding potential of -70 mV and -80 mV, respectively.

5.3.2. Type II neurons

I began by examining spontaneous synaptic events while clamping the voltage at -70 mV. Similar to Type I neurons these cells receive a large quantity of spontaneous inward going synaptic events. The frequency of these events did not differ with age (Young: 13 ± 3 Hz, n = 16, Aged: 7 ± 2 Hz, n = 14, Mann-Whitney U, p = 0.3, Z = -1.2 Figure 5-8), however the average amplitude of these events was a mean of 2.5 pA larger in the Young cohort (-16 ± 1 pA, n = 16) in comparison to the Aged (-13 ± 1 pA, n = 14, Mann-Whitney U p = 0.02, Z = -2.3 Figure 5-8). The holding potential required to hold Type II cells at -70 mV in voltage clamp mode did not differ with age (Young: -6 ± 5 pA, n = 16, Aged -9 ± 3pA, n = 14, Mann-Whitney U, p = 0.5, Z = -.07, Figure 5-8).

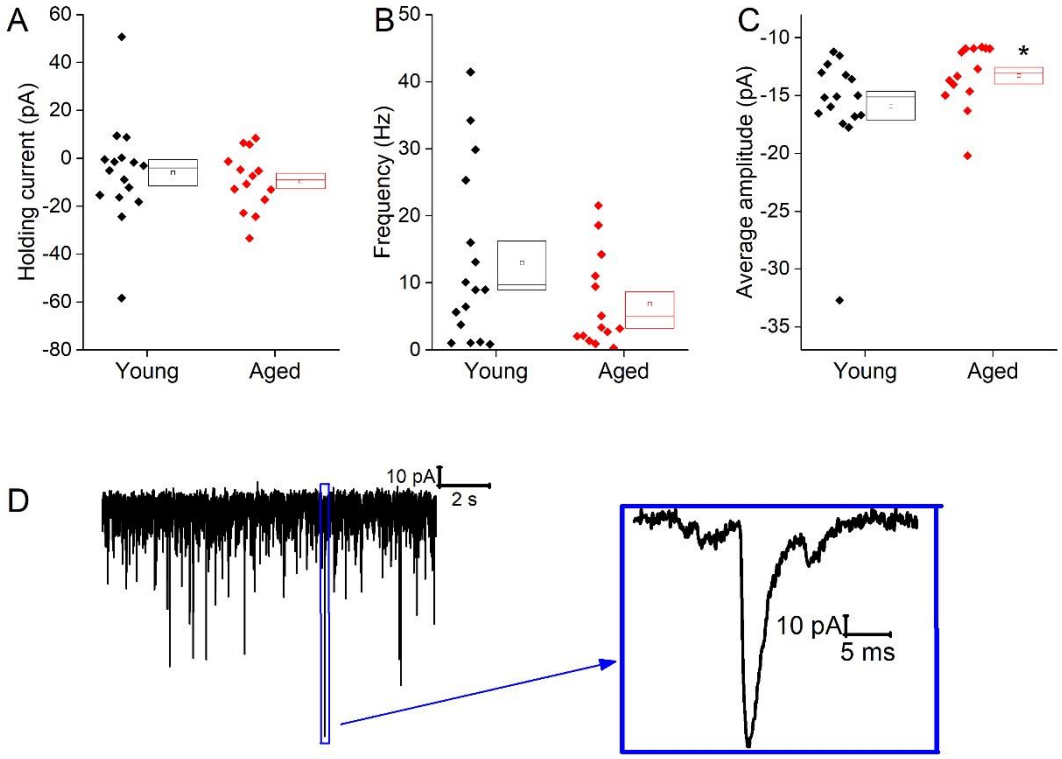

Figure 5-8 Spontaneous inward post-synaptic current properties of Type II neurons **A)** The holding current required to hold cells at -70 mV, **B)** Inward postsynaptic current frequency from 60 s voltage clamp recordings at -70 mV **C)** Corresponding mean inward postsynaptic current amplitudes **D)** Sample trace from a typical BNST neuron showing numerous spontaneous inward-going postsynaptic currents and a zoomed in image of a single spontaneous synaptic events. For all graphs in this figure Young n = 16, Aged n = 14.

Following these recordings I switched into current clamp mode and examined the cells at their resting membrane potential. The resting membrane potential was ~5 mV more depolarised in the aged cohort however this was not statistically significant (Young: -74 ± 2 mV, Aged: -69 ± 2 mV, unpaired t-test p = 0.1, t = -1.7, Figure 5-8). The proportion of cells spontaneously firing was far greater in the aged cohort with 10/16 aged cells firing while only 4/17 cells fired in the Young cohort (Chi squared p = 0.02). While this may be partly mediated by the RMP it could also be down to changes in cells excitability such as action potential threshold. Of the cells which were spontaneously firing there was no age effect on the firing frequency (Young 3 ± 2 Hz, n = 10, Aged 4 ± 2 Hz, n = 4, Mann-Whitney U, p = 0.8, Z = -0.3, Figure 5-9); equally of the cells which did not fire there was no age-dependent effect on the rheobase (Young 27 ± 4 pA, n = 10, Aged 18 ± 8 pA, n = 5, p = 0.2, t = 1.2, Figure 5-9).

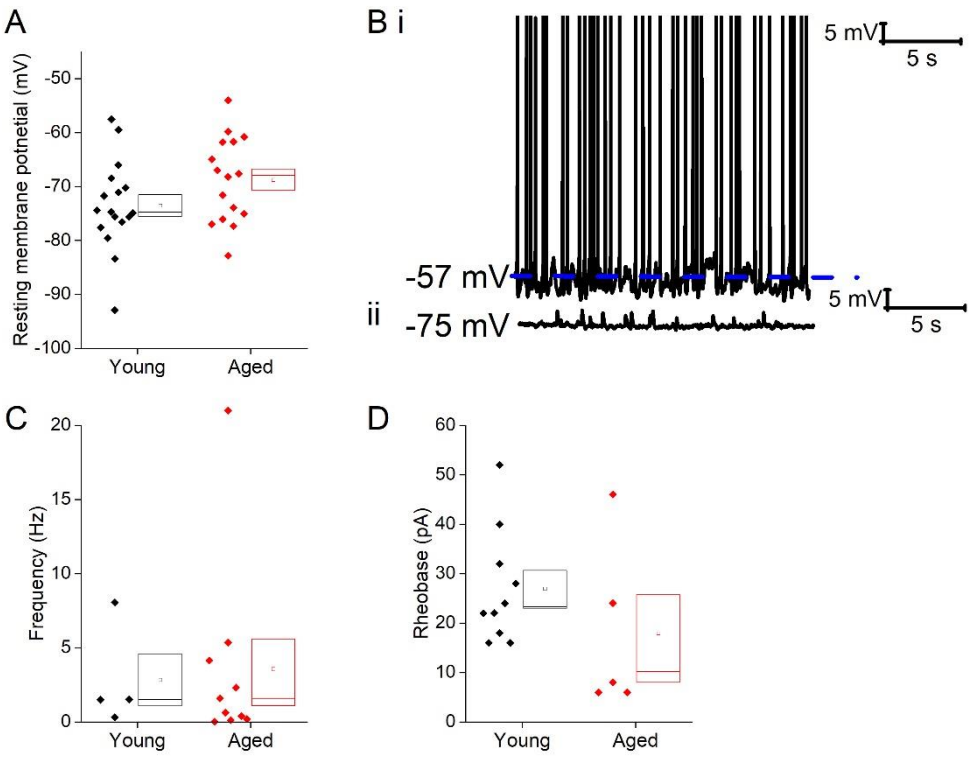

Figure 5-9 The Resting membrane potential properties of Type II neurons do not differ with age. **A)** Resting membrane potential (RMP) **B)** Sample cell firing spontaneously with current injection bellow, **C)** Firing frequency of cells which fired at RMP **D)** Rheobase at RMP.

From the -40 pA step of the current injection protocol (averages shown in Figure 5-10A) the input resistance, membrane time constant (tau), sag and capacitance were calculated. Input resistance (-70 mV Young 482 ± 56 MΩ, n = 18, Aged 582 ± 69 MΩ, n = 16, Mann-Whitney U p = 0.3, Z = -1.1; -80 mV, Young 433 ± 56 MΩ, n = 18, Aged 467 ± 68 MΩ, n = 16, Mann-Whitney U, p = 0.8, Z = -0.3), membrane time constant (-70 mV, Young 35 ± 4 ms, n = 18, Aged 32 ± 4 ms, n = 16, unpaired t-test p = 0.7, t = 0.4; -80 mV, Young 30 ± 4 ms, Aged 28 ± 4 ms, Mann-Whitney U p = 0.9, Z = -0.2) and were not age-dependent at either holding potential (Figure 5-10). Sag also did not differ with age (-80 mV, Young 17 ± 2 %, n = 18, Aged 21 ± 3 %, n = 16, unpaired t-test, p = 0.2, t = -1.3, Figure 5-10). Capacitance was a mean of over 10pF higher in the young cohort however this was not statistically significant (-70 mV, Young: 74 ± 6 pF, n = 18, Aged: 57 ± 3 pF, n = 16; -80 mV, Young 70 ± 6 pF, n = 18, Aged 60 ± 3 pF, n = 16, repeated measure one-way ANOVA, age p = 0.054 Figure 5-10).

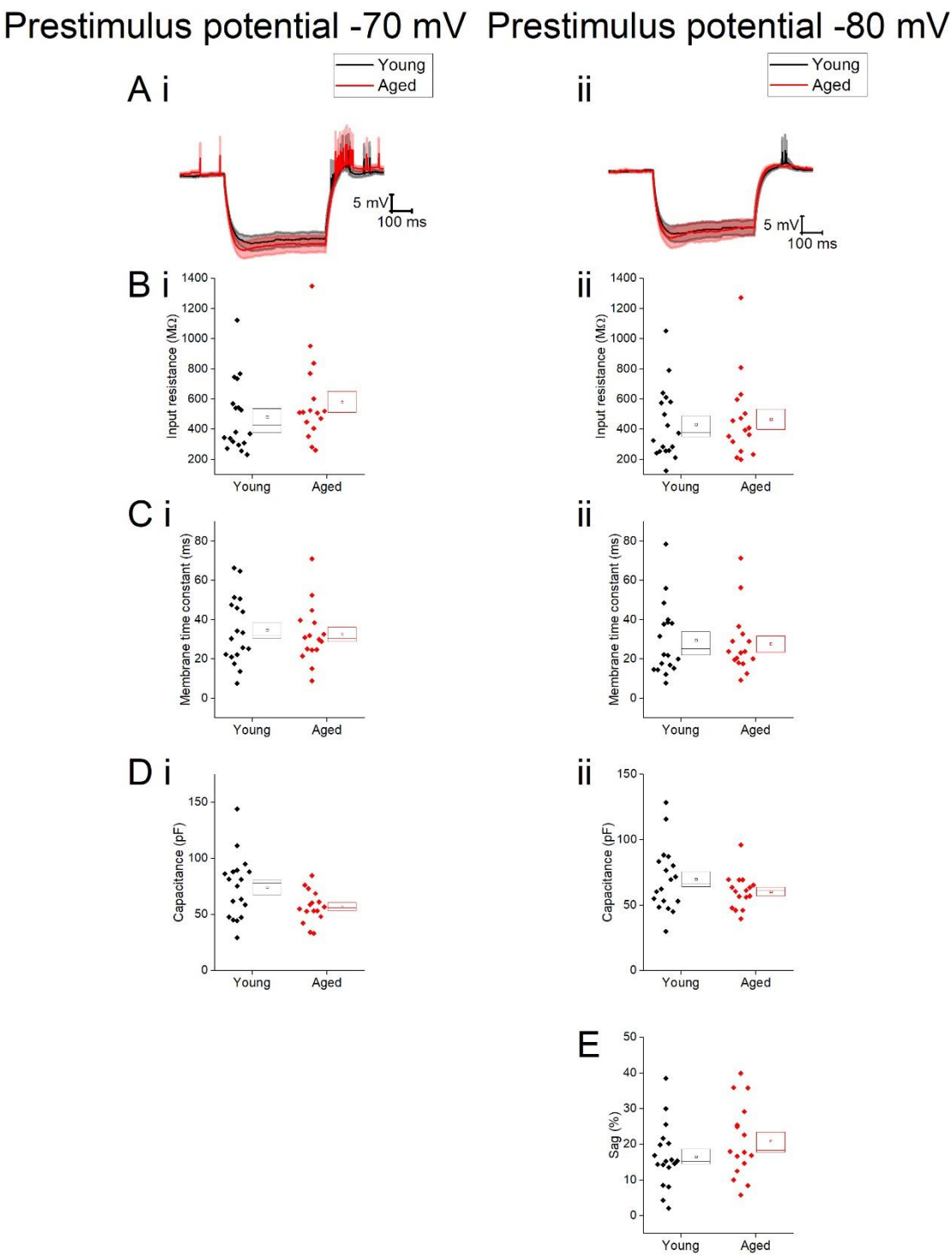

Figure 5-10. Passive membrane properties of Type II cells. **A)** Averaged traces of voltage response to a -40 pA current step in the Young and Aged cohort from a holding potential of -70 mV (i) and -80 mV (ii) respectively. The shaded areas are the standard error of the mean. **B)** Input resistance (R_{in}) from a holding current of -70 mV (i) and -80 mV (ii), **C)** membrane time constant from a holding potential of -70 mV (i) and -80 mV (ii), **D)** Capacitance from a holding potential of -70 mV (i) and -80 mV (ii), **E)** Sag from a holding potential of -80 mV.

The first action potential generated in response to the depolarising current injections was used to examine action potential properties. The averages for these action potentials are represented in Figure 5-12. No differences were observed in action potential zenith (-70 mV, Young 18 ± 2 mV, n = 18, Aged 17 ± 2 mV, n = 16; -80 mV, Young 17 ± 2 mV, Aged 18 ± 2 mV, repeated measure one-way ANOVA, age p = 0.97, t = 0.1, Figure 5-12) or action potential width at -20 mV from either holding current (-70 mV, Young 0.8 ± 0.02 ms, n = 18, Aged 0.8 ± 0.03 ms, n = 16; -80 mV, Young 0.7 ± 0.03 ms, Aged 0.8 ± 0.02 ms, repeated measure one-way ANOVA, age p = 0.14, F = 2.3, Figure 5-12). There were no differences in the maximum rate of rise of the action potential (-70 mV, Young 260 ± 18 mV/ms, n = 18, Aged 254 ± 20 mV/ms, n = 16; -80 mV Young: 283 ± 19 mV/ms, n = 18, Aged: 290 ± 17 mV/ms, n = 14, repeated measure one-way ANOVA, p = 0.12, F = 2.5, Figure 5-11) at either holding potential. Threshold was more depolarised in the young cells when examined from either holding potential (-70 mV, Young: -52 ± 1 mV, n = 18, Aged: -56 ± 1 mV, n = 16; -80 mV, Young: - 55 ± 1 mV, n = 18, Aged: -58 ±1 mV, n = 16, repeated measure one-way ANOVA, p = 0.03, F = 5.5, Figure 5-12). Interestingly, this shift in threshold appears to have no effect on the rheobase of the cells with no differences observed at either holding potential (-70 mV, Young 14 ± 2 pA, n = 16, Aged 15 ± 5 pA, n = 13, Mann-Whitney U, p = 0.3, Z = -1; -80 mV, Young 35 ± 3 pA, n = 15, Aged 34 ± 8 pA, n = 14. Mann-Whitney U p = 0.4, Z = -0.9, Figure 5-13).

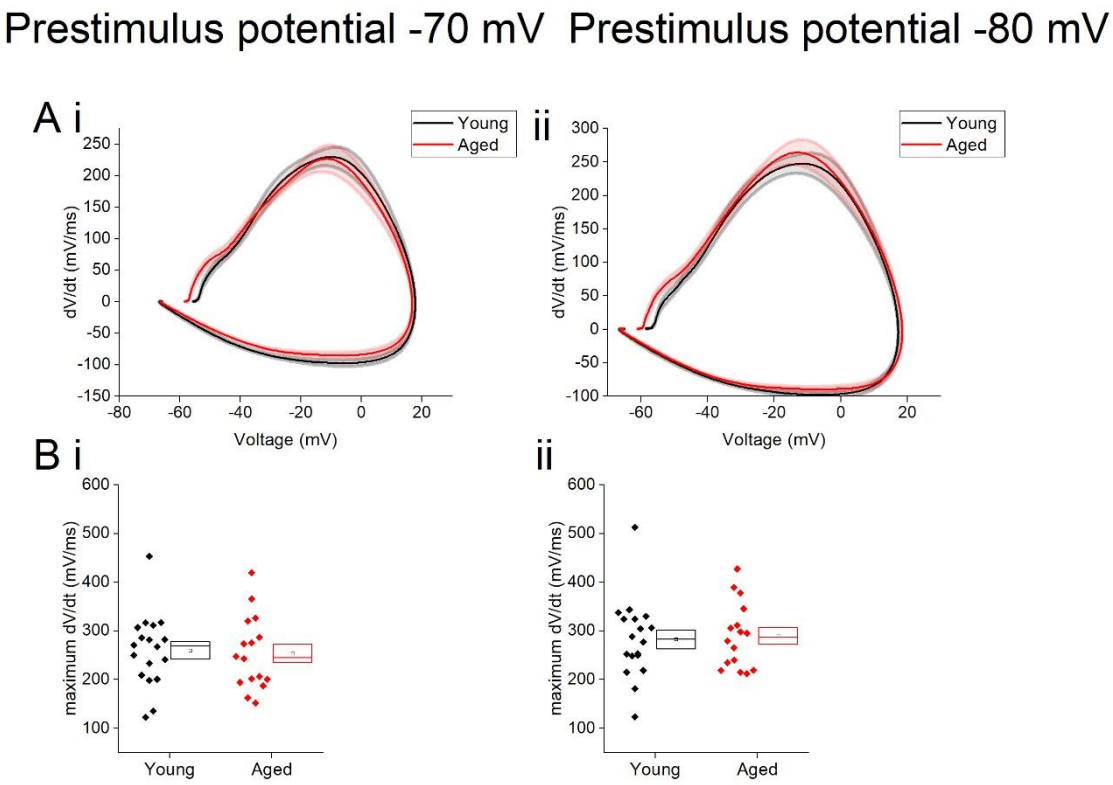

Figure 5-11. dV/dt of Type II neurons **A)** averaged dV/dt of cells plotted against the average action potential from a holding potential of -70 mV (i) and -80 mV (ii), **B)** dV/dt max of cells from a holding potential of -70 mV (i) and -80 mV (ii).

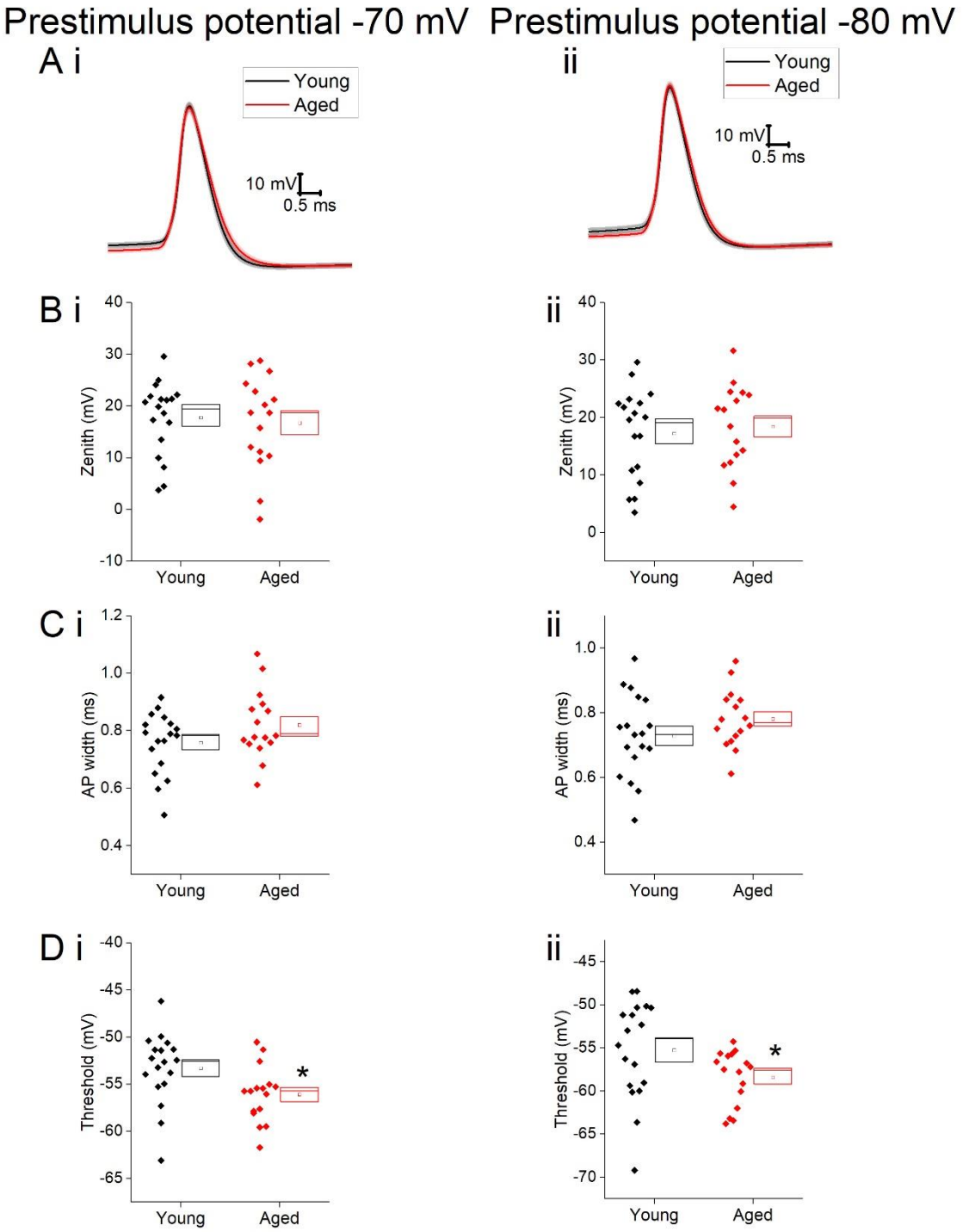

Figure 5-12. Aged Type II neurons have a more depolarised threshold**.** The properties of the first action potential produced by a 500 ms duration depolarizing pulse **A)** averaged action potential for 1st action potential from -70 mV (i) and -80 mV (ii). **B)** action potential Zenith from holding potential of -70 mV (i) and -80 mV (ii), **C)** action potential width measured at -20 mV from holding potential of -70 mV (i) and -80 mV (ii) **D)** Threshold from a holding potential of -70 mV (i) and -80 mV (ii).

Given the more hyperpolarised threshold in the aged animals I would have expected to see an increase in excitability of the aged neurons. Excitability was measured using the depolarising current injections. Sample traces containing components of these protocols can be seen in Figure 5-13; firstly I examined weather or not the cell fired in response to injections of depolarising currents (Figure 5-13). From a holding current of -70 the first step (5 pA) caused a higher proportion of Aged cells to fire with 11/16 aged cells firing while only 2/19 Young ones did (chi-squared $p = 0.0004$). There was no difference in the likelihood of firing in any other steps from this holding potential. This is most likely due to the fact that at the 20 pA injection the majority of both populations generated at least 1 spike, 15/19 Young cells and 13/16 Aged cells generated action potentials, by the 50pA step all cells in both cohorts were firing. From -80 mV the likelihood of firing did not differ on any of the current steps. Another measure of excitability is the frequency of action potentials in each of the current steps. From both prestimulus potentials there was significantly higher rates of firing in the aged cohort in comparison to the Young (repeated measure 2 way ANOVA $p = 0.02$, $F = 6.7$, Figure 5-13).

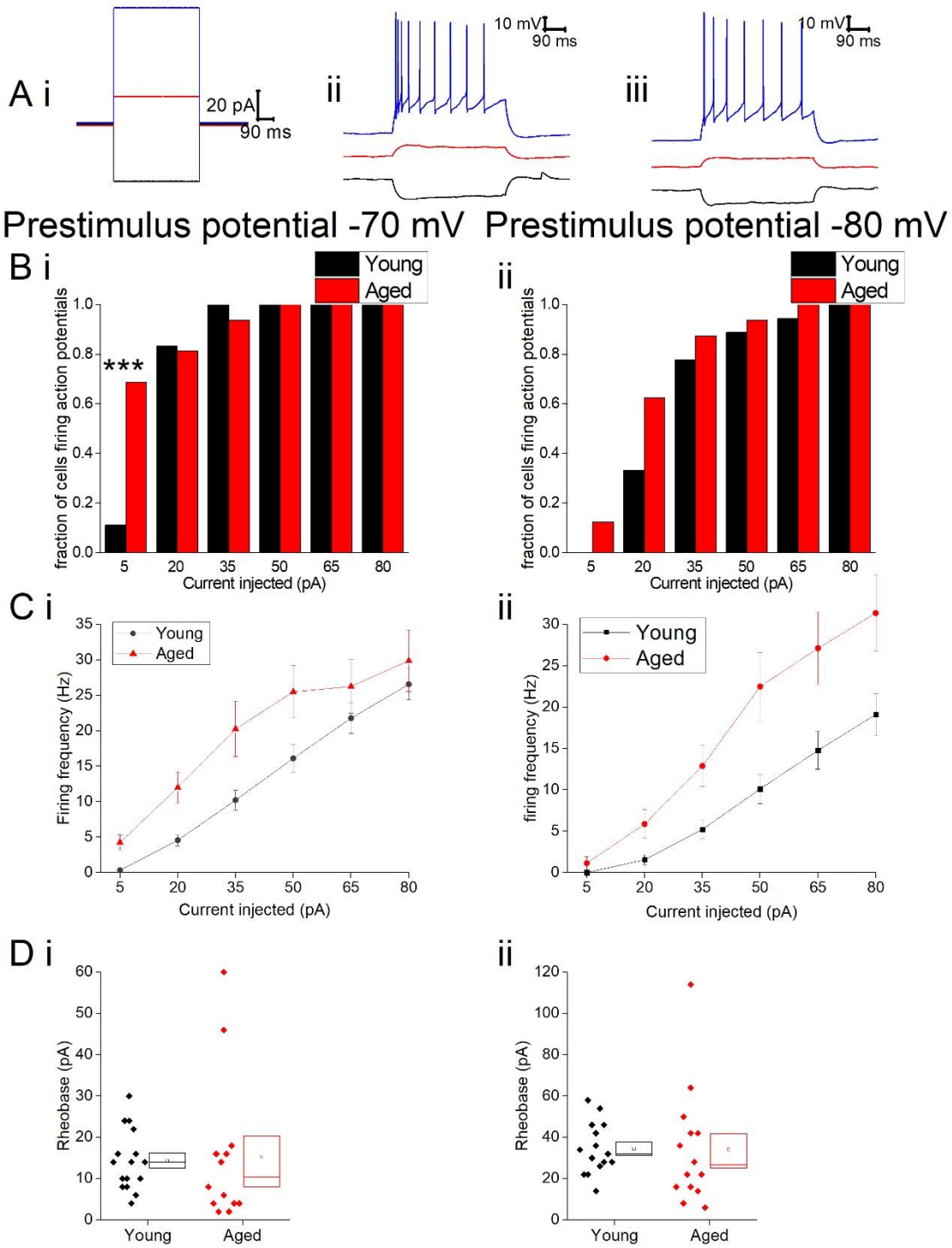

Figure 5-13. Type II neurons exhibit hyperexcitability in aged neurons in response to depolarising stimuli**. A)** For -40 pA, +20 pA and +80 pA stimuli applied at a prestimulus voltage of -80 mV the applied current injection (i) and observed voltage response from an example Young cell (ii) and Aged cell (iii) are presented. **B)** Fraction of cells which fired at least 1 action potential in response to each amplitude of depolarising current injection applied from holding potentials of -70 mV (i) and -80 mV (ii), significance based on chi Squared tests. **C)** Mean number of action potentials for each level of current injection from holding potentials of -70 mV (i) and -80 mV (ii), respectively (error bars SEM), **D)** rheobase from a holding potential of -70 mV (i) and -80 mV (ii).

When examining the latency in action potential generation, I found no differences in latency in the first action potential generated (-70 mV, Young 90 ± 15 ms, n = 18 Aged 82 ± 14 ms, n = 16, Mann-Whitney U, p = 1, Z = -0.07**;** -80 mV, Young 67 ± 9 ms, n = 18, Aged 89 ± 23 ms, n = 16, Mann-Whitney U, p = 0.8, Z = -0.3, Figure 5-14), however following the injection of 80 pA from both holding potentials there was a significant difference with the aged neuron generating spikes earlier (-70 mV, Young 9 ± 0.7 ms, Aged 6 ± 0.4 ms; -80 mV, Young 15 ± 1 ms, Aged 10 ± 0.7 ms, repeated measure one-way ANOVA, p = 0.002, F = 12, Figure 5-14).

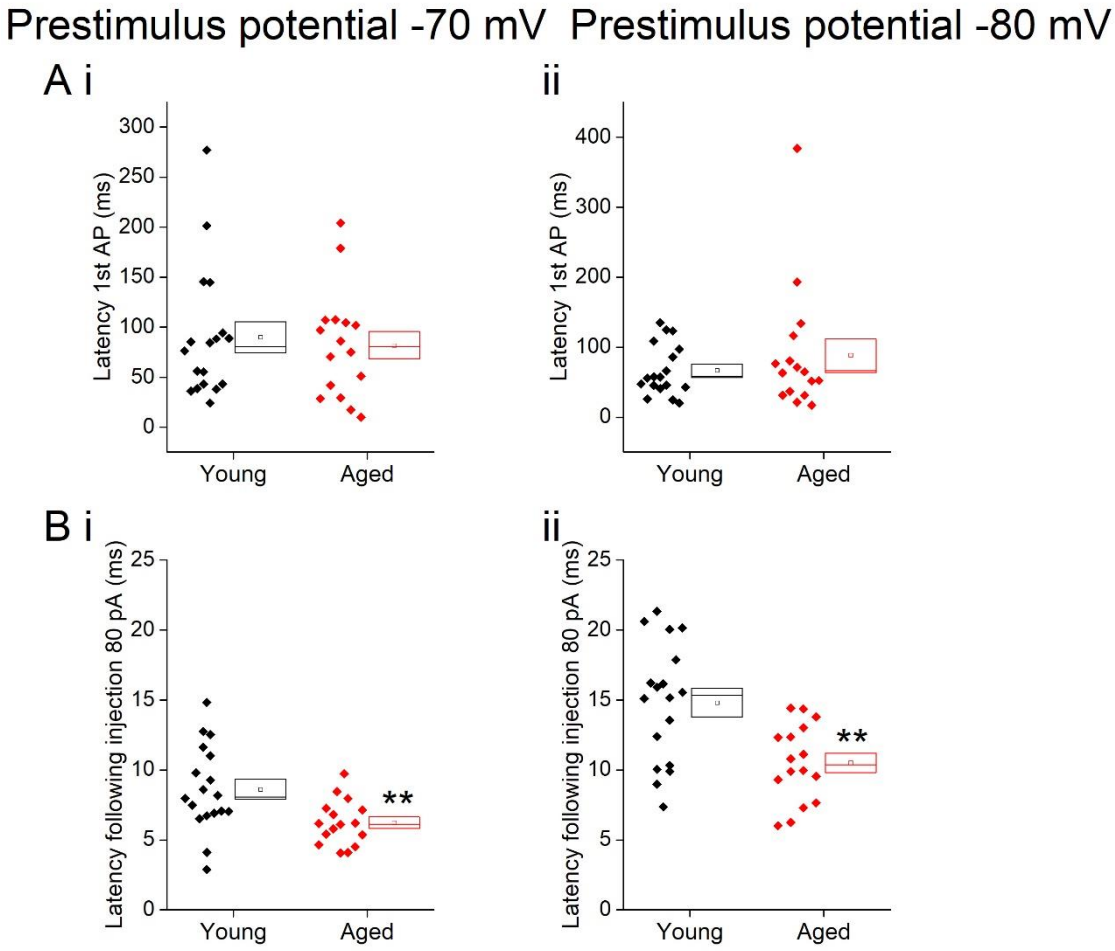

Figure 5-14. Latency to action potential **A)** Latency to the first action potential generated from depolarising steps from a membrane prestimulus of -70 mV (i) and -80 mV (ii) **B)** Latency to the first action potential generated in response to injection of 80 pA from a prestimulus potential of -70 mV (i) and -80 mV (ii).

5.4. Discussion

The data presented here represents differences in the intrinsic properties of BNST neurons observed when comparisons were made between patch clamp recordings performed in brain slices obtained either from post-pubescent Young (3-4 months) or very Aged (29-30 months) female C57BL/6 mice in the $BNST^{ALG}$. There are three Types of cells located within this area, due to the low numbers of Type III neurons their physiological role in aging was not addressed here. Overall, our data points to an intrinsic hyper-excitability associated with normal aging in Type II neurons and a more hyperpolarised resting membrane potential of Type I neurons with aging.

In Type I neurons the mean resting membrane potential of the Aged neurons was >10 mV more hyperpolarised. In theory this would drive the cells away from threshold making them less likely to fire, indeed only 12.5 % of the Aged cells fired at rest vs 47% of the Young, however this was not statistically significant. The change in holding current for both the voltage clamp recordings and the current clamp recording can be accounted for by these differences in resting membrane potential along with the changes in rheobase. The opposite was found in the Type II neurons with a higher proportion of aged cells firing, in this population these changes can be attributed to the differences in intrinsic excitability rather than changes in resting membrane potential.

The spontaneous action potential firing seen in these neuronal populations of the BNST suggest this area may be able to provide a substantial tonic synaptic drive to their various downstream synaptic targets, which included the CRF releasing cells of the PVN as well as the CRF circuit within the BNST. This does assume, however, that the intrinsic properties seen in acute brain slices are truly reflective of those present *in vivo*. This commonly made assumption is one that has certainly been questioned previously; intrinsic properties can be readily and persistently modified by “neurophysiological experiences” (e.g. periods of tonic depolarization) that might be expected to occur during the process of preparing acute brain slices (Brown & Randall, 2009).

In Type II neurons the average inward-going synaptic event is a mean of ~ 2.5 pA larger in the Young cohort. A higher average amplitude of synaptic events affect the probability of firing; given that I am unsure of the excitatory / inhibitory

nature of such inputs the effect of these events on firing rates could be either inhibitory or excitatory. Once the cells were switched into current clamp there was higher excitability in the aged cohort. This is unexpected as in my gender study (chapter 4) I found that the largest of the synaptic events were glutamatergic as such I would expect the large amplitude events seen here to be excitatory.

The use of brain slices will also impact on the “functional” connectivity of the BNST. Thus, although excitatory and inhibitory synapses onto BNST neurones remain (as evidenced by the spontaneous synaptic activity (Figure 5.1), their afferent axons are for the most part detached from their cell-bodies and, thus are highly likely to be silent. Consequently, one must also consider the level of spontaneous neural activity in the light of this functional denervation. For example, the preparation of slices and the use of a high chloride intracellular solution could have disrupted or truncated some form of strong inhibitory synaptic tone that in vivo holds BNST cells more negative or shunts their membrane potential reducing electrogenesis of spikes. Having said this, some of the very first neurophysiological studies of the BNST, in vivo recordings in anaesthetized female rats, revealed that the majority of BNST neurones that exhibited any activity fired at >1 Hz, and this activity may have to some degree been affected by oestrogen status (Bueno & Pfaff, 1976). More recently in vivo recordings from ventral BNST in male, awake mice indicate that, although hetrogenous, firing rates in active cells that project to VTA average around 5 Hz (Jennings *et al.*, 2013), this finding is similar, albeit slightly higher, than the spontaneous firing rates observed in firing Type II neurons.

When the membrane potential was pre-set to fixed levels of either -80 mV or -70 mV prior to application of current stimuli, the depolarization-induced action potential frequency was higher in Type II Aged animals. Theoretically such age-associated increase in excitability could result from a number of underlying sources. These include, but are not limited to, a negative shift in AP threshold (akin to that reported in hippocampal neurons (Randall et al. 2012), changes to the kinetics of Na^+ channel repriming, altered AHPs, or differences in membrane conductances active near threshold, that either promote (e.g. low threshold Ca^{2+} channels) or resist (low threshold K^+ channels) AP genesis.

Furthermore, quite subtle changes in combinations of these factors could synergize to promote enhanced excitability. In this cohort, action potential threshold undoubtedly played a key role in increasing excitability, in cells held at -80 mV the AP threshold was a mean of 3 millivolts more negative in the Aged animals. While this was not significant it undoubtedly contributed to the increased excitability observed in these cells. With regards to the actions of the cells at -70 mV, the depolarised threshold of the young cohort played a key role in the observed increases in frequency. Given the resting membrane potential of both cohorts was close to -70 mV, this shift in threshold most likely played a key role in the increases in proportion of cells firing at rest.

This increase in excitability in the Type II neurons could contribute to changes in anxiety with age. As this cell type is thought to act as an 'anxiety off' switch (Daniel & Rainnie, 2016) its increased excitability could lead to an inhibition of the CRF cells both in the PVN and within the BNST. Dami et al (2005) found a decrease in glucocorticoid in the morning in male C57BL/6 male mice in healthy aging; given that the animals used in this study were culled in the morning the behaviour of these Type II neurons could be contributing to decreases in glucocorticoid production. Given the anxiety off switch that has been attributed to this population it would make sense that increases in their excitability could contribute to decreases in glucocorticoid.

BNST originating GABAergic projections innervate multiple areas of the CNS, for example those involved in reward, feeding and stress. One key pathway is that monosynaptically linking BNST neurons to CRF producing cells of the PVN. It is likely that this pathway is predominant in mediating reductions in plasma glucocorticoid levels in response to BNST stimulation. Furthermore, BNST cells that are activated by excitatory inputs from limbic structures, such as the medial prefrontal cortex and hippocampal formation can, in turn, mediate a direct inhibitory, GABAergic drive to CRF-releasing neurons in the PVN (Cullinan *et al.*, 1993, 2008; Boudaba *et al.*, 1996).

Lesion of this system leads to exaggerated HPA activation by stressors (Radley & Sawchenko, 2011) suggesting that the mPFC inputs to the BNST can act as a brake on activity in the HPA axis. Afferent inputs to the BNST from the central amydala, in contrast, are inhibitory and thus relieve the influences of the

BNST (and consequently afferent inputs from mPFC) on PVN activity. To my knowledge no one has assessed whether these cells are Type I, Type II or Type III, given their inhibitory nature one would assume they are Type I or Type II.

Therefore, in aging the increased excitability of Type II BNST neurons might be expected to increase the inhibitory influence of BNST on the PVN and thus reducing overall HPA activity by limiting CRF output from parvocellular neurons. An interesting observation seen in Type I neurons was a widening of action potentials with age. If this outcome, seen here at the cell body, translated to similar changes in spike width at the presynaptic terminals formed by BNST neurons a substantial increase in release probability might be expected, and thus a corresponding increase in drive to down-stream synaptic targets of BNST neurons.

Although it can be proposed that neurophysiological changes in BNST neurons develop as a consequence of what might be regarded as autonomous aging-related processes within the BNST itself, another possibility is that the altered excitability I report represents an adaptive change in respond to an altered afferent synaptic drive from, for example, other limbic structures. Certainly other components of the limbic system with established BNST connectivity have been previously shown to exhibit significant neurophysiological changes associated with aging (Chang *et al.*, 2005*b*; Bodhinathan *et al.*, 2010; Coskren *et al.*, 2014).

Notably the BNST is well known for its sexually dimorphic nature as discussed in chapter 3. Due to their availability for this first study of BNST neurophysiology in Aged animals I focussed entirely on females. An interesting extension to this work would be to compare how aging alters the neurophysiological properties of male mice. This data provides no indication of when the neurophysiological changes I report develop within the mouse lifespan. A more detailed longitudinal study would be required for this, preferably sampling multiple age points from a large cohort of littermate animals raised throughout life in the same facility.

6. Changes in excitability of Type I and Type II neurons in the BNST of the CHMP2B mouse model of frontotemporal dementia

In the previous chapter I addressed the influence of healthy aging on the intrinsic properties of neurons located within the $BNST^{ALG}$. A key risk factor for a number of different dementias is aging, here I plan to examine weather expected changes in frontotemporal dementia differed from those observed during heathy aging.

6.1. Introduction

6.1.1. The CHMP2B model of frontotemporal dementia

Frontotemporal dementia (FTD) is the second most common form of young onset dementia following Alzheimer's disease (Ratnavalli *et al.*, 2002; Harvey *et al.*, 2003). A number of genes have been linked with familial FTD, the most common of which are those encoding tau (*MAPT*), *C9orf72* and progranulin (*GRN*). There are also a number of rarer genetic causes of the disease, one such gene encodes the charged multivesicular body protein 2B (*CHMP2B*) (Clayton *et al.*, 2015).

The CHMP2B mutation causes an inheritable form of frontotemporal dementia in a Danish family (Skibinski *et al.*, 2005; Isaacs *et al.*, 2011). These patients display less concern for others, an unkempt appearance, disinhibition, inappropriate emotional responses and restlessness sometimes along with increased aggression often followed by progressive aphasia (Isaacs *et al.*, 2011).

When this mutation was introduced into mice they displayed a progressive axonopathy, APP-positive swellings indicative of altered axonal function, this takes place through a gain of function mechanism (Ghazi-Noori *et al.*, 2012*b*). These mice also display both social and motor deficits in the later stages of the disease (Clayton *et al.*, 2015).

6.1.2. The role of the BNST in frontotemporal dementia

The impact of chronic stress on neurological function is unquestionable and greatly increases ones risk of developing various forms of dementia (Peavy *et al.*, 2009; Johansson *et al.*, 2010; Greenberg *et al.*, 2014*b*). One study has found a strong correlation between PTSD in veterans and the onset of dementia, with the biggest correlation observed in patients that developed frontotemporal dementia (Yaffe *et al.*, 2010; Greenberg *et al.*, 2014*a*). The BNST plays a key role in both chronic stress and PTSD as discussed in the introduction. Given this correlation, alongside the central role of BNST in stress, I propose that the BNST could be implicated in this disease and further study is required to identify altered functionality within this region.

A number of mouse models of frontotemporal dementia have shown a decrease in anxiety in various mazes. These include the V337M, THY-Tau22, PS19 mouse models which display decreases in anxiety on the elevated plus maze and the P301S model which had an increase in the amount of time spend in the middle of the open field. The R406W model found no differences in anxiety using the light dark box. Unlike these mouse models patients suffering from frontotemporal dementia often display increases in anxiety (Porter *et al.*, 2003; Koss *et al.*, 2016).

Patients in this Danish family also display an increase in aggression; impulse aggression is partly mediated by the BNST, this type of aggression often seen in PTSD patients has been attributed to feeling of helplessness. It is possible that the BNST is playing a role in this aggression observed in patients.

To my knowledge no one has assessed any aspect of BNST properties in any mouse model of frontotemporal dementia. At the time this research was carried out no studies examining changes in anxiety levels of this model had been published. Here I plan to address the effects of the CHMP2B mutation on anxiety levels of unstressed mice alongside the examination of the electrophysiological properties of BNST neurons within this novel model of frontotemporal dementia.

Hypothesis

Increased in anxiety observed in the human FTD may be associated with changes in excitability of neurons located within the $BNST^{ALG}$.

Aims

To determine if changes in excitability exist within the CHMP2B model of frontotemporal dementia.

6.2. Methods

CHMP2B mice were initially breed at UCL and transported to the University of Exeter and allowed to acclimatise for a week prior to commencing experiments. The animals had *ad lib* access to food and water for their entire lifespan. This experiment focused entirely on male animals.

Anxiety levels were tested on the elevated zero maze as previously described in the methods chapter. Ten animals from each cohort were tested twice on successive days and percentage time in the open portion was averaged across animals.

Brain slices containing the $BNST^{ALG}$ were prepared as previously described. A K-gluconate solution containing biocytin was used to carry out recordings. A series of electrophysiological characterisations were carried out as previously described in the methods chapter.

6.3. Results

6.3.1. Behavioural tests

Anxiety levels were assed using the elevated plus maze. I examined the percentage time spent in the open arm in 10 animals from each cohort averaged over two days. The wild type (WT) cohort spent an average of 16 ± 2 % (n = 10) in the open arm while the transgenic (TG) cohort spend an average of 13 ± 2 % (n = 10) in the open arm (unpaired t-test, p = 0.1, t = 1.6, Figure 6-1).

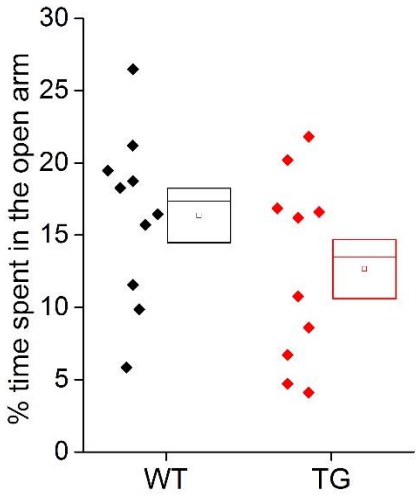

Figure 6-1 Percentage time spent in open arm of elevated zero maze

6.3.2. Electrophysiological characterisation of cells located in the anterolateral area of the BNST

In the WT cohort a total of 39 cells were recorded from the $BNST^{ALG}$ while 35 were recorded from the TG cohort. These cell types were then classified based on the electrophysiological properties as highlighted in the methods chapter. The WT cells comprised 15 Type I cells from 10 animals with a maximum of two cells per animal, 16 Type II cells from 11 animals with a maximum of two cells per animal and 6 Type III cells from four animals with a maximum of two cells per animal; the TG cohort was made up of 16 Type I cells from 10 animals with a maximum of 4 cells per animal, 12 Type II cells from nine animals with a

maximum of two cells being recorded from each animal and five type III cells from five animals with only one cell per animal being recorded. The other cells did not contain high enough numbers of any one population for valid comparison so were not included in this study.

6.3.2.1. Type I cells

Once whole cell acess to a cell was obtained the properties of the synaptic events were examined in voltage clamp mode while holding the cells at -70 mV. The amount of current required to hold these cells at -70 mV also did not differ averaging approxomitly 21 pA for each cohort (WT 22 ± 12 pA, n = 9, TG 21 ±13 pA, n =13, Mann-Whitney U, p = 0.9, Z = -0.1, Figure 6-2). There was no difference in eitheir the frequency (WT 4.5 ± 1.5 Hz, n = 9, TG 4.6 ±1.2 Hz, n = 13, Mann-Whitney U, p = 1, Z = -0.3) or averaged amplitude (WT -14 ± 0.8 pA, n = 9, TG -15 ± 0.9 pA, n = 13, Mann-Whitney U, p = 0.8, Z = -0.3 A) of these events (Figure 6-2).

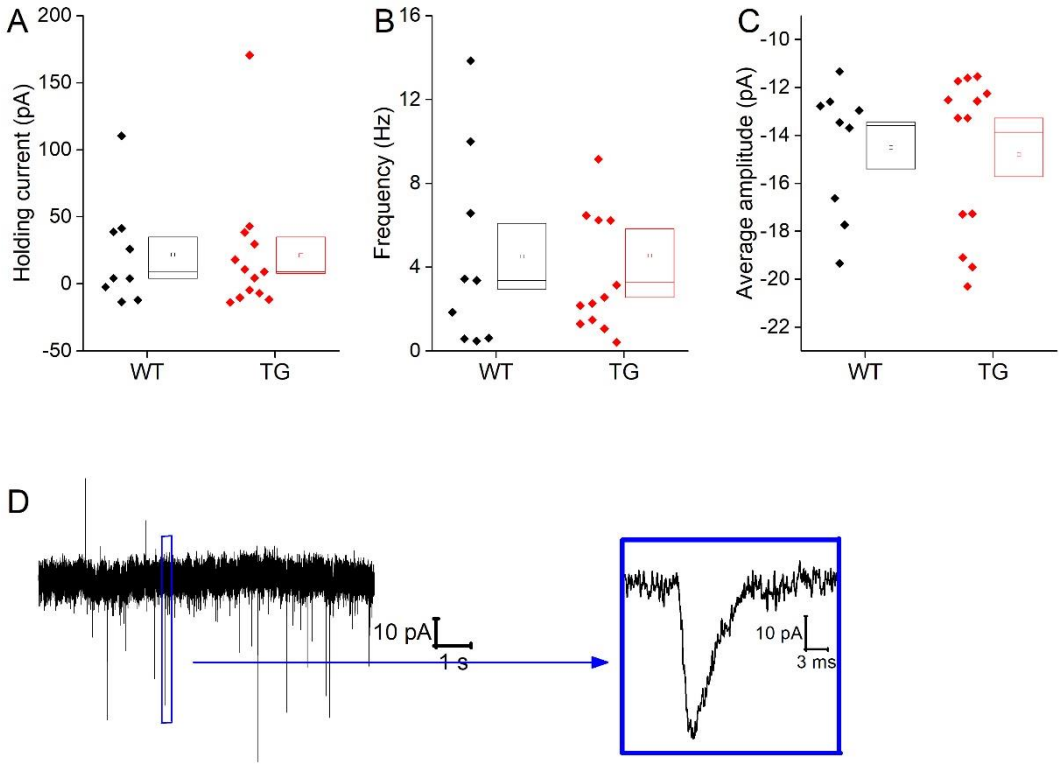

Figure 6-2. Synaptic events in type I cells. A) Current required to hold cells at -70 mV, B) frequency of post synaptic currents, C) average amplitude of post synaptic events, D) sample trace with a zoomed in voltage synaptic event.

Following this I switched into current clamp mode and looked at the resting membrane potential; genotype had no effect with both cohorts resting at ~ -76 mV (WT -77 ± 4 mV, n = 15, TG -75 ± 4 mV, n = 16, unpaired t-test, p = 0.6, t = -0.5, Figure 6-3). This was unsurprising given the similar holding currents observed in voltage clamp mode. The proportion of cells which generated at least 1 action potential in this 1 minute recording was not different with 5/15 WT cells firing and 2/16 TG cells firing (chi-squared p = 0.2).Cells were then held at a set potential of -80 mV for examination of intrinsic properties; the amount of current required to hold cells at -80 mV was not different between the cohorts (WT -6 ± 13 pA, n = 15, TG -23 ± 25 pA, n = 16, unpaired t-test, p = 0.6, t = 0.6).

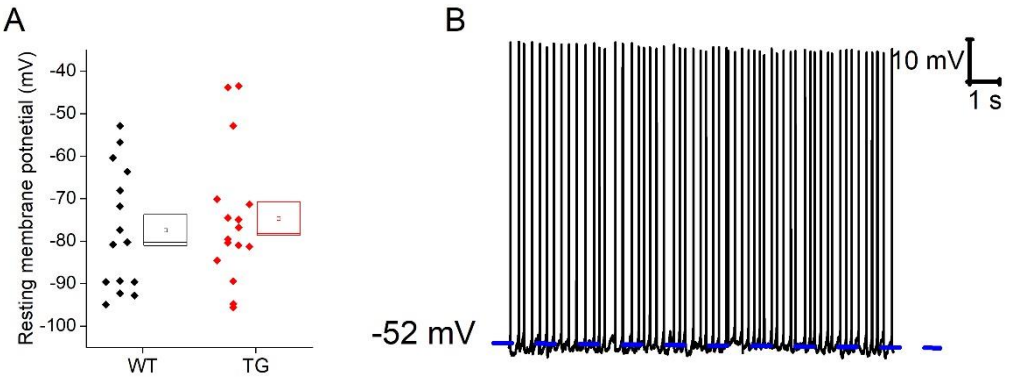

Figure 6-3. Resting membrane potential of type I cells A) Resting membrane potential, B) sample trace of cell firing at rest with current trace below.

The passive membrane properties were examined from the -40 pA current injection, the averages of these current injections is shown in Figure 6-4. No genotype specific differences were observed in input resistance (WT 305 ± 27 MΩ, n = 15, TG 247 ± 21 MΩ pA, n = 16, unpaired t-test, p = 0.1, t = 1.7), sag (WT 11 ± 1.5%, n = 15, TG 15 ± 2%, n =16, unpaired t-test, p = 0.2, t = -1.3) and capacitance (WT 82 ± 7 pF, n = 15, TG 81 ± 9 pF, n = 16, unpaired t-test, p = 0.9, t = 0.1) (Figure 6-4). From a holding potential of -80 mV the membrane time constant in the WT cohort was over 5 ms faster than in the TG cohort, however this was not statistically significant (WT 23 ± 1.3 ms, n = 16, TG 19 ± 2 ms, n = 15, unpaired t-test p = 0.07, t = 1.9, Figure *6-4*).

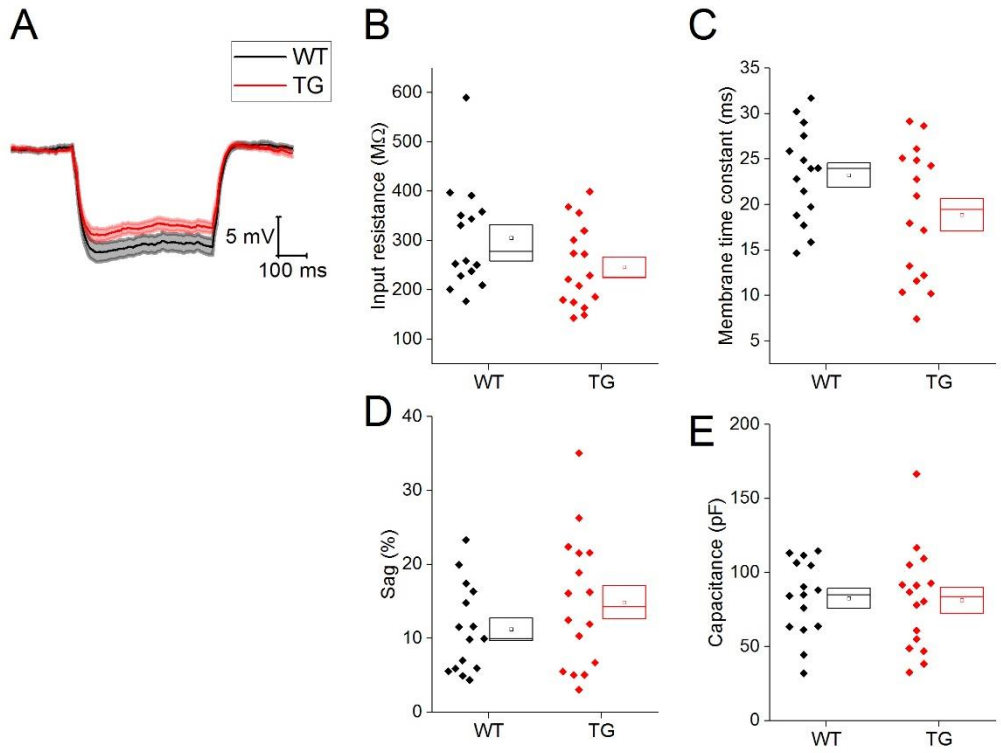

Figure 6-4. Passive membrane properties of Type I neurons A) Average of cells response to injection of -40 pA of current from a holding potential of -80 mV, B) input resistance, C) membrane time constant, D) % sag and E) Capacitance.

I then examined the action potential properties of the first action potential generated in each cell, these are averaged in Figure 6-5A. No differences in AP zenith (WT 22 ± 1 mV, n = 15, TG 19 ± 2 mV, n = 16 unpaired t-test, p = 0.2, t = 1.5), AP width (WT 0.9 ± 0.06 ms, n = 15, TG 0.8 ± 0.05 ms, n = 16, unpaired t-test, p = 0.15, t = 1.5) or Threshold (WT -55 ± 2 mV, n = 15, TG -54 ± 2 mV, n = 16, Mann-Whitney U, p = 0.7, Z = -0.4) were observed between the populations (Figure 6-5). Following this the first derivative of the action potentials were examined and the peak compared as shown in Figure 6-5, in the TG population the maximum rate of rise was ~60 mV/ms lower than its WT counterpart (WT 320 ± 23 mV/ms, n = 15, TG 258 ± 19 mV/ms, n = 16, unpaired t-test p = 0.04, t = 2.1).

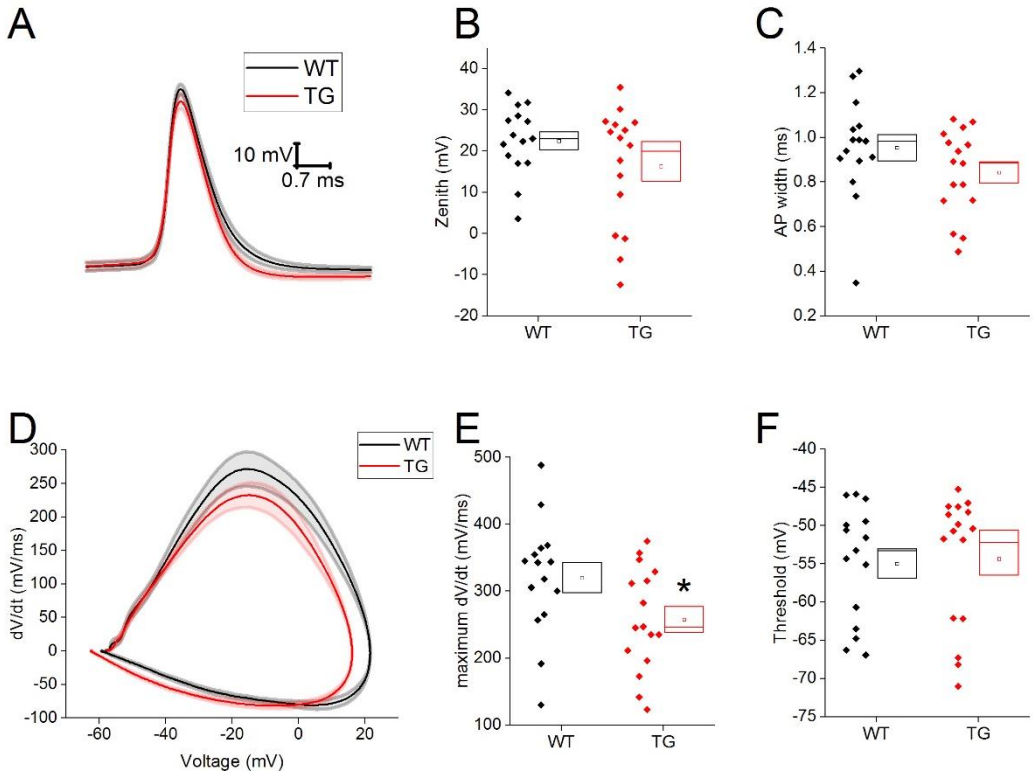

Figure 6-5. Action potential properties of Type I neurons A) Average of first action potential generated in response to depolarising current injections, B) AP zenith C) AP width at -20 mV, D) averaged dV/dt of cells plotted against the average voltage change of the action potential, E) maximum dV/dt and F) Threshold.

I then examined the excitability of neurons using two protocols, in the step protocol I examined the proportion of cells firing in each step and the frequency of said firing; in the Rheobase protocol I looked at the amount of current required to generate an action potential; no differences were observed in rheobase (WT 34 ± 6 pA, n = 6, TG 30 ± 2 pA, n = 7, unpaired t-test, p = 1, t = -0.2, Figure 6-6). Some differences were observed in the proportion of cells firing in response to the injection of depolarising current specifically following the injection of 35 pA of current where the TG cohort was more likely to fire action potentials (Table 6-1, Figure 6-6). A final measure of excitability is the delay between the onset of the current injections and the generation of the action potential referred to as latency. No differences in latency were observed when examining either the first action potential generated in response to depolarising current (WT 14 ± 2 ms, n = 15, TG 15 ± 3 ms, n = 16 Mann-Whitney U test, p =

0.6, Z = -0.5, Figure 6-6) or latency following the injection of 80 pA of current (WT 6 ± 3 ms, n = 14, TG 6 ± 2 ms, Mann-Whitney U, p = 0.8, Figure 6-6).

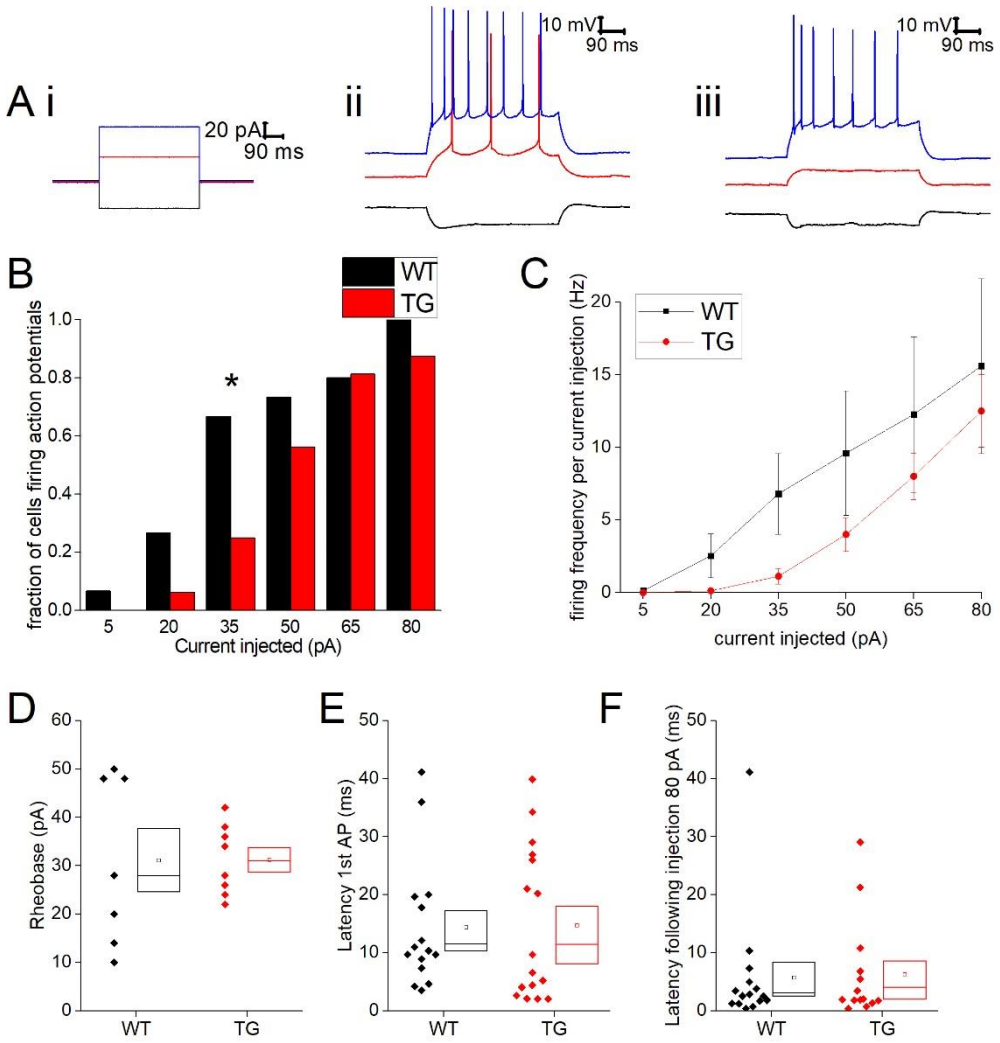

Figure 6-6. Excitability of Type I neurons. A sample trace of a WT (ii) and TG (iii) cell, i) sample current injections. B) Fraction of cells firing at least 1 action potential in response to a series of depolarising, C) frequency of firing in response to each depolarising current injection D) Rheobase, E) Latency to the first action potential generated in response to depolarising current injection and F) Latency to first action potential generated in response to the injection of 80 pA of current.

Current injected	Firing frequency following injection of depolarising current		Fraction of cells generating action potentials		
	WT (Hz)	TG (Hz)	WT	TG	P value
5 pA	0.1 ± 0.1	0 ± 0	0.07	0	0.3
20 pA	2.5 ± 1.5	0.1 ± 0.1	0.27	0.6	0.1
35 pA	6.8 ± 2.8	1.1 ± 0.5	0.67	0.25	0.02
50 pA	9.6 ± 4.2	4 ± 1.1	0.73	0.56	0.06
65 pA	12.3 ± 5.4	8 ± 1.6	0.8	0.82	0.9
80 pA	15.6 ± 6	12.5 ± 2.4	1	0.88	0.2

Table 6-1 Firing of frequency in response to each current injection and proportion of Type I cells firing in response to each current injection from both holding potentials. P values based on chi squared performed in Excel

6.3.2.2. Type II cells

A similar series of protocols was used to examine Type II cells. While holding these cell at -70 mV in voltage clamp mode there was no difference in the amount of current required, averaging 4 pA in each cohort (WT 4 ± 5 pA, n = 14, TG 4 ± 4 pA, n = 5, unpaired t-test, p = 0.9, t = -0.05); a sample trace is depicted in Figure 6-7. With regards to the frequency (WT 6.2 ± 2 Hz, n = 14, TG 3.4 ± 1, n = 5, Mann-Whitney U, p = 0.4, Z = -0.8) and average amplitude of synaptic events (WT -13 ± 0.6 pA, n = 14, TG -14 ± 1.4 pA, n = 5, unpaired t-test, p = 0.5, t = 0.6) there was no significant differences between the cohorts (Figure 6-7).

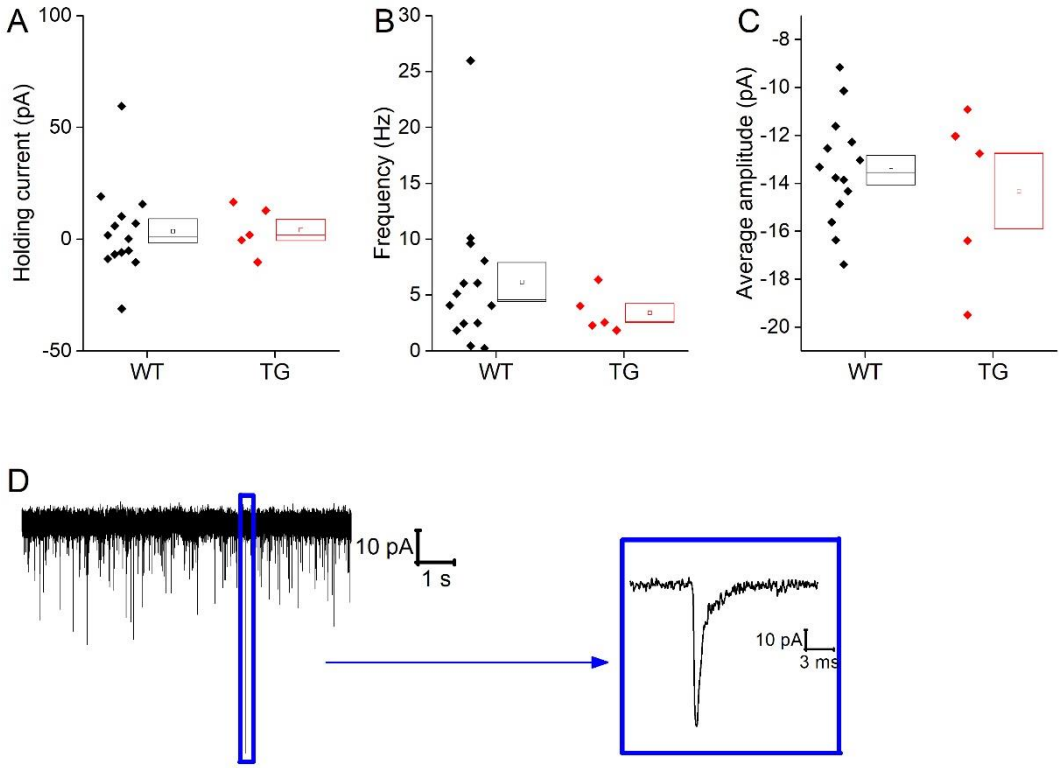

Figure 6-7. Synaptic events in type II cells A) Current required to hold cells at -70 mV, B) frequency of post synaptic currents, C) average amplitude of post synaptic events, D) sample trace with a zoomed in voltage synaptic event.

Cells were then switched into current clamp mode. There was no difference in the resting membrane potential with both cohorts resting at ~-71 mV (WT -72 ± 3 mV, n = 16, TG -71 ± 3 mV, n = 12, unpaired t-test, p = 0.7, t = -0.4, Figure 6-8). A similar proportion of cells were firing in each group with 7/16 TG cells firing and 6/12 WT cells firing (chi-squared, p = 0.7). Of the cells which were not firing the Rheobase was the same in the different populations with an average of 26 pA being required to generate an action potential in each group (WT 26 ± 7 pA, n = 6, TG 26 ± 6 pA, n = 5, unpaired t-test, p = 1, Figure 6-8). Of the cells which did fire in the TG cohort they fired at 2 ± 1 Hz while in the WT cohort they fired at 6 ± 2 Hz (Figure 6-8), this was not significantly different (Mann-U-Whitney, p = 0.1, Z = -1.6).

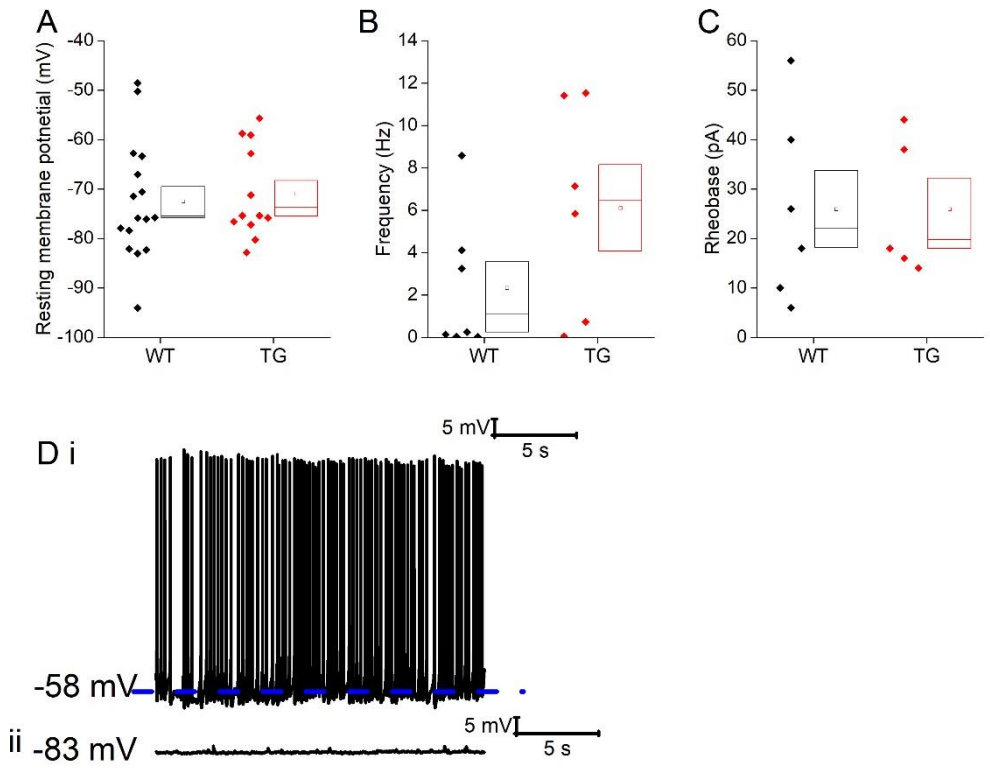

Figure 6-8. Type II cells at their Resting membrane potential. A) resting membrane potential of cells, B) frequency of cells which fired at their resting membrane potential, C) Rheobase of cells which did not fire at their resting membrane potential, D) sample cell firing at rest (i), sample cell not firing at rest (ii).

When examining the passive membrane properties of these cells I found no differences in input resistance (WT 429 ± 69 MΩ, n = 16, TG 317 ± 36 MΩ pA, n = 12, Mann-Whitney U, p = 0.4, Z = -0.9), membrane time constant (WT 27 ± 2 ms, n = 16, TG 24 ± 2 ms, n = 12, unpaired t-test, p = 0.3, t = 1), capacitance (WT 75 ± 7 pF, n = 16, TG 79 ± 7 pF, n = 14, unpaired t-test, p = 0.7, t = -0.396) or sag (WT 14 ± 3%, n = 16, TG 19 ± 3%, n = 12, Mann-Whitney U, p = 0.2, Z = -1.4,). The averages of the -40 pA step from each holding current for each genotype and the graphs are depicted in Figure 6-9.

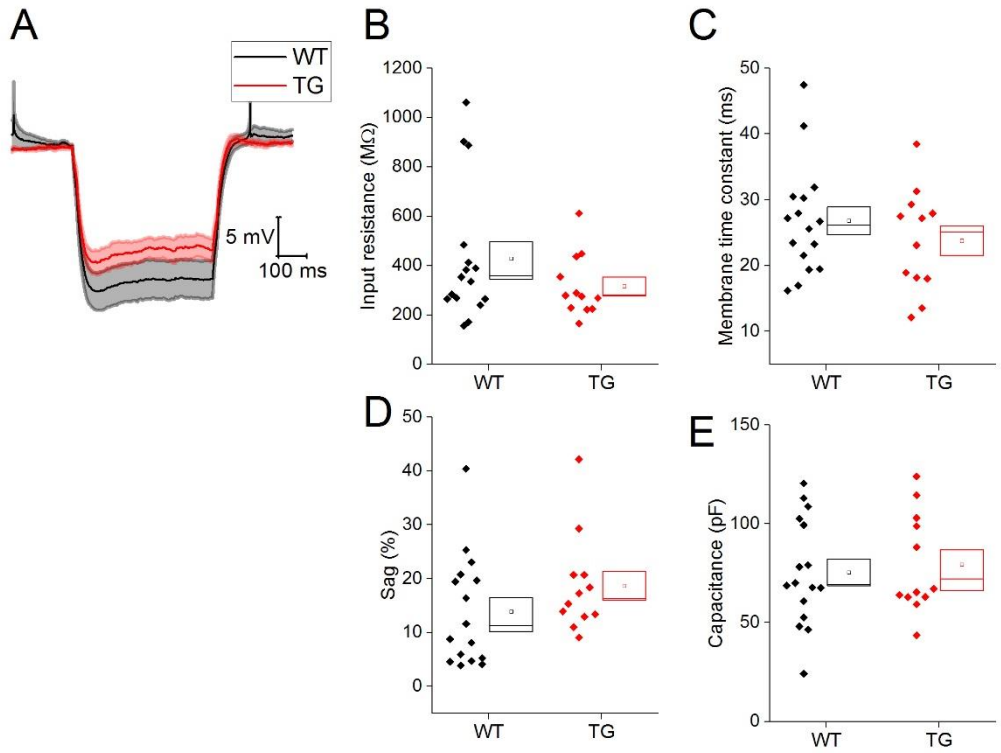

Figure 6-9. Passive membrane properties of type II BNST neurons A) Average of cells response to injection of -40 pA of current from a holding potential of -80 mV, B) input resistance, C) membrane time constant, D) % sag and E) Capacitance.

I then addressed the action potential properties from the first action potential generated in response to depolarising current injections shown in Figure 6-10. I found no differences in the width of the action potential at -20 mV (WT 0.8 ± 0.04 ms, n = 16, TG 0.9 ± 0.03 ms, n = 12, Mann-Whitney U, p = 0.3, Z = -1, Figure 6-10), zenith of the action potential (WT 20 ± 2 mV, n = 16, TG 18 ± 2 mV, n = 12, unpaired t-test, p = 0.5, t = 0.6, Figure 6-10) or the maximum dV/dt (WT 302 ± 17 mV/ms, n = 16, TG, 316 ± 27 mV/ms, n = 12, unpaired t-test, p = 0.6, t = -0.5, Figure 6-10). The mean threshold was significantly more depolarised in the WT cohort than in the TG cohort (WT -54 ± 1 mV, n = 16, TG -60 2 mV, n = 12, unpaired t-test, p = 0.02, t = 2.6, Figure 6-10).

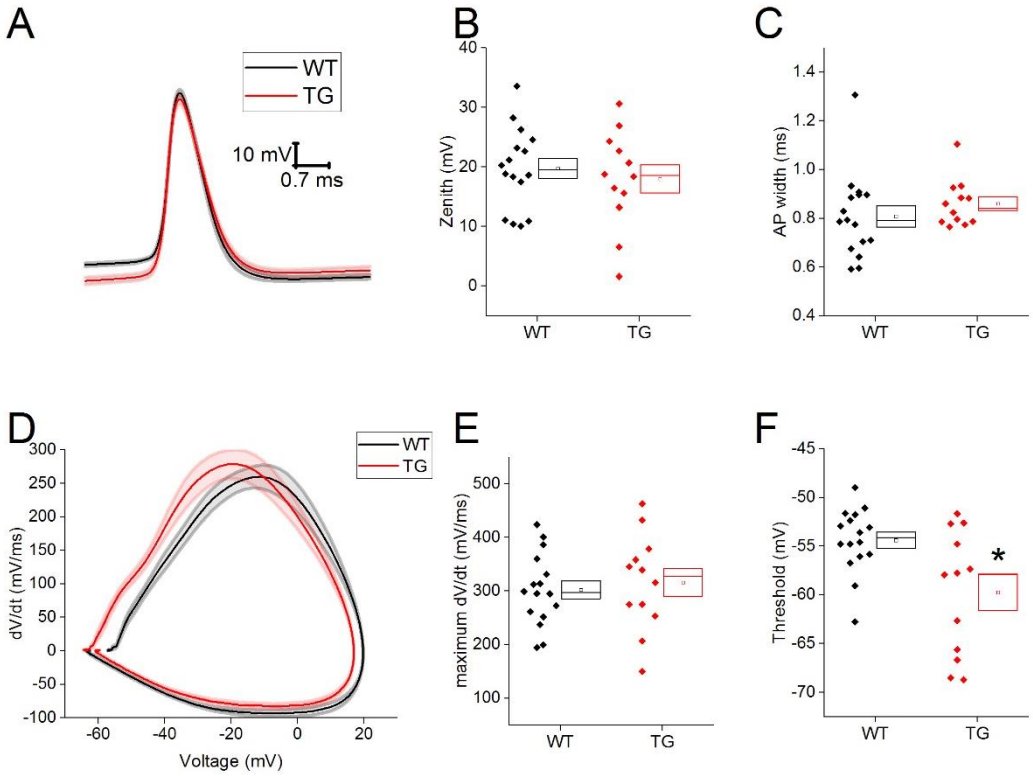

Figure 6-10. Action potential properties of Type II neurons. A) Average waveform of first action potential generated in response to depolarising current injections, B) AP zenith C) AP width at -20 mV, D) averaged dV/dt of cells plotted against the average voltage change of the action potential, E) maximum dV/dt and F) threshold.

A more depolarised threshold often leads to increases in excitability, however when I looked at firing frequency in each step (Table 6-2) and the proportion of cells firing in each step, I observed no differences (Figure 6-11,Table 6-2). Equally, genotype showed no effect on Rheobase (WT 24 ± 5 pA, TG 30 ± 7 pA, Mann-Whitney U, p = 1, Z = -0.1, Figure 6-11).

Finally, I examined the latency of action potential generation in the step protocol beginning with the first action potential generated. The TG cohort fired significantly earlier than the WT cohort (WT 12 ± 3 ms, n = 16, TG 7 ± 2 ms, n = 12, Mann-U-Whitney p = 0.047, Z = -2, Figure 6-11). No difference in latency were observed following the injection of 80 pA of current (WT 2 ± 0.5 ms, TG 2 ± 0.7 ms, Mann-Whitney U, p = 0.3, Z = -1, Figure 6-11).

Current injected	Firing frequency following injection of depolarising current		Fraction of cells generating action potentials		
	WT (Hz)	TG (Hz)	WT (%)	TG (%)	P value
5 pA	1 ± 1	1 ± 1	0.1	0.1	0.6
20 pA	6 ± 3	6 ± 4	0.2	0.2	0.7
35 pA	10 ± 4	11 ± 5	0.7	0.7	0.9
50 pA	15 ± 5	14 ± 6	0.9	0.8	0.09
65 pA	21 ± 5	18 ± 6	1	0.9	0.2
80 pA	24 ± 4	22 ± 6	1	1	

Table 6-2. Proportion of Type II cells firing in response to each current injection from both holding potentials. P values based on chi squared performed in Excel

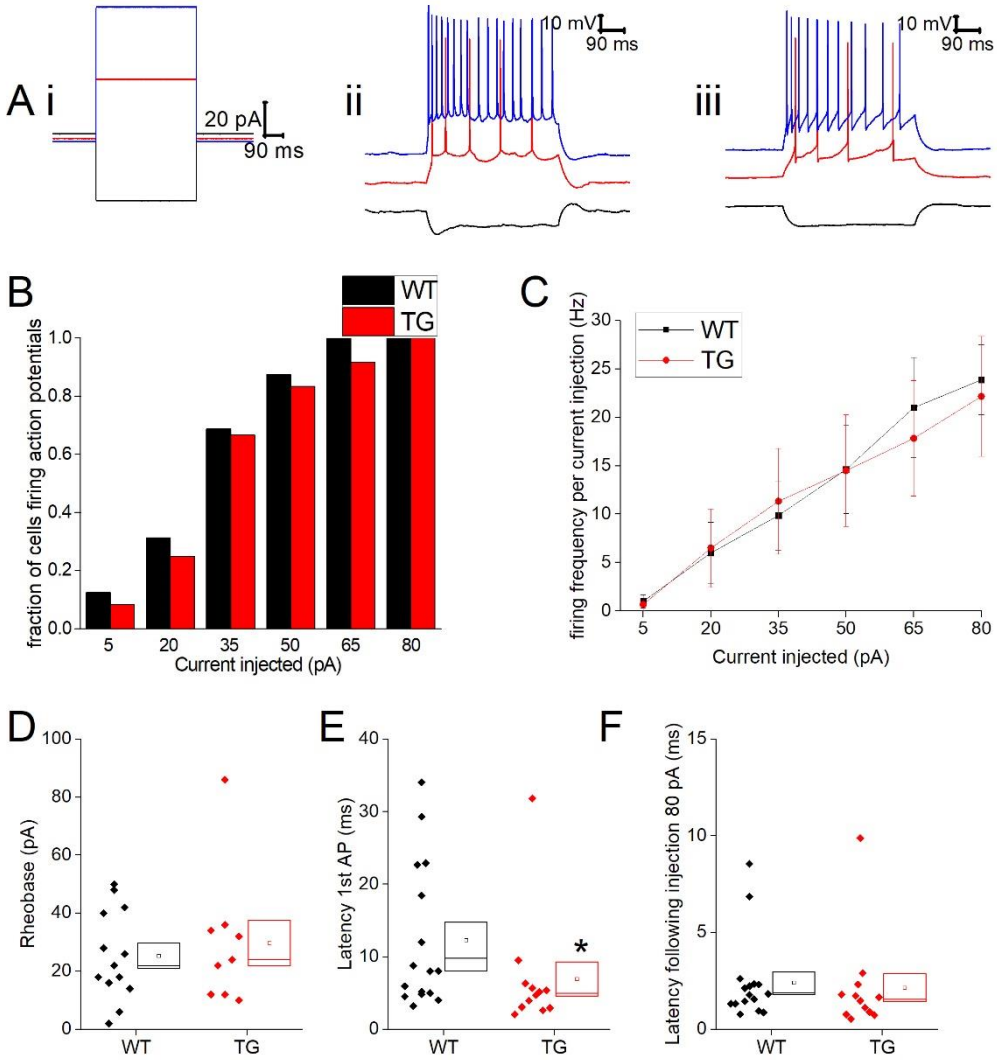

Figure 6-11. Firing properties of Type II neurons A sample trace of a WT (II) and TG (III) cell, i) sample current injections depicting the injection of -40 pA, +20 pA and +80 pA. Fraction of cells firing at least one action potential in response to a series of depolarising, C) frequency of firing in response to each depolarising current injection, D) Rheobase, E) Latency to the first action potential generated in response to depolarising current injection and F) Latency to first action potential generated in response to the injection of 80 pA of current.

1.1.1.1 Type III neurons

In type III cells the synaptic activity in voltage clamp was not included due to low n numbers; only 3 of each cohort had recording with low enough levels of noise to be included. Therefore I begin by looking at the resting membrane potential of these cells. Despite the TG cohort (-63 ± 6 mV) being a mean difference of 12 mV more depolarised then the WT (-75 ± 7 mV) population they did not significantly differ (unpaired t-test, p = 0.2, t = 1.3, Figure 6-12). Of the WT population 4/6 cells fired at least 1 action potential in the 1 minute while 2/5 TG cohort fired (chi-squared, p = 0.4). The firing frequencies here has n numbers too low for a valid comparison.

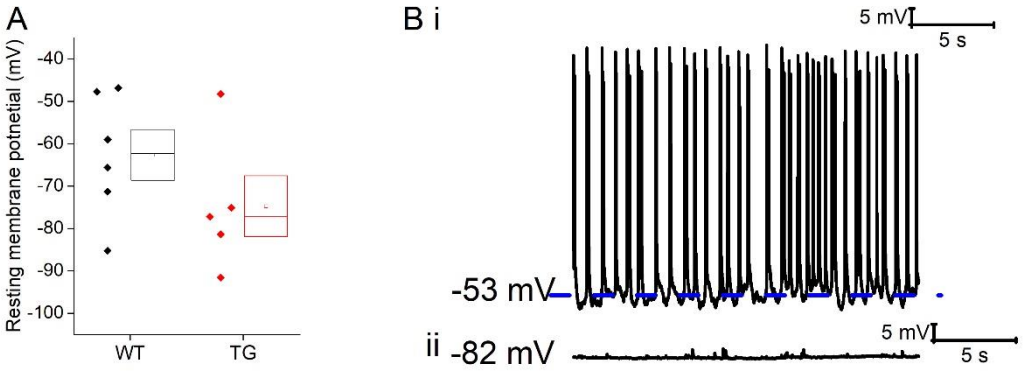

Figure 6-12 Resting membrane potential of Type III cells A) Resting membrane potential, Bi) Sample cell firing at rest, ii) sample cell not firing at rest.

The amount of current required to hold cells at -80 mV (WT -47 ± 16 pA, TG -9 ± 31 pA) was not genotype specific. Once cells were at their holding potentials the passive membrane properties of the cells were examined. I found no differences in input resistance (WT 545 ± 82 MΩ, n = 6, TG 358 ± 101 pA, n = 5, unpaired t-test, p = 0.2, t = 1.5), membrane time constant (WT 25 ± 5 ms, n = 6, TG 17 ± 3 ms, n = 5, unpaired t-test, p = 0.2, t = 1.4) or capacitance (WT 46 ± 4 pF, n = 6, TG 62 ± 16 pF, n = 5, unpaired t-test, p = 0.3, t = -1).

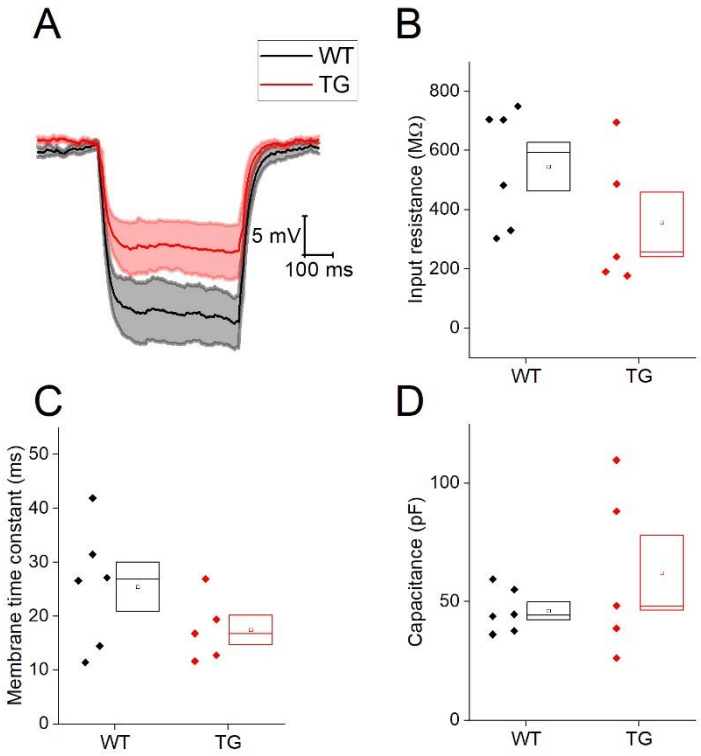

Figure 6-13 Passive membrane properties of Type III neurons A) Average of cells response to injection of -40 pA of current. B) Input resistance, C) membrane time constant and D) Capacitance.

Next I examined the action potential properties; no differences in action potential zenith (WT 13 ± 3 mV, n = 6, TG 13 ± 4 mV, n = 5, unpaired t-test, p = 0.9, t = 0.1, Figure 6-14 C, D), peak width at -20 mV (-80 mV, WT 0.8 ± 0.1 ms, n = 6, TG 0.9 ± 0.1 ms, n = 5, unpaired t-test, p = 0.7, Figure 6-14 E, F) or dV/dt max (-80 mV, WT 235 ± 24 mV/ms, TG 236 ± 24 mV/ms, unpaired t-test, p = 1, t = -0.2) were observed. While a mean difference of 6 mV existed in threshold (WT -62 ± 3 mV, n = 6, TG -56 ± 3 mV, n = 5, unpaired t-test p = 0.2, t = -1.3) a large amount of variability meant this was not statistically significant.

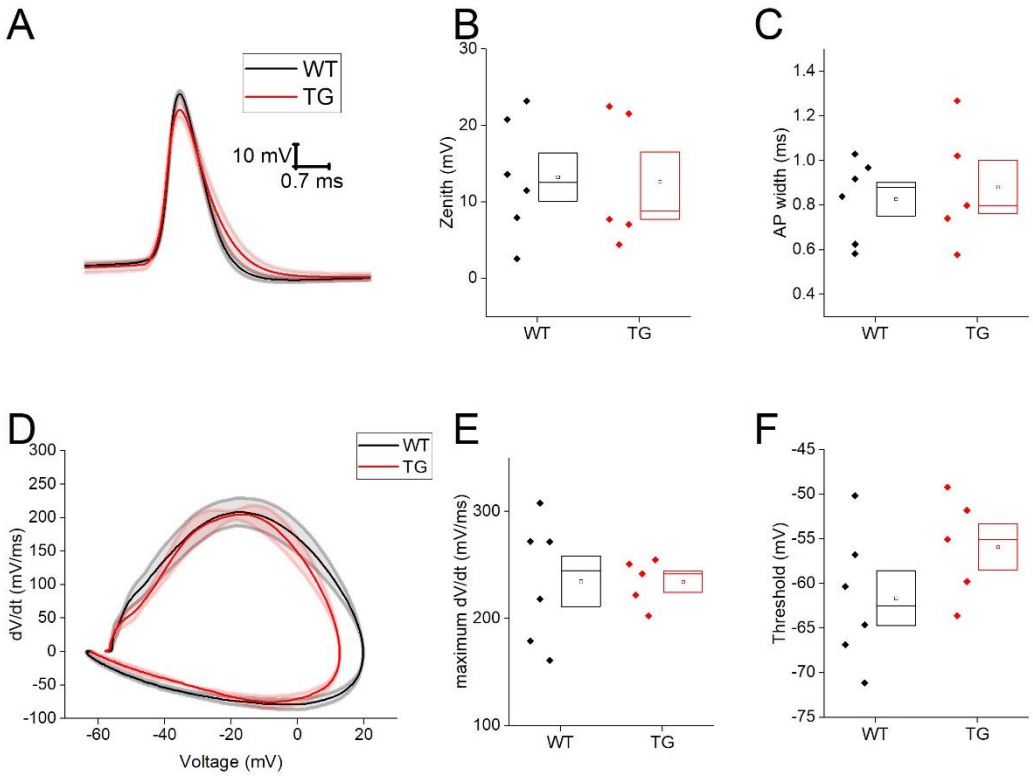

Figure 6-14 Action potential properties of type III neurons A) Average of first action potential generated in response to depolarising current injections. B) AP zenith, C) AP width at -20 mV, Averaged dV/dt of cells plotted against the average voltage change of cells, E) dV/dt max of cells and F) Threshold of cells from a holding potential of -70 mV and -80 respectively.

In examining excitability using the step protocol no differences in either proportion of cells firing (Table 6-3) or the frequency (Table 6-4) at which cells fire were observed.

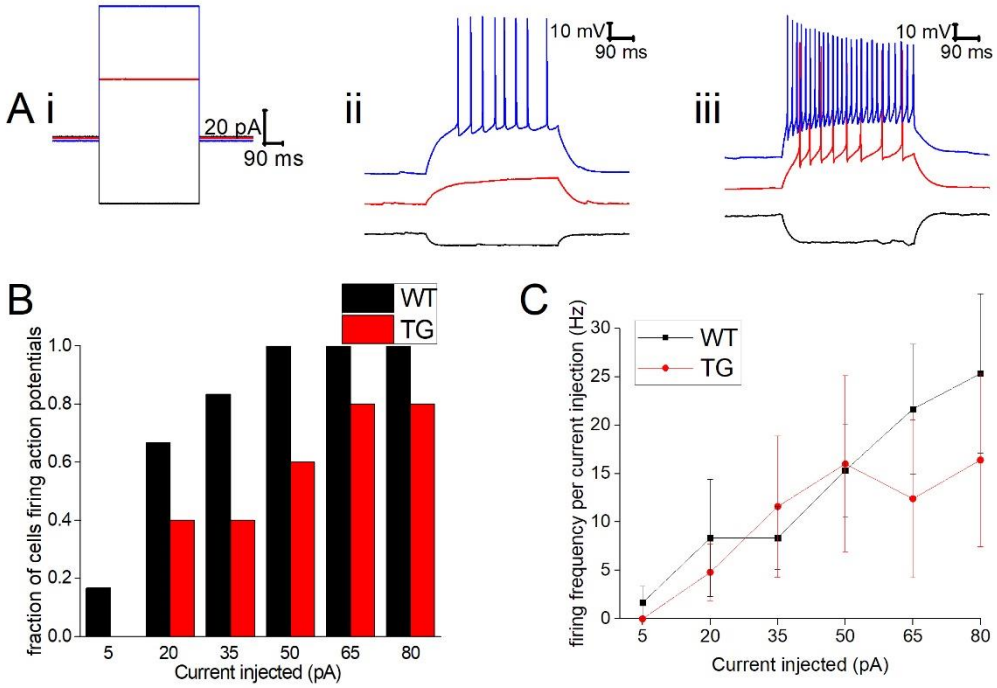

Figure 6-15 firing properties of Type III neurons A sample trace of a TG (II) and WT (III) cell, i) sample current injections. Fraction of cells firing at least 1 action potential in response to a series of depolarising pulses from a holding potential of -70 mV (B) and -80 mV (C). D, E) frequency of firing in response to each depolarising current injection from a holding potential of -70 mV and -80 mV respectively.

Current injected	WT (%)	TG (%)	P value
5 pA	17	0	0.4
20 pA	67	40	0.2
35 pA	83	40	0.1
050 pA	100	60	0.1
65 pA	100	80	0.2
80 pA	100	80	0.2

Table 6-3 Proportion of Type III cells firing in response to each current injection from both holding potentials. P values based on chi squared performed in Excel

Current injected	WT (Hz)	TG (Hz)
5 pA	2 ± 2 Hz	0 ± 0 Hz
20 pA	8 ± 6 Hz	5 ± 3 Hz
35 pA	8 ± 3 Hz	12 ± 7 Hz
50 pA	15 ± 5 Hz	16 ± 9 Hz
65 pA	21 ± 7 Hz	12 ± 8 Hz
80 pA	25 ± 8 Hz	16 ± 9 Hz

Table 6-4 Average frequency in response to each current injection from -70 mV and -80 mV of Type III cells

6.4. Discussion

This study examined the anxiety levels in the CHMP2B model of frontotemporal dementia, along with the electrophysiological properties of neurons located within the $BNST^{ALG}$. Overall, we found no differences in anxiety levels but observed some increases in excitability in the TG cohort in Type II neurons and a decrease in the maximum rate of rise in the action potential of type I neurons in the TG cohort.

TG Type II neurons display a hyperpolarised threshold, this would indicate that these cells would require less depolarising stimuli to generate an action potential and thereby lead to an increase in excitability. This was observed in decreased latency of these cells. Given the fast nature of synaptic events the differences in the period of time required for a cell to spike can be quite significant with regards to the cells response to synaptic input. With the assumed role of Type II neurons as anxiety off cells this increased excitability would in theory lead to a decrease in anxiety (Daniel *et al.*, 2017). However, the subtle nature of this increase, ie. that only 1 parameter appears to be affected while other measures of excitability like rheobase or firing frequency remain unaltered, may account for why this increase did not lead to decreases in anxiety in the maze. The opposing changes in excitability of the two populations may be cancelling out any behavioural effect.

The action potential waveform can have impact on various neurological functions; in Type I neurons the maximum rate of rise was significantly slower in the TG cohort. Changes in the maximum rate of rise can have effects on the action potential waveform leading to alterations in neurotransmitter release. While statisitically significant differences in action potential width or action potnetial zenith were not observed a trend towards a shorter thinner action potnetial was seen in the Type I neurons of the TG cohort. These two measurements would have opposing actions on neurotransmitter release; often a wider action potential would lead to increases in neurotransmitter release while a shorter action potential would lead to a decrease in neurotransmiter release. As the action potential width in this example is measured from a set potential of -20 mV the thinner aspect is most likely down to the fact that in the TG cohort the measurement was taken closer to the tip of the action potential

where it is most likely to be the thinnest. Unfortunatly due to large ADPs in a proportion of these cells AP width at threshold was not a viable measure.

These cells are classified using only their electrophysiological properties. The degree to which these forms of cell classification can be applied to dementia models is debatable. It is difficult to determine whether changes observed are down to changes in how the different cell types are behaving in the disease state or if changes within populations lead to misclassification of cells. For example classification of type II cells is based mostly on the hump observed in the depolarising step before the generation of an action potential thought to be driven by T-type calcium channels (Hammack *et al.*, 2007*a*). If these channels expression or function are changed by the dysfunction of the CHMP2B gene then there may be a resulting misclassification of the cell leading to potential differences in both the type II cells and in the other populations where the type II cells are misclassified.

While some of the electrophysiological properties differ in the different populations there is no effect on the anxiety levels of the animals, there is a number of possible reasons for this; it could be down to the fact that these animals were unstressed. This finding is consistent with the literature with Clayton et al 2017 finding no differences in anxiety levels in these mice using both the open field and the elevated plus maze. This finding is interesting as in the human population frontotemporal dementia is often associated with increases in anxiety(Clayton *et al.*, 2017). It may be that the mechanisms of dealing with stress become altered in disease state but given that all the animal testing so far has been carried out on unstressed models no differences have emerged. Of particular interest would be a PTSD model of stress in these animals given the strong correlation of PTSD and frontotemporal dementia in humans (Greenberg *et al.*, 2014*b*). This hypothesis was not tested as part of this project but it would be interesting to consider in the future.

This study has higlighted differences in intrinsic properties of neurons located within the anterolateral area of the BNST. These changes have no effect on anxiety in an unstressed model, however they highlight the potential for changes in stress processing which need to be adressed further.

7. General discussion

7.1. Summary and general discussion

Physiological manifestations of fear and anxiety appear to be conserved across mammalian species (Zhu *et al.*, 2014; Sotnikov *et al.*, 2014; Koch *et al.*, 2016). As the mouse's response to stress mimics a number of those observed in humans they are often used as a model to examine responses to stress and anxiety levels. A number of behavioural tests exist to determine anxiety in mouse models, this includes the elevated zero maze as used in this study. Further to these behavioural studies the use of mouse models allow numerous more invasive tests to be performed than cannot be carried out in a human, including electrophysiological characterisations of key brain regions associated with stress and anxiety such as the $BNST^{ALG}$. *In vitro* patch clamp recording is a robust way to gather real time electrophysiological information on neurons. The intrinsic electrophysiological properties of $BNST^{ALG}$ neurons have been characterised in the mouse, rat and non-human primate with similar populations being observed (Daniel *et al.*, 2017). This would indicate that the populations are conserved into higher mammalian species.

Overall, this thesis shows that a number intrinsic electrophysiological properties of neurons in the $BNST^{ALG}$ differ with gender, age and in the CHMP2B model of frontotemporal dementia. However the impact of the estrus cycle on BNST properties was minimal. I began by examining the effect of the estrus cycle on intrinsic properties in the $BNST^{ALG}$. A trend was observed in the dV/dt max of Type II neurons which was only significant in post hoc analysis: diestrus was slower than metestrus and proestrus. The trend observed in maximum rate of rise did not lead to any changes in either the shape of the action potential or the excitability of the different groups. The minimal effect of the estrus cycle on neurons located in the BNST meant that each of the stages of estrus could be grouped together for comparisons with an aged matched male cohort.

There were a number of intrinsic electrophysiological properties which were affected by gender; Type II cells showed an increased excitability in males driven by changes in passive membrane properties specifically input resistance. Progesterone or rather its metabolite ALLO plays a key role in regulating the expression of extrasynaptic $GABA_A$ receptors. These receptors can modulate

input resistance through tonic inhibition. In female mice, ALLO is 8-10 fold higher than in male mice and while progesterone is thought to be anxiolytic, the effects of fluctuations in ALLO are far more variable; the effect mediated can be both anxiolytic or anxiogenic (Dong *et al.*, 2001*a*; Gulinello *et al.*, 2003; Lovick, 2006; Matsumoto *et al.*, 2007; Shen *et al.*, 2007; Smith *et al.*, 2007; Jiang *et al.*, 2014; Nagaya *et al.*, 2015*a*). This increase in excitability in the Type II male neurons may lead to anxiolytic behaviour; Type II neurons are thought to be anxiolytic mediating their action through inhibition of the HPA axis (Daniel & Rainnie, 2016).

The differences in excitability and passive membrane properties of Type II neurons may contribute to changes in susceptibility to anxiety related disorders. The BNST is involved in a feedback mechanism of stress modulation between the HPA axis and the limbic system; dysregulation of this system has been implicated in PTSD (Lee *et al.*, 2008; McElligott *et al.*, 2010; Lebow *et al.*, 2012; Gafford & Ressler, 2015). Also, alteration in BNST function and CRF levels have been observed in patients with PTSD (Bremner *et al.*, 1997*b*). As the BNST is susceptible to modulation by stressful stimuli and mediates sustain fear states these changes in baseline processing may provide some basis for the altered susceptibility between the genders to PTSD.

Following this, I examined the effect of age on the intrinsic properties of neurons in the BNST. Due to the availability of tissue, this study was carried out in aging females. In aged mice, Type I neurons had a hyperpolarised resting membrane potential and wider action potentials, while Type II neurons from the aged cohort displayed smaller amplitudes of inward-going post synaptic events and an increase in excitability most likely due to the a more depolarised threshold. Increases in activity of Type II neurons are thought to decrease anxiety, if this hypothesis holds then in theory you would see a decrease in anxiety with aging in the female cohort. However, in the human population there is an increase in anxiety related disorders in menopausal females which has been attributed to decreases in sex hormones (Garrido, 2011; Ebner *et al.*, 2014). In chapter four, the correlation between behaviour and intrinsic properties of $BNST^{ALG}$ neurons was addressed; while a number of correlations were observed in the male

cohort, there were no significant correlations in any of the parameters examined in the female cohort.

An issue with the classification of this population was that it was based upon recordings in male rats and while most of the characteristics of these cells have led to similar classifications in the mouse there is a larger degree of variability in the female population. This may be attributable to changes in hormones leading to increased variability. However in chapter three this was addressed and I found that none of the electrophysiological properties examined displayed oestrous cycle dependent variations. Stress modulation changes over the lifespan occur in a sex specific manner (Bowman *et al.*, 2006) therefore in the future it would be interesting to expand upon this and examine the effect of age on males and see if a similar increase exists.

Finally I looked at the impact of frontotemporal dementia on the $BNST_{ALG}$, in Type I neurons the TG cohort had a significantly lower maximum rate of rise. This however did not lead to any changes in other aspects of the action potential waveform examined including width or zenith. Also TG Type II neurons had a more hyperpolarised threshold and faster latency. Changes in threshold often lead to alterations in excitability, however this was not the case in this cohort as no changes in excitability were observed. Similar to the previous two studies the largest differences were observed in Type II neurons, this may implicate that these neurons are more susceptible to changes in physiological conditions.

There is a third common cell type in these populations the Type III neurons, . The original classification of these cells was based upon two parameters, the absence of sag and the presence of an inwardly rectifying potassium current. The protocols used in this study did not address the presence or absence of inwardly rectifying potassium channels and were therefore based entirely upon the absence of sag. Therefore, the Type III neurons included here may be not accurately represent the Type III population present in these cohorts. The possible mixture of cells combined with low n number may be masking diffrences between the populations. These Type III neurons are thought to be CRF positive neurons and play a key role in stress modulation in the BNST as a whole and specifically within the $BNST^{ALG}$ (Sahuque *et al.*, 2006; Lee *et al.*,

2008; Sink *et al.*, 2013; Janitzky *et al.*, 2014; Gafford & Ressler, 2015; Henckens *et al.*, 2016). To fully understand how these circuits may be affected by gender, age and disease Type III cells should be examined further.

7.2. Future work

An interesting extension of this work would be a longitudinal study examining the effect of healthy aging on neurons in the BNST in both genders across their lifespan. In the introduction the genders specific effects of aging were addressed and while here we focused on the gender differences in young adults and healthy aging in females the changes in susceptibility to anxiety related disorders begins before puberty (Wesselhoeft *et al.*, 2015). In the prepubescent age range there is a higher incidence of anxiety related disorders in males. From the age of 12 onwards the incidences increase in both genders however they become more prevalent in females. I would propose the characterisation of these neurons from weening up to very aged animals at 30 months. This work would be carried out in conjunction with anxiety test measured on the elevated zero maze.

In conjunction with this, the optogenetic stimulation of afferent projections into the BNST would provide a more in depth understanding of the roles of these different population in stress modulation. To examine the functional connectivity between the ventral subiculum and mPFC onto the BNST I would use the two new variants of channelrhodopsin, Chronos and Chrimson. They would be injected into the mPFC and hippocampus respectively. These variants respond selectively to blue and red light allowing dual activation in the same slice prep. While the axonal projections would be removed optic stimulation still leads to EPSCs in connected cells. The $BNST^{ALG}$ receives dense afferents from both the ventral subiculum and the mPFC. I would expect a large proportion of the cells to respond to optic stimulation.

During the recordings I would fill the cells with biocytin. This will allow post recording characterisation of morphology and markers. While some initial work has been carried out into characterising these cells more research is needed. For example, no definitive markers have been found to tie electrophysiological characterisation to cell types. Some preliminary unpublished data (Daniel & Rainnie, 2015) from the Rainnie lab suggests that these different cell

populations do display certain markers specifically type III being CRF positive and type II being PCK-δ positive. One aspect of this project would be to address this post recording. This longitudinal study would provide vital insight into the mechanisms underlying stress processing over their lifetime.

References:

A.R Knight N. B (1996). The pharmacology of adenylyl cyclase modulation by GABAB receptors in rat brain slices. *Neuropharmacology* **35,** 703–712.

Adamec R, Head D, Blundell J, Burton P & Berton O (2006). Lasting anxiogenic effects of feline predator stress in mice: Sex differences in vulnerability to stress and predicting severity of anxiogenic response from the stress experience. *Physiol Behav* **88,** 12–29.

Admon R, Lubin G, Stern O, Rosenberg K, Sela L, Ben-Ami H & Hendler T (2009). Human vulnerability to stress depends on amygdala's predisposition and hippocampal plasticity. *Proc Natl Acad Sci U S A* **106,** 14120–14125.

Ahern T & Wu FCW (2015). New horizons in testosterone and the ageing male. *Age Ageing* **44,** 188–195.

Ahmed Z, Sheng H, Xu Y-F, Lin W-L, Innes AE, Gass J, Yu X, Wuertzer CA, Hou H, Chiba S, Yamanouchi K, Leissring M, Petrucelli L, Nishihara M, Hutton ML, McGowan E, Dickson DW & Lewis J (2010). Accelerated lipofuscinosis and ubiquitination in granulin knockout mice suggest a role for progranulin in successful aging. *Am J Pathol* **177,** 311–324.

ALBRIGHT F, SMITH PH & RICHARDSON AM (1941). POSTMENOPAUSAL OSTEOPOROSIS. *J Am Med Assoc* **116,** 2465.

Aloisi F (2001). Immune function of microglia. *Glia* **36,** 165–179.

Amat J, Tamblyn JP, Paul ED, Bland ST, Amat P, Foster AC, Watkins LR & Maier SF (2004). Microinjection of urocortin 2 into the dorsal raphe nucleus activates serotonergic neurons and increases extracellular serotonin in the basolateral amygdala. *Neuroscience* **129,** 509–519.

Bailey M & Silver R (2014). Sex differences in circadian timing systems: implications for disease. *Front Neuroendocrinol* **35,** 111–139.

Baker DG, West SA, Nicholson WE, Ekhator NN, Kasckow JW, Hill KK, Bruce AB, Orth DN & Geracioti TD (1999). Serial CSF corticotropin-releasing hormone levels and adrenocortical activity in combat veterans with posttraumatic stress disorder. *Am J Psychiatry* **156,** 585–588.

Bang J, Spina S & Miller BL (2015). Frontotemporal dementia. *Lancet* **386,** 1672–1682.

Barbaccia ML, Roscetti G, Trabucchi M, Mostallino MC, Concas A, Purdy RH & Biggio G (2008). Time-Dependent Changes in Rat Brain Neuroactive Steroid Concentrations and GABA_A Receptor Function after Acute Stress. *Neuroendocrinology* **63,** 166–172.

Batarseh Y, Duong Q-V, Mousa Y, Al Rihani S, Elfakhri K & Kaddoumi A (2016). Amyloid-β and Astrocytes Interplay in Amyloid-β Related Disorders. *Int J Mol Sci* **17,** 338.

Bayatti N, Hermann H, Lutz B & Behl C (2005). Corticotropin-Releasing

Hormone-Mediated Induction of Intracellular Signaling Pathways and Brain-Derived Neurotrophic Factor Expression Is Inhibited by the Activation of the Endocannabinoid System. *Endocrinology* **146,** 1205–1213.

Bettler B, Kaupmann K, Mosbacher J & Gassmann M (2004). Molecular structure and physiological functions of GABA(B) receptors. *Physiol Rev* **84,** 835–867.

Bodhinathan K, Kumar A & Foster TC (2010). Redox sensitive calcium stores underlie enhanced after hyperpolarization of aged neurons: role for ryanodine receptor mediated calcium signaling. *J Neurophysiol* **104,** 2586–2593.

Bormann J & Feigenspan A (1995). GABAc receptors. *Trends Neurosci* **18,** 515–519.

Boudaba C, Szabo K & Tasker JG (1996). Physiological Mapping of Local Inhibitory Inputs to the Hypothalamic Paraventricular Nucleus. *J Neurosci* **16,** 7151–7160.

Bowery NG, Bettler B, Froestl W, Gallagher JP, Marshall F, Raiteri M, Bonner TI & Enna SJ (2002). International Union of Pharmacology. XXXIII. Mammalian gamma-aminobutyric acid(B) receptors: structure and function. *Pharmacol Rev* **54,** 247–264.

Bowman RE, Maclusky NJ, Diaz SE, Zrull MC & Luine VN (2006). Aged rats: Sex differences and responses to chronic stress. *Brain Res* **1126,** 156–166.

Boyden ES (2015). Optogenetics and the future of neuroscience. *Nat Neurosci* **18,** 1200–1201.

Boyden ES, Zhang F, Bamberg E, Nagel G & Deisseroth K (2005). Millisecond-timescale, genetically targeted optical control of neural activity. *Nat Neurosci* **8,** 1263–1268.

Brack KE & Lovick TA (2007*a*). Neuronal excitability in the periaqueductal grey matter during the estrous cycle in female Wistar rats. *Neuroscience* **144,** 325–335.

Brack KE & Lovick TA (2007*b*). Neuronal excitability in the periaqueductal grey matter during the estrous cycle in female Wistar rats. *Neuroscience* **144,** 325–335.

Bremner JD, Licinio J, Darnell A, Krystal JH, Owens MJ, Southwick SM, Nemeroff CB & Charney DS (1997*a*). Elevated CSF corticotropin-releasing factor concentrations in posttraumatic stress disorder. *Am J Psychiatry* **154,** 624–629.

Bremner JD, Licinio J, Darnell A, Krystal JH, Owens MJ, Southwick SM, Nemeroff CB & Charney DS (1997*b*). Elevated CSF corticotropin-releasing factor concentrations in posttraumatic stress disorder. *Am J Psychiatry* **154,** 624–629.

Breslau N & Kessler RC (2001). The stressor criterion in DSM-IV posttraumatic stress disorder: an empirical investigation. *Biol Psychiatry* **50,** 699–704.

Brinkmann L, Buff C, Neumeister P, Tupak S V., Becker MPI, Herrmann MJ & Straube T (2017). Dissociation between amygdala and bed nucleus of the stria terminalis during threat anticipation in female post-traumatic stress disorder patients. *Hum Brain Mapp* **38,** 2190–2205.

Brinton RD, Thompson RF, Foy MR, Baudry M, Wang J, Finch CE, Morgan TE, Pike CJ, Mack WJ, Stanczyk FZ & Nilsen J (2008). Progesterone receptors: form and function in brain. *Front Neuroendocrinol* **29,** 313–339.

Brown JT & Randall AD (2009). Activity-dependent depression of the spike after-depolarization generates long-lasting intrinsic plasticity in hippocampal CA3 pyramidal neurons. *J Physiol* **587,** 1265–1281.

Bueno J & Pfaff DW (1976). Single unit recording in hypothalamus and preoptic area of estrogen-treated and untreated ovariectomized female rats. *Brain Res* **101,** 67–78.

Cain DW & Cidlowski JA (2015). Specificity and sensitivity of glucocorticoid signaling in health and disease. *Best Pract Res Clin Endocrinol Metab* **29,** 545–556.

Cairns NJ et al. (2007). TDP-43 in familial and sporadic frontotemporal lobar degeneration with ubiquitin inclusions. *Am J Pathol* **171,** 227–240.

Calcagnoli F, de Boer SF, Beiderbeck DI, Althaus M, Koolhaas JM & Neumann ID (2014). Local oxytocin expression and oxytocin receptor binding in the male rat brain is associated with aggressiveness. *Behav Brain Res* **261,** 315–322.

Caligioni CS (2009). Assessing reproductive status/stages in mice. *Curr Protoc Neurosci* **Appendix 4,** Appendix 4I.

Chang Y-M, Rosene DL, Killiany RJ, Mangiamele LA & Luebke JI (2005*a*). Increased action potential firing rates of layer 2/3 pyramidal cells in the prefrontal cortex are significantly related to cognitive performance in aged monkeys. *Cereb Cortex* **15,** 409–418.

Chang Y-M, Rosene DL, Killiany RJ, Mangiamele LA & Luebke JI (2005*b*). Increased action potential firing rates of layer 2/3 pyramidal cells in the prefrontal cortex are significantly related to cognitive performance in aged monkeys. *Cereb Cortex* **15,** 409–418.

Chang Y, Wang R, Barot S & Weiss DS (1996). Stoichiometry of a Recombinant GABAA Receptor. *J Neurosci*. Available at: http://www.jneurosci.org/content/16/17/5415.short [Accessed August 25, 2017].

Charmandari E, Tsigos C & Chrousos G (2005). ENDOCRINOLOGY OF THE STRESS RESPONSE. *Annu Rev Physiol* **67,** 259–284.

Chen-Plotkin AS et al. (2011). Genetic and Clinical Features of Progranulin-Associated Frontotemporal Lobar Degeneration. *Arch Neurol* **68,** 488.

Chen H, Liu J, Luo L & Zirkin BR (2004). Dibutyryl cyclic adenosine monophosphate restores the ability of aged Leydig cells to produce testosterone at the high levels characteristic of young cells. *Endocrinology*

145, 4441–4446.

Chen W, Shields J, Huang W & King JA (2009). Female fear: Influence of estrus cycle on behavioral response and neuronal activation. *Behav Brain Res* **201,** 8–13.

Cheney DL, Uzunov D, Costa E & Guidotti A (1995). Gas chromatographic-mass fragmentographic quantitation of 3 alpha-hydroxy-5 alpha-pregnan-20-one (allopregnanolone) and its precursors in blood and brain of adrenalectomized and castrated rats. *J Neurosci* **15,** 4641–4650.

Choi DC, Furay AR, Evanson NK, Ostrander MM, Ulrich-Lai YM & Herman JP (2007). Bed nucleus of the stria terminalis subregions differentially regulate hypothalamic-pituitary-adrenal axis activity: implications for the integration of limbic inputs. *J Neurosci* **27,** 2025–2034.

Chrousos GP & Gold PW (1992). The concepts of stress and stress system disorders. Overview of physical and behavioral homeostasis. *JAMA* **267,** 1244–1252.

Chrousos GP & Kino T (2005). Intracellular Glucocorticoid Signaling: A Formerly Simple System Turns Stochastic. *Sci Signal* **2005,** pe48-pe48.

Clark AK, Gruber-Schoffnegger D, Drdla-Schutting R, Gerhold KJ, Malcangio M & Sandkuhler J (2015). Selective Activation of Microglia Facilitates Synaptic Strength. *J Neurosci* **35,** 4552–4570.

Claro F, Segovia S, Guilamón A & Del Abril A (1995). Lesions in the medial posterior region of the BST impair sexual behavior in sexually experienced and inexperienced male rats. *Brain Res Bull* **36,** 1–10.

Clayton EL et al. (2017). Early microgliosis precedes neuronal loss and behavioural impairment in mice with a frontotemporal dementia-causing CHMP2B mutation. *Hum Mol Genet* **23,** ddx003.

Clayton EL, Mizielinska S, Edgar JR, Nielsen TT, Marshall S, Norona FE, Robbins M, Damirji H, Holm IE, Johannsen P, Nielsen JE, Asante EA, Collinge J, Isaacs AM & Isaacs AM (2015). Frontotemporal dementia caused by CHMP2B mutation is characterised by neuronal lysosomal storage pathology. *Acta Neuropathol* **130,** 511–523.

Conrad KL, Louderback KM, Gessner CP & Winder DG (2011*a*). Stress-induced alterations in anxiety-like behavior and adaptations in plasticity in the bed nucleus of the stria terminalis. *Physiol Behav* **104,** 248–256.

Conrad KL, Louderback KM, Gessner CP & Winder DG (2011*b*). Stress-induced alterations in anxiety-like behavior and adaptations in plasticity in the bed nucleus of the stria terminalis. *Physiol Behav* **104,** 248–256.

Conrad KL, Louderback KM, Gessner CP & Winder DG (2011*c*). Stress-induced alterations in anxiety-like behavior and adaptations in plasticity in the bed nucleus of the stria terminalis. *Physiol Behav* **104,** 248–256.

Conrad KL & Winder DG (2011). Altered anxiety-like behavior and long-term potentiation in the bed nucleus of the stria terminalis in adult mice exposed to chronic social isolation, unpredictable stress, and ethanol beginning in

adolescence. *Alcohol* **45,** 585–593.

Corpéchot C, Young J, Calvel M, Wehrey C, Veltz JN, Touyer G, Mouren M, Prasad V V, Banner C & Sjövall J (1993). Neurosteroids: 3 alpha-hydroxy-5 alpha-pregnan-20-one and its precursors in the brain, plasma, and steroidogenic glands of male and female rats. *Endocrinology* **133,** 1003–1009.

Coskren PJ, Luebke JI, Kabaso D, Wearne SL, Yadav A, Rumbell T, Hof PR & Weaver CM (2014). Functional consequences of age-related morphologic changes to pyramidal neurons of the rhesus monkey prefrontal cortex. *J Comput Neurosci*; DOI: 10.1007/s10827-014-0541-5.

Cox LE, Ferraiuolo L, Goodall EF, Heath PR, Higginbottom A, Mortiboys H, Hollinger HC, Hartley JA, Brockington A, Burness CE, Morrison KE, Wharton SB, Grierson AJ, Ince PG, Kirby J & Shaw PJ (2010). Mutations in CHMP2B in Lower Motor Neuron Predominant Amyotrophic Lateral Sclerosis (ALS) ed. Cookson MR. *PLoS One* **5,** e9872.

Crestani CC, Alves FH, Gomes F V, Resstel LB, Correa FM & Herman JP (2013). Mechanisms in the bed nucleus of the stria terminalis involved in control of autonomic and neuroendocrine functions: a review. *Curr Neuropharmacol* **11,** 141–159.

Cullinan WE, Herman JP & Watson SJ (1993). Ventral subicular interaction with the hypothalamic paraventricular nucleus: evidence for a relay in the bed nucleus of the stria terminalis. *J Comp Neurol* **332,** 1–20.

Cullinan WE, Ziegler DR & Herman JP (2008). Functional role of local GABAergic influences on the HPA axis. *Brain Struct Funct* **213,** 63–72.

Cummings JL (1997). The Neuropsychiatric Inventory: Assessing psychopathology in dementia patients. *Neurology* **48,** 10S–16S.

Dabrowska J, Hazra R, Guo J-D, Li C, Dewitt S, Xu J, Lombroso PJ & Rainnie DG (2013). Striatal-enriched protein tyrosine phosphatase-STEPs toward understanding chronic stress-induced activation of corticotrophin releasing factor neurons in the rat bed nucleus of the stria terminalis. *Biol Psychiatry* **74,** 817–826.

Dabrowska J, Martinon D, Moaddab M & Rainnie DG (2016). Targeting Corticotropin-Releasing Factor Projections from the Oval Nucleus of the Bed Nucleus of the Stria Terminalis Using Cell-Type Specific Neuronal Tracing Studies in Mouse and Rat Brain. *J Neuroendocrinol*; DOI: 10.1111/jne.12442.

Dalm S, Enthoven L, Meijer OC, van der Mark MH, Karssen AM, de Kloet ER & Oitzl MS (2005). Age-related changes in hypothalamic-pituitary-adrenal axis activity of male C57BL/6J mice. *Neuroendocrinology* **81,** 372–380.

Daniel SE, Guo J & Rainnie DG (2017). A comparative analysis of the physiological properties of neurons in the anterolateral bed nucleus of the stria terminalis in the Mus musculus , Rattus norvegicus , and Macaca mulatta. *J Comp Neurol* **525,** 2235–2248.

Daniel SE & Rainnie DG (2015). Stress Modulation of Opposing Circuits in the

Bed Nucleus of the Stria Terminalis. *Neuropsychopharmacology*; DOI: 10.1038/npp.2015.178.

Daniel SE & Rainnie DG (2016). Stress Modulation of Opposing Circuits in the Bed Nucleus of the Stria Terminalis. *Neuropsychopharmacology* **41,** 103–125.

Davis M, Walker DL, Miles L & Grillon C (2010). Phasic vs sustained fear in rats and humans: role of the extended amygdala in fear vs anxiety. *Neuropsychopharmacology* **35,** 105–135.

Day HE, Curran EJ, Watson SJ & Akil H (1999). Distinct neurochemical populations in the rat central nucleus of the amygdala and bed nucleus of the stria terminalis: evidence for their selective activation by interleukin-1beta. *J Comp Neurol* **413,** 113–128.

Devall AJ, Liu Z-W & Lovick TA (2009). Hyperalgesia in the setting of anxiety: Sex differences and effects of the oestrous cycle in Wistar rats. *Psychoneuroendocrinology* **34,** 587–596.

Disterhoft JF, Wu WW & Ohno M (2004). Biophysical alterations of hippocampal pyramidal neurons in learning, ageing and Alzheimer's disease. *Ageing Res Rev* **3,** 383–406.

Dobie DJ, Miller MA, Raskind MA & Dorsa DM (1992). Testosterone reverses a senescent decline in extrahypothalamic vasopressin mRNA. *Brain Res* **583,** 247–252.

Dobie DJ, Miller MA, Urban JH, Raskind MA & Dorsa DM (1991). Age-related decline of vasopressin mRNA in the bed nucleus of the stria terminalis. *Neurobiol Aging* **12,** 419–423.

Dong E, Matsumoto K, Uzunova V, Sugaya I, Takahata H, Nomura H, Watanabe H, Costa E & Guidotti A (2001*a*). Brain 5alpha-dihydroprogesterone and allopregnanolone synthesis in a mouse model of protracted social isolation. *Proc Natl Acad Sci U S A* **98,** 2849–2854.

Dong H-W, Petrovich G. & Swanson L. (2000). Organization of projections from the juxtacapsular nucleus of the BST: a PHAL study in the rat. *Brain Res* **859,** 1–14.

Dong H-W, Petrovich GD & Swanson LW (2001*b*). Topography of projections from amygdala to bed nuclei of the stria terminalis. *Brain Res Rev* **38,** 192–246.

Dong H-W & Swanson LW (2004*a*). Organization of axonal projections from the anterolateral area of the bed nuclei of the stria terminalis. *J Comp Neurol* **468,** 277–298.

Dong H-W & Swanson LW (2004*b*). Organization of axonal projections from the anterolateral area of the bed nuclei of the stria terminalis. *J Comp Neurol* **468,** 277–298.

Dong HW, Petrovich GD, Watts AG & Swanson LW (2001*c*). Basic organization of projections from the oval and fusiform nuclei of the bed nuclei of the stria terminalis in adult rat brain. *J Comp Neurol* **436,** 430–455.

Donner NC & Lowry CA (2013). Sex differences in anxiety and emotional behavior. *Pflügers Arch Eur J Physiol* **465,** 601–626.

Dumont EC, Mark GP, Mader S & Williams JT (2005). Self-administration enhances excitatory synaptic transmission in the bed nucleus of the stria terminalis. *Nat Neurosci* **8,** 413–414.

Ebner NC, Kamin H, Diaz V, Cohen RA & MacDonald K (2014). Hormones as "difference makers" in cognitive and socioemotional aging processes. *Front Psychol* **5,** 1595.

Ehrchen J, Sindrilaru A, Grabbe S, Schönlau F, Schlesiger C, Sorg C, Scharffetter-Kochanek K & Sunderkötter C (2004). Senescent BALB/c mice are able to develop resistance to Leishmania major infection. *Infect Immun* **72,** 5106–5114.

Emery DE & Sachs BD (1976). Copulatory behavior in male rats with lesions in the bed nucleus of the stria terminalis. *Physiol Behav* **17,** 803–806.

Erb S & Stewart J (1999). A role for the bed nucleus of the stria terminalis, but not the amygdala, in the effects of corticotropin-releasing factor on stress-induced reinstatement of cocaine seeking. *J Neurosci* **19,** RC35.

Faria MP, Miguel TT, Gomes KS & Nunes-de-Souza RL (2016). Anxiety-like responses induced by nitric oxide within the BNST in mice: Role of CRF1 and NMDA receptors. *Horm Behav* **79,** 74–83.

Funk D, Li Z & Lê AD (2006). Effects of environmental and pharmacological stressors on c-fos and corticotropin-releasing factor mRNA in rat brain: Relationship to the reinstatement of alcohol seeking. *Neuroscience* **138,** 235–243.

Gafford GM & Ressler KJ (2015). GABA and NMDA receptors in CRF neurons have opposing effects in fear acquisition and anxiety in central amygdala vs. bed nucleus of the stria terminalis. *Horm Behav* **76,** 136–142.

Gallo V & Deneen B (2014). Glial Development: The Crossroads of Regeneration and Repair in the CNS. *Neuron* **83,** 283–308.

Garrido P (2011). Aging and stress: past hypotheses, present approaches and perspectives. *Aging Dis* **2,** 80–99.

Gewirtz JC, Mcnish KA & Davis M (1998). Lesions of the bed nucleus of the stria terminalis block sensitization of the acoustic startle reflex produced by repeated stress, but not fear-potentiated startle. *Prog Neuro-Psychopharmacology Biol Psychiatry* **22,** 625–648.

Ghazi-Noori S, Froud KE, Mizielinska S, Powell C, Smidak M, Fernandez de Marco M, O'Malley C, Farmer M, Parkinson N, Fisher EMC, Asante EA, Brandner S, Collinge J & Isaacs AM (2012*a*). Progressive neuronal inclusion formation and axonal degeneration in CHMP2B mutant transgenic mice. *Brain* **135,** 819–832.

Ghazi-Noori S, Froud KE, Mizielinska S, Powell C, Smidak M, Fernandez de Marco M, O'Malley C, Farmer M, Parkinson N, Fisher EMC, Asante EA, Brandner S, Collinge J & Isaacs AM (2012*b*). Progressive neuronal

inclusion formation and axonal degeneration in CHMP2B mutant transgenic mice. *Brain* **135,** 819–832.

Gingerich S & Krukoff TL (2005). Estrogen Modulates Endothelial and Neuronal Nitric Oxide Synthase Expression via an Estrogen Receptor β-Dependent Mechanism in Hypothalamic Slice Cultures. *Endocrinology* **146,** 2933–2941.

Gingerich S & Krukoff TL (2006). Estrogen in the Paraventricular Nucleus Attenuates l-Glutamate–Induced Increases in Mean Arterial Pressure Through Estrogen Receptor β and NO. *Hypertension*. Available at: http://hyper.ahajournals.org/content/48/6/1130 [Accessed May 23, 2017].

Goldman SA, Nedergaard M & Windrem MS (2015). Modeling cognition and disease using human glial chimeric mice. *Glia* **63,** 1483–1493.

Greenberg MS, Tanev K, Marin M-F & Pitman RK (2014*a*). Stress, PTSD, and dementia. *Alzheimer's Dement* **10,** S155–S165.

Greenberg MS, Tanev K, Marin MF & Pitman RK (2014*b*). Stress, PTSD, and dementia. *Alzheimer's Dement* **10,** S155–S165.

Gresham R, Li S, Adekunbi DA, Hu M, Li XF & O'Byrne KT (2016). Kisspeptin in the medial amygdala and sexual behavior in male rats. *Neurosci Lett* **627,** 13–17.

Gulinello M, Gong QH & Smith SS (2003). Progesterone withdrawal increases the anxiolytic actions of gaboxadol: role of alpha4betadelta GABA(A) receptors. *Neuroreport* **14,** 43–46.

Guo J-D & Rainnie DG (2010). Presynaptic 5-HT1B receptor-mediated serotonergic inhibition of glutamate transmission in the bed nucleus of the stria terminalis. *Neuroscience* **165,** 1390–1401.

Gupta D & Morley JE (2014). Hypothalamic-Pituitary-Adrenal (HPA) Axis and Aging. In *Comprehensive Physiology*, pp. 1495–1510. John Wiley & Sons, Inc., Hoboken, NJ, USA. Available at: http://www.ncbi.nlm.nih.gov/pubmed/25428852 [Accessed May 23, 2017].

Hale MW, Stamper CE, Staub DR & Lowry CA (2010). Urocortin 2 increases c-Fos expression in serotonergic neurons projecting to the ventricular/periventricular system. *Exp Neurol* **224,** 271–281.

Hammack SE, Cooper MA & Lezak KR (2012). Overlapping neurobiology of learned helplessness and conditioned defeat: Implications for PTSD and mood disorders. *Neuropharmacology* **62,** 565–575.

Hammack SE, Guo J, Hazra R, Dabrowska J, Karyn M & Rainnie DG (2009). The response of neurons in the bed nucleus of the striatas terminalis to serotonin : Implications for anxiety. *Prog neuropsycopharmacology Biol Psyyciatry* **33,** 1309–1320.

Hammack SE, Mania I & Rainnie DG (2007*a*). Differential Expression of Intrinsic Membrane Currents in Defined Cell Types of the Anterolateral Bed Nucleus of the Stria Terminalis. *J Neurophysiol*.

Hammack SE, Mania I & Rainnie DG (2007*b*). Differential Expression of

Intrinsic Membrane Currents in Defined Cell Types of the Anterolateral Bed Nucleus of the Stria Terminalis. *J Neurophysiol* **98,** 638–656.

Hammels C, Pishva E, De Vry J, van den Hove DLA, Prickaerts J, van Winkel R, Selten J-P, Lesch K-P, Daskalakis NP, Steinbusch HWM, van Os J, Kenis G & Rutten BPF (2015). Defeat stress in rodents: From behavior to molecules. *Neurosci Biobehav Rev* **59,** 111–140.

Han X & Boyden ES (2007). Multiple-Color Optical Activation, Silencing, and Desynchronization of Neural Activity, with Single-Spike Temporal Resolution ed. Rustichini A. *PLoS One* **2,** e299.

Harvey RJ, Skelton-Robinson M & Rossor MN (2003). The prevalence and causes of dementia in people under the age of 65 years. *J Neurol Neurosurg Psychiatry* **74,** 1206–1209.

He C, Chen F, Li B & Hu Z (2014). Neurophysiology of HCN channels: From cellular functions to multiple regulations. *Prog Neurobiol* **112,** 1–23.

Hebda-Bauer EK, Simmons TA, Sugg A, Ural E, Stewart JA, Beals JL, Wei Q, Watson SJ & Akil H (2013). 3xTg-AD mice exhibit an activated central stress axis during early-stage pathology. *J Alzheimers Dis* **33,** 407–422.

Henckens MJAG, Printz Y, Shamgar U, Dine J, Lebow M, Drori Y, Kuehne C, Kolarz A, Eder M, Deussing JM, Justice NJ, Yizhar O & Chen A (2016). CRF receptor type 2 neurons in the posterior bed nucleus of the stria terminalis critically contribute to stress recovery. *Mol Psychiatry*; DOI: 10.1038/mp.2016.133.

Herman JP, Ostrander MM, Mueller NK & Figueiredo H (2005). Limbic system mechanisms of stress regulation: hypothalamo-pituitary-adrenocortical axis. *Prog Neuropsychopharmacol Biol Psychiatry* **29,** 1201–1213.

Herman JP, Tasker JG, Ziegler DR & Cullinan WE (2002). Local circuit regulation of paraventricular nucleus stress integration. *Pharmacol Biochem Behav* **71,** 457–468.

Hermann PM, Watson SN & Wildering WC (2014). Phospholipase A2 - nexus of aging, oxidative stress, neuronal excitability, and functional decline of the aging nervous system? Insights from a snail model system of neuronal aging and age-associated memory impairment. *Front Genet* **5,** 419.

Hines M, Allen LS & Gorski RA (1992). Sex differences in subregions of the medial nucleus of the amygdala and the bed nucleus of the stria terminalis of the rat. *Brain Res* **579,** 321–326.

HODGKIN AL & HUXLEY AF (1952). Movement of sodium and potassium ions during nervous activity. *Cold Spring Harb Symp Quant Biol* **17,** 43–52.

Huang G-B, Zhao T, Gao X-L, Zhang H-X, Xu Y-M, Li H & Lv L-X (2016). Effect of chronic social defeat stress on behaviors and dopamine receptor in adult mice. *Prog Neuro-Psychopharmacology Biol Psychiatry* **66,** 73–79.

Isaacs AM, Johannsen P, Holm I, Nielsen JE & FReJA consortium Fr (2011). Frontotemporal dementia caused by CHMP2B mutations. *Curr Alzheimer Res* **8,** 246–251.

Iwata S, Wakita M, Shin M-C, Fukuda A & Akaike N (2013). Modulation of allopregnanolone on excitatory transmitters release from single glutamatergic terminal. *Brain Res Bull* **93,** 39–46.

Janitzky K, D'Hanis W, Kröber A & Schwegler H (2015). TMT predator odor activated neural circuit in C57BL/6J mice indicates TMT-stress as a suitable model for uncontrollable intense stress. *Brain Res* **1599,** 1–8.

Janitzky K, Peine A, Kröber A, Yanagawa Y, Schwegler H & Roskoden T (2014). Increased CRF mRNA expression in the sexually dimorphic BNST of male but not female GAD67 mice and TMT predator odor stress effects upon spatial memory retrieval. *Behav Brain Res* **272,** 141–149.

Jedema HP & Grace AA (2004). Corticotropin-releasing hormone directly activates noradrenergic neurons of the locus ceruleus recorded in vitro. *J Neurosci* **24,** 9703–9713.

Jennings JH, Sparta DR, Stamatakis AM, Ung RL, Pleil KE, Kash TL & Stuber GD (2013). Distinct extended amygdala circuits for divergent motivational states. *Nature* **496,** 224–228.

Jiang H, Fang D, Kong L-Y, Jin Z-R, Cai J, Kang X-J, Wan Y & Xing G-G (2014). Sensitization of neurons in the central nucleus of the amygdala via the decreased GABAergic inhibition contributes to the development of neuropathic pain-related anxiety-like behaviors in rats. *Mol Brain* **7,** 72.

Johannessen M, Fontanilla D, Mavlyutov T, Ruoho AE & Jackson MB (2011). Antagonist action of progesterone at -receptors in the modulation of voltage-gated sodium channels. *AJP Cell Physiol* **300,** C328–C337.

Johansson L, Guo X, Waern M, Ostling S, Gustafson D, Bengtsson C & Skoog I (2010). Midlife psychological stress and risk of dementia: a 35-year longitudinal population study. *Brain* **133,** 2217–2224.

Johnson PL, Molosh A, Fitz SD, Truitt WA & Shekhar A (2012). Orexin, stress, and anxiety/panic states. *Prog Brain Res* **198,** 133–161.

Jolkkonen E, Miettinen R & Pitkänen A (2001). Projections from the amygdalo-piriform transition area to the amygdaloid complex: A PHA-l study in rat. *J Comp Neurol* **432,** 440–465.

Kandel ER, Schwartz JH (James H & Jessell TM (2000). *Principles of neural science*. McGraw-Hill, Health Professions Division.

Kash TL, Nobis WP, Matthews RT & Winder DG (2008). Dopamine Enhances Fast Excitatory Synaptic Transmission in the Extended Amygdala by a CRF-R1-Dependent Process. *J Neurosci* **28,** 13856–13865.

Kataoka N, Hioki H, Kaneko T & Nakamura K (2014). Psychological stress activates a dorsomedial hypothalamus-medullary raphe circuit driving brown adipose tissue thermogenesis and hyperthermia. *Cell Metab* **20,** 346–358.

Kayasuga Y, CHIBA S, SUZUKI M, KIKUSUI T, MATSUWAKI T, YAMANOUCHI K, KOTAKI H, HORAI R, IWAKURA Y & NISHIHARA M (2007). Alteration of behavioural phenotype in mice by targeted disruption

of the progranulin gene. *Behav Brain Res* **185,** 110–118.

Kc P & Dick TE (2010). Modulation of cardiorespiratory function mediated by the paraventricular nucleus. *Respir Physiol Neurobiol* **174,** 55–64.

Kent JM, Coplan JD & Gorman JM (1998). Clinical utility of the selective serotonin reuptake inhibitors in the spectrum of anxiety. *Biol Psychiatry* **44,** 812–824.

Kessler RC, Berglund P, Demler O, Jin R, Merikangas KR & Walters EE (2005). Lifetime Prevalence and Age-of-Onset Distributions of DSM-IV Disorders in the National Comorbidity Survey Replication. *Arch Gen Psychiatry* **62,** 593.

Kessler RC, Sonnega A, Bromet E, Hughes M & Nelson CB (1995). Posttraumatic stress disorder in the National Comorbidity Survey. *Arch Gen Psychiatry* **52,** 1048–1060.

Khakh BS & Sofroniew M V (2015). Diversity of astrocyte functions and phenotypes in neural circuits. *Nat Neurosci* **18,** 942–952.

Kirby L, Rice KC & Valentino RJ (2000). Effects of Corticotropin-Releasing Factor on Neuronal Activity in the Serotonergic Dorsal Raphe Nucleus. *Neuropsychopharmacology* **22,** 148–162.

Klaassens ER, Giltay EJ, Cuijpers P, van Veen T & Zitman FG (2012). Adulthood trauma and HPA-axis functioning in healthy subjects and PTSD patients: A meta-analysis. *Psychoneuroendocrinology* **37,** 317–331.

Klampfl SM, Brunton PJ, Bayerl DS & Bosch OJ (2016). CRF-R1 activation in the anterior-dorsal BNST induces maternal neglect in lactating rats via an HPA axis-independent central mechanism. *Psychoneuroendocrinology* **64,** 89–98.

Klimov LO, Fedoseeva LA, Ryazanova MA, Dymshits GM & Markel AL (2013). Expression of renin-angiotensin system genes in brain structures of ISIAH rats with stress-induced arterial hypertension. *Bull Exp Biol Med* **154,** 357–360.

Koch CE, Bartlang MS, Kiehn JT, Lucke L, Naujokat N, Helfrich-Förster C, Reber SO & Oster H (2016). Time-of-day-dependent adaptation of the HPA axis to predictable social defeat stress. *J Endocrinol* **231,** 209–221.

Koss DJ, Robinson L, Drever BD, Plucińska K, Stoppelkamp S, Veselcic P, Riedel G & Platt B (2016). Mutant Tau knock-in mice display frontotemporal dementia relevant behaviour and histopathology. *Neurobiol Dis* **91,** 105–123.

Kruijver FPM, Zhou J-N, Pool CW, Hofman MA, Gooren LJG & Swaab DF (2000). Male-to-Female Transsexuals Have Female Neuron Numbers in a Limbic Nucleus. *J Clin Endocrinol Metab* **85,** 2034–2041.

Kullmann DM, Ruiz A, Rusakov DM, Scott R, Semyanov A & Walker MC (2005). Presynaptic, extrasynaptic and axonal GABAA receptors in the CNS: where and why? *Prog Biophys Mol Biol* **87,** 33–46.

Kumar A & Foster TC (2002). 17beta-estradiol benzoate decreases the AHP amplitude in CA1 pyramidal neurons. *J Neurophysiol* **88,** 621–626.

Landfield PW & Pitler TA (1984). Prolonged Ca2+ -dependent afterhyperpolarizations in hippocampal neurons of aged rats. *Science (80-)* **226,** 1089–1093.

Lebow MA & Chen A (2016). Overshadowed by the amygdala: the bed nucleus of the stria terminalis emerges as key to psychiatric disorders. *Mol Psychiatry* **21,** 450–463.

Lebow M, Neufeld-Cohen A, Kuperman Y, Tsoory M, Gil S & Chen A (2012). Susceptibility to PTSD-like behavior is mediated by corticotropin-releasing factor receptor type 2 levels in the bed nucleus of the stria terminalis. *J Neurosci* **32,** 6906–6916.

Lee KM & MacLean AG (2015). New advances on glial activation in health and disease. *World J Virol* **4,** 42–55.

Lee VM, Goedert M & Trojanowski JQ (2001). Neurodegenerative tauopathies. *Annu Rev Neurosci* **24,** 1121–1159.

Lee Y & Davis M (1997). Role of the hippocampus, the bed nucleus of the stria terminalis, and the amygdala in the excitatory effect of corticotropin-releasing hormone on the acoustic startle reflex. *J Neurosci* **17,** 6434–6446.

Lee Y, Fitz S, Johnson PL & Shekhar A (2008). Repeated stimulation of CRF receptors in the BNST of rats selectively induces social but not panic-like anxiety. *Neuropsychopharmacology* **33,** 2586–2594.

Lein ES et al. (2007). Genome-wide atlas of gene expression in the adult mouse brain. *Nature* **445,** 168–176.

de Lera Ruiz M & Kraus RL (2015). Voltage-Gated Sodium Channels: Structure, Function, Pharmacology, and Clinical Indications. *J Med Chem* **58,** 7093–7118.

Levita L, Hammack SE, Mania I, Li X-Y, Davis M & Rainnie DG (2004). 5-hydroxytryptamine1A-like receptor activation in the bed nucleus of the stria terminalis: electrophysiological and behavioral studies. *Neuroscience* **128,** 583–596.

Lewis K, Li C, Perrin MH, Blount A, Kunitake K, Donaldson C, Vaughan J, Reyes TM, Gulyas J, Fischer W, Bilezikjian L, Rivier J, Sawchenko PE & Vale WW (2001). Identification of urocortin III, an additional member of the corticotropin-releasing factor (CRF) family with high affinity for the CRF2 receptor. *Proc Natl Acad Sci U S A* **98,** 7570–7575.

Li C, Pleil KE, Stamatakis AM, Busan S, Vong L, Lowell BB, Stuber GD & Kash TL (2012). Presynaptic inhibition of gamma-aminobutyric acid release in the bed nucleus of the stria terminalis by kappa opioid receptor signaling. *Biol Psychiatry* **71,** 725–732.

Liang KC, Chen HC & Chen DY (2001). Posttraining infusion of norepinephrine and corticotropin releasing factor into the bed nucleus of the stria terminalis enhanced retention in an inhibitory avoidance task. *Chin J Physiol* **44,** 33–43.

Liapakis G, Venihaki M, Margioris A, Grigoriadis D & Gkountelias K (2011). Members of CRF family and their receptors: from past to future. *Curr Med Chem* **18,** 2583–2600.

Liu W, Miller BL, Kramer JH, Rankin K, Wyss-Coray C, Gearhart R, Phengrasamy L, Weiner M & Rosen HJ (2004). Behavioral disorders in the frontal and temporal variants of frontotemporal dementia. *Neurology* **62,** 742–748.

Liu YC, Salamone JD & Sachs BD (1997). Lesions in medial preoptic area and bed nucleus of stria terminalis: differential effects on copulatory behavior and noncontact erection in male rats. *J Neurosci* **17,** 5245–5253.

Lörincz A, Notomi T, Tamás G, Shigemoto R & Nusser Z (2002). Polarized and compartment-dependent distribution of HCN1 in pyramidal cell dendrites. *Nat Neurosci* **5,** 1185–1193.

Lovick TA (2006). Plasticity of GABAA receptor subunit expression during the oestrous cycle of the rat: implications for premenstrual syndrome in women. *Exp Physiol* **91,** 655–660.

Lovick TA (2012). Estrous cycle and stress: influence of progesterone on the female brain. *Brazilian J Med Biol Res = Rev Bras Pesqui médicas e biológicas / Soc Bras Biofísica . [et al]* **45,** 314–320.

Mackenzie IRA et al. (2010). Nomenclature and nosology for neuropathologic subtypes of frontotemporal lobar degeneration: an update. *Acta Neuropathol* **119,** 1–4.

MacNamara A, Rabinak CA, Kennedy AE, Fitzgerald DA, Liberzon I, Stein MB & Phan KL (2016). Emotion Regulatory Brain Function and SSRI Treatment in PTSD: Neural Correlates and Predictors of Change. *Neuropsychopharmacology* **41,** 611–618.

Makino S, Gold PW & Schulkin J (1994). Effects of corticosterone on CRH mRNA and content in the bed nucleus of the stria terminalis; comparison with the effects in the central nucleus of the amygdala and the paraventricular nucleus of the hypothalamus. *Brain Res* **657,** 141–149.

Marcinkiewcz CA, Dorrier CE, Lopez AJ & Kash TL (2015). Ethanol induced adaptations in 5-HT2c receptor signaling in the bed nucleus of the stria terminalis: Implications for anxiety during ethanol withdrawal. *Neuropharmacology* **89,** 157–167.

Marowsky A & Vogt KE (2014). Delta-subunit-containing GABAA-receptors mediate tonic inhibition in paracapsular cells of the mouse amygdala. *Front Neural Circuits* **8,** 27.

Masugi-Tokita M, Flor PJ & Kawata M (2016). Metabotropic Glutamate Receptor Subtype 7 in the Bed Nucleus of the Stria Terminalis is Essential for Intermale Aggression. *Neuropsychopharmacology* **41,** 726–735.

Matsumoto K, Puia G, Dong E & Pinna G (2007). GABA $_A$ receptor neurotransmission dysfunction in a mouse model of social isolation-induced stress: Possible insights into a non-serotonergic mechanism of action of SSRIs in mood and anxiety disorders. *Stress* **10,** 3–12.

Mazure CM & Jones DP (2015). Twenty years and still counting: including women as participants and studying sex and gender in biomedical research. *BMC Womens Health* **15,** 94.

McDonald AJ, SHAMMAH-LAGNADO SJ, SHI C & DAVIS M (1999). Cortical Afferents to the Extended Amygdala. *Ann N Y Acad Sci* **877,** 309–338.

McElligott Z a & Winder DG (2008). Alpha1-adrenergic receptor-induced heterosynaptic long-term depression in the bed nucleus of the stria terminalis is disrupted in mouse models of affective disorders. *Neuropsychopharmacology* **33,** 2313–2323.

McElligott ZA, Klug JR, Nobis WP, Patel S, Grueter BA, Kash TL & Winder DG (2010). Distinct forms of Gq-receptor-dependent plasticity of excitatory transmission in the BNST are differentially affected by stress. *Proc Natl Acad Sci U S A* **107,** 2271–2276.

Miller BH & Takahashi JS (2014). Central Circadian Control of Female Reproductive Function. *Front Endocrinol (Lausanne)* **4,** 195.

Mironova VI, Rakitskaya V V, Pivina SG & Ordyan NE (2015). [STRESS-INDUCED PATTERNS OF THE HYPOTHALAMIC CRH AND VASOPRESSIN EXPRESSION IN FEMALE RATS IN A MODEL OF POSTTRAUMATIC STRESS DISORDER]. *Ross Fiziol zhurnal Im IM Sechenova* **101,** 1355–1365.

Mobbs D, Yu R, Rowe JB, Eich H, FeldmanHall O & Dalgleish T (2010). Neural activity associated with monitoring the oscillating threat value of a tarantula. *Proc Natl Acad Sci U S A* **107,** 20582–20586.

Münsterkötter AL, Notzon S, Redlich R, Grotegerd D, Dohm K, Arolt V, Kugel H, Zwanzger P & Dannlowski U (2015). SPIDER OR NO SPIDER? NEURAL CORRELATES OF SUSTAINED AND PHASIC FEAR IN SPIDER PHOBIA. *Depress Anxiety* **32,** 656–663.

Nagaya N, Acca GM & Maren S (2015*a*). Allopregnanolone in the bed nucleus of the stria terminalis modulates contextual fear in rats. *Front Behav Neurosci* **9,** 205.

Nagaya N, Acca GM & Maren S (2015*b*). Allopregnanolone in the bed nucleus of the stria terminalis modulates contextual fear in rats. *Front Behav Neurosci* **9,** 205.

Nautiyal KM, Tanaka KF, Barr MM, Tritschler L, Le Dantec Y, David DJ, Gardier AM, Blanco C, Hen R & Ahmari SE (2015). Distinct Circuits Underlie the Effects of 5-HT1B Receptors on Aggression and Impulsivity. *Neuron* **86,** 813–826.

Niswender CM & Conn PJ (2010). Metabotropic glutamate receptors: physiology, pharmacology, and disease. *Annu Rev Pharmacol Toxicol* **50,** 295–322.

Numan M & Numan M (1996). A lesion and neuroanatomical tract-tracing analysis of the role of the bed nucleus of the stria terminalis in retrieval behavior and other aspects of maternal responsiveness in rats. *Dev Psychobiol* **29,** 23–51.

Numan M & Numan MJ (1995). Importance of pup-related sensory inputs and maternal performance for the expression of Fos-like immunoreactivity in the preoptic area and ventral bed nucleus of the stria terminalis of postpartum rats. *Behav Neurosci* **109,** 135–149.

Nutsch VL, Bell MR, Will RG, Yin W, Wolfe A, Gillette R, Dominguez JM & Gore AC (2017). Aging and estradiol effects on gene expression in the medial preoptic area, bed nucleus of the stria terminalis, and posterodorsal medial amygdala of male rats. *Mol Cell Endocrinol* **442,** 153–164.

Oler JA, Fox AS, Shelton SE, Christian BT, Murali D, Oakes TR, Davidson RJ & Kalin NH (2009). Serotonin Transporter Availability in the Amygdala and Bed Nucleus of the Stria Terminalis Predicts Anxious Temperament and Brain Glucose Metabolic Activity. *J Neurosci* **29,** 9961–9966.

Olianas MC & Onali P (1999). GABA(B) receptor-mediated stimulation of adenylyl cyclase activity in membranes of rat olfactory bulb. *Br J Pharmacol* **126,** 657–664.

Olsen RW & Sieghart W (2008). International Union of Pharmacology. LXX. Subtypes of gamma-aminobutyric acid(A) receptors: classification on the basis of subunit composition, pharmacology, and function. Update. *Pharmacol Rev* **60,** 243–260.

Öngür D, Bechtholt AJ, Carlezon WA & Cohen BM (2014). Glial Abnormalities in Mood Disorders. *Harv Rev Psychiatry* **22,** 334–337.

Pal K, Swaminathan K, Xu HE & Pioszak AA (2010). Structural basis for hormone recognition by the Human CRFR2{alpha} G protein-coupled receptor. *J Biol Chem* **285,** 40351–40361.

Panatier A, Vallée J, Haber M, Murai KK, Lacaille J-C & Robitaille R (2011). Astrocytes are endogenous regulators of basal transmission at central synapses. *Cell* **146,** 785–798.

Paolicelli RC, Bolasco G, Pagani F, Maggi L, Scianni M, Panzanelli P, Giustetto M, Ferreira TA, Guiducci E, Dumas L, Ragozzino D & Gross CT (2011). Synaptic Pruning by Microglia Is Necessary for Normal Brain Development. *Science (80-)* **333,** 1456–1458.

Paxinos G & Franklin KBJ (2004*a*). *The mouse brain in stereotaxic coordinates*. Elsevier Academic Press. Available at: https://books.google.co.uk/books/about/The_Mouse_Brain_in_Stereotaxic_Coordinat.html?id=EHy1QN1xv0gC [Accessed June 8, 2017].

Paxinos G & Franklin KBJ (2004*b*). *The mouse brain in stereotaxic coordinates*. Elsevier Academic Press. Available at: https://books.google.co.uk/books/about/The_Mouse_Brain_in_Stereotaxic_Coordinat.html?id=EHy1QN1xv0gC&source=kp_cover&redir_esc=y [Accessed August 30, 2017].

Peavy GM, Salmon DP, Jacobson MW, Hervey A, Gamst AC, Wolfson T, Patterson TL, Goldman S, Mills PJ, Khandrika S & Galasko D (2009). Effects of Chronic Stress on Memory Decline in Cognitively Normal and Mildly Impaired Older Adults. *Am J Psychiatry* **166,** 1384–1391.

Perea-Rodriguez JP, Takahashi EY, Amador TM, Hao RC, Saltzman W & Trainor BC (2015). Effects of Reproductive Experience on Central Expression of Progesterone, Oestrogen α, Oxytocin and Vasopressin Receptor mRNA in Male California Mice (*Peromyscus californicus*). *J Neuroendocrinol* **27,** 245–252.

Pigott TA (2003). Anxiety disorders in women. *Psychiatr Clin North Am* **26,** 621–72, vi–vii.

Pleil KE, Rinker JA, Lowery-Gionta EG, Mazzone CM, McCall NM, Kendra AM, Olson DP, Lowell BB, Grant KA, Thiele TE & Kash TL (2015). NPY signaling inhibits extended amygdala CRF neurons to suppress binge alcohol drinking. *Nat Neurosci* **18,** 545–552.

Porter VR, Buxton WG, Fairbanks LA, Strickland T, O'Connor SM, Rosenberg-Thompson S & Cummings JL (2003). Frequency and Characteristics of Anxiety Among Patients With Alzheimer's Disease and Related Dementias. *J Neuropsychiatry Clin Neurosci* **15,** 180–186.

Prenderville JA, Kennedy PJ, Dinan TG & Cryan JF (2015). Adding fuel to the fire: the impact of stress on the ageing brain. *Trends Neurosci* **38,** 13–25.

Purdy RH, Moore PH, Rao PN, Hagino N, Yamaguchi T, Schmidt P, Rubinow DR, Morrow AL & Paul SM (1990). Radioimmunoassay of 3 alpha-hydroxy-5 alpha-pregnan-20-one in rat and human plasma. *Steroids* **55,** 290–296.

Radley JJ & Sawchenko PE (2011). A common substrate for prefrontal and hippocampal inhibition of the neuroendocrine stress response. *J Neurosci* **31,** 9683–9695.

Rainnie D (1999). Neurons of the bed nucleus of the stria terminalis (BNST): electrophysiological properties and their response to serotonin. *Ann N Y Acad Sci*695–699.

Ramos-Ortolaza DL, Doreste-Mendez RJ, Alvarado-Torres JK & Torres-Reveron A (2017). Ovarian hormones modify anxiety behavior and glucocorticoid receptors after chronic social isolation stress. *Behav Brain Res* **328,** 115–122.

Randall AD, Booth C & Brown JT (2012). Age-related changes to Na+ channel gating contribute to modified intrinsic neuronal excitability. *Neurobiol Aging* **33,** 2715–2720.

Rang H, Dale M, Ritter J & Flower R (2007). *Rang & Dale's Pharmacology E-Book - 6th Edition*. Available at: https://www.elsevier.com/books/rang-and-dales-pharmacology/ritter/978-0-7020-4074-0 [Accessed March 3, 2018].

Ransom BR & Ransom CB (2012). Astrocytes: multitalented stars of the central nervous system. *Methods Mol Biol* **814,** 3–7.

Ratnavalli E, Brayne C, Dawson K & Hodges JR (2002). The prevalence of frontotemporal dementia. *Neurology* **58,** 1615–1621.

Roberson ED (2012). Mouse models of frontotemporal dementia. *Ann Neurol* **72,** 837–849.

Rodríguez-Arellano JJ, Parpura V, Zorec R & Verkhratsky A (2016). Astrocytes in physiological aging and Alzheimer's disease. *Neuroscience* **323,** 170–182.

Rodriguez-Sierra OE, Goswami S, Turesson HK & Pare D (2016). Altered responsiveness of BNST and amygdala neurons in trauma-induced anxiety. *Transl Psychiatry* **6,** e857.

Ropert N, Miles R & Korn H (1990). Characteristics of miniature inhibitory postsynaptic currents in CA1 pyramidal neurones of rat hippocampus. *J Physiol* **428,** 707–722.

Sahuque LL, Kullberg EF, Mcgeehan AJ, Kinder JR, Hicks MP, Blanton MG, Janak PH & Olive MF (2006). Anxiogenic and aversive effects of corticotropin-releasing factor (CRF) in the bed nucleus of the stria terminalis in the rat: role of CRF receptor subtypes. *Psychopharmacology (Berl)* **186,** 122–132.

Sakanaka M, Shibasaki T & Lederis K (1986). Distribution and efferent projections of corticotropin-releasing factor-like immunoreactivity in the rat amygdaloid complex. *Brain Res* **382,** 213–238.

Saleeon W, Jansri U, Srikiatkhachorn A & Bongsebandhu-phubhakdi S (2016). Estrous Cycle Induces Peripheral Sensitization in Trigeminal Ganglion Neurons: An Animal Model of Menstrual Migraine. *J Med Assoc Thai* **99,** 206–212.

SAPOLSKY RM, KREY LC & McEWEN BS (1986). The Neuroendocrinology of Stress and Aging: The Glucocorticoid Cascade Hypothesis*. *Endocr Rev* **7,** 284–301.

Saudou F, Amara DA, Dierich A, LeMeur M, Ramboz S, Segu L, Buhot MC & Hen R (1994). Enhanced aggressive behavior in mice lacking 5-HT1B receptor. *Science* **265,** 1875–1878.

Sawada S, Takada S & Yamamoto C (1980). Electrical activity recorded from thin sections of the bed nucleus of the stria terminalis, and the effects of neurotensin. *Brain Res* **188,** 578–581.

Scharfman HE, Mercurio TC, Goodman JH, Wilson MA & MacLusky NJ (2003). Hippocampal excitability increases during the estrous cycle in the rat: a potential role for brain-derived neurotrophic factor. *J Neurosci* **23,** 11641–11652.

Schneeberger M, Gomis R & Claret M (2014). Hypothalamic and brainstem neuronal circuits controlling homeostatic energy balance. *J Endocrinol* **220,** T25-46.

Schneier FR, Campeas R, Carcamo J, Glass A, Lewis-Fernandez R, Neria Y, Sanchez-Lacay A, Vermes D & Wall MM (2015). COMBINED MIRTAZAPINE AND SSRI TREATMENT OF PTSD: A PLACEBO-CONTROLLED TRIAL. *Depress Anxiety* **32,** 570–579.

Shah NH & Aizenman E (2014). Voltage-Gated Potassium Channels at the Crossroads of Neuronal Function, Ischemic Tolerance, and Neurodegeneration. *Transl Stroke Res* **5,** 38–58.

Shaham Y, Shalev U, Lu L, De Wit H & Stewart J (2003). The reinstatement model of drug relapse: history, methodology and major findings. *Psychopharmacology (Berl)* **168,** 3–20.

Shen H, Gong QH, Aoki C, Yuan M, Ruderman Y, Dattilo M, Williams K & Smith SS (2007). Reversal of neurosteroid effects at alpha4beta2delta GABAA receptors triggers anxiety at puberty. *Nat Neurosci* **10,** 469–477.

Shen H, Gong QH, Yuan M & Smith SS (2005). Short-term steroid treatment increases delta GABAA receptor subunit expression in rat CA1 hippocampus: pharmacological and behavioral effects. *Neuropharmacology* **49,** 573–586.

Sheng H, Sun T, Cong B, He P, Zhang Y, Yan J, Lu C & Ni X (2008). Corticotropin-releasing hormone stimulates SGK-1 kinase expression in cultured hippocampal neurons via CRH-R1. *Am J Physiol Metab* **295,** E938–E946.

Shors TJ, Pickett J, Wood G & Paczynski M (1999). Acute stress persistently enhances estrogen levels in the female rat. *Stress* **3,** 163–171.

Silberman Y, Matthews RT & Winder DG (2013). A Corticotropin Releasing Factor Pathway for Ethanol Regulation of the Ventral Tegmental Area in the Bed Nucleus of the Stria Terminalis. *J Neurosci*. Available at: http://www.jneurosci.org/content/33/3/950.long [Accessed July 21, 2017].

Simons M & Nave K-A (2016). Oligodendrocytes: Myelination and Axonal Support. *Cold Spring Harb Perspect Biol* **8,** a020479.

Singh M & Su C (2013). Progesterone-induced neuroprotection: Factors that may predict therapeutic efficacy. *Brain Res* **1514,** 98–106.

Sink KS, Chung A, Ressler KJ, Davis M & Walker DL (2013). Anxiogenic effects of CGRP within the BNST may be mediated by CRF acting at BNST CRFR1 receptors. *Behav Brain Res* **243,** 286–293.

Skibinski G, Parkinson NJ, Brown JM, Chakrabarti L, Lloyd SL, Hummerich H, Nielsen JE, Hodges JR, Spillantini MG, Thusgaard T, Brandner S, Brun A, Rossor MN, Gade A, Johannsen P, Sørensen SA, Gydesen S, Fisher EM & Collinge J (2005). Mutations in the endosomal ESCRTIII-complex subunit CHMP2B in frontotemporal dementia. *Nat Genet* **37,** 806–808.

Skinner DC, Evans NP, Delaleu B, Goodman RL, Bouchard P & Caraty A (1998). The negative feedback actions of progesterone on gonadotropin-releasing hormone secretion are transduced by the classical progesterone receptor. *Proc Natl Acad Sci U S A* **95,** 10978–10983.

Smiałowska M, Szewczyk B, Woźniak M, Wawrzak-Wleciał A & Domin H (2013). Glial degeneration as a model of depression. *Pharmacol Rep* **65,** 1572–1579.

Smith KR, Damiano J, Franceschetti S, Carpenter S, Canafoglia L, Morbin M, Rossi G, Pareyson D, Mole SE, Staropoli JF, Sims KB, Lewis J, Lin W-L, Dickson DW, Dahl H-H, Bahlo M & Berkovic SF (2012). Strikingly different clinicopathological phenotypes determined by progranulin-mutation dosage. *Am J Hum Genet* **90,** 1102–1107.

Smith SS, Gong QH, Hsu F-C, Markowitz RS, ffrench-Mullen JMH & Li X (1998*a*). GABA(A) receptor alpha4 subunit suppression prevents withdrawal properties of an endogenous steroid. *Nature* **392,** 926–929.

Smith SS, Gong QH, Li X, Moran MH, Bitran D, Frye CA & Hsu FC (1998*b*). Withdrawal from 3alpha-OH-5alpha-pregnan-20-One using a pseudopregnancy model alters the kinetics of hippocampal GABAA-gated current and increases the GABAA receptor alpha4 subunit in association with increased anxiety. *J Neurosci* **18,** 5275–5284.

Smith SS, Shen H, Gong QH & Zhou X (2007). Neurosteroid regulation of GABA(A) receptors: Focus on the alpha4 and delta subunits. *Pharmacol Ther* **116,** 58–76.

Sofroniew M V. (2009). Molecular dissection of reactive astrogliosis and glial scar formation. *Trends Neurosci* **32,** 638–647.

Somerville LH, Whalen PJ & Kelley WM (2010). Human bed nucleus of the stria terminalis indexes hypervigilant threat monitoring. *Biol Psychiatry* **68,** 416–424.

Sotnikov S, Wittmann A, Bunck M, Bauer S, Deussing J, Schmidt M, Touma C, Landgraf R & Czibere L (2014). Blunted HPA axis reactivity reveals glucocorticoid system dysbalance in a mouse model of high anxiety-related behavior. *Psychoneuroendocrinology* **48,** 41–51.

Spencer TE & Bazer FW (2002). Biology of progesterone action during pregnancy recognition and maintenance of pregnancy. *Front Biosci* **7,** d1879-98.

Stanley DP & Shetty AK (2004). Aging in the rat hippocampus is associated with widespread reductions in the number of glutamate decarboxylase-67 positive interneurons but not interneuron degeneration. *J Neurochem* **89,** 204–216.

Stephens SBZ, Chahal N, Munaganuru N, Parra RA & Kauffman AS (2016). Estrogen Stimulation of *Kiss1* Expression in the Medial Amygdala Involves Estrogen Receptor-α But Not Estrogen Receptor-β. *Endocrinology* **157,** 4021–4031.

Stokes PE & Holtz A (n.d.). Fluoxetine tenth anniversary update: the progress continues. *Clin Ther* **19,** 1135–1250.

Straube T, Mentzel H-J & Miltner WHR (2007). Waiting for spiders: Brain activation during anticipatory anxiety in spider phobics. *Neuroimage* **37,** 1427–1436.

Suzuki A, Stern SA, Bozdagi O, Huntley GW, Walker RH, Magistretti PJ & Alberini CM (2011). Astrocyte-Neuron Lactate Transport Is Required for Long-Term Memory Formation. *Cell* **144,** 810–823.

Swarup V, Phaneuf D, Bareil C, Robertson J, Rouleau GA, Kriz J & Julien J-P (2011). Pathological hallmarks of amyotrophic lateral sclerosis/frontotemporal lobar degeneration in transgenic mice produced with TDP-43 genomic fragments. *Brain* **134,** 2610–2626.

Swerdlow NR, Geyer MA, Vale WW & Koob GF (1986). Corticotropin-releasing factor potentiates acoustic startle in rats: blockade by chlordiazepoxide. *Psychopharmacology (Berl)* **88,** 147–152.

Takahashi N & Sakurai T (2013). Roles of glial cells in schizophrenia: Possible targets for therapeutic approaches. *Neurobiol Dis* **53,** 49–60.

Tamagnini F, Novelia J, Kerrigan TL, Brown JT, Tsaneva-Atanasova K & Randall AD (2015). Altered intrinsic excitability of hippocampal CA1 pyramidal neurons in aged PDAPP mice. *Front Cell Neurosci* **9,** 372.

Tolin DF & Foa EB (2006). Sex differences in trauma and posttraumatic stress disorder: A quantitative review of 25 years of research. *Psychol Bull* **132,** 959–992.

Toufexis DJ, Davis C, Hammond A & Davis M (2004). Progesterone Attenuates Corticotropin-Releasing Factor-Enhanced But Not Fear-Potentiated Startle via the Activity of Its Neuroactive Metabolite, Allopregnanolone. *J Neurosci* **24,** 10280–10287.

Turesson HK, Rodríguez-Sierra OE & Pare D (2013). Intrinsic connections in the anterior part of the bed nucleus of the stria terminalis. *J Neurophysiol* **109,** 2438–2450.

Vasudevan N, Davidkova G, Zhu YS, Koibuchi N, Chin WW & Pfaff D (2001). Differential interaction of estrogen receptor and thyroid hormone receptor isoforms on the rat oxytocin receptor promoter leads to differences in transcriptional regulation. *Neuroendocrinology* **74,** 309–324.

Vasudevan N, Morgan M, Pfaff D & Ogawa S (2013). Distinct behavioral phenotypes in male mice lacking the thyroid hormone receptor α1 or β isoforms. *Horm Behav* **63,** 742–751.

Viau V (2002). Functional cross-talk between the hypothalamic-pituitary-gonadal and -adrenal axes. *J Neuroendocrinol* **14,** 506–513.

Vieira RT, Caixeta L, Machado S, Silva AC, Nardi AE, Arias-Carrión O & Carta MG (2013). Epidemiology of early-onset dementia: a review of the literature. *Clin Pract Epidemiol Ment Heal* **9,** 88–95.

Wagner KM, Roeder Z, Desrochers K, Buhler A V, Heinricher MM & Cleary DR (2013). The dorsomedial hypothalamus mediates stress-induced hyperalgesia and is the source of the pronociceptive peptide cholecystokinin in the rostral ventromedial medulla. *Neuroscience* **238,** 29–38.

Walf AA & Frye CA (2007). Estradiol decreases anxiety behavior and enhances inhibitory avoidance and gestational stress produces opposite effects. *Stress* **10,** 251–260.

Walker DL, Toufexis DJ & Davis M (2003). Role of the bed nucleus of the stria terminalis versus the amygdala in fear, stress, and anxiety. *Eur J Pharmacol* **463,** 199–216.

Watanabe E, Fujikawa A, Matsunaga H, Yasoshima Y, Sako N, Yamamoto T, Saegusa C & Noda M (2000). Nav2/NaG channel is involved in control of

salt-intake behavior in the CNS. *J Neurosci* **20,** 7743–7751.

Wei W, Zhang N, Peng Z, Houser CR & Mody I (2003). Perisynaptic localization of delta subunit-containing GABA(A) receptors and their activation by GABA spillover in the mouse dentate gyrus. *J Neurosci* **23,** 10650–10661.

Wesselhoeft R, Pedersen CB, Mortensen PB, Mors O & Bilenberg N (2015). Gender–age interaction in incidence rates of childhood emotional disorders. *Psychol Med* **45,** 829–839.

Wilson IA, Ikonen S, Gallagher M, Eichenbaum H & Tanila H (2005). Age-associated alterations of hippocampal place cells are subregion specific. *J Neurosci* **25,** 6877–6886.

Wright SH (2004). Generation of resting membrane potential. *Adv Physiol Educ*. Available at: http://advan.physiology.org/content/28/4/139.long [Accessed August 28, 2017].

Wu FCW et al. (2010). Identification of Late-Onset Hypogonadism in Middle-Aged and Elderly Men. *N Engl J Med* **363,** 123–135.

Wu FCW, Tajar A, Pye SR, Silman AJ, Finn JD, O'Neill TW, Bartfai G, Casanueva F, Forti G, Giwercman A, Huhtaniemi IT, Kula K, Punab M, Boonen S, Vanderschueren D & European Male Aging Study Group (2008). Hypothalamic-pituitary-testicular axis disruptions in older men are differentially linked to age and modifiable risk factors: the European Male Aging Study. *J Clin Endocrinol Metab* **93,** 2737–2745.

Yaffe K, Vittinghoff E, Lindquist K, Barnes D, Covinsky KE, Neylan T, Kluse M, Marmar C, S R, T H, C van D, RG T & LJ T (2010). Posttraumatic Stress Disorder and Risk of Dementia Among US Veterans. *Arch Gen Psychiatry* **67,** 608.

Yassa MA, Hazlett RL, Stark CEL & Hoehn-Saric R (2012). Functional MRI of the amygdala and bed nucleus of the stria terminalis during conditions of uncertainty in generalized anxiety disorder. *J Psychiatr Res* **46,** 1045–1052.

Yin F, Banerjee R, Thomas B, Zhou P, Qian L, Jia T, Ma X, Ma Y, Iadecola C, Beal MF, Nathan C & Ding A (2010). Exaggerated inflammation, impaired host defense, and neuropathology in progranulin-deficient mice. *J Exp Med* **207,** 117–128.

Zaba M, Kirmeier T, Ionescu IA, Wollweber B, Buell DR, Gall-Kleebach DJ, Schubert CF, Novak B, Huber C, Köhler K, Holsboer F, Pütz B, Müller-Myhsok B, Höhne N, Uhr M, Ising M, Herrmann L & Schmidt U (2015). Identification and characterization of HPA-axis reactivity endophenotypes in a cohort of female PTSD patients. *Psychoneuroendocrinology* **55,** 102–115.

Zhang F, Wang L-P, Boyden ES & Deisseroth K (2006). Channelrhodopsin-2 and optical control of excitable cells. *Nat Methods* **3,** 785–792.

Zhao J, O'Connor T & Vassar R (2011). The contribution of activated astrocytes to Aβ production: implications for Alzheimer's disease pathogenesis. *J Neuroinflammation* **8,** 150.

Zhu L-J, Liu M-Y, Li H, Liu X, Chen C, Han Z, Wu H-Y, Jing X, Zhou H-H, Suh H, Zhu D-Y & Zhou Q-G (2014). The Different Roles of Glucocorticoids in the Hippocampus and Hypothalamus in Chronic Stress-Induced HPA Axis Hyperactivity ed. Homberg J. *PLoS One* **9,** e97689.